

I. SPECTROSCOPIC EVIDENCE FOR SLOW VIBRATIONAL  
RELAXATION IN EXCITED ELECTRONIC STATES OF  
DIATOMICS IN RARE GAS SOLIDS

II. STATIC CRYSTAL FIELD EFFECTS IN THE ELECTRONIC  
SPECTRA OF ISOTOPICALLY MIXED BENZENE CRYSTALS

Thesis by

Dino Sabatino Tinti

In Partial Fulfillment of the Requirements

For the Degree of  
Doctor of Philosophy

California Institute of Technology  
Pasadena, California

1968

(Submitted September 29, 1967)

## ACKNOWLEDGEMENTS

I am indebted to Professor G. W. Robinson, my research advisor, for his encouragement throughout my graduate training and for his assistance in the completion of this work.

Special thanks must also go to E. R. Bernstein, S. D. Colson, and G. C. Nieman for their broad contributions to this thesis. The many hours spent in both experimental work and discussion with them has been a stimulating and productive experience.

I am also thankful for the continual encouragement and support given me by my parents.

The patience and understanding of my wife, Diana, has been a constant inspiration to the fulfillment of this work. I can not thank her enough.

Financial assistance from the California Institute of Technology and the National Aeronautics and Space Administration is gratefully appreciated. Various parts of this research were supported by the Atomic Energy Commission, the National Science Foundation, and the Army Research Office, Durham.



I. SPECTROSCOPIC EVIDENCE FOR SLOW VIBRATIONAL  
RELAXATION IN EXCITED ELECTRONIC STATES OF  
DIATOMICS IN RARE GAS SOLIDS

II. STATIC CRYSTAL FIELD EFFECTS IN THE ELECTRONIC  
SPECTRA OF ISOTOPICALLY MIXED BENZENE CRYSTALS

Thesis by

Dino Sabatino Tinti

ABSTRACT

PART I

Studies of vibrational relaxation in excited electronic states of simple diatomic molecules trapped in solid rare-gas matrices at low temperatures are reported. The relaxation is investigated by monitoring the emission intensity from vibrational levels of the excited electronic state to vibrational levels of the ground electronic state. The emission was in all cases excited by bombardment of the doped rare-gas solid with X-rays.

The diatomics studied and the band systems seen are:  $N_2$ , Vegard-Kaplan and Second Positive systems;  $O_2$ , Herzberg system; OH and OD,  $A^2\Sigma^+ - X^2\Pi_1$  system. The latter has been investigated only in solid Ne, where both emission and absorption spectra were recorded; observed fine structure has been partly interpreted in terms of slightly perturbed rotational motion in the solid. For  $N_2$ ,

OH, and OD emission occurred from  $v' > 0$ , establishing a vibrational relaxation time in the excited electronic state of the order, of longer than, the electronic radiative lifetime. The relative emission intensity and decay times for different  $v'$  progressions in the Vegard-Kaplan system are found to depend on the rare-gas host and the  $N_2$  concentration, but are independent of temperature in the range 1.7°K to 30°K.

## PART II

Static crystal field effects on the absorption, fluorescence, and phosphorescence spectra of isotopically mixed benzene crystals were investigated. Evidence is presented which demonstrate that in the crystal the ground, lowest excited singlet, and lowest triplet states of the guest deviate from hexagonal symmetry. The deviation appears largest in the lowest triplet state and may be due to an intrinsic instability of the  $^3B_{1u}$  state. High resolution absorption and phosphorescence spectra are reported and analyzed in terms of site-splitting of degenerate vibrations and orientational effects. The guest phosphorescence lifetime for various benzene isotopes in  $C_6D_6$  and sym- $C_6H_3D_3$  hosts is presented and discussed.

## TABLE OF CONTENTS

ACKNOWLEDGMENTS	ii
ABSTRACT	iii
I. EXPERIMENTAL PROCEDURES	1
II. THE ELECTRONIC SPECTRUM OF SIMPLE DIATOMICS IN SOLID RARE GASES	12
Spectroscopic Evidence for Slow Vibrational and Electronic Relaxation in Solids. The Vegard-Kaplan and Second Positive Systems of N <sub>2</sub> in Solid Rare Gases	12
Introduction	14
Experimental	16
Results	18
Discussion	39
References	46
Tables	49
Figures	72
Kinetics for a Model System Undergoing Vibrational Relaxation in an Excited Electronic State	93
The Emission Spectra of O <sub>2</sub> and CO in Solid Rare Gases	108
The Herzberg Bands of O <sub>2</sub>	109
The Cameron Bands of CO	114
References	120
The Absorption and Emission Spectra of OH and OD in Solid Neon. Evidence for Rotation	122
Introduction	123

Experimental	124
Results	125
Discussion	127
References	134
Tables	136
Figures	144
III. SPECTROSCOPIC STUDIES OF ISOTOPICALLY MIXED BENZENE CRYSTALS	150
Geometry of the Lowest Triplet State of Benzene	150
Introduction	152
Theoretical Background	154
Experimental	158
Results	161
Discussion	166
References	184
Table	187
Figures	188
Static Crystal Field Effects on the Vibronic Structure of the Phosphorescence, Fluorescence, and Absorption Spectra of Benzene Isotopic Mixed Crystals	193
Introduction	195
Theoretical Background	197
Experimental	198
Results	
Emission Spectra	200
Absorption Spectra	220

Discussion	222
References	226
Figures	228
Tables	243
The Guest Phosphorescence Lifetime in Isotopically Mixed Benzene Crystals	274
IV. PROPOSITIONS	279

## EXPERIMENTAL

In Part II of this thesis, studies of the electronic emission and absorption spectrum of diatomic guests in rare-gas solids is reported. The general technique of preparing such solids, which may contain chemically unstable diatomic radicals, is commonly termed matrix isolation. Since the experimental method is well known,<sup>1,2</sup> only the specifics of this work will be discussed. All gases were obtained from commercial sources (Matheson or Linde) and used without further purification.

The diatomic molecule, or its precursor, plus rare-gas mixtures were prepared in one of two different ways. In the first method, the mixture is prepared in a Pyrex glass vacuum line and stored in a glass flask fitted with a stopcock. The mixing manifold is shown schematically in Fig. 1a. Throughout Fig. 1, "X" denotes either a stopcock or a metal valve and "P" denotes a pressure gauge, which is either an ionization, thermocouple, or mechanical type. The volume of bulb A was determined by weighing A empty and then filled with water at a known density. The volumes of the other parts of the system were easily determined, assuming the perfect gas law and the volume of A, from the pressure changes occurring when a given amount of gas in A expanded throughout the system. A given mixture could be prepared by filling A and B with the diatomic and rare-gas respectively to the appropriate pressures. The gases were transferred to the storage flask C by immersing the side arm in liquid helium. The liquid helium was contained in a small, portable double dewar,<sup>3</sup> consisting of a

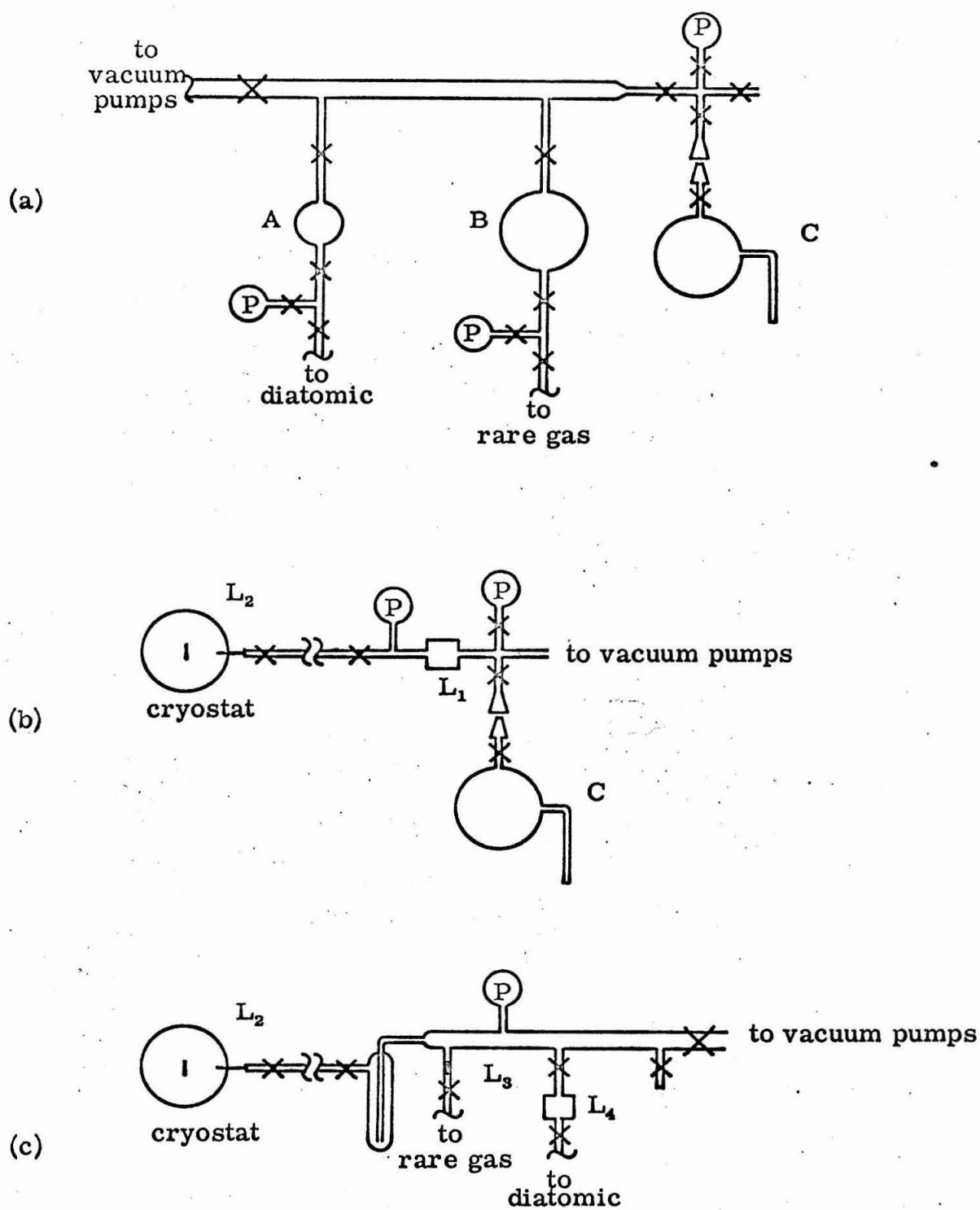


Fig. 1. Schematic of manifolds used to prepare rare-gas plus diatomic mixtures.

commercial 1/2 gal bulb-type dewar inside a one gal straight-side dewar. The pressures in A and B were chosen to give less than one atmosphere in C. The actual volumes used were:  $A = 55.82 \text{ cm}^3$ ,  $B = 1109 \text{ cm}^3$ , and  $C = 1036 \text{ cm}^3$ . The flask C is then attached to an auxillary vacuum line by which the mixture can be admitted to the vacuum chamber of a liquid helium cooled cryostat. The gases were allowed to mix overnight in the storage flask before depositing.

This auxillary deposit system is shown in Fig. 1b. The flask C is separated from the vacuum chamber surrounding the cold-finger by a variable leak, (Nupro, Series M), labelled  $L_1$  in Fig. 1b. This leak is continuously adjusted during the deposition to maintain a constant pressure of roughly 3 mm Hg between  $L_1$  and the fixed leak  $L_2$ , which leads to the dewar vacuum chamber. These conditions correspond to a deposition rate of  $\sim 5 \mu\text{mole/sec}$ , which is continued for roughly one hour. During this time the pressure remaining in C is monitored by a gauge.

Alternately, the mixture is prepared and deposited using the continuous flow system shown in Fig. 1c. The solvent flow rate is determined by a Pyrex capillary leak  $L_3$ . The solute flow rate, and therefore its concentration, is controlled by means of a variable leak  $L_4$  (Granville-Phillips Series 203). The respective flow rates were checked using an electric clock and pressure gauges before each experiment. However, this was found to be an unnecessary precaution. The rate through  $L_3$  changed only very slightly with time, apparently due to foreign material becoming trapped in the capillary from the high pressure gas cylinders and the variable leak could be reproducibly



set to any desired flow rate once it was calibrated. The gases mix in the glass manifold and then impinge on the liquid helium cooled cold-finger through a fixed leak  $L_2$ . During deposition a steady state condition exists and the pressure in the manifold equilibrates at roughly 5 mm Hg for a manifold volume of 500 cm<sup>3</sup>. The mixture enters the dewar vacuum chamber at approximately the same rate as the rare-gas enters the manifold, which was  $\sim 3 \mu\text{mole/sec}$  for most of the experiments. Deposit times were of the order of one hour. Both methods worked equally well. The only modification suggested is replacement of the fixed leak  $L_3$  with a variable leak, so that the deposition rate could be varied in the continuous flow technique.

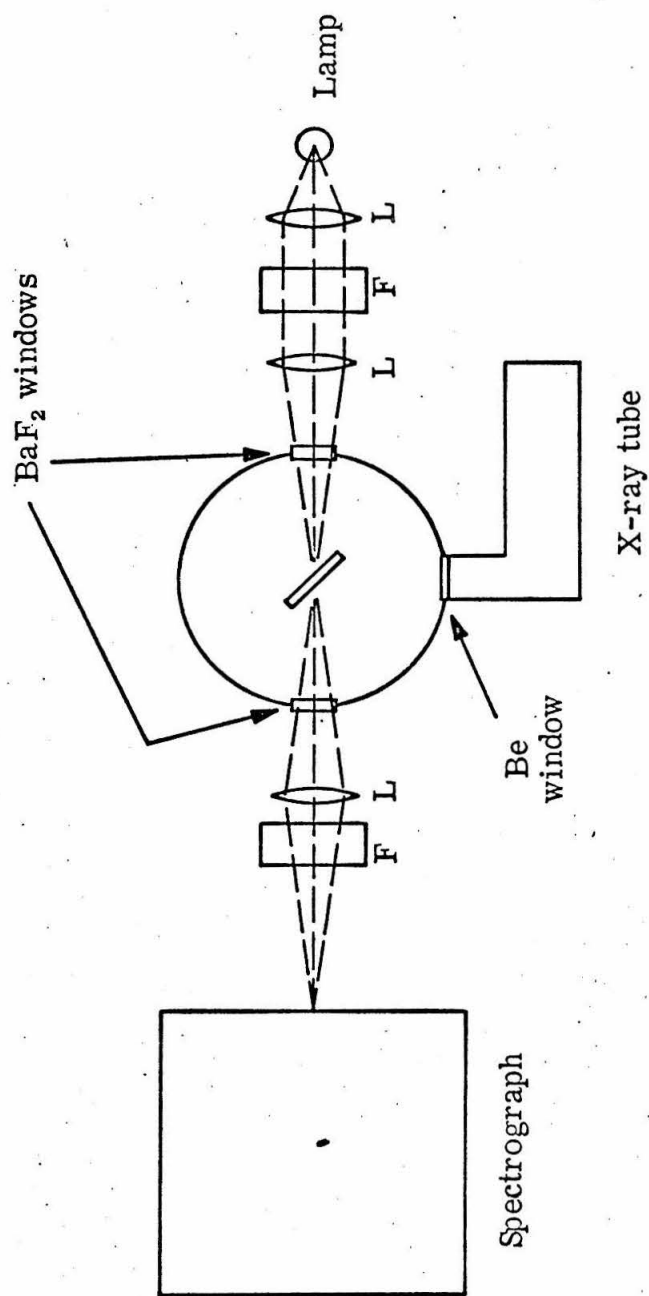
The additional access to the vacuum manifold shown in Fig. 1c is mainly for solutes or precursors which are liquids at room temperature. These are degassed and vacuum distilled into the cold trap, where they are maintained at the appropriate reduced temperature.

The cold finger on which the gas mixture is deposited is either an optical window or a copper plate. The latter was used at  $T \leq 4.2^\circ\text{K}$  when only emission spectra were required. Front surface irradiation was of course necessary. The optical window for  $T \leq 4.2^\circ\text{K}$  was sapphire in direct contact with liquid helium. The dewar and cold finger design has been described by R. P. Frosch.<sup>4</sup> Typical pressures in the cryostat are as follows. Without addition of liquid  $\text{N}_2$  to the outer jacket, the dewar pressure after overnight pumping with a diffusion pump is  $\sim 6 \times 10^{-5}$  mm Hg. The pressure quickly drops to  $< 1 \times 10^{-6}$  mm Hg when liquid  $\text{N}_2$  is added. A small amount of liquid  $\text{N}_2$  is also added to the inner helium dewar to remove air vapor. This  $\text{N}_2$  must be removed

before liquid helium is transferred. After liquid helium has been transferred, the pumping port to the cryostat is closed and the pressure in the dewar remains  $< 1 \times 10^{-6}$  mm Hg. For deposition of all mixtures except those which have large amounts of Ne or H<sub>2</sub>, the pumping port to the cryostat remains closed during the actual depositing. The pressure equilibrates at  $\approx 1 \times 10^{-3}$  mm Hg by the efficient cryopumping of the liquid helium. While depositing Ne or H<sub>2</sub>, the dewar pumping port is left open. The internal pressure equilibrates at about the same value, but if the dewar is isolated the helium boil-off rate becomes excessive. Moreover, to deposit these two gases good thermal contact is required and sapphire is recommended if an optical window is required.

For the temperature studies, a previously described<sup>5</sup> dewar, which has been slightly modified to be completely interchangeable with the system used for  $T \leq 4.2^\circ\text{K}$ , is employed. The cold finger in this case is a quartz window, mounted in a copper holder. A carbon resistance thermometer served as the temperature sensor. The actual temperature measured was that of the copper frame and not that of the optical window. One would, therefore, expect the sample temperature to be somewhat greater than the temperatures reported.

In all cases reported in Part II the diatomic emission spectrum was excited by irradiation with 50 kV X-rays from a tungsten target at a tube current load of 45 ma. The experimental apparatus was designed by Frosch, who has adequately described it. The optical set-up for spectral observations is shown in Fig. 2. Light sources used for the absorption experiments include General Electric tungsten



L = Quartz Lens

F = Glass and/or solution filter

Fig. 2. Schematic Optical set up.

filament ( $\lambda = 4000\text{-}12000\text{ \AA}$ ) and PEK high pressure xenon ( $\lambda = 2500\text{-}4000\text{ \AA}$ ).

The spectra were recorded either photographically or photoelectrically. A Jarrell-Ash 0.75 m spectrograph with a 7500 grooves/in grating, blazed for  $1\mu$  in a Czerny-Turner optical mount was used for nearly all experiments. This instrument has an entrance aperture of  $f/6.3$  and with the grating employed gave a first order plate factor of about  $40\text{ \AA/mm}$ . Spectra was taken in the first four orders using Kodak 103a-O, 103-F, I-N, and hypersensitized I-M and I-Z plates in the appropriate spectral regions. Slit widths varied, but in all cases the natural line widths reported were determined with much narrower slit widths. Some preliminary spectra were taken with a Bausch and Lomb medium quartz prism spectrograph and a McPherson Model 235 0.5 m scanning monochrometer. However, all line measurements reported were taken from plates exposed on the Jarrell-Ash spectrograph. The appropriate Corning glass and/or liquid Kasha filters were used to order sort. For the most extensively studied Vegard-Kaplan bands of  $\text{N}_2$ , the combinations of filters, grating order, and photographic plate used for the different wavelength ranges are recorded in Table I. Plate measurements were done with a travelling microscope (CIT Chemistry No. 4067 ). Lines from an Fe-Ne hollow cathode lamp served as wavelength standards. Reproductions of spectra were made with either a Jarrell-Ash recording microphotometer or a Joyce-Loeb recording microdensitometer. The former records the spectrum on a percent transmission scale, whereas the latter gives the optical density

Table I. Filter, grating order, and photographic plate combinations used for the Vegard-Kaplan bands of  $N_2$ .

$\lambda(\text{\AA})$	Kodak <sup>a</sup> plate	grating orders	filters
2300-3400	108a-O	3, 4	$NiSO_4-CoSO_4$ <sup>b</sup>
3000-5000	103a-O	2, 3	Corning 7740 <sup>c</sup>
4200-6500	103 -F	1, 2	Corning 3389 <sup>c</sup>
6000-9000	I-N	1	Corning 3384 <sup>c</sup>

<sup>a</sup>Kodak photographic plate number.

<sup>b</sup>M. Kasha, J. Opt. Soc. Amer. 38, 929 (1947).

<sup>c</sup>Corning glass number.

on the plate directly. This should be borne in mind when comparing the spectra presented in later parts of this thesis.

The Jarrell-Ash spectrograph could be easily converted to a spectrometer by replacing the plateholder racking assembly with a commercial (Jarrell-Ash) photoelectric attachment. This has been ultimately modified<sup>6</sup> to include bilateral adjustable exit slits and an easily adjustable photomultiplier tube holder. The latter has been designed so that with slight modifications the photomultiplier may be cooled. In addition a motor drive has been added. Decay time measurements were performed using this system. The X-rays could be shut off in about 0.005 msec by a spring driven brass shutter and this, therefore, set a lower limit on the decays which could be monitored. Both RCA IP28 and EMI 6256S photomultiplier tubes were used. The photomultiplier signal was developed across a  $1\text{M}\Omega$  load resistor, which was then fed to a simple cathode follower made from a Philbrick P65AU operational amplifier. A range of capacitances could be inserted into the circuit in parallel with the load resistor to reduce high frequency noise. The resulting RC time constants were  $\sim 0$  and 0.001 to 0.1 sec. These were always chosen  $\approx 10^{-2}$  times the lifetime of the decay being monitored. The follower signal was displayed on a Tektronix type 531 oscilloscope and photographed in the usual manner. If the decays were quite long, they were occasionally recorded on a Bristol strip chart recorder. The photomultiplier signal in this case is amplified by a Victoreen electrometer (Model VTE 1) before being fed to the recorder.

The experiments on isotopically mixed benzene crystals, reported in Part III of this thesis, were performed with additional experimental apparatus and techniques than that described above. However, this is described either in the particular section or elsewhere.<sup>7</sup>

## REFERENCES

1. H. W. Brown and G. C. Pimentel, J. Chem. Phys. 29, 883 (1958);  
D. E. Milligan and G. C. Pimentel, J. Chem. Phys. 29, 1405 (1958).
2. M. McCarty and G. W. Robinson, J. Chem. Phys. 28, 349 (1958);  
ibid., 350 (1958); G. W. Robinson, J. Molec. Spectroscopy 6, 58  
(1961).
3. The author thanks Professor S. I. Chan for loan of this dewar.
4. R. P. Frosch, Thesis, California Institute of Technology, 1965.
5. L. F. Keyser, Thesis, California Institute of Technology, 1965;  
L. F. Keyser and G. W. Robinson, J. Chem. Phys. 44, 3225 (1966).
6. Part of these modifications were performed by S. D. Colson.
7. G. C. Nieman, Thesis, California Institute of Technology, 1965;  
S. D. Colson, Thesis, California Institute of Technology, 1968;  
E. R. Bernstein, Thesis, California Institute of Technology, 1968.



Spectroscopic Evidence for Slow Vibrational and Electronic  
Relaxation in Solids. The Vegard-Kaplan and Second  
Positive Systems of N<sub>2</sub> in Solid Rare Gases.\*

D. S. TINTI AND G. W. ROBINSON

Gates and Crellin Laboratories of Chemistry,<sup>†</sup> California Institute  
of Technology, Pasadena, California 91109

ABSTRACT

The spectra emitted from N<sub>2</sub> doped rare-gas solids at low temperatures, irradiated with X-rays, has been investigated in detail. The molecular N<sub>2</sub> emission seen in the spectral range 2300 Å to 5000 Å consists of the Vegard-Kaplan (VK)  $A^3\Sigma_u^+ \rightarrow X^1\Sigma_g^+$  and the second positive  $C^3\Pi_u \rightarrow B^3\Pi_g$  band systems. The latter is observed only in solid Ne. Forbidden transitions of N-atoms and sometimes impurity O-atoms are also seen.

Both N<sub>2</sub> band systems show emission from  $v' > 0$ , establishing a relatively slow vibrational relaxation rate in the  $A^3\Sigma_u^+$  and  $C^3\Pi_u$  states in solid rare gases. For the VK system the relative intensity of emission from  $v' > 0$  is strongly dependent on the rare-gas host and on the N<sub>2</sub> concentration. No  $v' > 0$  is seen for a Ne host, whereas in Ar, Kr, and Xe the relative intensity of  $v' > 0$  increases with decreasing N<sub>2</sub> concentrations and a maximum  $v' = 6$  is found in these three hosts.

---

\* Supported in part by the Atomic Energy Commission.

<sup>†</sup> Contribution No.

Decay times for isolated VK bands were measured and appeared exponential within experimental error. From the measured lifetime in Ar, we conclude that the vibrational relaxation time in the  $A^3\Sigma_u^+$  state of  $N_2$  in solid Ar is greater than 0.4 sec. The effect of temperature on the relaxation was found to be small in the range 1.7°K to 30°K.

## I. INTRODUCTION

Relaxation of electronically excited molecules in solids has received considerable attention in the last few years. Most of this work has assumed that vibrational relaxation of molecules in van der Waals solids occurs in a time fast compared with the radiative and nonradiative processes that depopulate electronic levels. This seems to be true for complex molecules as well as for some diatomics. However, systems are known where the vibrational relaxation rate in a solid environment is roughly the same as that for radiative transitions: e.g.,  $C_2 \ A^3\Pi_g \rightarrow X^3\Pi_u$  (Swan bands);<sup>1</sup>  $N_2 \ A^3\Sigma_u^+ \rightarrow X^1\Sigma_g^+$  (Vegard-Kaplan bands);<sup>2-7</sup>  $O_2 \ A^3\Sigma_u^+ \rightarrow X^3\Sigma_g^-$  (Herzberg bands);<sup>7</sup> and  $S_2 \ B^3\Sigma_u^- \rightarrow X^3\Sigma_g^-$ .<sup>8</sup> The slow vibrational relaxation in these systems is evidenced by emission originating from higher vibrational levels in the upper electronic state. The highest  $v'$  observed is that for  $N_2$ , and, therefore, we have chosen this system for further study of vibrational relaxation processes in simple van der Waals solids.

Diatomics and small polyatomics with few internal degrees of freedom and large vibrational spacings should lose vibrational energy rather slowly in the solid phase, since multiphonon processes are required. In particular, a homonuclear diatomic with large vibrational energy spacing might be expected to have the slowest rate of vibrational relaxation. A recent theoretical study by Sun and Rice<sup>9</sup> also suggests that vibrational relaxation of diatomic molecules in the solid might be slow. We present here further evidence emphasizing that vibrational relaxation in the solid phase can indeed be very slow.

Experiments are also described that demonstrate the occurrence of radiative transitions between two excited molecular electronic states in the solid state.

## II. EXPERIMENTAL

The general technique of matrix isolation, which is used in this work to study diatomic guest molecules in rare-gas solids, has been described previously,<sup>10</sup> as has the use of X-irradiation to excite the emission spectrum of the guest molecule.<sup>11</sup>

The rare gases employed were Linde MSC grade. High purity diatomic gases were obtained from either Matheson or Linde.  $^{14}\text{N}^{15}\text{N}$  was obtained from the Isomet Corporation with a stated isotopic purity of 98%. All gases were used without further purification. The mixtures of the diatomic molecule and the rare-gas were prepared in one of two different ways. In the first method, the mixture was prepared in a glass vacuum line and stored in a glass flask fitted with a stopcock. The gases were then transferred to the storage flask by immersing a side arm in liquid helium and were allowed to mix in the flask overnight. The flask was then attached to an auxiliary vacuum line from which the mixture could be slowly admitted to the vacuum chamber of the cryostat for deposition. Alternately, the mixture could be admitted to the cryostat without prior mixing using a continuous flow system. The flow rate of the host gas was determined by a Pyrex capillary leak. The flow rate of the guest, and therefore its concentration, was controlled by means of a variable leak. For both techniques the deposit rate was roughly  $15 \pm 10$  mmole/hour. Deposit times were of the order of one hour.

For the studies at  $\leq 4.2^\circ\text{K}$ , the cold-finger on which the mixed gases impinged is either a copper plate or a sapphire window, both of which are in direct contact with the liquid coolant. Identical spectra are obtained in both cases.



For the variable temperature studies a previously described dewar,<sup>12</sup> which has been slightly modified, was used. In this case the optical window on which the gas mixture was deposited is not in direct contact with the coolant. The temperature measured and reported is not that of the window, but rather is the temperature of the copper frame in which the window is clamped with indium washers. A calibrated carbon resistor served as the temperature sensor. The lowest measured temperature in this dewar was about 8°K and could be continuously adjusted up to about 30°K. The window temperature was probably several degrees higher, especially at the lower temperatures.

The diatomic emission spectrum was excited with 50 kV X-rays from a tungsten target at a tube current load of 45 ma. The X-ray excitation could be shut off by means of a brass shutter in about 0.005 sec to facilitate lifetime measurements. The lifetimes were obtained mainly from photographs of oscilloscope traces. RCA IP28 and EMI 6356S photomultiplier tubes were used. The emission spectra were photographed on Kodak O- or F-plates with a 0.75 meter f/6.3 Jarrell-Ash spectrograph, which also served as a monochromator to isolate individual vibronic transitions for lifetime determinations. The spectra were taken in the second and third orders of a grating with a first-order plate factor of about 40 Å/mm. Exposure times varied from approximately 10 min to a few hours. Order-sorting, where necessary, was accomplished by means of the appropriate combination of solution and glass filters.

### III. RESULTS

The emission of light from solid  $N_2$  and from dilute solid solutions of  $N_2$  has been investigated previously by numerous authors, employing varying excitation techniques. These include electron bombardment,<sup>2,3,6,7</sup> application of ac and dc discharges,<sup>5</sup> and the condensation at low temperatures of the products from a gas discharge.<sup>4</sup> Most of this work, since the pioneering work of Vegard<sup>2</sup> some 40 years ago, was carried out at the National Bureau of Standards where Broida and co-workers<sup>4-7</sup> extensively studied free-radial stabilization at low temperatures. The most common molecular emission seen in all these studies is the Vegard-Kaplan band system of  $N_2$   $A^3\Sigma_u^+ - X^1\Sigma_g^+$ .

The molecular  $N_2$  emission observed in the spectral range 2300 Å to 5000 Å when a deposited mixture of  $N_2$  plus rare-gas is irradiated with X-rays consists of the Vegard-Kaplan (VK) and the second positive  $C^3\Pi_u - B^3\Pi_g$  band systems. A discussion of the second positive group, which is observed only in solid Ne, will be reserved until Sec. III D. Emission from N-atoms  $2p^3\ ^2D - 2p^3\ ^4S$  and sometimes from impurity O-atoms  $2p^4\ ^1S - 2p^4\ ^1D$  is also observed. These two transitions are designated the  $\alpha$  and  $\beta$  groups, respectively, in the publications of Broida and co-workers. The Herzberg bands of  $O_2$   $A^3\Sigma_u^+ - X^2\Sigma_g^-$  are also sometimes weakly seen as an impurity.

#### A. Atomic Emissions

The atomic emissions are generally less sharp than the molecular bands and appear as doublets with the blue component sharper and more intense. The  $\alpha$ -group is typically sharper and more intense than the

$\beta$ -group. Approximate frequencies for the most intense feature of the atomic emissions  $\alpha$  and  $\beta$  are shown in Table I.

### B. Vegard-Kaplan System

The vibronic spectrum--The VK bands are sharpest in solid Ne, becoming progressively broader and degraded to the red in the heavier rare-gases or with increasing  $N_2$  concentration. The narrowest observed bandwidths at half intensity in the four rare gases are approximately:  $\leq 10 \text{ cm}^{-1}$  in Ne,  $20 \text{ cm}^{-1}$  in Ar,  $40 \text{ cm}^{-1}$  in Kr and  $40 \text{ cm}^{-1}$  in Xe. Besides the red shading, additional fine structure is often observed. For example, in solid Ar the VK bands are all at least double-headed under the usual experimental conditions. This is discussed in more detail below.

Tables II to V summarize the observed VK band frequencies, assignments, and the corresponding matrix shifts for solid Ne, Ar, Kr and Xe, respectively. The gas phase transition energies were computed from the molecular constants given by Benesch et al.<sup>13</sup> The tabulated frequencies in the Ar host are for the highest energy band component, which is generally the most intense. In Kr and Xe solids the broader lines cause the frequency measurements to be less precise and also results in considerable overlap of different bands. The overlap makes some of the vibrational assignments in Kr and Xe somewhat uncertain.

The vibrational constants of the A and X states in the four rare-gases were calculated from a least-squares fit of the experimental line frequencies to the equation<sup>14</sup>



$$\nu = \nu_{00} + (\omega'_e - \omega'_e x'_e) v' - \omega'_e x'_e v'^2 - (\omega''_e - \omega''_e x''_e) v'' + \omega''_e x''_e v''^2 \quad (1)$$

These constants are shown in Table VI. The difference between the band frequencies calculated from these constants using Eq. (1) and the observed frequencies is included in Tables II to V. The average standard error in the four rare-gases between observed and calculated frequencies is  $2.2 \text{ cm}^{-1}$ , which is about the experimental measurement error. A progressive red shift in  $\nu_{00}$  is found from gas to solid and from Ne to Xe. The solid perturbations on  $\omega_e$  and  $\omega_e x_e$ , as shown in Table VI, are small. The general decrease of  $\omega_e$  and increase of  $\omega_e x_e$  in the  $X^1\Sigma_g^+$  state from Ne to Xe presumably results from an overall increasing attractive interaction in the heavier rare-gases.

The vibrational assignments in Ar were confirmed using  $^{14}\text{N}^{15}\text{N}$  of 98% isotopic purity. The band frequencies and assignments are tabulated in Table VII for 0.25%  $^{14}\text{N}^{15}\text{N}$  in solid Ar at 8°K. The ratios of the reduced masses  $\rho^2$ , deduced from the vibrational constants of the  $\text{N}_2$  isotopes in solid Ar calculated by Eq. (1), are in excellent agreement with the theoretical value of 0.9668. The comparison is shown in Table VIII, which also gives the vibrational constants of  $^{14}\text{N}^{15}\text{N}$  in the A and X states. Table VIII also gives the vibrational constants determined for  $^{14}\text{N}^{15}\text{N}$  in natural abundance ( $\sim 0.7\%$ ) in a  $^{14}\text{N}_2$  sample in solid Ne. The observed band frequencies for  $^{14}\text{N}^{15}\text{N}$  in Ne are presented in Table IX. These measurements are less precise than those of the major isotope present due to the overall weakness of the bands. However, within the experimental error the inferred values for  $\rho^2$  are again in agreement with the theoretical value.

Intensities--Rough estimates of the relative intensities within each  $v'$  progression are given only in the case of Ar in Table III. No large changes from this intensity distribution were noticed for the other matrices. The overall intensity distribution for  $^{14}\text{N}_2$  is in good qualitative agreement with Rydberg-Klein-Rees Franck-Condon factors<sup>15</sup> for the VK system, giving further support to the vibrational assignments. Most of the  $v'$ ,  $v''$  transitions labeled "not observed" in Tables II through V have Franck-Condon factors  $\lesssim 10^{-2}$ . In Ar (Table III) some of these very weak bands were observed on heavily overexposed plates.

The intensity distribution in the different  $v''$  progressions of the VK system depends strongly on the host rare-gas and on the  $\text{N}_2$  concentration. Several bands of the VK system as observed in solid Ar at 4.2 °K are shown in Fig. 1 for different  $\text{N}_2$  concentrations. At high concentrations ( $> 1\%$ ) of  $\text{N}_2$  in Ar most of the emitted intensity arises from  $v' = 0$ , with higher  $v'$  very weak. However, as the  $\text{N}_2$  concentration is decreased, more of the emitted intensity originates from  $v' > 0$ . Levels as high as  $v' = 6$  have been identified for  $\lesssim 0.3\%$   $\text{N}_2$  in Ar. For concentrations less than about  $0.1\%$   $\text{N}_2$ , no changes in the relative intensity distribution occur and no higher  $v'$  than 6 is observed. A series of plates for  $0.3\%$   $\text{N}_2$  in Ar at 1.7 °K were purposely overexposed to search for weak emission from  $v' > 6$ . Although lines due to  $^{14}\text{N}^{15}\text{N}$  in natural abundance ( $\sim 0.7\%$ ) were seen to the high energy side of the stronger VK bands, no emission from  $v' > 6$  was found.

Very similar results are obtained in Kr and Xe solids except that more VK emission occurs from  $v' > 0$  for a fixed  $\text{N}_2$  concentration in these heavier rare-gases. Figure 2 compares the VK emission in Ne,

Ar, Kr and Xe for 1%  $N_2$ . Concentration studies again indicate that  $v'_{\max} = 6$ , as shown for the Kr studies in Fig. 3. The absence of emission from  $v > 6$  of the A state is not, of course, due to predissociation since higher vibrational levels of A are known from the first positive system of  $N_2$ .<sup>16</sup> Furthermore, the lowest dissociation limit of  $N_2$  has been conclusively determined to be 9.78 eV,<sup>17</sup> some 2.5 eV above  $v = 6$  of the A state. A possible explanation for this breaking off is presented in Sec. IV in terms of the excitation mechanism.

For the 0.1-1.3% range of  $N_2$  concentrations studied in a Ne host, no bands of  $^{14}N_2$  with  $v' > 0$  were photographed on plates where the  $v' = 0$  progression of  $^{14}N^{15}N$  is seen in natural abundance. We estimate, therefore, that the steady state population of  $v = 0$  in the A state must exceed that of  $v > 0$  by roughly two or more orders of magnitude in the Ne host.

In the recent investigations by Broida and co-workers, only bands with  $v' = 0, 1$ , and 2 were observed, and these decreased in intensity with increasing  $v'$ . However, the concentration of  $N_2$  was approximately 3% or greater and the resolution employed was less than ours. At these high  $N_2$  concentrations the VK bands are typically broad and, therefore, bands with  $v' \geq 3$  overlap bands originating from  $v' \leq 2$ . Vegard originally observed bands with higher  $v'$  but in agreement with our results only  $v' \leq 6$  were seen. Vegard also assigned a few bands for which  $v' > 0$  in solidified Ne, but they were very weak and this could explain our failure to photograph them.

The conclusive observation of emission from  $v' > 0$  in Ar, Kr, and Xe establishes a vibrational relaxation time in the  $A^3\Sigma_u^+$  state of the order of, or longer than, the electronic lifetime of the spin-forbidden

VK bands in these solid hosts. This will be discussed more fully in Sec. IV.

Temperature studies--The VK system in solid Ar and Kr hosts was photographed over a temperature range 1.8 to 30°K. In Ne the range was limited to the two temperatures 1.8 and 4.2°K. Figure 4 shows microphotometer tracings of part of the VK system for 0.2% N<sub>2</sub> in Ar at various temperatures. The upper tracing is the spectrum of the unannealed sample at the deposition temperature, approximately 8°K. The lower spectra show emission from this same deposit after annealing at around 28°K for roughly 30 min. Further annealing at 28°K did not change the spectrum in any way, implying that "annealing" is complete in less than 30 min.

The spectrum from a gas mixture of nearly the same composition deposited at 4.2°K in a different dewar system and photographed at 4.2°K and 1.8°K was the same as the unannealed spectrum in Fig. 4 except for an overall line sharpening and the absence of the continuum. The annealed spectra in Fig. 4 also do not show the broad emission present in the unannealed sample. Although various broad continua have been seen at various times in all rare-gas solvents, they are not always present. The source of these continua and the reason for their disappearance with annealing are unknown.

The relative intensity of emission from higher  $v'$  is slightly reduced after the first annealing. However, for later temperature cycling between 4°K and 30°K, the only spectral effects observed are a general line broadening and an apparent reduction in the relative intensity of the red components at higher temperatures (cf. Fig. 4).

These latter two effects are completely reversible. Since the relative  $v'$  intensity does not vary with temperature after the initial annealing, the vibrational relaxation rate in the A state is not a strong function of temperature below 30°K.

Completely analogous results, although not as complete, are obtained in Ne and Kr hosts. Identical spectra were observed at 1.7 and 4.2°K in solid Ne. Sharper lines are obtained if the Ne sample is prepared at 4.2° rather than at 1.7°K. When 0.2% N<sub>2</sub> in Kr was deposited at 8°K, additional spectral features were observed that were absent in the spectra taken at 4.2°K. These consisted of a broad emission band approximately 220 cm<sup>-1</sup> to low energy of each VK band as shown in Fig. 5 for some representative bands at the two temperatures 9 and 32°K. The sample was annealed at ~30°K before these spectra were taken. In Kr some line sharpening of the higher energy component occurs with deposition at ~10 rather than 4.2°K. Annealing at ~30°K does not lead to any further reduction in the linewidth. The intensity of the low energy component, contrary to the results in solid Ar, increases with increasing temperature, which may explain why it was not found at 4.2°K. Neglecting the broad components, the relative  $v'$  intensity remains approximately constant, independent of temperature, below 30°K.

Fine structure--The VK bands in solidified Ar, as seen from the spectra presented earlier, are all at least doublets. This fine structure, which has been noted by previous workers,<sup>2-7</sup> is not seen in Kr or Xe hosts. However, this may be due to the increased linewidth in the latter two hosts. The fine structure in Ar appears to the low frequency side of the main line reported in Table II. The energy separation of the red



components from the main line is  $(40 \pm 4) \text{ cm}^{-1}$  and  $(61 \pm 2) \text{ cm}^{-1}$ . The  $61 \text{ cm}^{-1}$  component is seen only on the  $v' = 0$  progression. Both features are seen for both  $^{14}\text{N}_2$  and  $^{14}\text{N}^{15}\text{N}$  in Ar. For completeness we note that on one very heavily exposed plate an additional feature was seen in the  $v' = 0$  progression  $\sim 306 \text{ cm}^{-1}$  to the red of the main line. This has a sharp blue edge but is very strongly degraded to the red, which could explain why it is not usually photographed.

The relative intensity of the various components varies somewhat with experimental conditions. However, the only changes which appear systematic are as follows. Under all conditions investigated in Ar the relative intensity of the red components decreases with increasing  $v'$ . At  $4.2^\circ\text{K}$  the  $60 \text{ cm}^{-1}$  removed feature is usually slightly more intense and the  $40 \text{ cm}^{-1}$  feature less intense than the main  $v' = 0$  line. For progressions with  $v' > 0$  the single additional component  $40 \text{ cm}^{-1}$  to the red is always weaker than the main line. These relative intensities are generally independent of  $\text{N}_2$  concentration as seen from Fig. 1. The  $40$  and  $60 \text{ cm}^{-1}$  red components in Ar decrease in intensity reversibly with increasing temperature, while the much further removed red component in Kr increases in intensity reversibly with increasing temperature (cf. Figs. 4 and 5).

In Ne fine structure is seen mainly to high energy of the strong main line reported in Table II, although weaker structure and shading appears to low energy. For example, the 0, 10 VK band for low concentrations of  $\text{N}_2$  in Ne has additional features at  $+90(\text{vw})$ ,  $+60(\text{w})$ ,  $+43(\text{w})$ ,  $+28(\text{m})$ ,  $-15(\text{w})$ ,  $-34(\text{vw})$ , and  $-54(\text{vbw}) \text{ cm}^{-1}$  removed from the

main line. Intensity estimates relative to the very strong main line are given in parenthesis. As in Ar this fine structure is somewhat variable. At high  $N_2$  concentrations ( $\geq 1\%$ ) only the main line and structureless red shading is seen.

The origin of this varied multiplet structure remains unknown. The theoretical frequency spectrum<sup>18</sup> for both solid Ne and Ar have two maxima at about 40 and 60  $\text{cm}^{-1}$  which is within the range of the observed splittings. However, it is clear that phonon emission alone is insufficient to explain all the observations. Other possible explanations include multiple trapping sites and restricted translational motion.

### C. Decay Times for Vegard-Kaplan Bands and the $\alpha$ -Group

Atomic emissions--The  $\beta$ -group, reportedly due to the  $^1S - ^1D$  transition of the O-atom,<sup>8</sup> decayed faster than the  $\sim 5$  msec limit imposed by the X-ray shutter. The forbidden atomic N emission  $^2D - ^4S$ , on the other hand, is very long lived and deviates considerably from a first-order decay law at short time, as is shown in Fig. 6 for Ne and Ar hosts. The decay of the  $\alpha$ -group was partially studied only for these two rare-gas hosts and only at 4.2°K. The atomic decay in Kr was measured only once and decayed non-exponentially, very similar to the decay in Ar, but in a shorter time. The initial half-life in Kr is  $\sim 5$  sec, increasing to  $\sim 7$  sec at the end of the first decade decay. In Ar the corresponding half-lives are  $\sim 7.5$  and  $\sim 10$  sec, respectively. The atomic decays were measured with a relatively large monochromator band pass ( $40 \text{ cm}^{-1}$ ), so that the decay does not represent an isolated component of the  $\alpha$ -group. The latter is not a single line, but

consists of at least two components which could explain a non-exponential decay. Alternately, the non-exponential behavior could arise from recombination reactions involving  $^2\text{D}$  N-atoms, e. g.,  $^2\text{D} + ^2\text{D}$  and  $^2\text{D} + ^4\text{S}$ . If recombination reactions were large contributors to the decay kinetics, highly non-exponential decays would be predicted.

The atomic decays do not appear to follow the same kinetics in Ne and Ar. For example, in Ne the initial decay seems to follow second-order kinetics since a plot of  $I^{-1}$  versus time is linear during the first  $\sim 150$  sec of the decay. However, in Ar such a plot is not linear. It seems reasonable to ascribe the exponential decay at long times in Ne to the  $^2\text{D} \rightarrow ^4\text{S}$  radiative transition of the N-atom. This then has a lifetime of  $(340 \pm 10)$  sec in solid Ne, compared to 41 sec<sup>19</sup> in solid nitrogen and  $\sim 12$  hours in the free atom.<sup>20</sup> If the exponential tail indicated in Fig. 6 for the  $\alpha$ -group in solid Ar persists to longer times, then the  $^2\text{D} \rightarrow ^4\text{S}$  radiative lifetime is roughly 18 sec in Ar. The short time non-exponential behavior in Ne, Ar, and Kr is assigned to atom recombination. In Ne the recombination is apparently mainly  $^2\text{D} + ^2\text{D}$  which gives second-order kinetics at short times for the  $^2\text{D}$  decay. In Ar and Kr presumably other recombinations are also occurring to a substantial degree, yielding a complicated decay. The atomic decays were not investigated as a function of X-irradiation time, which might help to elucidate the kinetics. We note that in all three rare-gases the atomic decay times are much longer than the initial VK decays.

Vegard-Kaplan system--The decay times for the  $\text{N}_2$  VK bands were measured in the rare-gas solvents for different  $\text{N}_2$  concentrations and sample temperatures. The data obtained for the VK bands are



summarized in Table X. The lifetime in Xe is shorter than the X-ray excitation shut-off time and, therefore, only an upper limit could be set. Considerable difficulty was encountered in obtaining the VK decays in a Kr host because of lower signal-to-noise and since the emission intensity had already partly decayed from its mean steady state value before the exciting X-rays were completely off. Therefore, lifetimes were determined only for  $\sim 1\%$   $N_2$  in Kr which roughly corresponds to the lowest concentration for which the decay could be monitored with the available sensitivity.

The lifetimes reported are averages for different isolated bands with the same  $v'$ . Care was taken to use only well-resolved bands in clean spectral regions. Therefore, the number of different bands measured, especially at low concentrations, was limited. The decay for each band used was measured several times and at least two bands were used for each  $v'$ . The decay constants for a given band agreed to better than 10% with each other and with the constants for other bands of the same  $v'$  progression for any particular sample. However, the reproducibility between different experiments at the same  $N_2$  concentration and temperature is around 10%.

The monochromator band pass was nearly always sufficiently large that the measured decay represents some mean of the high and low energy components. The wavelength setting of the monochromator was slightly adjusted to maximize the photomultiplier current, so that the wavelength at which the intensity decay was monitored for the same band in different experiments is not necessarily the same.

Individual decay times were determined graphically from the slope of a logarithm of intensity versus time plot, examples of which are shown in Fig. 7. As nearly as can be determined, the initial decay of the VK bands appears exponential. However, with the experimental signal-to-noise ratio a definitive conclusion on the decay law can not be reached, since the intensity of an isolated VK band is usually too weak to follow its decay over much more than one decade change in intensity. Nevertheless, it is important to note that for short times after the excitation shut-off, where the signal-to-noise is maximum, no certain deviation from an exponential decay law is apparent for any of the isolated bands studied. For this reason the initial points of the  $\log I$  versus time plot were weighted slightly more in the graphical determination of the decay time. Thus, the reported values represent mainly the initial decay with an assumed first-order rate law and accordingly are referred to as "lifetimes". More correctly these values are the times for the emission intensity to decay to  $1/e$  of its steady state value. When "half-life" is used, we mean the time for the intensity to decay to  $1/2$  its initial value.

In solid Ne where only  $v' = 0$  is seen for the VK bands, it was possible by using a larger slit width and electrical high-frequency filtering to increase the signal-to-noise and, thereby, follow the decay for longer times. A typical decay is shown in Fig. 8 for 0.1%  $N_2$  in solid Ne at 4.2°K. The initial decay is exponential, but a very long lived nonexponential tail is present. This tail, however, does not contribute appreciably to the initial decay which

we take to be the lifetime of the A state in the Ne host. The tail most likely arises from atom recombination in the solid which repopulates the A state after the X-rays are extinguished. Presumably, atom recombination also occurs in the other rare-gas hosts as suggested by the non-exponential decay of the  $\alpha$ -group. However, no evidence of this is present in the initial VK decays, so that the pumping from recombination occurs much more slowly than the rate for disappearance of the A state. Moreover, the results for Ne imply that atom recombination is not the dominant mechanism for exciting the A state.

If the lifetimes are rigorously exponential, then no vibrational cascading is occurring during the lifetime of the A state, even in the hosts where  $v' > 0$  are seen in the VK system. If the decays were obviously nonexponential at short times, or if greater sensitivity were available, it would be possible with certain assumptions to analyze the decay curve and obtain information concerning the relaxation kinetics. It is, therefore, of interest to determine the decay law much more accurately than was possible in this work. However, as will be discussed in Sec. IV, the limited experimental results do permit a rough quantitative limit to be set on the vibrational relaxation rate in the A  $^3\Sigma_u^+$  state of  $N_2$ .

The lifetime of the  $N_2$  A  $^3\Sigma_u^+$  state in solid Ne should be compared with the gas phase radiative lifetime, since previous (limited) experience in this laboratory has indicated that the solid Ne perturbation on molecular lifetimes is not usually very severe. Moreover, since  $v' > 0$  are not seen in the VK system for a Ne host, the decays are not affected by slow vibrational cascading.

However, considerable uncertainty exists as to the free molecule radiative lifetime. A direct measurement of the gas phase lifetime is most desirable, but because of the small radiative transition probability such measurements are very difficult and easily distorted by radiationless quenching of the long-lived A state. A direct measurement by Zipf<sup>21</sup> resulted in  $\tau_A \approx 0.9$  sec. A more recent determination<sup>22</sup> gave  $\tau_A^{v=0} \approx 10$  sec. Both of these measurements involve significant corrections for diffusion and quenching of  $A^3\Sigma_u^+$  molecules at the walls of the discharge vessel. Alternately  $\tau_A$  can be indirectly determined from the ratio of the radiative lifetimes of the A and B states, which has been determined in an elegant experiment by Carleton and Oldenberg.<sup>23</sup> From the absorption strength of the  $1.0 B \leftarrow A$  transition and the absolute intensity emitted in the VK  $A \rightarrow X$  0,6 band simultaneously measured in a discharge through purified  $N_2$ , they obtain  $\tau_A^{v=0} / \tau_B^{v=1} = (1.0 \pm 0.4) \times 10^6$  sec. Although  $\tau_B$  was for a long time very uncertain, recent direct determinations<sup>24</sup> appear to be converging to  $\tau_B^{v=1} = (7.8 \pm 1.0) \times 10^{-6}$  sec, which yields  $\tau_A^{v=0} = (12.5 \pm 4.9)$  sec if the Carleton and Oldenberg ratio is accepted. Thus, even the recent determinations of  $\tau_A$  have a range 0.9 to 17 sec.

The VK lifetime of 3.3 sec in solid Ne lies within the range of the gas phase values and may be very close to the actual radiative lifetime. This measured lifetime reflects of course both the radiative and nonradiative mechanisms for depopulating the A state. For highly forbidden transitions, it is well known that measured lifetimes in

solids can be considerably shortened by nonradiative mechanisms. The nonradiative rate for internal electronic relaxation from  $v=0$  in the A state to high  $v$  in the ground state should be very small since the density of vibrational levels of X in the vicinity of A is very coarse.<sup>25</sup> However, it should be emphasized that the presence of N-atoms, besides giving a long lived tail to the decay from recombination reactions, might also in some fashion help quench excited  $N_2$  molecules.

Large changes in the decay times for both the atomic and molecular emissions occur with changing the solid environment since the heavier rare-gas solids shorten the lifetime of a spin-forbidden transition. A mechanism whereby the transition acquires additional probability has been discussed by Robinson and Frosch<sup>10,25</sup> and in detail by Robinson.<sup>26</sup> In brief, the states of the host heavy-atoms, which have large spin-orbit coupling, are mixed with the guest states so that the guest states of different multiplicities are more strongly coupled in the heavy-atom environment relative to the free molecule.

A scheme for estimating the additional oscillator strength  $f'$  due to heavy atom perturbations has been given by Robinson, who concludes from a second-order perturbation treatment that for heavy rare-gas solvents,

$$f' \approx \frac{(2.5)^2 C^2 \lambda^2 \nu_m}{F_0 (F_0 - \nu_m)^4} f_p \quad (2)$$

Here  $C$  is a semiempirical interaction matrix element,  $\lambda$  is the spin-orbit coupling constant in the rare-gas,  $F_0$  is the center-of-gravity of



the lowest  $P_1$  states of the rare-gas,  $\nu_m$  is the appropriate guest transition energy, and  $f_p$  is the total perturber oscillator strength for the  $^1_3P_1 - ^1S_0$  transition. The factor  $(2.5)^2$  roughly accounts for contributions to the perturbed oscillator strength from other than the lowest resonance transitions. Robinson suggests that the value of the interaction matrix element is  $10\text{-}25\text{ cm}^{-1}$ . Although this range is based on experimental interaction energies in organic crystals, we assume the magnitude to be correct for nitrogen in solid rare-gases. The values of the host parameters used in Eq. (2), which were also taken from Robinson, and the calculated perturbed oscillator strength and lifetime for the VK system in the three hosts, Ar, Kr, and Xe, respectively, are given in Table XI. The VK lifetimes refer to the zeroth vibrational level of the A state. The rare-gas oscillator strength given in Table XI is 12 times the gas value since each guest molecule is perturbed by roughly 12 host heavy atoms.

The observed dipole strength should equal the sum of the free molecule plus the heavy-atom induced dipole strengths. If the longest lifetime measured in Ne, 3.3 sec, is taken as the unperturbed radiative lifetime of the VK transition, then with the calculated perturbed lifetimes shown in Table XI the radiative lifetimes for the  $v = 0$  level of the A state in the heavy-atom hosts become: 0.5 sec in Ar, 0.024 sec in Kr, and 0.008 sec in Xe. These lifetimes are only in fair agreement with the experimental lifetimes. However, if the interaction constant  $C$  is increased somewhat, then the calculated perturbed lifetimes can be made to agree with the observed lifetimes, as shown in Table XI. Since there is no reason to expect the interaction constant

to be either  $25 \text{ cm}^{-1}$  or constant for all the rare-gases, we take this near agreement between calculated and experimental lifetimes as support for both the theory of Robinson and the correctness of the experimental lifetimes.

In the free  $\text{N}_2$  molecule, the  $A \rightarrow X$  transition probability is expected to depend on the vibrational level of A. This arises mainly from a large variation of the electronic transition moment with internuclear distance,<sup>27</sup> together with a smaller frequency factor. The overall effect acts to increase the transition probability, i. e., decrease the radiative lifetime, for VK emission from  $v' > 0$ . The magnitude change in the VK radiative lifetime relative to  $v' = 0$  can be estimated as  $\lesssim 15\%$  for low  $v'$ . This small change in the lifetime results from the large Franck-Condon envelope for the VK system, which causes the varying transition moment, to be averaged over many bands. Such effects are expected to show up where the transition is highly forbidden and become of diminished importance as the transition gains allowedness. Thus, in a heavy-atom environment these effects are not expected to appear for the VK bands. The concentration dependence of the VK lifetimes, as shown in Table X, suggests that the lifetime shortening for high  $v'$  is due to some form of concentration quenching. This is supported by the concentration dependence of the steady state intensities discussed earlier and shown in Figs. 1 and 3.

### D. Second Positive System of N<sub>2</sub> in Solid Neon

The second positive (2+) band system of N<sub>2</sub>,  $C^3\Pi_u \rightarrow B^3\Pi_g$  is well known in the gas phase,<sup>16</sup> but has not previously been observed in condensed phases. However, when a solid mixture of Ne plus low concentrations of N<sub>2</sub> is irradiated with X-rays the (2+) system of N<sub>2</sub> is readily emitted. The observed bands belonging to the sequences  $\Delta v = -1, -2$ , and  $-3$  are shown in Fig. 9a. The overall VK intensity from the 1% N<sub>2</sub> in Ne sample corresponding to Fig. 9a is roughly two orders of magnitude greater than the (2+) intensity. Therefore, the  $\Delta v = 0$  and  $+1$  sequences are strongly overlapped by the structure associated with the heavily overexposed 0, 8 and 0, 9 VK bands. These latter two sequences are shown in Fig. 9b which corresponds to 0.2% N<sub>2</sub> in Ne where the (2+) intensity is increased relative to the VK. This concentration dependence can also be seen by comparing the emission spectrum from  $\sim 1\%$  N<sub>2</sub> in Ne shown earlier in Fig. 2 with the spectra displayed in Fig. 9.

The transition energies, vibrational assignments and matrix shifts are given in Table XII. The vibrational constants in the C and B states, calculated from Eq. (1), are compared with the gas phase values in Table XII. Although the vibrational numbering was not checked by isotopic substitution, the agreement of the calculated constants and observed band positions with the gas phase values leaves little doubt as to the correctness of the assignment. The solid perturbations on  $\omega_e$  and  $\omega_e x_e$  are small for both the B and the C states. The transition shows a relatively uncommon blue shift in the



solid, but it is quite small, amounting to only  $80 \text{ cm}^{-1}$  for the 0,0 band and is not unreasonable for a transition between two excited states. Furthermore, as in the VK system, the intensity distribution in the three observed  $v''$  progressions of the (2+) system agrees with the relative intensities predicted from Franck-Condon factors.<sup>28</sup>

The potential curve for the C state is rather complicated in the gas phase. Presumably, at least four bound vibrational levels exist, each of which shows a breaking off on account of predissociation.

No emission is seen from  $v' > 4$ .<sup>29</sup> Carroll<sup>30</sup> has suggested that part of the observed irregularities in the C' state (upper state of the Goldstein-Kaplan bands) is due to interaction with the C state and concludes that the potential curves for the two states are possibly joined together to form an overall  ${}^3\Pi_u$  curve with a double minimum separated from the  ${}^4S + {}^2D$  dissociation limit by a potential hump. Unfortunately, no emission from  $v' > 2$  in the C  ${}^3\Pi_u$  state nor any evidence of the Goldstein-Kaplan system was seen in the solid spectrum, so that we are unable to investigate possible solid perturbations on the interesting features outlined above.

The vibrational relaxation rate in the C state must again be slow compared to the gas phase radiative lifetime of  $40 \times 10^{-9} \text{ sec}$ ,<sup>31</sup> since emission from  $v' = 0, 1$ , and 2 is seen. However, the intensity of  $v' > 0$  is less than that of  $v' = 0$  for all  $N_2$  concentrations studied and does not appear to change with either guest concentration or temperature between 4.2 and 1.7° K. The absence of emission from  $v' > 2$  in solid Ne might be due to an absence of bound vibrational levels

in the C state for  $v > 2$  in the solid. However, this explanation for the breaking off of emission appears unlikely. As Schnepf and Dressler<sup>32</sup> have shown for the dissociation of the  $B^3\Sigma_u^-$  state of  $O_2$  in solid Ar and  $N_2$  hosts, the repulsive interactions in the solid often increase the dissociation limit or at least introduce a potential maximum. Moreover, larger changes in the vibrational constants of the C state than are observed would be expected if the change in the potential curve in the solid were sufficient to reduce the number of bound levels. We, thus, conclude that either  $v > 2$  in the C state is not populated or, if populated, relaxes within the radiative lifetime to lower vibrational levels.

The observation of the (2+) system of  $N_2$  in a solid environment is at first sight surprising since molecular emission in solids normally comes only from the lowest excited state of a given spin multiplet. For polyatomic molecules radiationless processes are nearly always sufficiently rapid to depopulate the higher electronic states, even though they may have allowed radiative transitions to lower states. For diatomics, however, electronic relaxation might be expected to be somewhat slower since the molecule has fewer and more coarsely spaced internal modes. Following the theoretical model of Robinson and Frosch,<sup>25</sup> this implies the density of available final states in the relaxation process will be lower and thus the overall relaxation rate reduced. Nevertheless, only a few band systems originating from higher electronic states have been reported and none are known to terminate in other than the ground state. Presumably this is partly due to the difficulty of exciting these high energy states

in a solid environment. We note that the (2+) system is not observed in Ar, Kr, or Xe matrices, where the excited states of the rare-gas solid<sup>33</sup> lie near or below the  $\sim 11$  eV gas phase energy of the C state.<sup>16</sup> This suggests that fast relaxation takes place in the heavier rare-gases at least down to the lowest host states or band so that the C state is excited only in solid Ne. It is most likely a general rule for solids that molecular radiative transitions can not compete with nonradiative transitions when the upper state is imbedded in or lies above the host band. The guest and host states will be strongly mixed under these conditions and both inter- and intramolecular relaxation processes will proceed faster than radiation of light.

One experimental attempt was made to observe the first positive system in absorption ( $B^3\Pi_g \leftarrow A^3\Sigma_u^+$ ). Since the lifetime of the A ( $v = 0$ ) state is quite long in solid Ne and the VK system rather intense, it was felt that perhaps the 0,0 of the allowed B-A transition could be observed, while irradiating with X-rays. However, no absorption was seen for  $\sim 1\%$  N<sub>2</sub> in Ne in the spectral region 9000 to 12,000 Å, which brackets the gas phase 0,0 of the first positive system<sup>16</sup> at 10,510 Å.

#### IV. DISCUSSION

##### A. Excitation Mechanism

Rather complicated mechanisms are available for exciting the  $N_2$  VK bands in a solid irradiated with X-rays. The actual mechanism or mechanisms must explain the breaking off of the VK emission above  $v' = 6$ . The gas phase potential energy diagram of  $N_2$ ,<sup>34</sup> shown in Fig. 10, suggest a possible radiationless path for populating the A state which would not populate  $v > 6$ . Fig. 10 shows a near resonance of the  $v = 0$  level of the B state with the  $v = 7$  level of the A state. If relaxation to the  $v = 0$  level of the B state were relatively fast and if only the transfer  $B \rightarrow A$  were important, then the observation  $v' \leq 6$  in the VK bands could be understood providing the relative energy shifts of the states in the solid were not too large. Faster relaxation in the B and higher states occurs, we believe, because the overall density of states is much greater than in the low vibrational levels of the A state.

The  $N_2$  molecule is probably excited mainly by energy transfer from the lowest host exciton band, which lies<sup>33</sup> at 8.4, 10.0, 11.6 and roughly 17eV for Xe, Kr, Ar and Ne, respectively. Only in solid Ne does the C state lie below the host band and, thus, the  $(2+) C \rightarrow B$  system is seen only in Ne. The only experimental observation inconsistent with the proposed mechanism is the presence of  $^2D$  N-atoms in all four rare-gases. If relaxation were sufficiently fast above the lowest host band, then from energy considerations excited  $^2D$  N-atoms would occur only in Ne and possibly Ar solids (cf. Fig. 10). Perhaps the atoms are formed from the fraction of molecules that directly absorb energy from the X-ray photons.

That a substantial number of atoms are present in these solids is evidence by an intense  $\alpha$ -group emission. This is often the single most intense feature in the emission spectrum after prolonged X-irradiation, although the integrated VK intensity is always one or more orders of magnitude greater than that of the atomic  $\alpha$ -group. The total N-atom concentration is of course not known. No  $^2P \rightarrow ^4S$  emission is seen, but this would be very weak since most  $^2P$  N-atoms will decay by  $^2P \rightarrow ^2D$  whose transition energy is outside the spectral region investigated here. Atom recombination also leads to excited  $N_2$  molecules. Evidence for recombination is present in the VK decays for a Ne host as discussed earlier. The non-exponential atomic decay in Ne, Ar, and Kr also suggests recombination reactions.

#### B. Vibrational Relaxation Time

It is obvious that emission from  $v' > 0$  in a molecular band system can occur only if the radiative lifetime of the band system is of the order or shorter than, the vibrational relaxation time. If the radiative lifetime is much shorter than the relaxation time, the observed intensities of different  $v''$  progressions reflect the different excitation rates and the variation of the radiative lifetime with vibrational level. On the other hand, if the radiative lifetime is much longer than the vibrational relaxation time, then all emission occurs from the lowest vibrational level of the excited state regardless of the initial vibrational level or levels excited. In these two limiting cases the observed decay after the excitation cut off for  $v' = 0$  will appear exponential. However, if the electronic radiative lifetime and the vibrational relaxation time are nearly equal, then the observed decays will not appear exponential.

Since  $v' > 0$  are seen for the VK bands in Ar, Kr, and Xe and since the decays for Ar and Kr are exponential at short times within experimental error, the vibrational relaxation time must be longer than the VK radiative lifetime. Thus, in solid Ar the vibrational relaxation time in the  $A \ ^3\Sigma_1^+$  state of  $N_2$  is longer than 0.4 sec. In the other rare-gases where  $v' > 0$  are seen, a lower limit for the vibrational relaxation time may be similarly set.

This lower bound to the vibrational relaxation time does not depend on the measured VK decay times being the radiative lifetimes. It only depends on the relative magnitudes for populating a given vibrational level by cascading from higher levels and for depopulating that level by either radiative or nonradiative transitions to the ground electronic state. This conclusion is not affected by such factors as atom recombination as long as the time scales are sufficiently different.

### C. Concentration Dependence

Without the decay measurements, it is attractive to relate the concentration dependence of the steady state intensities to a concentration dependent vibrational relaxation. The competition between a roughly constant vibrational relaxation time and the changing VK radiative lifetime might then account for the different steady state populations of  $v \geq 0$  in the A state among the four rare-gases for a given  $N_2$  concentration. However, this requires that the vibrational relaxation time be very nearly equal to the VK lifetime in solid Ar, in which case non-exponential behavior at short times is expected. Although we



cannot completely eliminate such a mechanism, it is probably not important.

The concentration dependence of both the steady state populations and the decay time for  $v > 0$  is presumably due to a selective concentration quenching of higher vibrational levels of A, assuming that the excitation mechanism is not appreciably concentration dependent. Intermolecular transfer of the total electronic plus vibrational excitation energy between  $N_2$  molecules in a solid is most probable in the resonance case. Considering only resonance transfer between  $A^3\Sigma_u^+$   $N_2$  molecule with  $v > 0$  and a ground state  $N_2$  molecule, the largest Franck-Condon factors<sup>15</sup> and band oscillator strengths<sup>27</sup> occur for high  $v$  and, therefore, the maximum energy transfer to "relaxation centers" occurs for high  $v$ . These centers could be, for example, lattice defects, atoms, dimers, or impurities. These are all expected to increase in number with increasing concentration. During the long time scales involved, a very small non-nearest-neighbor coupling between  $N_2$  molecules, as suggested by Sun and Rice,<sup>9</sup> could thus lead to significant energy transfer and concentration quenching.

#### D. Comparison with Other Systems

A number of other light atom diatomics have also shown emission from  $v' > 0$  when present as guests in solid rare-gases. Table XIV presents the pertinent data for all these known systems. Also tabulated are data for some diatomics for which  $v' > 0$  is not seen in solid rare-gases.

With the exception of  $O_2$  and  $S_2$ , the diatomic band systems tabulated were all studied in these laboratories using X-ray excitation



techniques. We have reinvestigated the Herzberg system of  $O_2$  ( $A \rightarrow X$ ) in the rare-gases employing X-ray excitation and also see  $v' > 0$  only in solid Xe, where weak emission from what seems to be  $v' = 1$  is observed. The spectrum in Xe is quite diffuse whereas in Ar and Kr, where only  $v' = 0$  is seen, the linewidths are similar to those observed for the VK system. The  $S_2$   $B \rightarrow X$  system was excited<sup>8</sup> by absorbing into  $v = 3, 7$ , and  $9$  of the  $B$  state. In all cases only  $v' = 0$  and  $1$  was reported for the Xe host.

It is obvious from Table XIV that emission from  $v' > 0$  for diatomics in solids is a relatively frequent occurrence. It occurs for both homonuclear and heteronuclear diatomics and in the lowest and higher lying excited states. This is much different than the usual case for larger polyatomics where emission only occurs from the zeroth vibrational level of the lowest excited state of a given spin multiplet. This is probably related to faster relaxation rates in the larger molecules because of the greater number of internal degrees of freedom.

Based on the available data, it is not possible to draw any major conclusions or make generalizations at this time. However, the following features seem noteworthy. Even among the simple diatomic molecules shown in Table XIV, the vibrational relaxation time in excited electronic states varies from  $\sim 1$  sec to  $10^{-9}$  sec. The highest  $v'$  observed occur for the  $N_2$  VK bands where  $v' = 6$  is observed. Moreover, this band system has the longest radiative lifetime. As seen from Fig. 10, the  $A$  state is the lowest excited state of  $N_2$  and is far removed in energy from other known  $N_2$  electronic states. Furthermore, the VK emission breaks off when the upper state vibrational level lies very near or above

the next lowest lying excited state. Thus, it appears that an increased density of states where present may preclude observation of high  $v'$  in solid phases by increasing the number of paths for relaxation and increasing the relaxation rate. It is also interesting to note that for CH, OH, and OD fine structure is observed<sup>35, 56</sup> which can at least in part be assigned to rotational structure. Thus, even if the molecule is undergoing rotational motion in the site, the vibrational relaxation time can remain long relative to electronic radiative lifetimes. This is particularly significant for heteronuclear diatomics since the rotational motion is coupled to the "quasi-translational" motion of the guest molecule in the rare-gas cage.<sup>37</sup> This coupling might be expected to increase the relaxation rates. It would in fact predict the apparent faster relaxation for OH relative to OD.

For polyatomics in solids the only estimates of vibrational relaxation rates at low temperatures comes from spectral line widths. Robinson and Frosch have pointed out that at 4.2°K the typical line widths are  $\sim kT = 3 \text{ cm}^{-1}$  so that from the uncertainty principle the vibrational relaxation time is  $\sim 10^{-11}$  sec. More recent studies<sup>38</sup> on isotopically mixed aromatic crystals have shown that the guest phosphorescence linewidth of  $\text{C}_6\text{H}_6$  is  $\lesssim 0.1 \text{ cm}^{-1}$ , which corresponds to vibrational relaxation time in the ground electronic state of  $\gtrsim 10^{-10}$  sec.

The vibrational relaxation times imposed by the above data are much longer than the often quoted times of  $\leq 10^{-13}$  sec. This is in qualitative agreement with the recent theoretical conjecture of Sun and Rice (SR). These authors calculate a collision induced vibrational relaxation time for a ground state  $\text{N}_2$  molecule in solid Ar of 0.01 sec

(at 65°K ?). Since  $\omega_e$  for  $N_2$  in its ground state is 1.6 times that in the  $A^3\Sigma_u^+$  state, one reasonably expects the vibrational relaxation time in the ground state to be even longer than our value of  $> 0.4$  sec for the excited state. Moreover, the rate expression given by SR suggests a relatively large temperature dependence at moderate temperatures, contrary to our observations.

Other models for vibrational relaxation in solids have also recently been reported.<sup>39,40</sup> These involve resonance interaction between the vibrational quantum and the appropriate number of lattice phonons at the Debye maximum. Fairly good agreement is obtained between rates deduced from acoustic measurements and calculated rates. All examples, however, are near room temperature and involve only a small number of phonons. For  $N_2$  in solid Ar more than 20 phonons at the Debye maximum are required and any numerical calculation along these lines is probably not meaningful. However, these models do suggest that higher-order multiphonon processes, as required for  $N_2$  in Ar, are slow. They also are in agreement with experiment in predicting no temperature effect at temperatures well below the Debye maximum.

#### ACKNOWLEDGMENTS

The authors thank Dr. A. S. Dubin for making available to them the least-squares fitting program used in this work.

# REFERENCES

- <sup>1</sup>(a) M. McCarty and G.W. Robinson, J. Chim. Phys. 56, 723 (1959); (b) R. P. Frosch, Thesis, California Institute of Technology, Pasadena, California (1964).
- <sup>2</sup>L. Vegard and S. Stensholt, Skrifter Norske Videnskaps--Akad. Oslo, I: Mat.--Naturv. Kl. No. 9 (1935). This paper contains references to the large number of articles published by Vegard and co-workers on the spectra of condensed systems.
- <sup>3</sup>J. C. McLennan and G. M. Shrum, Proc. Roy. Soc. (London) A106, 138 (1924).
- <sup>4</sup>H. P. Broida and M. Peyron, J. Chem. Phys. 32, 1068 (1960); M. Peyron and H. P. Broida, ibid. 30, 139 (1959); A. M. Bass and H. P. Broida, Phys. Rev. 101, 1790 (1956).
- <sup>5</sup>L. J. Schoen and R. E. Rebbert, J. Mol. Spectry. 3, 417 (1959).
- <sup>6</sup>E. M. Hörl, J. Mol. Spectry. 3, 425 (1959).
- <sup>7</sup>L. J. Schoen and H. P. Broida, J. Chem. Phys. 32, 1184 (1960).
- <sup>8</sup>L. Brewer and G. D. Brabson, J. Chem. Phys. 44, 3274 (1966).
- <sup>9</sup>H.-Y. Sun and S. A. Rice, J. Chem. Phys. 42, 3826 (1965).
- <sup>10</sup>G. W. Robinson, J. Mol. Spectry. 6, 58 (1961).
- <sup>11</sup>R. P. Frosch and G. W. Robinson, J. Chem. Phys. 41, 367 (1964).
- <sup>12</sup>L. F. Keyser and G. W. Robinson, J. Chem. Phys. 44, 3225 (1966).
- <sup>13</sup>W. Benesch, J. T. Vanderslice, S. G. Tilford, and P. G. Wilkinson, Astrophys. J. 142, 1227 (1965).
- <sup>14</sup>G. Herzberg, Molecular Spectra and Molecular Structure. I. Spectra of Diatomic Molecules (D. Van Nostrand, Inc., New York, 1950).

<sup>15</sup>W. Benesch, J. T. Vanderslice, S. G. Tilford, and P. G. Wilkinson, *Astrophys. J.* 143, 236 (1966).

<sup>16</sup>G. H. Dicke and D. F. Heath, Johns Hopkins Spectroscopic Report No. 17, 1959.

<sup>17</sup>L. Brewer and A. W. Searcy, *Ann. Rev. Phys. Chem.* 7, 259 (1956).

<sup>18</sup>J. Grindlay and R. Howard, Lattice Dynamics, edited by R. F. Wallis (Pergamon Press, New York, 1965) p. 129; G. L. Pollock, *Rev. Mod. Phys.* 36, 748 (1964).

<sup>19</sup>M. Peyron, E. M. Hörnl, H. W. Brown and H. P. Broida, *J. Chem. Phys.* 30, 1304 (1959).

<sup>20</sup>W. L. Wiese, M. W. Smith, and B. M. Glennon, Atomic Transition Probabilities (U. S. Government Printing Office, 1962), Vol. I, p. 55.

<sup>21</sup>E. C. Zipf, Jr., *J. Chem. Phys.* 38, 2034 (1963).

<sup>22</sup>H. H. Brömer and F. Spieweck, *Planet. Space Sci.* 15, 689 (1967).

<sup>23</sup>N. P. Carleton and O. Oldenberg, *J. Chem. Phys.* 36, 3460 (1962).

<sup>24</sup>M. Jeunehomme, *J. Chem. Phys.* 45, 1805 (1966); T. Wentink, Jr. and L. Isaacson, *ibid.* 46, 822 (1967); W. Brennen, *ibid.* 44, 1793 (1966).

<sup>25</sup>G. W. Robinson and R. P. Frosch, *J. Chem. Phys.* 37, 1962 (1962); *ibid.* 38, 1187 (1963).

<sup>26</sup>G. W. Robinson, *J. Chem. Phys.* 46, 572 (1967).

<sup>27</sup>D. C. Jain and R. C. Sahni, *J. Quant. Spectry. Radiat. Transfer* 7, 475 (1967); R. N. Zare, E. O. Larsson, and R. A. Berg, *J. Mol. Spectry.* 15, 117 (1965).

<sup>28</sup>W. Benesch, J. T. Vanderslice, S. G. Tilford, and P. G. Wilkinson, *Astrophys. J.* 144, 408 (1966).

<sup>29</sup>Ref. 16. However, Y. Tanaka and A. S. Jursa have recently reported [*J. Opt. Soc. Am.* 51, 1239 (1961)] emission from what may be a strongly perturbed  $v = 5$  level of the C state.

<sup>30</sup>P. K. Carroll, *Proc. Roy. Soc. (London)* A272, 270 (1963).

<sup>31</sup>M. Jeunehomme, *J. Chem. Phys.* 44, 2672 (1966).

<sup>32</sup>O. Schnepf and K. Dressler, *J. Chem. Phys.* 42, 2482 (1965).

<sup>33</sup>G. Baldini, *Phys. Rev.* 128, 1562 (1962).

<sup>34</sup>W. Benesch, J. T. Vanderslice, S. G. Tilford, and P. G. Wilkinson, *Astrophys. J.* 142, (1965).

<sup>35</sup>L. F. Keyser, Thesis, California Institute of Technology, Pasadena, California (1965).

<sup>36</sup>D. S. Tinti, manuscript in preparation.

<sup>37</sup>H. Friedmann and S. Kimel, *J. Chem. Phys.* 43, 3925 (1965).

<sup>38</sup>E. R. Bernstein, S. D. Colson, D. S. Tinti, and G. W. Robinson, manuscript in preparation.

<sup>39</sup>L. Liebermann, *Phys. Rev.* 113, 1052 (1959); R. A. Rasmussen, *J. Chem. Phys.* 36, 1821 (1961); *ibid.* 46, 211 (1967).

<sup>40</sup>H. G. Danielmeyer, *Acustica* 17, 102 (1966).

TABLE I.

Most Intense Feature of the  $\alpha$  and  $\beta$  Groups in Solid Rare-Gases

Host	$\alpha$	$\beta$
	N $^2D - ^4S$ ( $\text{cm}^{-1}$ )	O $^1S - ^1D$ ( $\text{cm}^{-1}$ )
gas <sup>a</sup>	19227	17925
Ne	19217	17926
Ar	19185	17833
Kr	19136	17763
Xe	18964	

<sup>a</sup>C. E. Moore, Natl. Bur. Std. (U. S.) Circ. No. 467, Vol. I (1949) pp. 32, 95; III (1958), p. 239.



TABLE II.

Vegard-Kaplan System of N<sub>2</sub> in Solid Neon

$v'$	$v''$	$\nu_{\text{vac}}(\text{cm}^{-1})$	$\Delta\nu_{\text{matrix}}(\text{cm}^{-1})$ gas-solid	$\Delta\nu(\text{cm}^{-1})$ $\nu_{\text{vac}}$ -calculated
0	3	42749	102	-0.2
0	4	40506	101	-0.3
0	5	38292	100	-0.5
0	6	36109	96	1.3
0	7	33953	94	1.0
0	8	31824	94	-1.3
0	9	29728	91	0.4
0	10	27661	87	1.9
0	11	25617	90	-2.5
0	12	23607	88	2.1
0	13	21630	82	2.3

TABLE III.

Vegard-Kaplan System of N<sub>2</sub> in Solid Argon

$v'$	$v''$	relative <sup>a</sup> intensity	$\nu_{\text{vac}}(\text{cm}^{-1})$	$\Delta\nu_{\text{matrix}}(\text{cm}^{-1})$ gas-solid	$\Delta\nu(\text{cm}^{-1})$ $\nu_{\text{vac}}$ -calculated
0	3	w	42717	134	-2.0
0	4	m	40477	130	0.6
0	5	ms	38263	129	1.2
0	6	s	36080	125	1.2
0	7	s	33925	122	1.3
0	8	s	31799	119	1.2
0	9	ms	29700	119	-1.1
0	10	m	27635	113	1.4
0	11	w	25595	112	-0.3
1	3	w	44151	133	-1.4
1	4	m	41909	131	-0.8
1	5	m	39698	126	1.6
1	6	not observed			
1	7	mw	35359	121	1.9
1	8	m	33232	119	0.8
1	9	ms	31134	118	-0.5
1	10	s	29065	116	-2.0
1	11	ms	27030	110	1.4
1	12	w	25018	110	-1.5
1	13	vw	23042	103	2.5
2	4	w	43312	133	-3.2
2	5	w	41102	128	0.2
2	6	m	38917	126	-0.5
2	7	m	36763	122	0.5
2	8	w	34638	118	1.4
2	9	vvw	32540	117	0.1
2	10	ms	30473	113	0.6

TABLE III (cont.)

$v'$	$v''$	relative <sup>a</sup> intensity	$\nu_{\text{vac}}(\text{cm}^{-1})$	$\Delta\nu_{\text{matrix}}(\text{cm}^{-1})$ gas-solid	$\Delta\nu(\text{cm}^{-1})$ $\nu_{\text{vac}}$ -calculated
2	11	s	28432	113	-2.0
2	12	s	26421	112	-3.9
2	13	ms	24442	108	-2.9
2	14	w	22493	104	-1.1
2	15	vw	20572	101	-0.5
3	5	w	42480	127	0.8
3	6	w	40296	124	1.0
3	7	not observed			
3	8	overlap with 0, 6			
3	9	overlap with 0, 7			
3	10	w	31851	113	1.1
3	11	not observed			
3	12	m	27802	108	-0.4
3	13	s	25819	109	-3.4
3	14	ms	23871	104	-0.6
3	15	mw	21951	100	1.0
3	16	w	20060	97	2.5
4	5	w	43827	130	-1.8
4	6	not observed			
4	7	m	39490	122	0.5
4	8	m	37366	118	2.4
4	9	vvw	35269	115	2.0
4	10	w	33199	114	-0.4
4	11	m	31162	110	0.9
4	12	m	29152	108	0.1
4	13	not observed			
4	14	m	25220	104	-1.1
4	15	s	23300	101	0.5

TABLE III (cont.)

$v'$	$v''$	relative <sup>a</sup> intensity	$\nu_{\text{vac}}(\text{cm}^{-1})$	$\Delta\nu_{\text{matrix}}(\text{cm}^{-1})$ gas-solid	$\Delta\nu(\text{cm}^{-1})$ $\nu_{\text{vac}}$ -calculated
4	16	m	21408	99	0.9
4	17	vw	19546	96	2.2
5	6	w	42966	126	-0.2
5	7	w	40813	121	1.9
5	8	not observed			
5	9	mw	36589	117	0.4
5	10	m	34521	114	-0.0
5	11	not observed			
5	12	overlap with 2, 10			
5	13	s	28492	107	-1.6
5	14	ms	26541	105	-1.8
5	15	vw	24621	101	-0.1
5	16	s	22730	98	1.3
5	17	s	20868	96	2.6
6	7	not observed			
6	8	m	39981	118	2.0
6	9	m	37881	118	-1.3
6	10	not observed			
6	11	ms	33776	112	-0.4
6	12	ms	31766	110	-1.2
6	13	not observed			
6	14	ms	27835	105	-1.5
6	15	s	25914	102	0.8
6	16	w	24024	98	1.6
6	17	not observed			
6	18	vw	20323	99	-2.0

a. The strongest band in each  $v''$  progression (constant  $v'$ ) is called strong.

TABLE IV:

Vegard-Kaplan System of N<sub>2</sub> in Solid Krypton

$v'$	$v''$	$\nu_{\text{vac}} (\text{cm}^{-1})$	$\Delta\nu_{\text{matrix}} (\text{cm}^{-1})$ gas-solid	$\Delta\nu (\text{cm}^{-1})$ $\nu_{\text{vac}} - \text{calculated}$
0	3	42621	230	-3.2
0	4	40385	222	0.1
0	5	38176	216	1.1
0	6	35996	209	2.1
0	7	33845	202	2.9
0	8	31720	198	0.5
0	9	29626	192	0.1
0	10	27563	185	1.5
0	11	25525	182	-1.3
1	4	41812	228	-1.8
1	5	39600	224	-3.7
1	6	not observed		
1	7	*		
1	8	33147	204	-1.3
1	9	31052	200	-2.8
1	10	28992	189	1.6
1	11	26957	183	1.9
1	12	*		
2	5	41005	225	0.2
2	6	38826	217	2.1
2	7	36671	214	-1.1
2	8	*		
2	9	not observed		
2	10	30388	198	-3.5
2	11	28356	189	-0.2
2	12	26348	185	-2.1
2	13	24373	177	-0.2

TABLE IV (cont.)

$\nu'$	$\nu''$	$\nu_{\text{vac}}(\text{cm}^{-1})$	$\Delta\nu_{\text{matrix}}(\text{cm}^{-1})$ gas-solid	$\Delta\nu(\text{cm}^{-1})$ $\nu_{\text{vac}}^{\text{calculated}}$
2	14	22423	174	-2.3
3	5	42385	222	6.7
3	6	40203	217	5.7
3	7	not observed		
3	8	overlap with 0, 6		
3	9	*		
3	10	overlap with 0, 8		
3	11	not observed		
3	12	27723	187	-0.6
3	13	25750	178	3.4
3	14	23800	175	1.2
4	6	not observed		
4	7	39391	221	-0.3
4	8	37266	218	-2.6
4	9	not observed		
4	10	33114	200	3.3
4	11	31077	195	1.5
4	12	29066	194	-3.4
4	13	not observed		
4	14	25142	182	-2.5
4	15	23228	173	2.2
4	16	21334	172	-2.3
5	6	42857	235	-4.2
5	7	40710	224	0.6
5	8	not observed		

TABLE IV (cont.)

$v'$	$v''$	$\nu_{\text{vac}}(\text{cm}^{-1})$	$\Delta\nu_{\text{matrix}}(\text{cm}^{-1})$ gas-solid	$\Delta\nu(\text{cm}^{-1})$ $\nu_{\text{vac}}\text{-calculated}$
5	9	36495	211	1.8
5	10	*		
5	11	not observed		
5	12	overlap with 2, 10		
5	13	28407	192	-3.5
5	14	not observed		
6	7	41997	231	-2.8
6	8	39877	222	-0.1
6	9	37783	216	-0.6
6	10	not observed		
6	11	33684	204	-0.0
6	12	31678	198	0.1
6	13	not observed		
6	14	27753	187	-0.0
6	15	25840	176	5.7
6	16	23945	177	0.2

\* observed but not accurately measured



TABLE V  
Vegard-Kaplan System of N<sub>2</sub> in Solid Xenon

$v'$	$v''$	$\nu_{\text{vac}}(\text{cm}^{-1})$	$\Delta\nu_{\text{matrix}}(\text{cm}^{-1})$ gas-solid	$\Delta\nu(\text{cm}^{-1})$ $\nu_{\text{vac}}$ -calculated
0	3	42529	322	2.0
0	4	40289	318	-1.4
0	5	38080	312	-3.0
0	6	35905	300	-0.0
0	7	33759	288	2.7
0	8	31640	278	3.1
0	9	29548	270	1.2
0	10	27486	262	-0.0
0	11	25457	250	2.5
1	4	41717	323	1.6
1	5	39509	315	0.9
1	6	not observed		
1	7	35178	302	-3.3
1	8	33061	290	-0.9
1	9	30971	281	-0.8
1	10	28910	271	-1.0
1	11	26865	255	5.4
1	12	24872	256	-5.4
2	5	40902	328	-3.0
2	6	38726	317	-1.0
2	7	36577	308	-1.3
2	8	34455	302	-3.9
2	9	not observed		
2	10	30307	279	-1.0
2	11	28277	268	0.5

TABLE V (cont.)

$\nu'$	$\nu''$	$\nu_{\text{vac}}(\text{cm}^{-1})$	$\Delta\nu_{\text{matrix}}(\text{cm}^{-1})$ gas-solid	$\Delta\nu(\text{cm}^{-1})$ $\nu_{\text{vac}}\text{-calculated}$
2	12	26273	260	-1.4
2	13	24301	249	-0.5
2	14	*		
3	5	42277	330	3.0
3	6	40093	327	-2.9
3	7	not observed		
3	8	not observed		
3	9	overlap with 0, 7		
3	10	overlap with 0, 8		
3	11	not observed		
3	12	27646	264	2.7
3	13	25669	259	-1.4
3	14	23721	254	-5.9
4	6	not observed		
4	7	39293	319	4.9
4	8	37170	314	1.3
4	9	not observed		
4	10	*		
4	11	overlap with 1, 9		
4	12	28985	275	0.8
4	13	not observed		
4	14	25072	252	4.2
4	15	23157	244	3.4
5	7	40601	333	0.0
5	8	not observed		
5	9	36390	316	-1.4
5	10	34339	296	8.3

TABLE V (cont.)

$v'$	$v''$	$\nu_{\text{vac}}(\text{cm}^{-1})$	$\Delta\nu_{\text{matrix}}(\text{cm}^{-1})$ gas-solid	$\Delta\nu(\text{cm}^{-1})$ $\nu_{\text{vac}}^{\text{calculated}}$
5	11	not observed		
5	12	overlap with 2, 10		
5	13	28325	274	0.8
5	14	26380	266	-0.6
6	8	39764	335	-2.4
6	9	37678	321	1.7
6	10	not observed		
6	11	33577	311	-7.0
6	12	*		
6	13	not observed		
6	14	overlap with 3, 12		
6	15	25750	266	-1.2

\* Observed, but not accurately measured.

TABLE VI

Molecular Constants of  $N_2$  from the Vegard-Kaplan System in Solid Rare Gases

State	$(cm^{-1})$	Gas <sup>a</sup>	Ne	Ar	Kr	Xe	Error <sup>b</sup>
$A^3\Sigma_u^+$	$\nu_{00}$	49754.8	49652	49624	49517	49413	$\pm 4$
	$\omega_e$	1460.4		1461.3	1456.5	1453.1	$\pm 0.8$
	$\omega_e^x$	13.83		13.96	13.84	14.02	$\pm 0.1$
$X^1\Sigma_g^+$	$\omega_e$	2358.0	2359.1	2359.3	2355.8	2353.9	$\pm 0.8$
	$\omega_e^x$	14.14	14.53	14.59	14.57	14.66	$\pm 0.04$

<sup>a</sup>Ref. 13<sup>b</sup>The uncertainties represent the average standard deviation for Ne, Kr and Xe. For Ar the errors are roughly one half the values given.

TABLE VII

Vegard-Kaplan System of  $^{14}\text{N}^{15}\text{N}$  In Solid Argon

$v'$	$v''$	$\nu_{\text{vac}} (\text{cm}^{-1})$	$\Delta\nu (\text{cm}^{-1})$ $\nu_{\text{vac}} - \text{calculated}$
0	4	40634	1.4
0	5	38453	-1.5
0	6	36305	0.5
0	7	34182	-0.6
0	8	32089	0.1
0	9	30024	0.7
0	10	27989	3.2
0	11	25975	-1.5
1	6	not observed	
1	7	not observed	
1	8	33497	-0.6
1	9	31431	-1.1
1	10	29396	1.4
1	11	27385	-0.2
1	12	25405	1.0
2	6	39094	-1.2
2	7	36975	1.6
2	8	34871 (?)	-8.7
2	9	not observed	
2	10	30772	-4.5
2	11	28769	1.8
2	12	26786	0.0
2	13	24833	0.2
2	14	22904	-3.9
3	8	overlap with 0, 6	
3	9	34170	0.8

TABLE VII (cont.)

$v'$	$v''$	$\nu_{\text{vac}}(\text{cm}^{-1})$	$\Delta\nu(\text{cm}^{-1})$ $\nu_{\text{vac}} - \text{calculated}$
3	10	32129	-2.7
3	11	not observed	
3	12	28141	-0.2
3	13	26190	-0.1
3	14	24263	-1.2
3	15	22365	-2.2
4	8	37561	-2.2
4	9	not observed	
4	10	33460	-0.2
4	11	31451	0.2
4	12	29472	2.4
4	13	not observed	
4	14	25592	0.5
4	15	23696	1.3
4	16	21826	0.1
5	8	not observed	
5	9	*	
5	10	34767	5.2
5	11	not observed	
5	12	overlap with 2,10	
5	13	28818	-0.1
5	14	26894	0.8
5	15	not observed	
5	16	23128	0.4
5	17	21289	0.2
6	9	38072	-2.2
6	10	not observed	
6	11	34027	-0.3
6	12	32047	0.9

TABLE VII (cont.)

$v'$	$v''$	$\nu_{\text{vac}}(\text{cm}^{-1})$	$\Delta\nu(\text{cm}^{-1})$ $\nu_{\text{vac}} - \text{calculated}$
6	13	not observed	
6	14	28163	-5.0
6	15	26270	-1.2

\* Observed, but not accurately measured.



TABLE VIII  
Molecular Constants of  $^{14,15}\text{N}_2$  from the Vegard-Kaplan System in Solid Argon and Neon

State	$(\text{cm}^{-1})$	Ar <sup>a</sup>	$\rho^2$ <sup>b</sup>	Ne <sup>a</sup>	$\rho^2$ <sup>b</sup>
$A^3\Sigma_u^+$	$\nu_{00}$	49626		49665	
	$\omega_e$	1435.5	$0.9651 \pm 0.001$		
	$\omega_e^x$	13.39	$0.959 \pm 0.01$		
$X^1\Sigma_g^+$	$\omega_e$	2318.8	$0.9659 \pm 0.003$	2322.1	$0.969 \pm 0.003$
	$\omega_e^x$	14.06	$0.964 \pm 0.003$	14.25	$0.981 \pm 0.02$

<sup>a</sup>For solid Ar the standard deviations are those given in Table VI. The corresponding error limits for solid Ne are roughly five times as great.

<sup>b</sup>The theoretical value is  $\rho^2 = 0.9668$

TABLE IX  
Vegard-Kaplan System of  $^{14}\text{N}^{15}\text{N}$  in Solid Neon

$v'$	$v''$	$\nu_{\text{vac}}(\text{cm}^{-1})$	$\Delta\nu(\text{cm}^{-1})$ $\nu_{\text{vac}}\text{-calculated}$
0	4	40662	0.3
0	5	34482	-0.1
0	6	36330	-0.9
0	7	34208	-0.3
0	8	32117	3.0
0	9	30046	-2.5
0	10	28012	0.6

TABLE X

Decay Times for the Vegard-Kaplan Bands in Solid Rare-Gases

Interpreted as an Exponential Decay

host	% N <sub>2</sub>	T(°K)	$\tau$ (sec)				
			v'=0	v'=1	v'=2	v'=3	v'=4
Ne	0.6	1.7	2.8				
	1.0	4.2	3.3				
	0.1	4.2	3.2				
Ar	0.1	1.7	0.42				
	1.0	4.2	0.35	0.31	0.24		0.21
	0.5	4.2	0.38	0.34	0.28		
	0.1	4.2	0.38	0.38	0.41	0.35	0.27
	0.8	8.0	0.37				
	0.2	8.0	0.4 <sub>2</sub>		0.38	0.34	0.24
	0.8	20	0.39				
	1.0	4.2	0.015	0.014	0.013		
Xe	1.0	4.2	<0.005				

TABLE XI

Calculated Perturbed Lifetimes for the  $A^3\Sigma_u^+$  State of  $N_2$  in the  
Heavy Rare Gases

	Ar	Kr	Xe
$f_p$	3.0	3.7	6.1
$\lambda(\text{cm}^{-1})$	-664	-2460	-4304
$F_0(\text{cm}^{-1})$	94341	82513	71095
$C(\text{cm}^{-1})$	25	25	25
$f'$	$8.44 \times 10^{-10}$	$5.52 \times 10^{-8}$	$1.73 \times 10^{-6}$
$\tau'(\text{sec})$	1.54	0.024	0.0008
$C(\text{cm}^{-1})$	49	32	
$f'$	$3.24 \times 10^{-9}$	$8.84 \times 10^{-8}$	
$\tau'(\text{sec})$	0.40	0.015	

TABLE XII

Second Positive System of N<sub>2</sub> in Solid Neon

v'	v''	intensity	$\nu_{\text{vac}}(\text{cm}^{-1})$	$\Delta\nu_{\text{matrix}}(\text{cm}^{-1})^a$ solid-gas	$\Delta\nu(\text{cm}^{-1})$ $\nu_{\text{vac}}$ -calculated
0	0	s	29751	76	0.2
0	1	ms	28042	72	-0.7
0	2	m	26364	71	-0.0
0	3	w	24716	70	1.3
0	4	vvw	23094	67	-0.8
1	0	w	31745	75	0.1
1	1	not observed			
1	2	w	28359	71	0.9
1	3	w	26709	68	0.2
1	4	vw	25088	66	-0.9
1	5	vvw	23498	65	-0.3
2	0	vw	33687	75	(1.4) <sup>b</sup>
2	1	vw	31977	71	-0.5
2	2	not observed			
2	3	not observed			
2	4	vw	27029	65	-0.6
2	5	vw	35440	66	1.0
2	6	vvw	33878	64	0.1

<sup>a</sup>Gas values taken from Ref. 16.<sup>b</sup>This band was not included in the analysis for the vibrational constants.

TABLE XIII

Molecular Constants of  $N_2$  from the Second  
Positive System in Solid Neon

State	( $\text{cm}^{-1}$ )	gas <sup>a</sup>	Ne
	$\nu_{00}$	29675	29751
$C^3\Pi_u$	$\omega_e$	2047.09	$2047.5 \pm 0.9$
	$\omega_e x_e$	28.446	$26.70 \pm 0.5$
$B^3\Pi_g$	$\omega_e$	1735.42	$1737.5 \pm 0.4$
	$\omega_e x_e$	15.198	$14.69 \pm 0.07$

<sup>a</sup>Ref. 16

TABLE XIV

Selected Summary of Light Atom Diatomic Band Systems Observed in Emission in Solid Rare Gases

diatomic	transition	$\omega'_e$ <sup>a</sup>	radiative lifetime (sec)	v' observed	host	ref. <sup>b</sup>
C <sub>2</sub>	$A^3\Pi_g \rightarrow X'^3\Pi_u$	1788	$\sim 10^{-6}$	0, 1	Ar, Kr, Xe	1
N <sub>2</sub>	$A^3\Sigma_u^+ \rightarrow X^1\Sigma_g^+$	1460	3.3 $\leq 0.4$	0 0 to 6	Ne Ar, Kr, Xe	
N <sub>2</sub>	$C^3\Pi_u \rightarrow B^3\Pi_g$	2035	$5 \times 10^{-8}$	0, 1, 2	Ne	31
O <sub>2</sub>	$A^3\Sigma_u^+ \rightarrow X^3\Sigma_g^-$	819	$\sim 10^{-3}$	0 0, 1	Ar, Kr Xe	7 7
O <sub>2</sub>	$b^1\Sigma_g^+ \rightarrow X^3\Sigma_g^-$	1432	$\sim 10$	0	Ne	7
S <sub>2</sub>	$B^3\Sigma_u^- \rightarrow X^3\Sigma_g^-$	434	$\sim 10^{-6}$	0 0, 1	Ne, Ar, Kr Xe	8 8
NO	$a^4\Pi \rightarrow X^2\Pi$	1019 <sup>c</sup>	$\leq 0.1$	0	Ar, Kr	11 11
NO	$B^2\Pi \rightarrow X^2\Pi$	1037	$\sim 10^{-6}$	0	Ar, Kr	11
CH	$C^2\Sigma^+ \rightarrow X^2\Pi$	2824		0	Ar	35



TABLE XIV (cont.)

diatomic	transition	$\omega_e^a$ ( $\text{cm}^{-1}$ )	radiative lifetime (sec)	$v'$ observed	host	$\text{ref.}^b$
CH	${}^2\Sigma^- \rightarrow X^2\Pi$	2452	$1 \times 10^{-6}$	0, 1	Ar	35
CH	${}^2\Delta \rightarrow X^2\Pi$	2921	$5.6 \times 10^{-7}$	0	Ar	35
OH	${}^2\Sigma^+ \rightarrow X^2\Pi$	3180	$1 \times 10^{-6}$	0, 1, 2	Ne	36
OD	${}^2\Sigma^+ \rightarrow X^2\Pi$	2320		0 to 4	Ne	36

<sup>a</sup>Ref. 14.

<sup>b</sup>The first column gives the reference for the band system; the second column for the radiative lifetime. The reference numbers relate to references quoted in the text. If no reference is given, the lifetimes shown are our estimates for the perturbed lifetime in the solid.

<sup>c</sup>M. Ogawa, *Sci. of Light* (Tokyo) **3**, 39 (1954).

<sup>d</sup>M. Jeunehomme and R. P. Schwenker, *J. Chem. Phys.* **42**, 2406 (1965); R. I. Barger and H. P. Broida, *ibid.* **43**, 2371 (1965).

<sup>e</sup>R. G. Bennett and F. W. Dalby, *J. Chem. Phys.* **32**, 1716 (1960); **40**, 1414 (1964).

Fig. 1. Microphotometer tracings of part of the Vegard-Kaplan system of  $N_2$  at various concentrations in solid Ar. The  $v'$ ,  $v''$  assignments are given below the tracings. " $O_2$ " designates part of the Herzberg system of  $O_2$ .  $T = 4.2^\circ K$ .

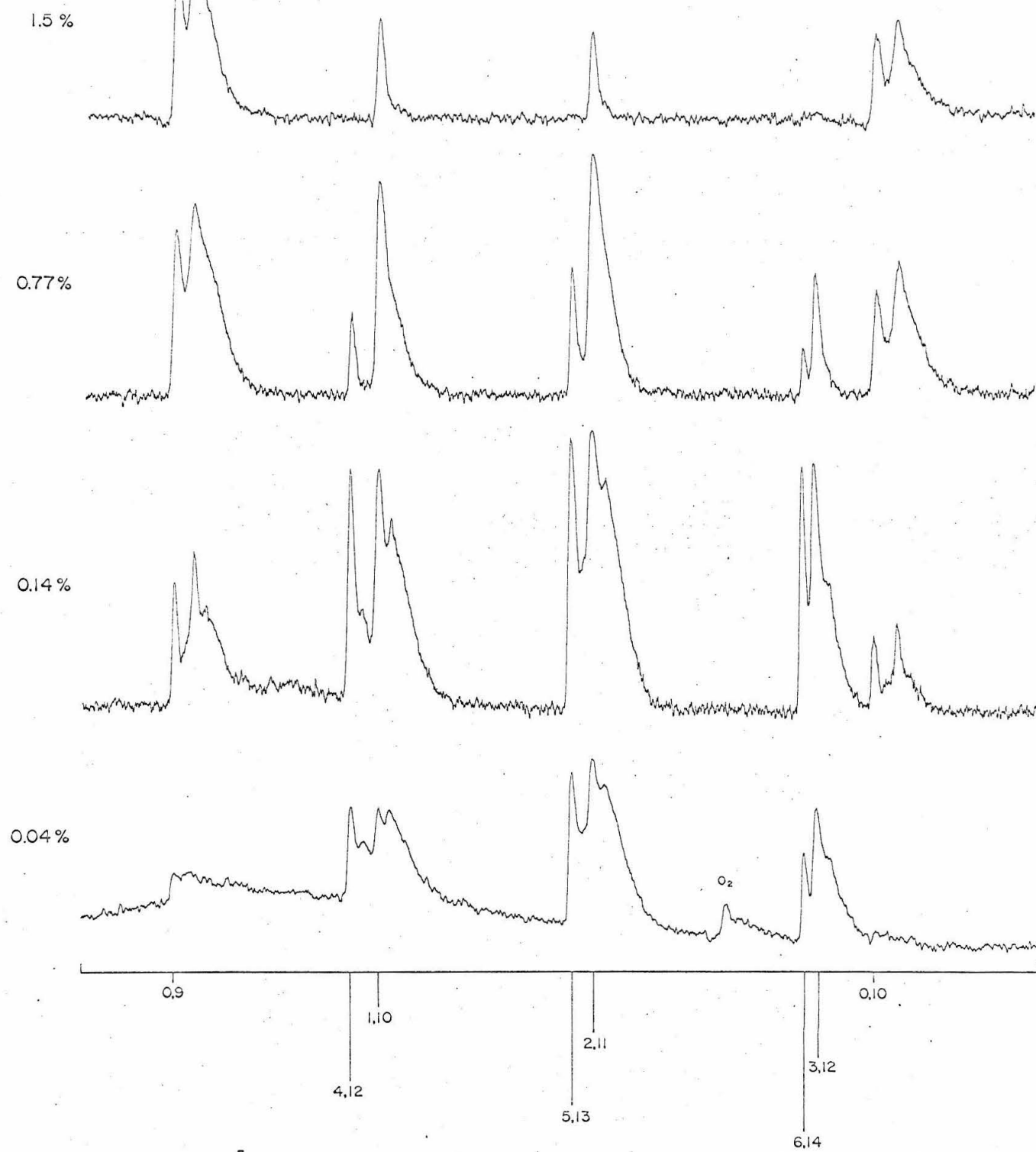


Fig. 2. Microphotometer tracings of part of the Vegard-Kaplan system of 1%  $N_2$  in solid rare-gases. The  $v'$ ,  $v''$  assignments are given below the tracings. "2+" designates the second positive group of  $N_2$ .  $T = 4.2^\circ K$ .

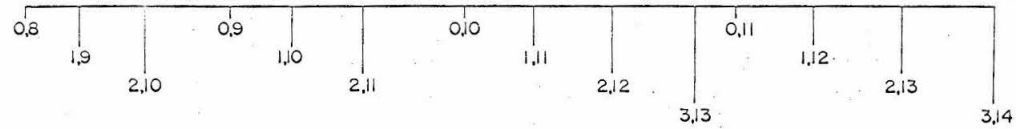
75

Ne

(2+)

(2+)

Ar



Kr

Xe

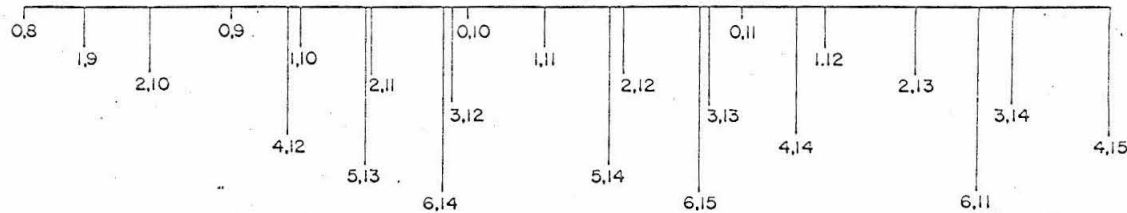


Fig. 3. Microphotometer tracings of part of the Vegard-Kaplan system of  $N_2$  at various concentrations of solid Kr. The  $v'$ ,  $v''$  assignments are given below the tracings.  $T = 4.2^\circ K$ .

1.2 %

77

0.44 %

0.12 %

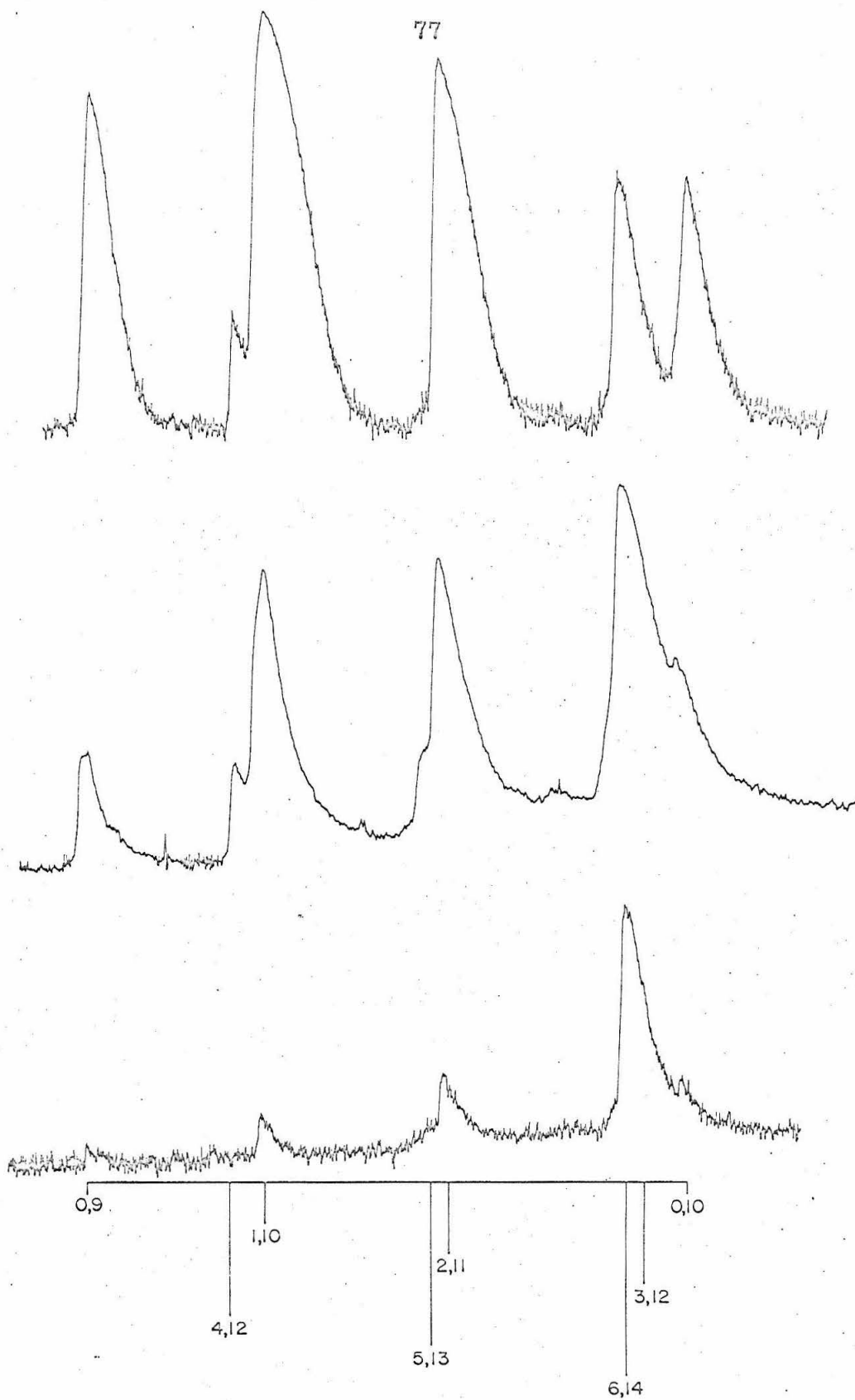




Fig. 4. Microphotometer tracings of part of the Vegard-Kaplan system of 0.2%  $N_2$  in solid Ar at various temperatures. (a) not annealed; (b) annealed at 30°K. The  $v'$ ,  $v''$  assignments are given below the tracings.

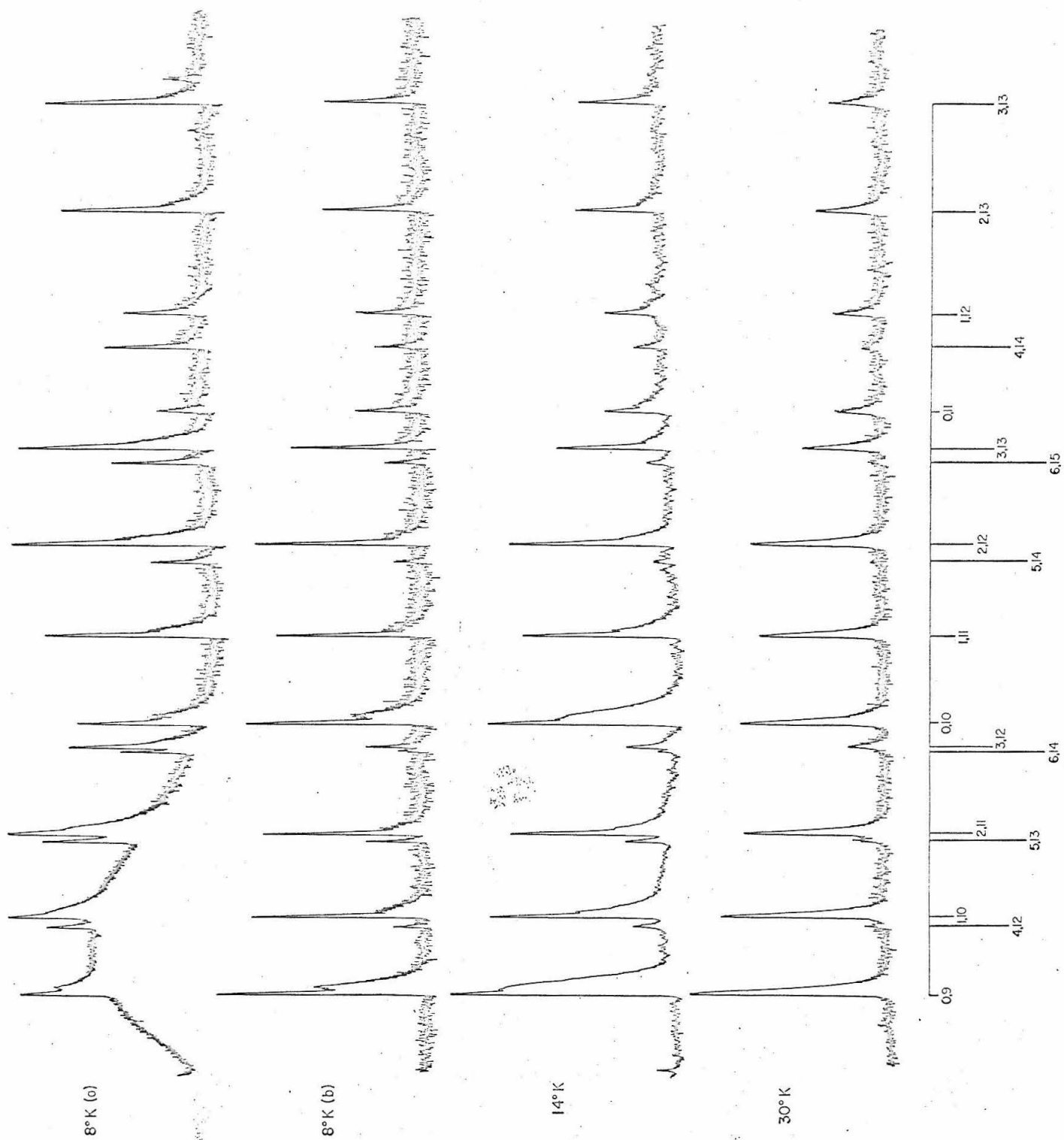


Fig. 5. Microphotometer tracings of part of the Vegard-Kaplan system of 0.2% N<sub>2</sub> in solid Kr at 9°K and 32°K. The v', v'' assignments are given below the tracings.

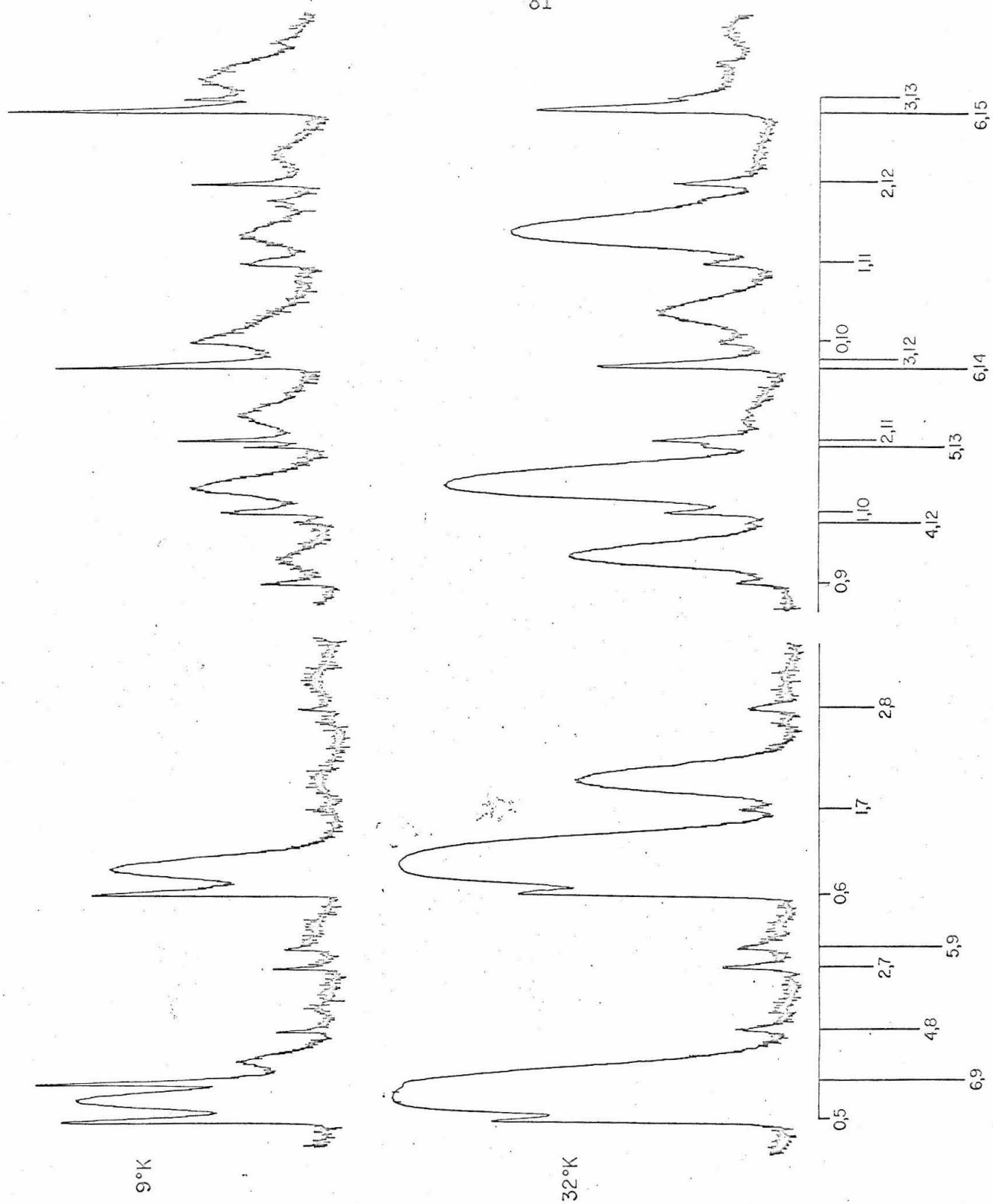
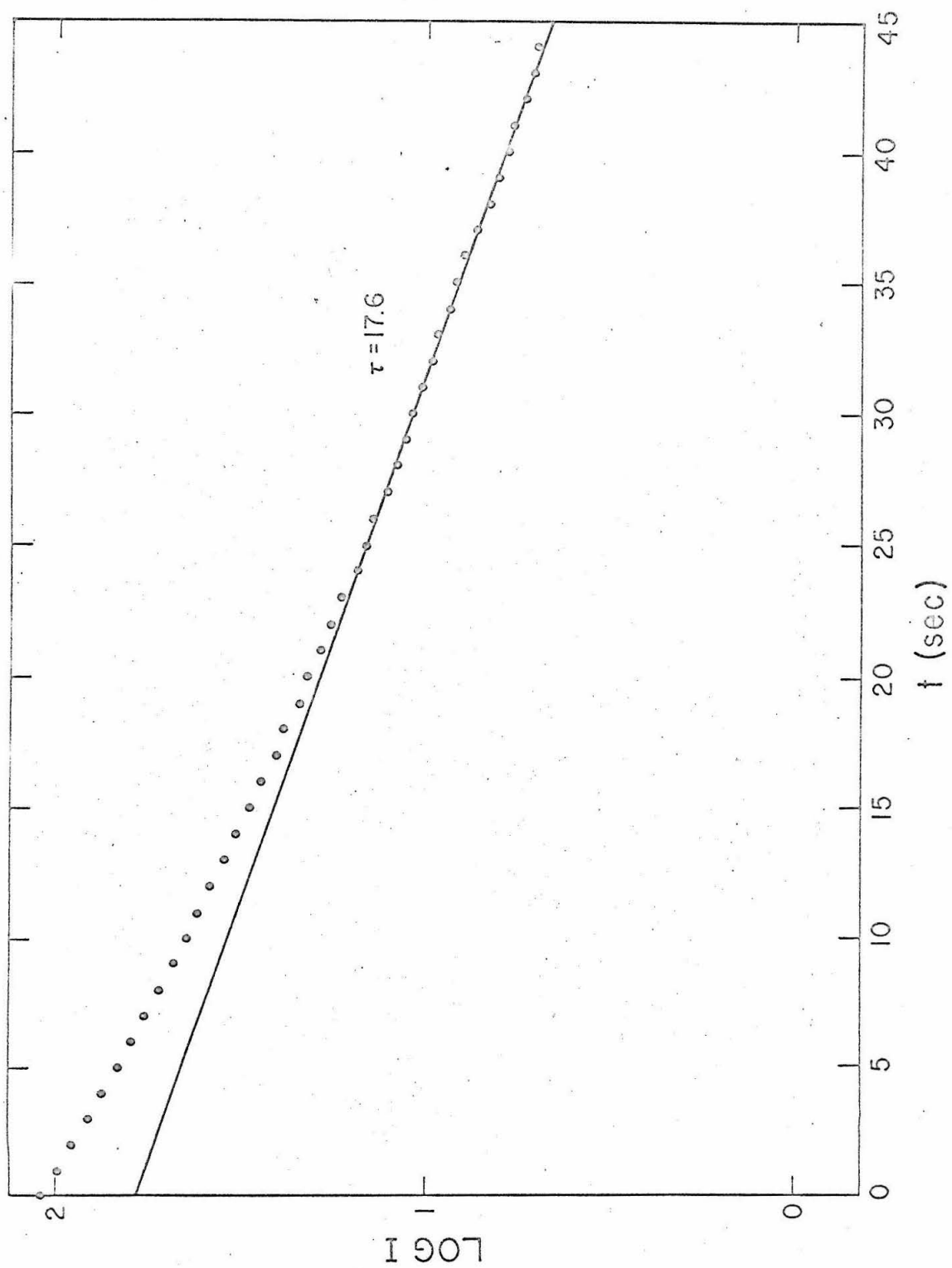


Fig. 6. Decay of the  $\alpha$ -group for 0.1%  $N_2$  in solid Ar (a) and Ne (b).  $T = 4.2^\circ K$ .



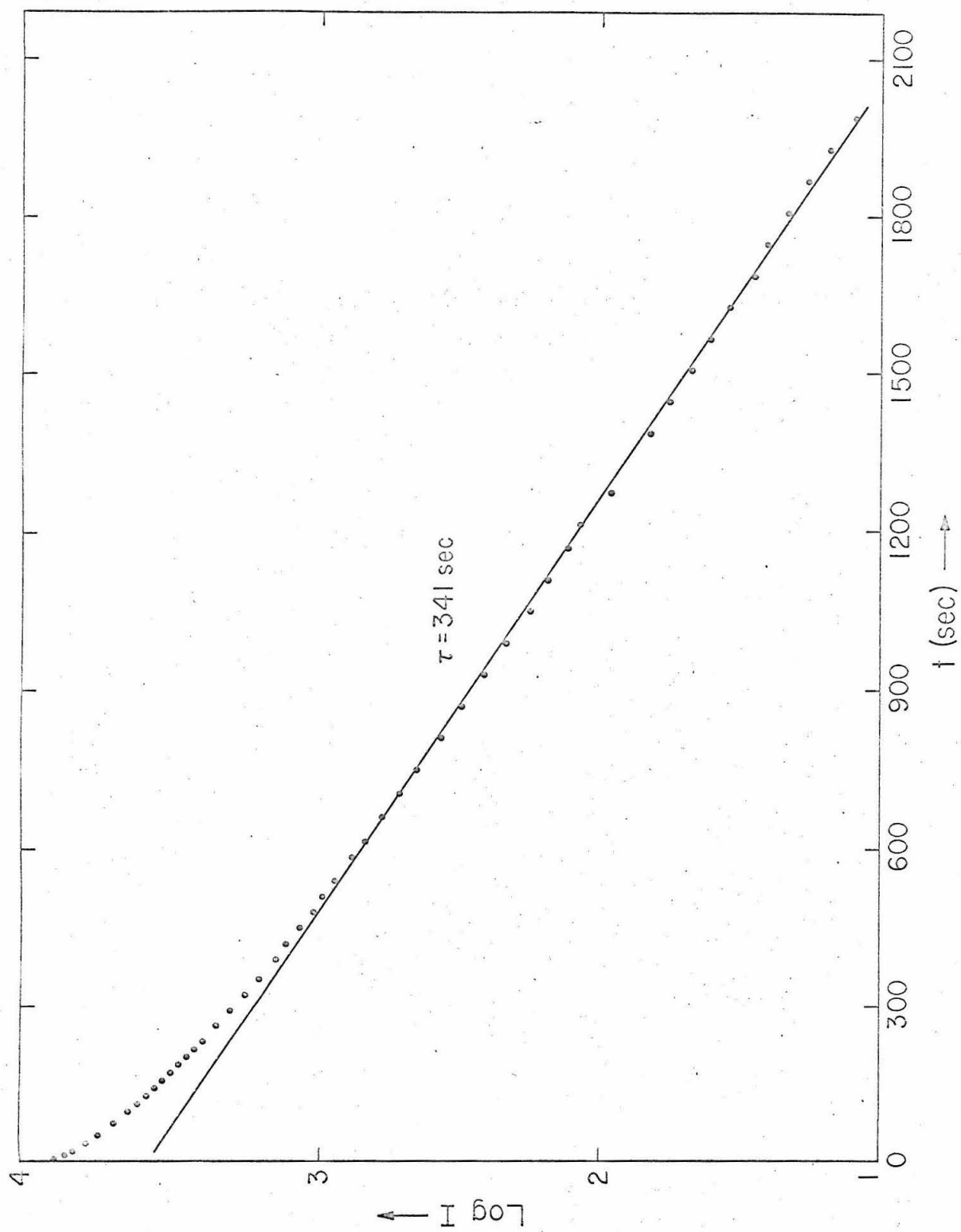




Fig. 7. Representative decay curves of the Vegard-Kaplan bands for 0.1% N<sub>2</sub> in solid Ar. T = 4.2°K.

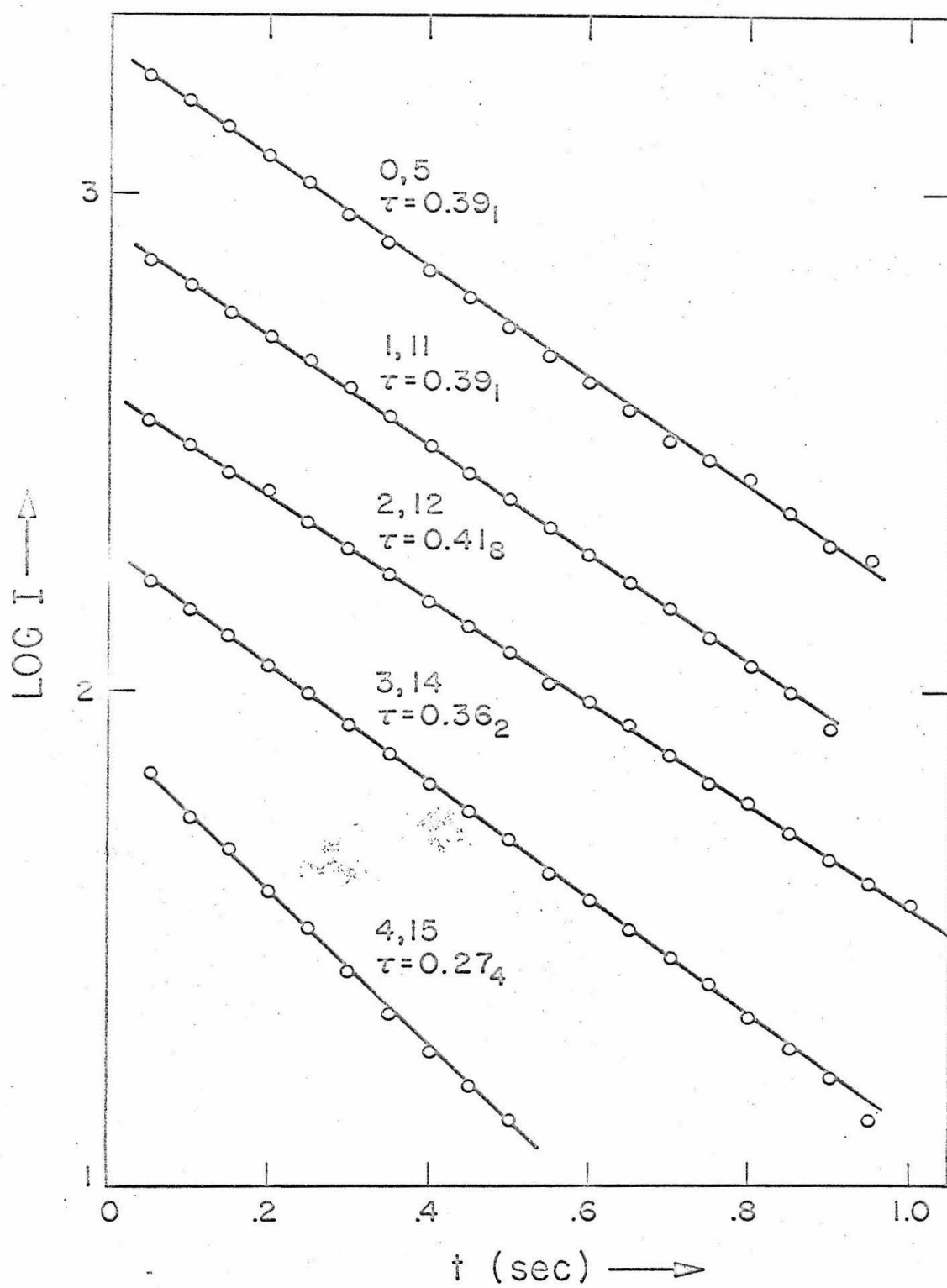


Fig. 8. Decay of the Vegard-Kaplan 0,7 band for 0.1% N<sub>2</sub> in solid Ne. T = 4.2°K.

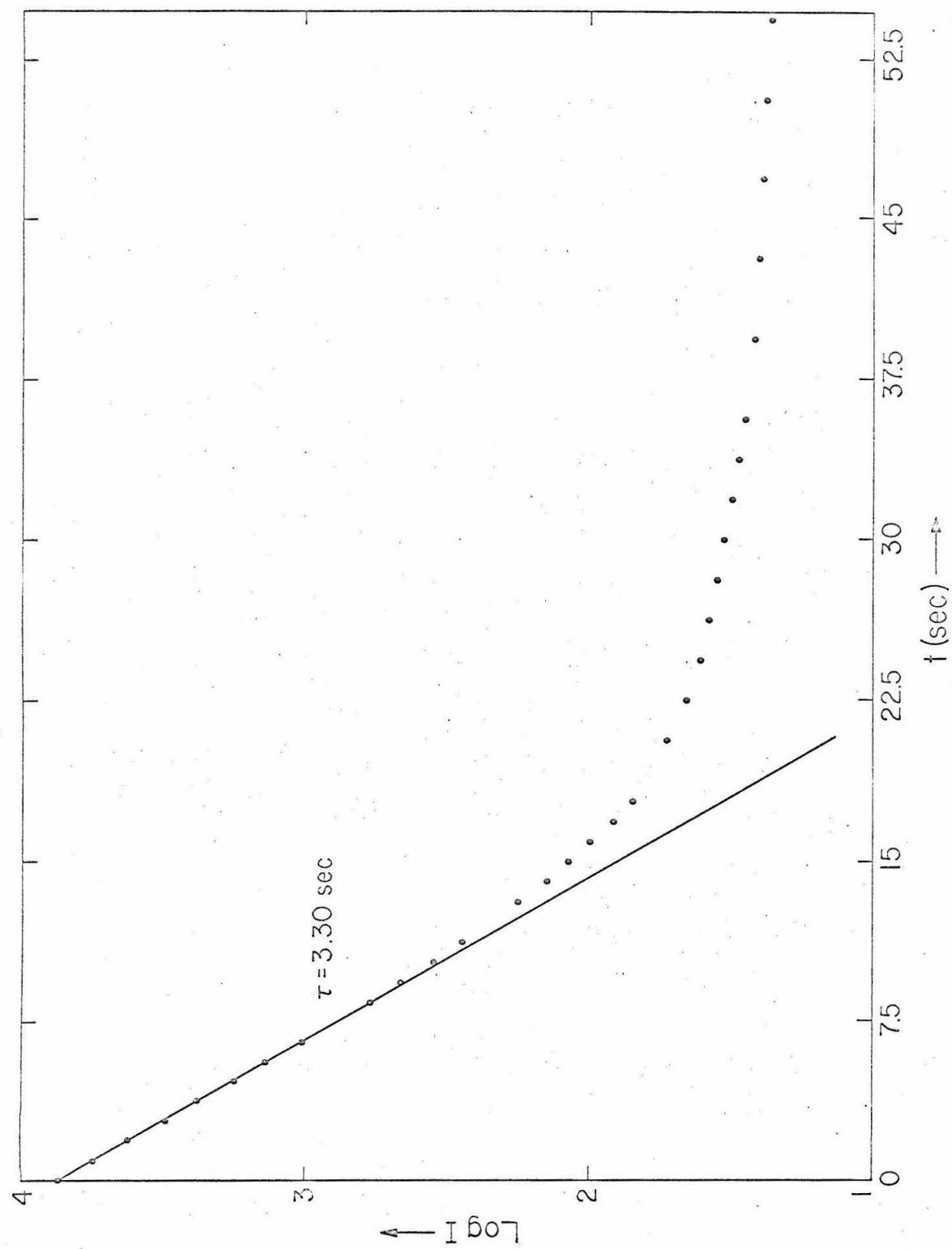


Fig. 9. Microphotometer tracings of part of the second positive (2+) system of  $N_2$  in solid Ne. (a) 1.0%  $N_2$ ; (b) 0.1%  $N_2$ .  $T = 4.2^\circ K$ . The  $v'$ ,  $v''$  assignments are given below the tracings.

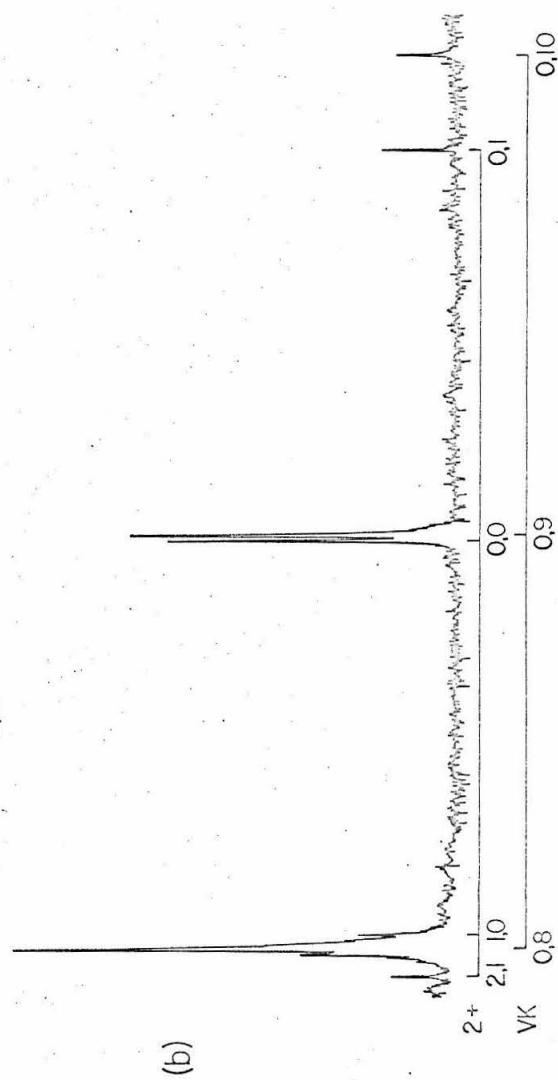
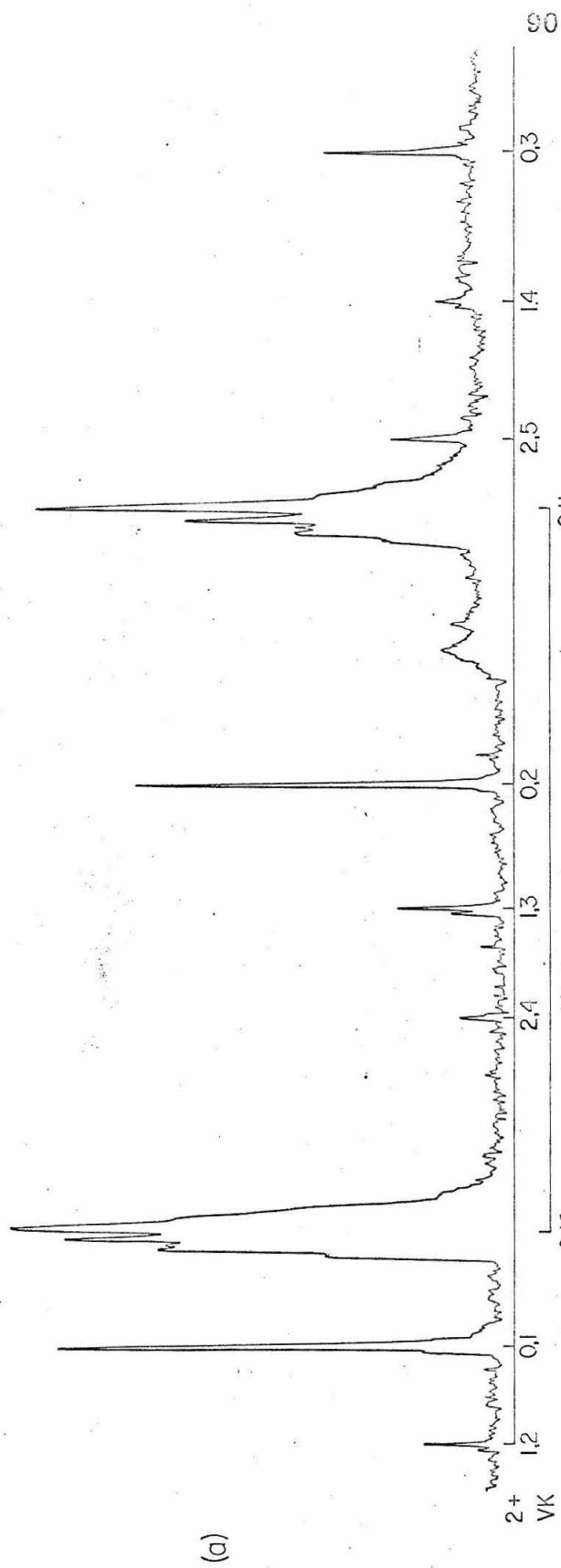
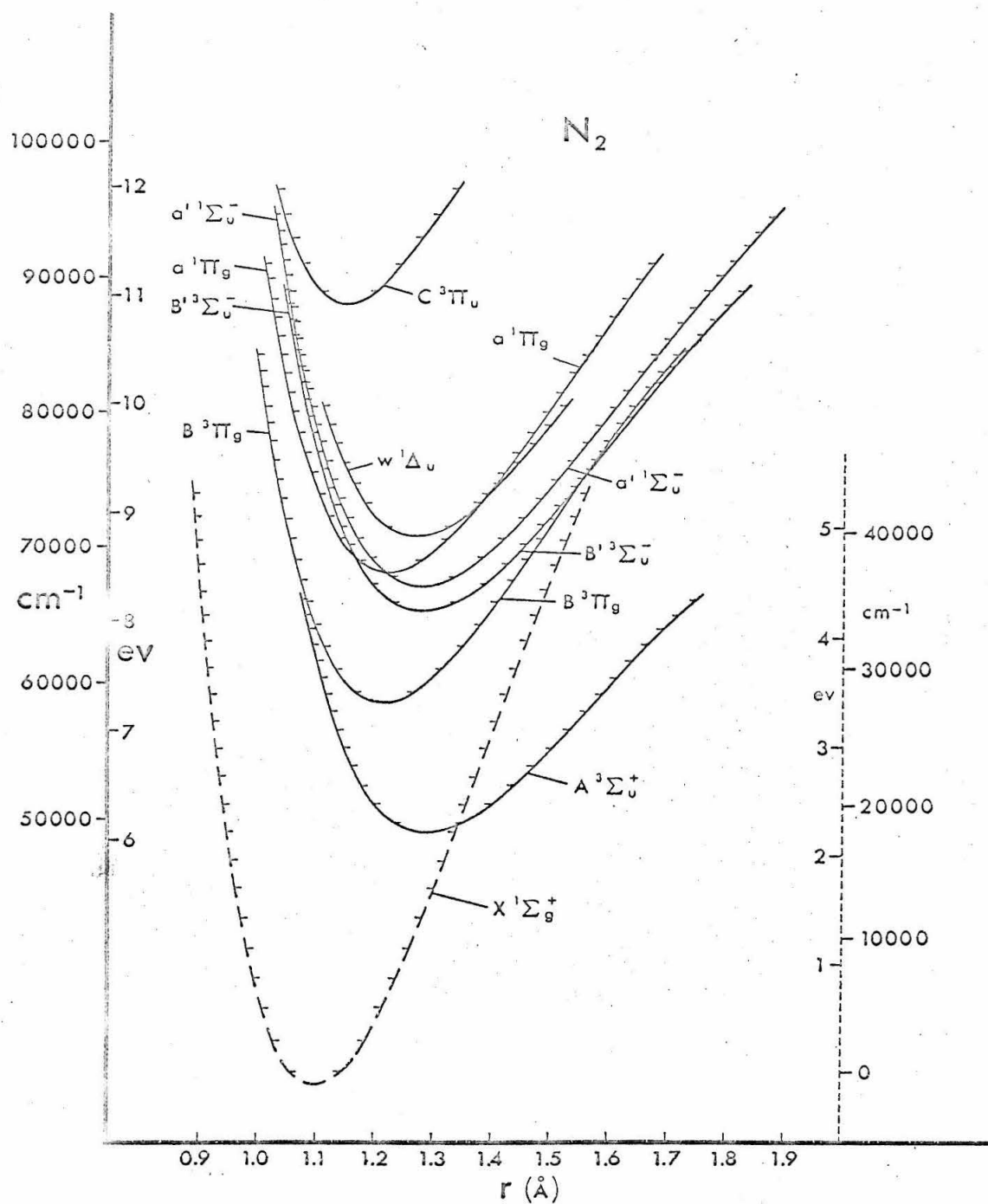


Figure 10. Potential energy curves for known states of  $N_2$  below 12 eV, taken from Ref. 34. The right hand scale corresponds to the  $X^1\Sigma_g^+$  state.





KINETICS FOR A MODEL SYSTEM UNDERGOING VIBRATIONAL  
RELAXATION IN AN ELECTRONICALLY EXCITED STATE.

We now consider the kinetics for the relaxation of a system of diatomic oscillators prepared initially in a nonequilibrium vibrational distribution. The analysis given here closely resembles that of Montroll and Shuler.<sup>1</sup> The diatomic molecules are present as guests in a solid rare-gas crystal which acts as a heat bath. The states of the guest molecule which we are interested in are A and X, the excited and ground electronic states, with vibrational levels  $v'$  and  $v''$  respectively. The system of oscillators consists of the molecules in the  $v'$  levels of the A state prepared by electronic excitation of the diatomic molecule.

The concentration of diatomic guest molecules is assumed to be sufficiently small that energy exchange takes place only between guest and host molecules, that is the relaxation processes in the vibrational manifold of the A state are first order with respect to the concentrations. This is apparently the experimental situation for less than about 0.2% by volume guest for the system  $N_2$  in solid Ar.

The rate of change in the population of the level  $v' = i$  may be written

$$\dot{N}_i = K_i - k_i N_i + \sum_{l < i} g_{il} N_l - \sum_{l > i} g_{li} N_l \quad (1)$$

where  $N_i$  is the population of the level  $v' = 1$ ,  $g_{ij}$  is the rate constant for vibrational relaxation between levels  $v' = i$  and  $v' = j$  ( $i > j$ ), and  $k_i$  is the rate constant for all other mechanisms of depopulating the level  $i$ . Thus, for example,  $k_i$  includes the rate of spontaneous emission  $A \rightarrow X$  and the rate of the electronic radiationless transition  $A \rightsquigarrow X$  from the  $i$ th vibrational level of the A state to the vibrational levels  $v''$  of the ground electronic state X. The vibrational relaxation rate  $g_{ij}$  may similarly be made up of radiative and nonradiative parts.  $K_i$  is the rate, assumed small, at which oscillators are produced by external pumping into the  $i$ th vibrational level of the A state. For example, if the A state were excited by the absorption of light,  $K_i$  would depend on such factors as the diatomic concentration, the intensity of the radiation at frequency  $\nu_i$  and the oscillator strength  $f_i$ . In writing Eq. (1) we have assumed the temperature to be sufficiently low that the Boltzmann equilibrium population of  $v > 0$  is negligible and that the probability of the diatomic absorbing phonons from the surrounding lattice, thereby undergoing "up transitions" from lower vibration levels to  $v' = i$  and from  $v' = i$  to higher vibrational levels is much less than the rate of vibrational relaxation.

To proceed further we must have some knowledge of the transition probabilities. We will assume that the potential function for the A electronic state is harmonic. Since we are primarily interested in low  $v'$ , this is a relatively good approximation to the actual potential function. Thus, a diatomic molecule vibrating in the potential function of the A state must obey the rather strict selection rules for transitions between levels of a simple harmonic oscillator.

For the radiative transitions of a harmonic oscillator, the selection rules and transition probabilities are well known to be given by

$$g_{ij} = 0 \quad j \neq i \pm 1 \quad (2a)$$

$$g_{i,i-1} = i g_{10} \quad (2b)$$

If the perturbation which induces the radiationless transition between vibrational levels is linear in the normal coordinate of the diatomic oscillator and sufficiently small for a first order perturbation calculation, then the matrix elements for relaxation are identical, except for a constant factor, with those for radiative transitions of a harmonic oscillator.<sup>2</sup> Thus, the selection rule  $\Delta v = \pm 1$  and the relationship among the transition probabilities given in Eqs. (2) will hold for radiationless as well as radiative transitions. Even if the diatomic vibrates in an anharmonic potential, the squared matrix elements<sup>3</sup> and, therefore, the transition probabilities would still be very nearly proportional to the upper state quantum number for a perturbation linear in the oscillator coordinate.

This linearization of the intermolecular potential assumes a nearly adiabatic interaction,<sup>2</sup> i. e., the amplitude of the oscillator vibration is small compared with the effective range of the intermolecular force field. This approximation becomes increasingly inaccurate

as the amplitude increases in the higher vibrational levels. Thus, we do not expect Eqs. (2) to be generally true for radiationless transitions, but a possible starting point for comparison with experiment.

However, the selection rule  $\Delta v = \pm 1$  probably holds, or at least dominates, independent of the form of the coupling. Calculations<sup>4</sup> show that in low energy collisions of a particle with a harmonic oscillator one quantum transfers have the greatest probability. In a solid, as compared to a gas, transitions with  $\Delta v > 1$  probably have relatively lower probabilities since higher multiphonon processes are required.

Assuming only nearest neighbor transitions and limiting the discussion to the lowest  $(\alpha + 1)$  vibrational levels of the A state ( $v'_{\max} = \alpha$ ), Eq. (1) may be written

$$\dot{N}_i = K_i - (a_i g + b_i k) N_i + a_{i+1} g N_{i+1} \quad (3)$$

where

$$b_i = k_i / k_0 = k_i / k \quad i = 0, 1, \dots, \alpha$$

$$a_i = g_{i,i-1} / g_{10} = g_i / g \quad i = 1, 2, \dots, \alpha$$

$$a_i = 0 \quad i = 0, i > \alpha$$

The constants  $a_i$ ,  $b_i$  represent the relative change with vibrational level of the ratios  $(g_i/g)$ ,  $(k_i/k)$ . In general both of these are dependent

on the vibrational level  $i$ . For example, if  $k_i$  is the rate of spontaneous emission, then  $b_i$  depends on the variation of the electronic transition dipole moment with internuclear distance for the  $A \rightarrow X$  band system. Note that  $\dot{N}_i$  for  $i = 0, \alpha$  contain fewer terms, since we have assumed  $a_0 = a_j = 0$  for  $j > \alpha$ .

Eq. (3) can be put into a more compact form by letting

$$\beta_i = (a_i + b_i k/g) \quad (4)$$

whence

$$\dot{N}_i = K_i - g \beta_i N_i + a_{i+1} g N_{i+1} \quad (5)$$

The set of  $(\alpha + 1)$  differential difference equations Eq. (5) governs the kinetics of the model system. We proceed to obtain first the steady state solutions and then find the general solution with the steady state populations as initial conditions.

#### Steady State Solution

At steady state, the level populations are at equilibrium and  $\dot{N}_i = 0$ . By iteration the steady state populations  $N_i^0$  are easily found.

$$N_i^o = (K_i/g\beta_i) + (g\beta_i)^{-1} \sum_{j=1}^{\alpha-i} K_{i+j} \prod_{l=1}^j \left( \frac{a_{i+l}}{\beta_{i+l}} \right) \quad (6)$$

For  $i = \alpha$ , the second term on the right hand side of Eq. (6) is not present.

The real experimental system generally falls into one of three possible limits of Eq. (6). If the rate of spontaneous emission is much less than the rate of vibrational relaxation,  $k \ll g$ , then

$$N_i^o = (K_i/ga_i) + (ga_i)^{-1} \sum_{j=1}^{\alpha-i} K_{i+j} \quad i \neq 0 \quad (7a)$$

$$N_0^o = (K_0/k) + k^{-1} \sum_{j=1}^{\alpha} K_j \quad (7b)$$

Thus, only the zeroth vibrational level of the A state is significantly populated and emission of the A  $\rightarrow$  X band system should consist of a single  $v''$  progression with  $v' = 0$ . This is the usual case for polyatomics in solids and for some diatomics. This is definitely not the case for  $N_2$  in solid rare-gases.

On the other hand if  $k \gg g$ , then

$$N_i^o = (K_i/b_i k) + (b_i k)^{-1} \sum_{j=1}^{\alpha-i} K_{i+j} \left( \frac{g}{k} \right)^j \prod_{l=1}^j \left( \frac{a_{i+l}}{b_{i+l}} \right) \quad (8)$$

$$\approx K_i/b_i k$$

and most of the observed A  $\rightarrow$  X band system is resonance emission.



Therefore, the intensities of different  $v''$  progressions reflect the different pumping rates  $K_i$  and the  $b_i$ .

For the most interesting case of  $k \approx g$ , Eq. (6) reduces to

$$N_i^0 = \frac{K_i}{g(a_i + b_i)} + g^{-1}(a_i + b_i)^{-1} \sum_{j=1}^{\alpha-i} K_{i+j} \prod_{l=1}^j \left(1 + \frac{b_{i+l}}{a_{i+l}}\right)^{-1} \quad (9)$$

and, thus, emission occurs from all energetically available vibrational levels of the excited electronic state.

A further simplification of Eq. (6) results if the vibrational manifold of A is populated by external pumping only at the level  $v = \alpha$ . This would be the case, for example, if the A state were excited by absorption of monochromatic light of frequency  $\nu_{v', v''} = \nu_{\alpha 0}$ . For this limit where only  $K_\alpha$  is non zero, Eq. (6) simplifies and only the last term of the sum remains.

$$N_i^0 = (g\beta_i)^{-1} K_\alpha \prod_{l=1}^{\alpha-i} \left( \frac{a_{i+l}}{\beta_{i+l}} \right) \quad (10)$$

This condition can generally be chosen by the experimenter or often results from the requirement of conservation of energy during an excitation energy transfer to the A state. Moreover,  $b_i k$ , which in most cases equals the rate of spontaneous emission, can be determined from lifetime measurements. If the lifetime of A is independent of vibrational level, then of course  $b_i = 1$ . By measuring the relative

populations

$$N_i^{\circ}/N_0^{\circ} = (\beta_0/\beta_i) \prod_{\ell=1}^i (\beta_{\ell}/a_{\ell}) \quad (11)$$

$\alpha$ -equations are obtained in the  $\alpha$ -unknowns  $g_i$ , i. e.,  $g$  and the  $a_i$  for  $i = 2, 3, \dots, \alpha$ . Thus, the relative steady state populations of the  $(\alpha + 1)$ -vibrational levels in the A state determine in principle the vibrational relaxation rate and its change with vibrational level if the  $b_{ik}$  are known.

The applicability of the model can be experimentally checked by varying the initial level excited. Thus, by exciting into say  $v' = 1$  and determining  $N_1^{\circ}/N_0^{\circ}$ ,  $g_{10}$  is obtained. By next exciting into  $v' = 2$  and measuring relative populations  $N_2^{\circ}$ ,  $N_1^{\circ}$ , and  $N_0^{\circ}$ ,  $g_{21}$  and  $g_{10}$  are obtained. This can obviously be extended, at least in principle, indefinitely. If the rates so calculated do not agree, multiquantum jumps are strongly implied. The model can in fact be easily extended to include  $\Delta v = 2$  transitions and the results show that the rates for these double quantum jumps can be obtained if the populations are experimentally determined for the levels removed by  $\Delta v = 2$  from the level excited. A system wherein this may be possible is suggested in Part IV of this thesis.

If as suggested earlier  $a_i = i$ , Eq. (11) becomes

$$N_i^{\circ}/N_0^{\circ} = \frac{1}{i!} \prod_{\ell=0}^{i-1} (\ell + b_{\ell} k/g) \quad (12)$$

These equations have a total of  $(\alpha + 2)$ -unknowns. If the  $b_{ik}$  are again assumed known, the rate constant  $g$  is overdetermined from only a few steady state populations.

### General Solution

We now proceed to determine the time behavior of the system of oscillators which is prepared initially in the vibrational distribution set up by the steady state conditions. The equations to be solved are

$$-\dot{N}_\alpha = g \beta_\alpha N_\alpha \quad (13a)$$

$$-\dot{N}_i = g \beta_i N_i - a_{i+1} g N_{i+1} \quad i=0,1,\dots,(\alpha-1) \quad (13b)$$

These equations are identical to Eq. (5) except that the pumping rate  $K_1$  is set equal to zero. This assumes no pumping of the A state after the primary excitation is shut off. Thus, for example, atom recombination and cascading from higher electronic states are neglected. If these processes occur either much faster or much slower than either  $k$  or  $g$ , they do not appreciably distort the analysis. These are linear differential equations of the first order whose general solutions are

$$N_\alpha = C_\alpha \exp(-g \beta_\alpha t) \quad (14a)$$

$$N_i = C_i \exp(-g \beta_i t) + \exp(-g \beta_i t) \int \exp(g \beta_i t) \times a_{i+1} g N_{i+1} dt \quad (14b)$$

Substitution of Eq. (14a) into Eq. (14b) yields a solution for  $N_{\alpha-1}$ .

The general solution can then be obtained by iteration for  $N_{\alpha-j}$  :

$$N_i(t) = C_i \exp(-g\beta_i t) + \frac{a_{i+1}}{\gamma_{\alpha-i}'} C_{i+1} \exp(-g\beta_{i+1} t) \\ + \dots + \frac{a_{i+1} a_{i+2} \dots a_{\alpha}}{\gamma_1' \gamma_2' \dots \gamma_{\alpha-i}'} C_{\alpha} \exp(-g\beta_{\alpha} t) \quad (15a)$$

where

$$\gamma_l^m = \beta_{\alpha-l} - \beta_{\alpha-l+m} = (k/g)(b_{\alpha-l} - b_{\alpha-l+m}) \\ + (a_{\alpha-l} - a_{\alpha-l+m}) \quad (16)$$

The solution Eq. (15) does not apply if  $\gamma_1^m = 0$ , which only occurs, except for an accidental cancellation of the terms in Eq. (16), if  $a_i = b_i = 1$ .

This condition is not expected to occur in practice.

The general solution Eq. (15) may be written in a more compact form by treating the populations  $N_i(t)$  as a column vector. In matrix notation Eq. (15) reads

$$\underline{N}(t) = \underline{D} \underline{C}(t) \quad (15b)$$

The matrix  $\underline{D}$  is triangular with elements

$$D_{ii} = 1 \quad (17a)$$

$$D_{ij} = \frac{\prod_{l=1}^{j-i} a_{i+l}}{\prod_{l=1}^{j-i} \gamma_{\alpha-j+l}^2} \quad j > i \quad (17b)$$

$$D_{ij} = 0 \quad j < i \quad (17c)$$

$\underline{C}(t)$  is a column vector whose elements are the time independent coefficients  $C_i$  times the factor  $\exp(-g\beta_i t)$ . The constants  $C_i$  are obtained from the initial conditions at time  $t = 0$ , i. e., the steady state population  $N_i^0$  determined earlier. Substituting Eq. (6) into Eq. (15) for  $t = 0$ ,

$$\underline{C} = \underline{D}^{-1} \underline{N}^0 \quad (19)$$

The problem is now formally solved. Eq. (15) describes the approach to thermal equilibrium for the system of oscillators having an initial vibrational distribution in the A electronic state prescribed by Eq. (6). We note that as  $t \rightarrow \infty$ ,  $N_i \rightarrow 0$ . Thus, all of the guest diatomic molecules are in the ground electronic state, as required for Boltzmann equilibrium at the low temperatures under consideration. For intermediate times the populations  $N_i(t)$  approach their thermal

equilibrium values by a sum of first order decays. Thus, unless one term of the sum dominates, the observed decay of the population  $N_i(t)$  will not follow an exponential law. This will be the case for short times if vibrational relaxation is taking place.

### Comparison with Experiment

It is not possible to directly apply the kinetic model to the VK system in solid rare-gases. The reasons for this are obvious from earlier discussion and will only be sketched here. With X-ray excitation, the pumping mechanism for populating the vibrational levels of A is not known. Thus, the vibrational relaxation rate can not be evaluated from the steady state spectrum. Even if the excitation mechanism were known, the relative populations in the A state are not well known. These in principle can be calculated from the experimental band intensities if Franck-Condon factors and the variations of the electronic transition moment were known for the VK system in the solid rare-gas hosts. Even allowing certain approximations for the above quantities, the experimental band intensities were not accurately obtained.

A major difficulty is how to treat the observed fine structure, which is not completely resolved from the main line. For example, as discussed earlier (cf. p. ), the red components in solid Ar are usually more intense than the main line for the  $v' = 0$  progression, whereas the opposite is true for progressions with  $v' > 0$ . However, even in the latter case, the intensity in the red components is a large fraction of the total band

intensity. If the red components are due to molecules in defect sites, then the intensity in these features should be neglected.

The following very approximate approach was taken. Band intensities were obtained by photographic photometry neglecting entirely the red components. Peak height rather than integrated area was used. Relative populations were then estimated in a standard manner<sup>5</sup> using gas phase Rydberg-Klein-Ress Franck-Condon factors<sup>6</sup> and assuming a constant transition moment.

Although the results show considerable scatter, they indicate that for low concentrations of  $N_2$  in Ar the relative populations in the A state increase with vibrational level,  $v' = 2$  to 6 being roughly a factor of 2-4 more populated than  $v' = 0$ . However, if the red components are included, then the maximum population shifts strongly towards  $v' = 0$ . No actual determinations were made in this latter case.

Clearly many different sets of the variables in the kinetic equations will yield the population distribution. However, a large number of these produce highly nonexponential decays. Thus, if lower vibrational levels of the A state are pumped entirely relaxation from higher  $v'$ , very nonexponential decays result. Numerical calculations show that this "amount of nonexponentiality" would have been immediately obvious in the experimental decay curves.

Assuming the correctness of the model, the following conclusions are imposed by comparing numerical calculations with the experimental population distribution and the observed "exponential decay." Lower vibrational levels of A are populated by unknown mechanisms other than one quantum vibrational relaxation. If we assume that the vibra-

tional relaxation rate depends linearly on the upper level quantum number ( $a_i = i$ ) and that the electronic radiative rate is independent of vibrational level ( $b_i = 1$ ), then the radiative rate  $k$  is at least three times as large as the vibrational relaxation rate  $g$ . The lower limit to the ratio  $k/g$  increases as the population distribution favors higher  $v'$ . On the other hand, if the steady state populations strongly favor low  $v'$ , the decays become more nearly exponential and the lower limit for  $k/g$  is decreased.



## References

1. E. W. Montroll and K. E. Shuler, J. Chem. Phys. 26, 454 (1957).
2. J. F. Clarke and M. McChesney, The Dynamics of Real Gases (Butterworths and Co., London, 1964), pp. 296-306.
3. N. W. Bazley, E. W. Montroll, R. J. Rubin and K. E. Shuler, J. Chem. Phys. 28, 700 (1958).
4. D. Secrest and B. R. Johnson, J. Chem. Phys. 45, 4556 (1966).
5. See, for example, R. W. Nicholls and A. T. Stewart, Atomic and Molecular Physics, ed. D. R. Bates (Academic Press, New York, 1962), Ch. 2.
6. W. Benesch, J. T. Vanderslice, S. G. Tilford, and P. G. Wilkinson, Astrophys. J. 143, 236 (1966).

## THE EMISSION SPECTRA OF O<sub>2</sub> AND CO IN SOLID RARE GAS MATRICES

The results discussed in earlier sections demonstrate that vibrational relaxation of diatomics in solid matrices can be quite slow. This was evidenced by the appearance of bands with  $v' > 0$  in the diatomic emission spectrum. The Vegard-Kaplan bands of N<sub>2</sub> were particularly significant in this respect since the system is spin-forbidden and, therefore, has a very long radiative lifetime. Thus, the observation of  $v' > 0$  emphasizes the slow vibrational relaxation. It was hoped that the results obtained with N<sub>2</sub> could be extended to other forbidden band systems. The two first row diatomics CO and O<sub>2</sub> were chosen since both have well known forbidden transitions connecting their lowest excited triplet state with the ground state: viz., the Cameron bands of CO,  $a^3\Pi - X'^1\Sigma^+$ , and the Herzberg bands of O<sub>2</sub>,  $A^3\Sigma_u^+ - X^3\Sigma_g^-$ . The Cameron bands are spin-forbidden, whereas the Herzberg bands are forbidden since  $\Sigma^+$  states cannot combine with  $\Sigma^-$  states. The results to be described are highly preliminary and incomplete, but will serve as a guide for future work.

Experimental conditions were generally the same as previously described. CO or O<sub>2</sub> concentration of 0.2-1.0% were chosen, employing the continuous flow technique. The guest emission spectrum was excited by X-irradiation of the solid guest plus rare-gas mixture. Some preliminary spectra were taken on a Bausch and Lomb medium quartz spectrograph, but all measurements reported herein were from plates taken with the Jarrell-Ash 0.75 meter grating spectrograph. The latter was used in second, third and fourth orders. The first order plate factor was roughly 40 Å/mm.

1. The Herzberg bands of O<sub>2</sub>

The Herzberg bands of O<sub>2</sub> have been previously observed in solid Ar, Kr and Xe hosts by Schoen and Broida,<sup>1</sup> who used electron bombardment of the solid to excite the diatomic emission spectrum.  $v' > 0$  were seen only in the Xe host where emission from  $v' = 1$  is reported. The Herzberg bands were not seen in solid Ne. Instead the Second Negative system of O<sub>2</sub><sup>+</sup> was observed. In addition a strong line of 7943 Å was assigned in the Ne host to the 0, 0 band of the  $A^1\Sigma_g^+ \rightarrow X^3\Sigma_g^-$  transition of O<sub>2</sub>. The  $\beta$  group, attributed to the  $^1S \rightarrow ^1D$  transition of the O-atom, was seen in all four rare-gases. Our results in the main part agree with the observations of Schoen and Broida (SB). There are, however, certain differences which will be discussed.

The spectral region covered herein for the molecular bands is that encompassed by Kodak 103a-O plates, i. e.,  $\lambda \lesssim 5000$  Å. The appropriate plates were also taken for slightly longer wavelengths, but the exposures were such that only rather intense features were photographed. Thus, we also saw the  $\beta$  group in all four rare-gases. The frequency of this feature in O<sub>2</sub> doped rare-gas solids is the same as that reported earlier in Part II of this thesis for N<sub>2</sub> doped solids. Its intensity is, however, usually greater when O<sub>2</sub> is intentionally added. The frequencies for the  $\beta$  group in all four rare-gases agree well with those reported by SB.

Our measurements of the Herzberg system of O<sub>2</sub> are given in Table I. The  $v'$ ,  $v''$  assignments are based on the work of SB. In Ar and Kr the bands are relatively sharp ( $\sim 30$  cm<sup>-1</sup>) and red shaded. However, in Xe the bands are more diffuse and appear superimposed

on a broad structured continuum. The intensity maxima in the continuum have the frequencies given in Table II. We were not able to photograph any molecular emission from an O<sub>2</sub> doped Ne solid. When X-rays first impinged on the Ne solid, it glowed blue. The afterglow was similar at short times and then turned deep red at longer times. After approximately 15 mins of X-irradiation, the glow from the sample was a whitish-yellow and no afterglow lasting longer than ~0.1 sec was visually observed. The deep red afterglow seen initially may well be due to the forbidden atmosphere bands of O<sub>2</sub> which SB assigned in solid Ne. The yellow glow was identified as the  $\beta$  group. This experiment was repeated twice with identical results.

The measurements of the Herzberg system reported in Table I are generally slightly to the red (0-37 cm<sup>-1</sup>) of those reported by SB. This difference may well be less than the combined experimental errors. However, it appears somewhat systematic in that the difference either increases (Ar) or decreases (Kr and Xe) with increasing  $v''$ . SB do not report frequencies for the six members of the  $v' = 1$  progression which they assigned in solid Xe. However, their published spectrum confirms six bands roughly midway between adjacent members of the  $v' = 0$  progression as expected. We observed the two strong members of this progression which fall in the spectral range covered here.

The vibrational constants of the X  $^3\Sigma_g^-$  state of O<sub>2</sub> in Ar and Kr were calculated from the data given in Table I with the results

Table I. Herzberg bands of O<sub>2</sub> in solid rare-gases.

v''	Ar		Kr		Xe	
	v' = 0 (cm <sup>-1</sup> )		v' = 0 (cm <sup>-1</sup> )		v' = 0 (cm <sup>-1</sup> )	v' = 1 (cm <sup>-1</sup> )
3			29443	vw		
4	28041	vw	27968	mw		
5	26590	w	26511	m	26574	w
6	25152	m	25079	s	25130	m
7	23739	ms	23670	vs	23710	m
8	22351	ms	22283	vs	*	23104 w
9	20979	m	20918	s	*	21678 mw
10			*			

\* observed, but not accurately measured.

Table II. Unassigned bands observed from 1% O<sub>2</sub> in solid Xe.

$\nu(\text{cm}^{-1})$	intensity
26155	m
25547	w
24963	vw
24546	mw
23935	vw
23452	vvw

shown in Table III. The data for Xe are too incomplete to allow such an analysis. The calculated constants are in relatively good agreement with both the gas values and those reported earlier by SB. However, our calculated 0,0 frequency shows a progressive red shift, whereas SB report the 0,0 for Kr at higher energy than for Ar. An unusual feature of this system is the very large red shift observed in solid Ar and Kr. This amounts to about  $1000\text{ cm}^{-1}$  and is the largest observed for any first-row diatomic.<sup>2</sup> Typically these shifts are  $\approx 300\text{ cm}^{-1}$ .

If Morse Franck-Condon factors<sup>3</sup> calculated for the free molecule are applicable to the solid spectrum, the most intense transitions from  $v' = 1$  should terminate in  $v'' = 5, 6, 7$  and  $8$ . The Franck-Condon maximum of the  $v' = 0$  progression should similarly occur between  $v'' = 8$  and  $v'' = 10$ . The intensity maximum in Ar, Kr, and Xe for the  $v' = 0$  progression occurs at  $v'' \approx 8$  in good agreement with the simple theoretical prediction. However, the  $v' = 1$  progression is not seen until  $v'' = 8$ . Our estimate of the intensity maximum from SB's published spectrum is  $v'' = 9$ . Moreover, an apparent intensity anomaly occurs even in the  $v' = 0$  progression for solid Xe at 0,9.<sup>1</sup> This band is much weaker than expected, while 0,10 has what seems to be the correct relative intensity.

In summary no  $v' > 0$  are seen for the Herzberg bands in Ar or Kr solids. In Xe the observations suggest emission from  $v' = 1$ , but they are not totally convincing. The results appear very similar to that obtained for  $S_2$ <sup>4</sup> in that emission from  $v' > 0$  occurs only in Xe. For the Herzberg bands this could be due to a competition between the radiative lifetime, which would be shortened in the Xe matrix,

Table III. Vibrational constants of  $O_2$  in solid rare-gases. All entries are in  $cm^{-1}$ .

State		Gas <sup>a</sup>	Ar	Kr
$A^3\Sigma_u^+$	$\nu_{00}$	35000	$34075 \pm 15$	$34010 \pm 4$
	$\omega_e$	802.8		
	$\omega_e x_e$	14.64		
$X^3\Sigma_g^-$	$\omega_e$	1580.4	$1561.4 \pm 5$	$1567.3 \pm 1.3$
	$\omega_e x_e$	12.07	$10.63 \pm 0.4$	$11.26 \pm 0.1$

<sup>a</sup>Ref. 3

and a nearly constant vibrational relaxation time. This cannot be the explanation for  $S_2$  since the band system observed is allowed.

## 2. The Cameron bands of CO

No emission from CO has been previously assigned in a solid matrix.<sup>5</sup> We find relatively strong emission from ~1% CO in Ar while irradiating with X-rays. However, the spectrum is somewhat complicated and has only been partially analyzed. New features appear in the spectrum and grow in intensity as the length of time X-rays have impinged on the sample lengthens.

Initially the spectrum consists primarily of two well separated band systems, one of which is the Herzberg system of  $O_2$ . This presumably results from  $O_2$  impurity in the commercial CO, since an air leak would have also shown the typically stronger Vegard-Kaplan bands of  $N_2$ . These were sometimes seen, but always much weaker than the Herzberg  $O_2$  system. The other, much stronger, system consists of five very broad bands with a relatively sharp blue edge. The width of these bands at half intensity is roughly  $500\text{ cm}^{-1}$ . They are tentatively assigned to the Cameron system of CO. The positions of the bands are shown in Table IV and are compared with the gas frequencies for the Cameron system. Measurements were made at the intensity maximum as determined from densitometer tracings. The spectral region to the blue of the highest energy band reported in Table IV was not searched.

If these are the Cameron bands, a red shift in the 0,0 of  $(764 \pm 50)\text{ cm}^{-1}$  occurs in solid Ar. If the blue edge is measured, the shift is reduced to  $\sim 600\text{ cm}^{-1}$ . This is a relatively large matrix shift,



Table IV. Cameron bands of CO in solid Ar. All entries are in  $\text{cm}^{-1}$ .

		gas		Ar	
$v'$	$v''$	$\nu^a$	$\Delta G$	$\nu^b$	$\Delta G$
0	0	48474		47710	
			2144		2193
0	1	46330		45517	
			2116		2133
0	2	44214		43384	
			2089		2062
0	3	42125		41322	
			2063		1982
0	4	40062		39340	

<sup>a</sup>G. Herzberg, Molecular Spectra and Molecular Structure I. Spectra of Diatomic Molecular (D. Van Nostrand Co., Inc., New York, 1950), p. 520

<sup>b</sup>measurement error  $\pm 20 \text{ cm}^{-1}$

but similar size shifts have been previously observed (vide supra). More unusual is the excessive width of the bands. Leroi, Ewing and Pimentel<sup>6</sup> have investigated the infrared spectrum of CO in solid Ar and note that the spectrum is extremely dependent upon a variety of experimental conditions. In particular, their results show that a considerable clustering of CO occurs in a deposited sample. This agrees with the more recent work<sup>7</sup> on the equilibrium phase diagram of Ar-CO. These aggregates would be expected to produce diffuse bands. However, Leroi, et al. observe the aggregate ground state fundamental to be red shifted from the gas by  $5\text{ cm}^{-1}$  to the value observed in the pure solid, whereas the monomer is blue shifted by the same amount. Our results seem to indicate a rather large blue shift and increased anharmonicity (cf. Table IV).

An alternate explanation of both the large red shift and the excessive line width involves the recently determined<sup>8</sup> large change in dipole moment resulting from excitation of CO to the  $a^3\Pi$  state. The ground state moment<sup>9</sup> is only 0.112 D. This small value in the ground state is attributed to a balancing of the polarity of the C-O bond by the "lone pair" of electrons on the carbon atom. In the excited state the dipole moment increases to  $1.38\text{ D}^8$ , since qualitatively one of these lone pair electrons is excited into a  $\pi$ -orbital. Therefore, the excited state energy is reduced more than that of the ground state by dipole-induced dipole interactions with the surrounding polarizable medium. A net overall red shift above that usually present for small guests from dispersion interactions results. Applying the Franck-Condon principle to the entire system of guest plus host, the excessive

line width can then be explained. In the relatively long lived a  $^3\Pi$  state, the system has a chance to adjust to its minimum energy position before emission occurs. Not only might this cause a further red shift, but, and more importantly, rather broad bands would result. If we assume that the CO occupies a substitutional site in the Ar lattice and make the point dipole approximation, the shift due to dipole-induced dipole interactions is given by <sup>10</sup>

$$\frac{\Delta E}{hc} = 14.45 \alpha (\mu'^2 - \mu''^2) / r^6$$

where  $\alpha = 1.63 \times 10^{-24} \text{ cm}^3$  is the polarizability of Ar, <sup>11</sup>  $r = 3.76 \text{ \AA}$  is the nearest neighbor distance in solid Ar <sup>12</sup> and  $\mu$  is the CO dipole moment in the excited (') and ground (") electronic states. This leads to an additional red shift of about  $80 \text{ cm}^{-1}$ , which still leaves a rather large shift. However, the point dipole approximation is probably not applicable at these intermolecular distances.

A disturbing feature of even the assignment is the fact that the 0,0 band of the Cameron system for solid CO, observed in absorption by Hexter, <sup>13</sup> is red shifted from the gas by only  $\sim 74 \text{ cm}^{-1}$ . It is clear that more experimental work, aimed primarily towards reducing the linewidth of the observed bands and confirming the assignment, is necessary. The only experimental condition varied here was the CO concentration from 1.0 to 0.2%. No changes were observed in the features ascribed to the Cameron system. In particular no  $v' > 0$  are seen.

Besides the features described above, new spectral lines appear

and grow in intensity with X-irradiation. These features are grouped in Table V. Those lines whose intensity grows in are noted. For the weak lines, it could not be determined if the relative intensity changed with X-irradiation time. The group of lines at around  $33800\text{ cm}^{-1}$  is assigned to the  $^1\text{S} \rightarrow ^3\text{P}$  transition of the O-atom, which occurs<sup>14</sup> at  $33700\text{ cm}^{-1}$  in the free atom. The  $\beta$ -group is seen in these solids, supporting the presence of  $^1\text{S}$  O-atoms. The relative intensities of the  $^1\text{S} \rightarrow ^1\text{D}$  and  $^1\text{S} \rightarrow ^3\text{P}$  emission features are roughly equal in solid Ar, whereas the free atom transition probabilities<sup>14</sup> predict  $^1\text{S} \rightarrow ^1\text{D}$  to be about 20 times more intense than  $^1\text{S} \rightarrow ^3\text{P}$ . This could be due to an increased  $^1\text{S} \rightarrow ^3\text{P}$  transition probability resulting from mixing with the Ar states, which have large spin-orbit coupling. However, these arguments depend on the assignment of the  $\beta$ -group which is still not certain.<sup>1</sup> Moreover, in other systems where the  $\beta$ -group is observed, the features at  $33800\text{ cm}^{-1}$  are not seen. We did not, for example, see them in an  $\text{O}_2$  doped Ar solid. This may have been only an intensity effect since relatively weak exposures were taken. Assignments are not conjectured for the remaining lines in Table V. It appears that CO is not the carrier of these bands, but that they belong to some product or products formed in the solid. Jacox, et al.<sup>15</sup> have, for example, shown that in Ar matrices C-atoms react with CO to form CCO.

Table V. Unassigned bands observed from 1% CO in solid Ar

$\nu_{\text{vac}}$ ( $\text{cm}^{-1}$ )	X-ray <sup>a</sup> time	relative intensity	$\Delta\nu$ ( $\text{cm}^{-1}$ )	assignment
33908	+	m	30	$\text{O } ^1\text{S} \rightarrow ^3\text{P} ?$
33839	+	s	50	
33733	+	s	50	
25939	+	s	25	
24354	+	m	25	
22786	?	w	25	
22723	?	w	25	
21571	?	w	25	

<sup>a</sup>+ indicates that the features grow in intensity with the length of X-irradiation time.

## REFERENCES

1. L. J. Schoen and H. P. Broida, J. Chem. Phys. 32, 1184 (1960).
2. See for example G. W. Robinson, J. Molec. Spectroscopy 6, 58 (1961) for a partial summary. References to other band systems may be obtained from Table XIV in the section of this thesis on N<sub>2</sub> in solid rare gases.
3. R. W. Nicholls, J. Res. Natl. Bur. Stds. (U. S.) 69A, 369 (1965).
4. L. Brewer and G. D. Brabson, J. Chem. Phys. 44, 3274 (1966).
5. R. P. Frosch (Thesis, California Institute of Technology, 1965) has tentatively assigned the Herzberg system of CO in solid Kr. However, this assignment seems doubtful. His reported values are all displaced to the blue nearly a constant amount ( $\sim 10 \text{ cm}^{-1}$ ) from our measurements of the Herzberg O<sub>2</sub> system.
6. G. E. Leroi, G. E. Ewing, and G. C. Pimentel, J. Chem. Phys. 40, 2298 (1964).
7. G. S. Burrett and L. Meyer, J. Chem. Phys. 43, 3502 (1965).
8. R. S. Freund and W. Klemperer, J. Chem. Phys. 43, 2422 (1965).
9. C. A. Burrus, J. Chem. Phys. 28, 427 (1958).
10. J. D. Hirschfelder, C. F. Curtis and R. B. Bird, Molecular Theory of Gases and Liquids (John Wiley and Sons, Inc., New York, 1954), p. 984.
11. Landolt-Bornstein, Zahlenwerte und Functionen (Springer-Verlog, Berlin, 1951), Vol. 1, part 3, p. 510.
12. G. L. Pollack, Rev. Mod. Phys. 36, 748 (1964).
13. R. M. Hexter, J. Chem. Phys. 46, 2300 (1967).

14. W. L. Wiese, M. W. Smith, and B. M. Glennen, Atomic Transition Probabilities (U. S. Government Printing Office, 1962), Vol. I, p. 82.
15. M. E. Jacox, D. E. Milligan, N. G. Moll, and W. E. Thompson, J. Chem. Phys. 43, 3734 (1965).

Absorption and Emission Spectra of OH and OD in Solid Ne.  
Evidence for Rotation\*

D. S. TINTI

Gates and Crellin Laboratories of Chemistry, California Institute<sup>†</sup>  
of Technology, Pasadena, California

(Received

Abstract

The  $A^2\Sigma^+ - X^2\Pi_1$  system of OH and OD has been studied in solid Ne at 4.2°K. Both absorption and emission spectra have been recorded, the latter for the first time in a solid matrix. Emission is seen from  $v' > 0$ , establishing a relatively slow vibrational relaxation rate in the  $A^2\Sigma^+$  state for OH and OD in solid Ne. Considerable fine structure is seen that differs for the two isotopes and is not a mirror image in absorption and emission. This structure bears no resemblance to the structure previously observed for OH and OD in the other rare gases. The observed structure can be partly interpreted in terms of slightly perturbed rotational motion in the solid. The larger perturbation for OH compared with OD suggests that translation-rotation coupling may be important. Rotational relaxation times shorter than  $\approx 10^{-6}$  sec have been established from the lack of "hot-band" structure in the emission spectrum.

<sup>†</sup>Contribution No. 3555

\*Supported in Part by the Atomic Energy Commission.



## 1. INTRODUCTION

Many small molecules have been shown to undergo nearly free rotation when trapped in solid rare gas hosts. These include  $\text{CH}_4$ ,<sup>1</sup>  $\text{H}_2\text{O}$ ,<sup>2</sup>  $\text{HCl}$ ,<sup>3</sup>  $\text{NH}_3$ ,<sup>4</sup>  $\text{NH}_2$ ,<sup>5</sup> and  $\text{NH}$ .<sup>6</sup> Most of these investigations of rotational motion in solids have employed infrared spectroscopy. However, the latter two molecules, viz.  $\text{NH}_2$  and  $\text{NH}$ , have shown rotational structure in their electronic spectra. In the case of  $\text{NH}$  in solid Ar, McCarty and Robinson<sup>6</sup> have observed four lines of the  $A^3\Pi - X^3\Sigma^-$  transition in absorption and four lines in resonance fluorescence, assigning all eight lines to individual rotational transitions with nearly constant solid shifts. By analogy to  $\text{NH}$ , it may be anticipated that  $\text{OH}$  and  $\text{CH}$  should also show considerable rotational freedom in solid rare gases. However, the evidence to date has not completely confirmed this expectation. Keyser<sup>7</sup> has studied  $\text{CH}$  in solid Ar and partly explained fine structure observed in both emission and absorption to rotation. Robinson and McCarty<sup>8</sup> have assigned the 0,0 band of the  $A^2\Sigma^+ - X^2\Pi_1$  system of  $\text{OH}$  and  $\text{OD}$  in solid Ar and Kr. Although fine structure is observed, it could not be consistently assigned to rotational motion. More recently Wei<sup>9</sup> has reaffirmed the results of Robinson and McCarty and, in addition, investigated the  $A - X$  system of  $\text{OH}$  and  $\text{OD}$  in solid Xe. For the three hosts Ar, Kr and Xe the fine structure is very similar. However, the structure is also only slightly dependent on whether the guest is  $\text{OH}$  or  $\text{OD}$ . This implies that, if the fine structure is due to rotation, the rotational motion is strongly perturbed.

We have studied the A-X system of OH and OD in solid Ne at 4.2°K. Both absorption and emission spectra have been recorded. This is the first time that the emission spectrum of OH or OD have been observed in a solid matrix. The fine structure of these molecules in solid Ne bears no resemblance to that in the other rare gases. The present results can be partly interpreted in terms of rotation in the solid.

## 2. EXPERIMENTAL

The molecular fragment OH in solid Ne was prepared by X-irradiation of H<sub>2</sub>O-Ne solid mixtures. The solid was formed by deposition of the gaseous mixture on a sapphire window maintained at 4.2°K by direct contact with liquid helium. After deposition the sample was radiated with 50 kV X-rays from a tungsten target at a tube current load of 45 ma. The intensity of the features assigned to OH did not change appreciably with the length of time of irradiation after about 30 minutes.

The gaseous mixture was prepared during deposition by flowing the rare-gas from a tank through a capillary leak and over a cold trap containing water at a reduced temperature. Water concentrations between 0.1 and 1.0% were typically used. The H<sub>2</sub>O employed was triply distilled. The D<sub>2</sub>O was obtained from General Dynamics Corporation with a specified purity of 99.7%. The rare-gases were Linde MSC grade and were used without further purification.

The spectra were taken with a Jarrell-Ash 0.75 meter grating spectrograph. In the neighborhood of 0,0 band of OH at 3125Å the linear dispersion was roughly 14Å/mm. A high pressure Xe lamp was used as a source for the absorption studies. The emission

spectra of the solids were excited using X-irradiation. Exposure times for the latter ranged from approximately 15 minutes to one hour.

### 3. RESULTS

The observed spectral lines assigned to OH and OD are listed in Tables I and II respectively. The only other molecular band systems observed were the Vegard-Kaplan and Second Positive systems of the  $N_2$  molecule in emission. These occurred presumably because of either an air leak in the vacuum system or  $N_2$  impurity in the commercial Ne. Although some overlap of the OH and OD bands with the  $N_2$  systems resulted, this was not excessively serious and no attempt was made to remove this trace of  $N_2$ . Overlapped lines are noted in Tables I and II. The band systems of  $N_2$  in solid Ne will be discussed elsewhere.<sup>10</sup>

Microphotometer tracings of a portion of the OH and OD spectra are shown in Figs. 1 and 2. OH could not be completely removed from the OD spectrum, even though the system was purged with  $D_2O$  overnight. The corresponding lines are, however, sufficiently resolved even for the 0,0 band, as seen from Figs. 1 and 2. Note that the line widths of the absorption features increase with increasing energy, while for the emission bands the line widths increase with decreasing energy.

It is readily seen from Fig. 1 that the fine structure observed in the 0,0 band for OD is compressed relative to OH, as expected

for rotational levels. By comparing Figs. 1 and 2, one also notes that the observed fine structure is not a mirror image in absorption and emission.

Emission from excited vibrational levels of the upper  $A^2\Sigma^+$  state occurs for both OH and OD. The maximum  $v'$  observed is 2 for OH and 4 for OD. Emission from  $v' > 4$  in a solid environment has been observed<sup>10</sup> only for the Vegard-Kaplan bands of  $N_2$  in solid Ar, Kr and Xe, where  $v'$  as high as 6 are seen. The observation of  $v' > 0$  for OH in the  $A^2\Sigma^+ \rightarrow X^2\Pi_1$  system establishes a vibrational relaxation time in the A state the order of, or longer than, the radiative A-X lifetime. In the gas phase, the radiative lifetime is  $1 \times 10^{-6}$  sec.<sup>11</sup> We can only set a limit of  $\lesssim 5 \times 10^{-3}$  sec, imposed by the X-ray shut-off time, for the A state lifetime in solid Ne. On the other hand, no emission from excited rotational levels is assigned (vide infra) so that rotational relaxation occurs much more rapidly than the radiative lifetime.

Employing the highest energy line for each emission band observed, the vibrational constants for the A and X states for OH and OD were calculated. The results are given in Table III, where the usual spectroscopic notation<sup>12</sup> is employed. The corresponding gas phase values are included for comparison.<sup>12</sup> It should be noted that the gas constants refer to "null lines", whereas the highest energy solid line is here assigned to a rovibronic transition. The results show only small perturbations on the vibrational constants by the Ne environment and confirm the vibrational analysis given in Tables I and II.

#### 4. DISCUSSION

The lower rotational levels in the energy diagram of the  $A^2\Sigma^+-X^2\Pi_i$  system of OH in the gas phase are given in Fig. 3. The A-doubling of the rotational levels of the  $^2\Pi_i$  state and the spin-doubling in the  $^2\Sigma^+$  state are neglected since they are both small ( $<1\text{ cm}^{-1}$ ). The allowed transitions from the lowest rotational level in both absorption and emission are shown in Fig. 3 by vertical lines. A more complete energy diagram is given by Mulliken.<sup>13</sup> Three allowed rotational transitions from  $K'=0$  occur in emission. Six transitions from the  $J''=3/2$  level of the  $^2\Pi_{3/2}$  substate are allowed in absorption, but only four lines are expected since the satellite bands  $R_{21}(1)$  and  $Q_{21}(1)$  are nearly degenerate with  $R_1(1)$  and  $Q_1(1)$  respectively.

Table IV lists the gas phase energies<sup>14, 15</sup> and the relative intensities of the transitions designated in Fig. 3 for the 0, 0 band of OH and OD. The intensities were calculated from the expressions given by Earls<sup>16</sup> for  $^2\Sigma-^2\Pi$  transitions. The observed lines and intensity estimates for OH and OD in solid Ne are given in columns 5 and 6 of Table IV. All observed absorption lines are shown; however, only the three stronger emission lines are tabulated. The remaining, much weaker, emission features are given in Tables I and II. These will be discussed later. The three stronger emission lines for both OH and OD are assigned to the  $P_1(1)$ ,  $P_{12}(1)$  and  $O_2(2)$  transitions. The intensities observed in solid Ne agree approximately with the

intensities predicted for the free molecule. These transitions all originate from the lowest rotational level of the  $A^2\Sigma^+$  state, but only  $P_{12}(1)$  and  $O_2(2)$  terminate in the  $X^2\Pi_{1/2}$  substate. The separation between these two lines gives the  $J''=1/2$ ,  $J''=3/2$  energy difference in the solid (cf. Fig. 3). The measured energy separation for the 0,0 band is 51 and 36  $\text{cm}^{-1}$  for OH and OD respectively, while the average  $P_{12}(1)$ - $O_2(2)$  separation for all vibrational bands is 52 and 38  $\text{cm}^{-1}$ .

The corresponding gas phase values for the 0,0 band are 61 and 32  $\text{cm}^{-1}$ . For OD the line assigned to  $O_2(2)$  is not clearly resolved from  $P_{12}(1)$ , as seen from Fig. 2. Thus, the measured separation could easily be too large by  $\sim 6 \text{ cm}^{-1}$ , which is the solid-gas difference in  $P_{12}(1)$ - $O_2(2)$ . However, the  $\sim 9 \text{ cm}^{-1}$  difference in the splitting for OH between gas and solid is real. The  $P_1(1)$ - $P_{12}(1)$  separation depends not only on the rotational term values, but also on the multiplet splitting in the  $^2\Pi_1$  ground state. The mean  $P_1(1)$ - $P_{12}(1)$  splitting in Ne is 144 and 152  $\text{cm}^{-1}$  for OH and OD respectively. For both isotopes these are roughly 20  $\text{cm}^{-1}$  smaller than the gas values. The energy separations discussed above are summarized in Table V.

The other, much weaker, emission features can not be readily assigned to rotational structure. For OH two additional broad lines can usually be seen to lower energy of  $P_1(1)$  by about 35 and 70  $\text{cm}^{-1}$ . Only one such feature is seen for OD roughly 55  $\text{cm}^{-1}$  to the red of  $P_1(1)$ . However, this could correspond to the two features seen in

OH if these were unresolved for OD. These additional emission lines remain unassigned.

In absorption the two lowest energy lines are quite sharp ( $\sim 5 \text{ cm}^{-1}$ ) for both OH and OD. These have been assigned to  $P_1(1)$  and  $Q_1(1) + Q_{21}(1)$ , which terminate at  $K'=0$  and  $K'=1$  respectively. The observed intensities disagree with those for the free molecule. However, the predicted intensities are quite sensitive to the ratio of the spin-orbit coupling constant to the rotational constant.<sup>16</sup> Moreover, if the rotational levels are perturbed as discussed later, significant departure from the free molecule intensities could result. The perturbation on the  $A^2\Sigma^+$  rotational levels, as given by  $[Q_1(1) + Q_{21}(1)] - P_1(1)$ , is much less for OD than OH. The appropriate differences are shown in Table V.

The next higher energy absorption feature should be  $R_1(1) + R_{21}(1)$  which terminates in  $K' = 2$ . Two lines are seen at about the correct energy for  $R_1(1) + R_{21}(1)$ , separated by 40 and  $20 \text{ cm}^{-1}$  for OH and OD, respectively. In the reduced symmetry of the crystalline site, the  $K' = 2$  rotational level could be split by static crystal interactions. Two different substitutional site symmetries are possible for a doped rare-gas crystal, corresponding to either the normal face-centered-cubic (fcc) or the hexagonal-close-packed (hcp) structure, which is stabilized by certain impurities.<sup>17</sup> The substitutional site symmetry  $\bar{D}_{3h}$  in a hcp crystal is much lower than the  $O_h$  site symmetry of the fcc crystal. In a  $\bar{D}_{3h}$  site even the  $K' = 1$  level can split, and this splitting is predicted to be roughly the



same as the overall splitting for  $K'=2$  for low values of the rotational barrier.<sup>18</sup> However, the  $Q_1(1)+Q_{21}(1)$  line ( $K'=1$ ) is much sharper than even the individual features assigned to  $R_1(1)+R_{21}(1)$  ( $K'=1$ ). In an  $O_h$  site only levels with  $K' \geq 2$  are split.<sup>19</sup> Again for low values of the barrier the band widths for  $K'=2$  and  $K'=3$  are roughly the same. However,  $K'=2$  splits into two levels while  $K'=3$  is split into three levels. As seen from Fig. 1, the features assigned to  $R_1(1)+R_{21}(1)$  and  $S_1(1)$ , where  $K'=2$  and 3 respectively, have roughly equal widths for OD. The  $S_1(1)$  line was not seen for OH, presumably because of the lower  $H_2O$  concentrations employed. Thus, one possible explanation for the observed structure is the existence of a rotational barrier which splits the  $K'=2$  and  $K'=3$  rotational levels. The individual components of  $K'=3$  are presumably unresolved, but contribute to the line width of the  $S_1(1)$  transition. If this explanation were completely correct, the splitting of  $K'=2$  level is a very sensitive measure of the rotational barrier. Determining the barrier from the splitting of the  $K'=2$  level and the data given by Devonshire,<sup>19</sup> the results shown in Table VI arise for the rotational levels. The rotational constant has been assumed to remain unchanged in the solid. Even within our rather large experimental error, the observations can not be explained by a rotational barrier alone. In particular the  $[Q_1(1)+Q_{21}(1)] - P_1(1)$  separation for OH is in violent disagreement.

The much larger solid perturbation in  $[Q_1(1)+Q_{21}(1)] - P_1(1)$  for OH can be explained by rotation-translation coupling.<sup>20, 3</sup> This



results if in the solid the molecule rotates about a point, called the center of interaction, which does not correspond to the center of mass. This leads to a coupling between the constrained translational and the rotational motion of the molecule. The coupling depends on the difference between the center of mass and the center of interaction, which is given by A. Friedmann and Kimel<sup>20</sup> show that the energy perturbation on the  $K^{\text{th}}$  rotational level,  $\Delta E(K)$ , is approximately given by

$$\frac{\Delta E(K)}{hc} = \frac{BmA^2\xi}{2I} \left[ 1 - \frac{2\xi(K^2+K+1)-4K(K+1)}{(\xi-2K)(\xi+2K+2)} \right] \quad (1)$$

Here  $B$  is the rotational constant,  $m$  is the molecular mass,  $I$  the moment of inertia, and  $\xi$  is the translational frequency in units of  $B$  of the diatomic in the solid site. The other parameters have either been previously defined or have their usual meaning. Employing this perturbation approach, the coupling parameter  $A$  can be determined from the observed  $[Q_1(1)+Q_{21}(1)]-P_1(1)$  separation for OH. The other necessary quantity is the translational frequency  $\xi$  of OH in the Ne site. This was estimated by a method suggested by Friedman and Kimel<sup>20</sup> from a harmonic-oscillator model using a Leonard-Jones (6, 12) interaction potential with parameters for Ne-Ne approximating the OH-Ne parameters. The translational frequency for OH is reasonably expected to be roughly the value given in Table VI, which is near the Debye maximum for solid Ne.<sup>21</sup> Given the translational frequency and the coupling parameter, the relative positions of all the

OH and OD rotational levels are in principle calculable from Eq. (1). The results are presented in Table VI. The important point to note is that the large  $Q_1(1)$ - $P_1(1)$  perturbation for OH and at the same time the very small perturbation for OD can be readily explained.

The  $K' = 2$  rotational level in OD is also only slightly perturbed. This level can not be calculated from perturbation theory for OH since a near resonance with the translational frequency occurs. Similar behavior occurs for OD at  $K' = 3$ . It may be that one of the two lines observed in the  $R_1(1) + R_{21}(1)$  region corresponds to absorption to the level wherein one quantum of the translational motion is excited. This mixes with the rotational states by the translation-rotation coupling and thereby steals intensity. The lines at  $32415 \text{ cm}^{-1}$  for OH and  $32506 \text{ cm}^{-1}$  for OD are  $67$  and  $72 \text{ cm}^{-1}$ , respectively, to high energy of the  $P_1(1)$  line and could possibly be the translational quantum. This leaves the line at  $32486 \text{ cm}^{-1}$  as the  $R_1(1) + R_{21}(1)$  line for OD which then has a very small rotational energy shift from the gas phase. For OH the line at  $32455 \text{ cm}^{-1}$  is then assigned to  $R_1(1) + R_{21}(1)$ . It is presumably perturbed quite strongly by the nearby, but lower lying, translational level and is, thus, pushed to higher energy. Although the local translational frequency appears closer to the  $R_1(1) + R_{21}(1)$  line for OD, the translation-rotation coupling is much less for OD so that resonance interactions do not push the levels apart. A serious problem with the above assignment is the relative intensities of the various lines in OH and OD. The line that is tentatively assigned to the translation is more intense in OD than in OH.

Neither of the two mechanisms discussed above need by themselves explain the data since both the static crystal-field interaction and the dynamic translation-rotation coupling can simultaneously occur. Moreover, coupling to lattice phonons can perturb the levels further. In summary, it seems that the  $K'=1$ ,  $K'=0$  separation in the  $A^2\Sigma^+$  state can be reasonably explained by rotation-translation coupling. However, for  $K'>1$  the situation is less clear. An "exact" fit of the experimental data could possibly be made by treating both the coupling parameter and the translation frequency as parameters and diagonalizing the Hamiltonian matrix.<sup>3</sup> However, our experimental data does not warrant this at present.

The author gratefully acknowledges the support and encouragement given him by Professor G. W. Robinson. He also thanks S. Wei for allowing him to examine his unpublished data.

REFERENCES

- <sup>1</sup>A. Cabana, G. B. Savitsky, and D. F. Hornig, J. Chem. Phys. 39, 2942 (1963).
- <sup>2</sup>R. L. Redington and D. E. Milligan, J. Chem. Phys. 39, 1276 (1963); 37, 2162 (1962).
- <sup>3</sup>L. F. Keyser and G. W. Robinson, J. Chem. Phys. 44, 3225 (1966) and references therein.
- <sup>4</sup>D. E. Milligan, R. M. Hexter, and K. Dressler, J. Chem. Phys. 34, 1009 (1961).
- <sup>5</sup>G. W. Robinson and M. McCarty, Jr., J. Chem. Phys. 30, 999 (1959).
- <sup>6</sup>M. McCarty, Jr. and G. W. Robinson, J. Am. Chem. Soc. 81, 4472 (1959) and references therein.
- <sup>7</sup>L. F. Keyser, Thesis, California Institute of Technology, 1965.
- <sup>8</sup>G. W. Robinson and M. McCarty, Jr., J. Chem. Phys. 28, 350 (1958); Can. J. Phys. 36, 1590 (1958); M. McCarty, Jr., Thesis, The John Hopkins University, 1960.
- <sup>9</sup>S. Wei, private communication.
- <sup>10</sup>D. S. Tinti and G. W. Robinson, manuscript in preparation.
- <sup>11</sup>R. G. Bennett and F. W. Dalby, J. Chem. Phys. 40, 1414 (1964).
- <sup>12</sup>G. Herzberg, Molecular Spectra and Molecular Structure. I. Spectra of Diatomic Molecules (D. Van Nostrand, Inc., New York, 1950), pp. 151, 560.

- <sup>13</sup>R. S. Mulliken, Phys. Rev. 32, 388 (1928).
- <sup>14</sup>C. E. Moore and H. P. Broida, J. Res. Natl. Bur. Std. (U.S.) A63, 279 (1959).
- <sup>15</sup>H. Oura and M. Ninomiya, Proc. Phys. Math. Soc. (Japan) 25, 335 (1943).
- <sup>16</sup>L. T. Earls, Phys. Rev. 48, 423 (1935).
- <sup>17</sup>C. S. Barrett and L. Meyer, J. Chem. Phys. 42, 107 (1965); 43, 3502 (1965); C. S. Barrett, L. Meyer, and J. Wasserman, J. Chem. Phys. 44, 998 (1966).
- <sup>18</sup>M. T. Bowers and W. H. Flygare, J. Chem. Phys. 44, 1389 (1966).
- <sup>19</sup>A. F. Devonshire, Proc. Roy. Soc. (London) A153, 601 (1936); W. H. Flygare, J. Chem. Phys. 39, 2663 (1963).
- <sup>20</sup>H. Friedmann and S. Kimel, J. Chem. Phys. 43, 3925 (1965).
- <sup>21</sup>J. Grindlay and R. Howard, in Lattice Dynamics, edited by R. F. Wallis (Pergamon Press, New York, 1965), p. 129; G. L. Pollack, Rev. Mod. Phys. 36, 748 (1964).

TABLE I.  $A^2\Sigma^+-X^2\Pi_1$  system of OH in solid neon.

	$v', v''$	$\nu_{\text{vac}}$ ( $\text{cm}^{-1}$ )	Relative Intensity	Assignment
Absorption	0,0	32455	m	$Q_1(1)+Q_{21}(1)$ $P_1(1)$
		32415	w	
		32372	m	
		32348	s	
	1,0	*		
Emission	0,0	32347	vs	$P_1(1)$
		32310	vw	
		32277	vw	$P_{12}(1)$ $O_2(2)$
		32203	s	
		32152	w	
	0,1	28774	vw	$P_1(1)$ $P_{12}(1)$
		*		
	1,0	35317	ms	$P_1(1)$
		35245	vw	
		35174	m	$P_{12}(1)$ $O_2(2)$
		35119	vw	
	1,1	31745	s	$P_1(1)$
		31718	vw	
		31678	vw	$P_{12}(1)$ $O_2(2)$
		31597	m	
		31548	vw	
	2,0	38101	w	$P_1(1)$ $P_{12}(1)$ $O_2(2)$
		37958	vw	
		*		
	2,1	34528	ms	$P_1(1)$
		34452	vw	
		34383	m	$P_{12}(1)$ $O_2(2)$
		*		
	2,2	31120	m	$P_1(1)$ $P_{12}(1)$ $O_2(2)$
		30976	w	
		*		

\* observed, but not accurately measured.

TABLE II.  $A^2\Sigma^+-X^2\Pi_i$  system of OD in solid neon.

	$v', v''$	$\nu_{\text{vac}}$ ( $\text{cm}^{-1}$ )	Relative Intensity	Assignment
Absorption	0, 0	32560	vw	$S_1(1)$
		32506	m	
		32486	w	
		32449	m	$Q_1(1)+Q_{21}(1)$
		32434	s	
	1, 0	34702	w, b	$Q_1(1)+Q_{21}(1)$
		34650	w	
		34636	m	
	2, 0	*		
Emission	0, 0	32434	vs	$P_1(1)$
		32386	vw	
		32282	s	$P_{12}(1)$
		32246	vw	$O_2(2)$
	0, 1	overlap with VK 0, 9 <sup>†</sup>		
	1, 0	34634	ms	$P_1(1)$
		34573	vw	
		34486	m	$P_{12}(1)$
		34447	vw	$O_2(2)$
	1, 1	32000	s	$P_1(1)$
		overlap with VK 0, 8		
	1, 2	29450	vw	$P_1(1)$
		29298	vvw	$P_{12}(1)$
	2, 0	36733	w	$P_1(1)$
		36580	vw	$P_{12}(1)$
	2, 1	34101	ms	$P_1(1)$
		overlap with VK 0, 7		
	2, 2	31554	m	$P_1(1)$
		31401	mw	$P_{12}(1)$
		*		$O_2(2)$

TABLE II. (Cont'd.)

2,3	29092 28936	vw vvw	$P_1(1)$ $P_{12}(1)$
3,1	overlap with VK 0,6		
3,2	33555 33406 33367	m mw vvw	$P_1(1)$ $P_{12}(1)$ $O_2(2)$
3,3	*		
4,3	32999 32849	vw vvw	$P_1(1)$ $P_{12}(1)$

\* Observed, but not accurately measured.

† VK = Vegard-Kaplan system of  $N_2$ .



TABLE III. Molecular constants of OH and OD in solid neon.  
All entries are in  $\text{cm}^{-1}$ .

State		OH		OD	
		Gas <sup>a</sup>	Solid	Gas <sup>a</sup>	Solid
$A^2\Sigma^+$	$\omega_e$	3180.5	3154.5±0.3	2319.9	2295.1±1.4
	$\omega_e x_e$	94.93	92.6±0.7	52.0	48.5±0.3
$X^2\Pi_1$	$\omega_e$	3735.2	3735.2±0.4	2720.9	2716.5±1.5
	$\omega_e x_e$	82.81	81.2±0.3	44.2	41.9±0.5

<sup>a</sup>Ref. 12.

TABLE IV. Summary of gas and solid data for 0, 0 band.

Isotope	Transition	Gas <sup>a</sup>		Solid		Gas-Solid (cm <sup>-1</sup> )
		cm <sup>-1</sup>	Relative Intensity	cm <sup>-1</sup>	Relative Intensity	
OH	S <sub>1</sub> (1)	32643	0.49			
	R <sub>1</sub> (1)+R <sub>21</sub> (1)	32542	4.30	32455	m	87
				32415	w	127
	Q <sub>1</sub> (1)+Q <sub>21</sub> (1)	32474	10.00	32372	m	102
	P <sub>1</sub> (1)	32441	6.18	32348	s	93
	P <sub>12</sub> (1)	32314	3.50	32203	m	112
OD	O <sub>2</sub> (2)	32253	0.81	32152	vw	101
	S <sub>1</sub> (1)	32637	0.70	32560 <sup>b</sup>	vvw	77 <sup>b</sup>
	R <sub>1</sub> (1)+R <sub>21</sub> (1)	32583	4.70	32506	m	77
				32486	w	97
	Q <sub>1</sub> (1)+Q <sub>21</sub> (1)	32547	10.00	32449	m	98
	P <sub>1</sub> (1)	32530	5.97	32434	s	96
	P <sub>12</sub> (1)	32399	3.57	32282	m	117
	O <sub>2</sub> (2)	32367	1.17	32246	w	121

<sup>a</sup>OH, Ref. 14; OD, Ref. 15.<sup>b</sup>± 10 cm<sup>-1</sup>.

TABLE V. Summary of discussed energy differences.  
All entries in  $\text{cm}^{-1}$ .

	OH		OD	
	Gas <sup>a</sup>	Solid	Gas <sup>b</sup>	Solid
$P_1(1)-P_{12}(1)$	126	144	131	152
$P_{12}(1)-O_2(2)$	61	52	32	38
$Q_1(1)-P_1(1)$	33	24	17	16
$R_1(1)-Q_1(1)$	68	43, 83	36	37, 57
$S_1(1)-R_1(1)$	101		54	68, 48

<sup>a</sup>Ref. 14.

<sup>b</sup>Ref. 15.

TABLE VI. Observed structure in the 0, 0 band interpreted in terms of a static crystal field interaction.  
All entries are in  $\text{cm}^{-1}$ .

Barrier <sup>a</sup>		$Q_1(1)-P_1(1)$	$R_1^a(1)-Q_1(1)$	$R_1^b(1)-Q_1(1)$
OH	Obs.	24	43	83
	-97	35	48	88
	+85	34	56	96
OD	Obs.	16	37	57
	-45	18	30	50
	+41	18	27	47

<sup>a</sup>Barrier determined from splitting of  $K'=2$  level ( $R_1^b-R_1^a$ ) as discussed in text.

TABLE VII. Observed structure in the 0, 0 band interpreted in terms of rotation-translation coupling. All entries are in  $\text{cm}^{-1}$ , except where noted.

	Translation Frequency	$A_{\text{O}}^{\dagger}$ (Å)	$Q_1(1)-P_1(1)$		$R_1(1)-Q_1(1)$	
			Calc.	Obs.	Calc.	Obs.
OH	58	0.15	--	24	n. r.	43, 83
OD	57	0.094	16	16	32	37, 57

$^{\dagger}$  Difference between the center of mass and the center of interaction.

n. r. = near resonance.

Fig. 1. Microphotometer tracing of a portion of the absorption spectra of OH and OD in solid Ne.

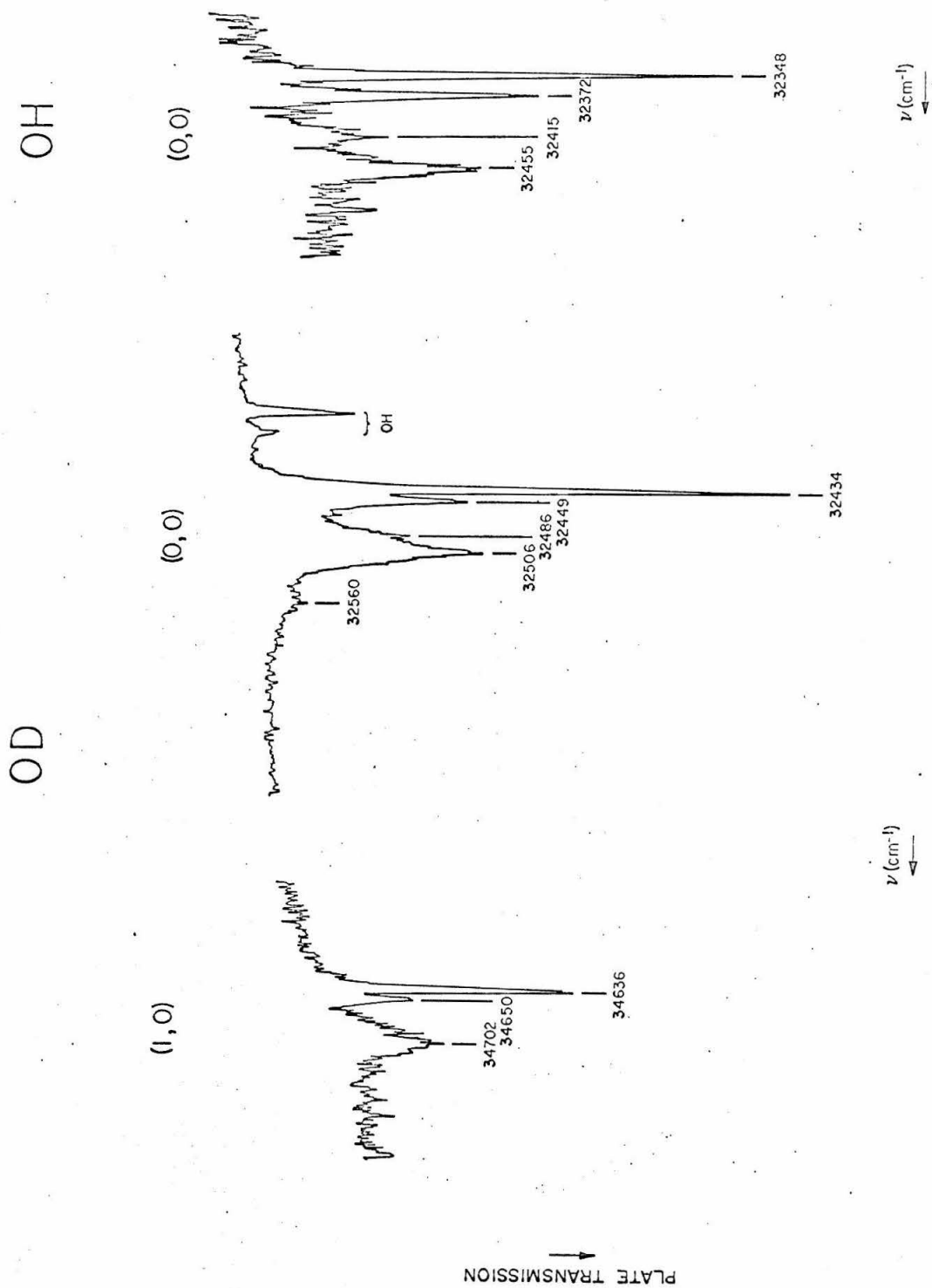


Fig. 2. Microphotometer tracing of the 0,0 band of OH and OD observed in emission in solid Ne.



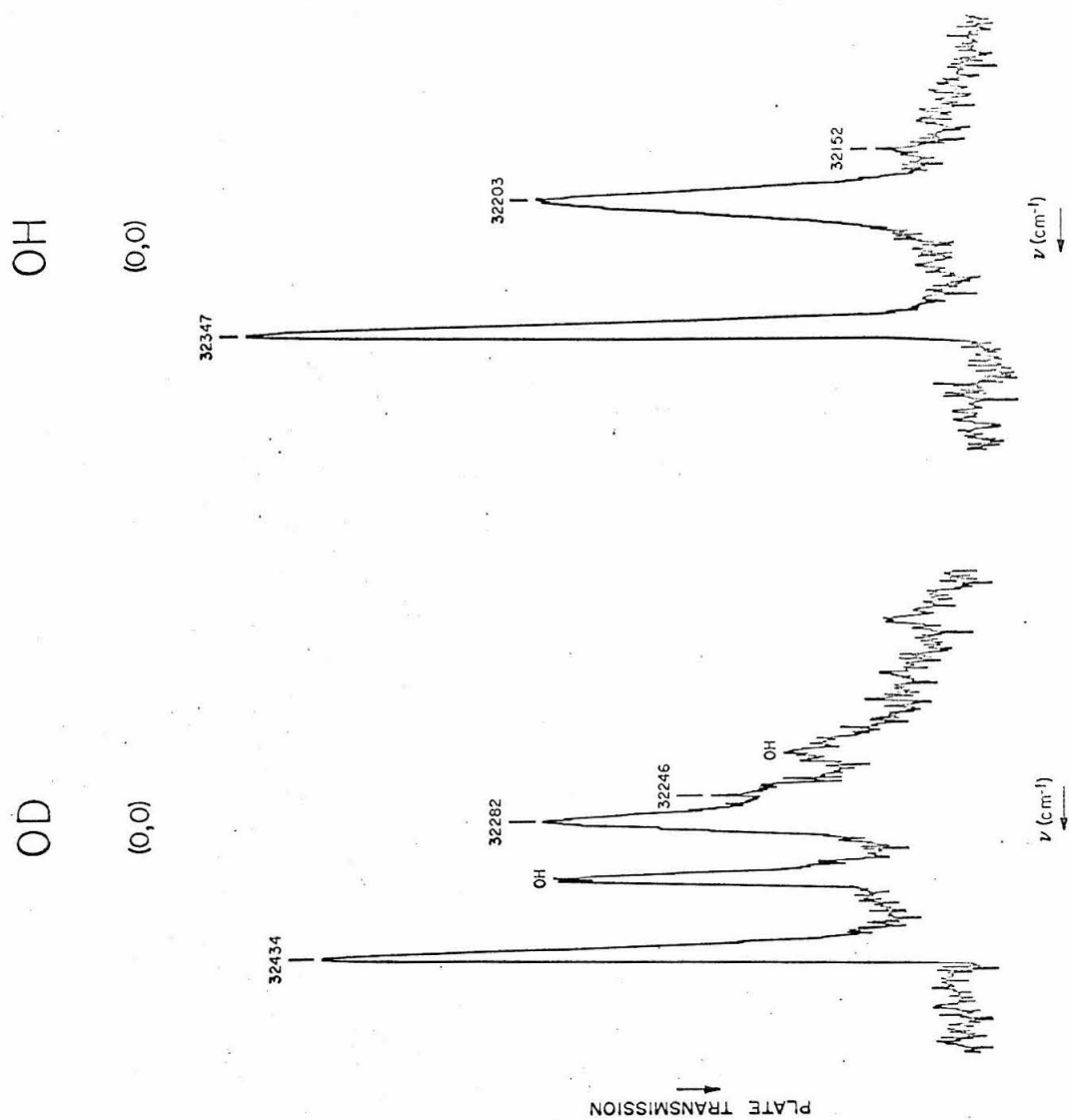
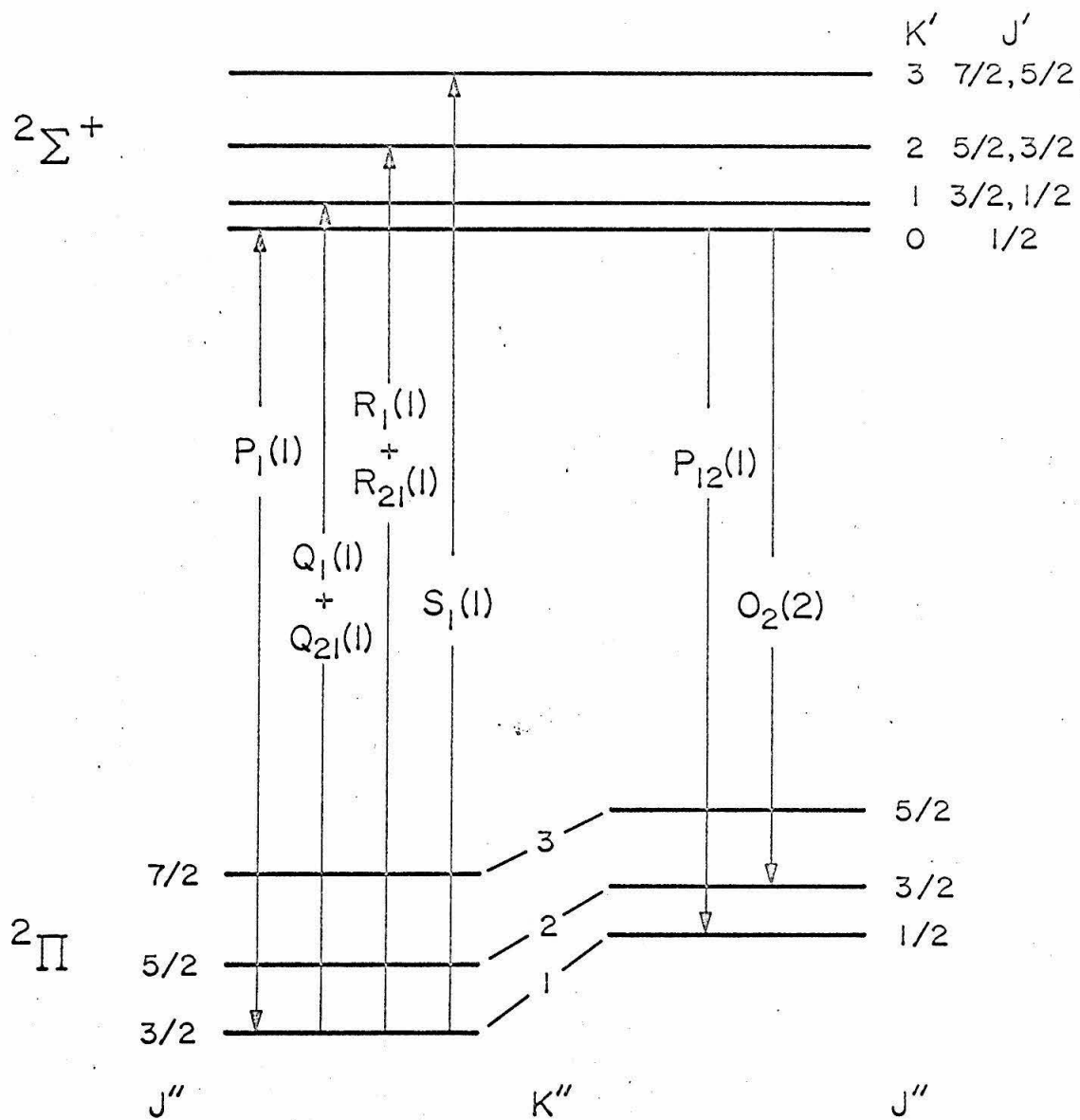


Fig. 3.  $A^2\Sigma^+ - X^2\Pi_1$  schematic energy level diagram.



Geometry of the Lowest Triplet State of Benzene\*

G. C. NIEMAN<sup>†</sup> AND D. S. TINTI<sup>‡</sup>

Gates and Crellin Laboratories of Chemistry<sup>§</sup>

California Institute of Technology, Pasadena, California 91109

(Received

ABSTRACT

The phosphorescence, fluorescence and absorption spectra of seven isotopic benzenes in a  $C_6D_6$  host crystal were obtained at 4.2° K. The isotopes having less than  $D_{3h}$  symmetry show splittings in their phosphorescence and singlet absorption spectra. Expected splittings in the fluorescence spectrum have not yet been observed because of the greater difficulty in obtaining the required high resolution fluorescence spectra. The splittings are interpreted in terms of a distortion, which may arise either from extrinsic or intrinsic perturbations, in the  $^1B_{2u}$  and  $^3B_{1u}$  states of crystalline benzene. This distortion causes conformers of isotopic benzenes with less than trigonal symmetry to have different zero-point energies and leads to the observed line multiplicity. The vibronic

---

\* Work supported in part by the U. S. Army Research Office.

<sup>†</sup> NSF Predoctoral Fellow. Present Address: Department of Chemistry, University of Rochester, Rochester, New York. A portion of this work was included in a thesis presented by G. C. Nieman in partial fulfillment of the requirements of the degree of Doctor of Philosophy in Chemistry at the California Institute of Technology, Pasadena, California, 1965.

<sup>‡</sup> NASA Trainee.

<sup>§</sup> Contribution No. 3374. This section originally appeared in J. Chem. Phys. 46, 1432 (1967).

structure of the phosphorescence and fluorescence emissions implies that the magnitude of the distortion is small.

Benzene molecules in the low-symmetry crystalline field are not expected to retain a hexagonal shape. However, the splittings in the fluorescence are only about  $1/8$  as large as those in the phosphorescence, implying that the distortion in the  $^3B_{1u}$  state is larger than that in the  $^1B_{2u}$  state. There is therefore some cause to believe that the distortion in the  $^3B_{1u}$  state is partly intrinsic and thus has the significance attached to it by theorists. Our experiments, however, cannot actually distinguish between intrinsic and extrinsic distortions, but certainly give the impression that the distortion of the  $^3B_{1u}$  state of benzene in the crystal is not very substantial and is either wholly or partly caused by the effect of the crystal field.

The relative intensities of the components of the multiplet structure in the phosphorescence are strongly concentration dependent because of trap-to-trap excitation migration in the crystal. At low guest concentrations, where little migration can occur, the intensity ratio gives the statistical weights of the components; at high concentrations a Boltzmann intensity ratio is obtained. The interpretation of the available optical data can be made to agree with the interpretation of ESR results by de Groot, Hesselmann, and van der Waals that a distorted  $^3B_{1u}$  benzene is preferentially oriented in the site cavity of the solid phase, but the resulting picture is not a wholly satisfying one.


## 1. INTRODUCTION

Over twenty years ago in the classic paper entitled "Phosphorescence and the Triplet State" by Lewis and Kasha<sup>1</sup> it was stated "...there must be a peculiar distortion of the benzene molecule in the phosphorescent state." That supposition was based on two arguments: 1) The weakness of the 0,0 band relative to other vibronic components of the spectrum, and 2) an energetic argument that predicted no resonance energy in the triplet state. In addition, chemical intuition seemed to dictate a quinoidal structure for benzene in its lowest triplet state. These arguments were extended by Redlich and Holt.<sup>2</sup>

We know that this line of reasoning would probably not now lead to the conclusion that the benzene molecule is distorted in its phosphorescent state. It is now known that the weakness of the 0,0 band is caused not by the Franck-Condon effect operating between a distorted excited state and a hexagonal ground state but instead is a manifestation of the  $D_{6h}$  symmetry selection rules for transitions,<sup>3,4</sup> which in the absence of external fields or molecular distortions would predict a zero electric dipole contribution to the 0,0 band of the  $^3B_{1u} - ^1A_{1g}$  transition. In addition, the energetic arguments of Lewis and Kasha are now difficult to follow in view of modern knowledge about molecular electronic energy computations. A loss of "resonance energy" in the triplet state would imply a major distortion of the molecule, an effect that does not appear to take place in view of the similarity between the vibronic structure in the phosphorescence spectrum and the fluorescence spectrum of benzene. This latter point still requires clarification though a more detailed study of the  $^3B_{1u} - ^1A_{1g}$  absorption spectrum, a difficult experiment considering the  $\sim 10^{-10}$  oscillator strength<sup>5</sup> for the transition!

Even though the arguments of Lewis and Kasha might not be used today, the fact remains that in 1944 the suggestion that a polyatomic molecule could completely change its shape on electronic excitation was bold indeed and would not be proved by spectroscopists to be a common phenomenon among polyatomics until fully ten years later.<sup>6</sup> Our intuition, based now on a large amount of experimental data, would suggest that there is no general reason to expect any excited electronic state to have the same nuclear configuration as the ground state. In particular, excitation of an electron into an antibonding orbital might be expected to lead to energy stabilization and molecular distortion through bond rehybridization. When the change of geometry is subtle, as it may be in the benzene triplet, rather more than a casual look at a low resolution optical spectrum may be needed, however, to prove the point for or against distortion.

The present paper begins by giving a brief theoretical background to the problem of nonhexagonal benzene. Optical experiments are then described that show the lowest excited states of benzene in the crystalline state to be nonhexagonal.





## 2. THEORETICAL BACKGROUND

More recent interest in the structure of triplet benzene was kindled by the work of Moffitt and Liehr. A paper by Moffitt<sup>7</sup> on the electronic structure of cyclic polyenes having the general formula  $C_{4\nu+2}H_{4\nu+2}$  lays the theoretical ground work for the later calculation by Liehr<sup>8</sup> of vibronic interactions in benzene. Moffitt considers the ground state and the four states from the lowest excited configuration  $(a_1)^2 (e_1)^4 \dots (e_\nu)^3 (e_{\nu+1})$ . Mixing only among the four excited states was taken into account. In benzene,  $\nu = 1$ , and it is well known<sup>9</sup> that the four excited states in question belong to spatial representations  $B_{1u}$ ,  $B_{2u}$ , and  $E_{1u}$  of the point group  $D_{6h}$ . Triplet states were not considered explicitly, but within the framework of Moffitt's approximations, the results for singlets and triplets are identical. Moffitt showed that if atomic orbital overlap were neglected in a  $2p\pi$  basis representation, "one-electron perturbations" mixing the four excited states take a remarkable and particularly simple form. In the first place, such one-electron perturbations do not connect the  $B_{1u}$  state with the  $B_{2u}$  state nor can they mix the components of the doubly degenerate  $E_{1u}$  state. Thus a splitting of the  $E_{1u}$  state will not take place in first order; splitting will take place in second order, however, since one component of the  $E_{1u}$  state is mixed with  $B_{1u}$  and the other component is mixed with  $B_{2u}$  (see Fig. 1 of Ref. 7).



Moffitt defined even and odd perturbations, respectively, as those which arise in the perturbation problem by connecting atomic orbital basis functions on carbon atom positions whose numbering differs by even (including zero) and odd integers. He showed that a purely even one-electron perturbation would mix the  $B_{2u}$  state with one component of the  $E_{1u}$  state, and a purely odd one-electron perturbation would mix  $B_{1u}$  with the other component of  $E_{1u}$ . As a first approximation, vibronic interactions can be expressed as a sum of single electron operators, the effects of nuclear displacements on electron-electron repulsion supposedly giving an energy contribution in a higher order. Thus, roughly speaking, vibronic interactions can be considered one-electron perturbations and Moffitt's results can be applied. Furthermore, considering C-C stretching vibrations only, the vibronic perturbation is "odd", and only the  $B_{1u}$  state mixes with the  $E_{1u}$  state. This means that a vibronic interaction of the type considered is expected to be much more effective in perturbing the  $^{1,3}B_{1u}$  states of benzene than the  $^{1,3}B_{2u}$  states. Consistent with this theoretical viewpoint is the experimental observation<sup>4</sup> that a primarily "C-C stretching" vibration is responsible for intensity in the  $^3B_{1u} - ^1A_{1g}$  transition but not in the  $^1B_{2u} - ^1A_{1g}$  transition. It is presumed here that intensity enhancement depends on vibronic mixing with the respective  $^3E_{1u}$  or  $^1E_{1u}$  state. A "carbon bending" vibration would give rise to much smaller odd-type perturbation terms and would contain even terms as well. Thus carbon bending vibrations can perturb both  $B_{1u}$  and  $B_{2u}$  states, but to a smaller extent than the stretching vibrations. Moffitt's general conclusions would therefore indicate that the  $^3B_{1u}$  state of benzene stands to be distorted to a greater extent than does the  $^1B_{2u}$  state through coupling of the electrons to C-C bond stretching motions. The larger energy denominator for the

singlet ( $\sim 16,500 \text{ cm}^{-1}$ )<sup>10</sup> compared with that for the triplet ( $\sim 6900 \text{ cm}^{-1}$ )<sup>11</sup> would further decrease the extent of  $E_{1u}$  mixing and distortion of the lowest singlet compared with the lowest triplet of benzene.

Extension of Moffitt's theory to include the variation of electronic energy with nuclear displacement and the numerical evaluation of the matrix elements themselves has been supplied by Liehr.<sup>8</sup> Considering the  $^1B_{1u}$  and  $^1E_{1u}$  states to be exactly degenerate in the hexagonal configuration, instead of being split by around 1 e.v. by interelectronic repulsion as they are in the real molecule, Liehr found that the Jahn-Teller depression energy for a  $D_{2h}$  distortion is  $2005 \text{ cm}^{-1}$  and  $2510 \text{ cm}^{-1}$ , respectively, depending on whether the molecule has two short bonds in the 1, 2 and 4, 5 positions as in a quinoidal structure, or two long bonds in these positions ("nonquinoidal  $D_{2h}$  structure"). He concluded therefore that there was a definite possibility that the molecule is deformed in such a  $B_{1u}$  state. According to this calculation, there is a  $505 \text{ cm}^{-1}$  barrier for pseudo-rotation between the three possible minima corresponding to the low energy structure. When one takes into account the empirical 1 e.v. energy difference between the  $^3B_{1u}$  and  $^3E_{1u}$  states, Liehr's vibronic energies would have to be approximately doubled to give second-order contributions of comparable magnitude as those quoted in his paper.

A rather serious criticism of Liehr's paper concerns his use of the Lennard-Jones or harmonic approximation<sup>12</sup> for the estimation of the bond length dependence of  $\pi$ -electron energies. More recent work<sup>13</sup> has indicated that this is a relatively poor approximation. A better one for some purposes is an exponential dependence used by Longuet-Higgins and Salem.<sup>14</sup> As pointed out by Hobey and McLachlan,<sup>13</sup> the Lennard-Jones approximation leads to a positive value of the second derivative of the  $\pi$ -electron resonance energy

with distance, while the Longuet-Higgins and Salem approximation leads to a negative value for  $\beta''(r)$ . Hobe and McLachlan show that for the negative ions of molecules having in their undistorted configuration a 3- or 6-fold symmetry axis (e.g., benzene, coronene, and triphenylene), the total  $\underline{D}_{2h}$  distortion energy consists of two parts: a Jahn-Teller energy depending upon  $\beta'(r)$  and equal in magnitude for the two distorted forms, and a contribution depending upon  $\beta''(r)$  which has a positive sign for one distorted configuration and a negative sign for the other. Thus the nature of the energetically lowest configuration depends upon the sign of  $\beta''$ , and the theoretically predicted stable configuration may therefore be different depending upon what approximation is used for  $\beta(r)$ . In particular, the Longuet-Higgins and Salem approximation favors the quinoidal structure of the benzene ion while the Lennard-Jones approximation favors the nonquinoidal structure! These same arguments can be carried over to the neutral molecule states.

de Groot and van der Waals<sup>15</sup> have considered the theoretical problem of conformational isomerism in the benzene  $^3B_{1u}$  state. Using the Longuet-Higgins and Salem approximation for  $\beta(r)$  and assuming  $\underline{D}_{2h}$  distortions, these authors found a stabilization energy of  $1520 \text{ cm}^{-1}$  for the quinoidal structure and  $1000 \text{ cm}^{-1}$  for the nonquinoidal  $\underline{D}_{2h}$  structure. The  $520 \text{ cm}^{-1}$  separation between these two forms is in good quantitative agreement with the calculation of Liehr except that the stabilization energy is in an opposite sense (!), the quinoidal structure being more stable, according to deGroot and van der Waals, than the nonquinoidal structure. This is just what one would expect following the Hobe and McLachlan arguments. But it is certainly disconcerting to the experimentalist who might well conclude that the theoretical calculations thus far have shown the quinoidal and nonquinoidal  $\underline{D}_{2h}$  forms of benzene to have the same energy within a rather wide limit of uncertainty.

Yet the calculations so far have been relatively crude in the kinds of approximations they have employed. Only C-C bond stretching distortions have been considered. Bond bending and the out-of-plane degree of freedom might well be considered in future calculations.

Lacking at the moment these more sophisticated results, one must resort to experimentation in order to shed light on the question of the structure of benzene in its lowest triplet state. In the next few sections results of fluorescence and phosphorescence measurements in isotopic mixed crystals of benzene will be discussed. Some new absorption measurements will be mentioned briefly. These results show that the lowest triplet state and, to a lesser extent, the lowest excited singlet state of crystalline benzene deviate from the hexagonal form. Afterwards, the ESR results of deGroot and van der Waals<sup>15</sup> will be compared with the optical spectroscopic results.

### 3. EXPERIMENTAL

Spectra of seven partially deuterated benzenes dissolved as guests in a  $C_6D_6$  host crystal have been photographed at 4.2° K. The molecules studied are:  $C_6H_6$ ,  $C_6H_5D$ , 1,4- $C_6H_4D_2$ , 1,3- $C_6H_4D_2$ , 1,3- $C_6H_2D_4$ , 1,3,5- $C_6H_3D_3$ , and 1,2,4- $C_6H_3D_3$ . Because of zero-point effects (vide infra) there is a shift of the 0,0 transition to lower energy by approximately  $33\text{ cm}^{-1}$  per hydrogen atom substituted into  $C_6D_6$ . Thus at 4.2° K more highly protonated species act as effective energy traps from which emission is observed. To avoid effects caused by trap-to-trap excitation transfer to chemical impurities,<sup>16</sup> solute concentrations between 0.01% and 1.0% were generally used.

All benzenes were obtained from commercial sources except for the 1,2,4- $C_6H_3D_3$  which was synthesized by one of us (GCN). The isotopic

purity was found to be adequate for all the benzenes since emission from isotopic impurities was spectroscopically well resolved and could easily be characterized. Samples of adequate chemical purity were prepared by vacuum sublimation. Further purification with metallic cesium<sup>11</sup> did not alter the emission spectra assigned to the isotopes of benzene.

Crystals having a thickness of 1-10 $\mu$  were prepared by freezing the liquid mixture between quartz plates, the entire process being carried out in a nitrogen atmosphere. Crystals 1-3mm thick were grown from the liquid mixture in a sealed-off quartz cell. The cell was later broken open under the liquid helium to achieve good thermal contact with the helium bath. Both methods of growing the isotopically mixed crystals gave identical emission spectra, but, presumably because of more complete absorption of the exciting light and better degassing, emission from the thicker crystals was more intense.

Most of the phosphorescence spectra were obtained in the second or third orders of a 15,000 line-per-inch grating in a two-meter mount. Fluorescence and absorption spectra were taken in third order. A few plates, showing better than double this resolution, of the phosphorescence and the absorption spectra, were obtained<sup>17</sup> in the third and fourth orders of a Jarrell-Ash 3.4 meter photographic instrument equipped with a 15,000 line/in. grating. Good fluorescence spectra have been more difficult to obtain on the higher resolution instrument. Such spectra will be reported at some future time. When more accurate intensity measurements were desired, the spectra were studied using a Jarrell-Ash 1.8 meter photoelectric scanning spectrometer. No absorption from chemical impurities was seen to the long wavelength side of the benzene cutoff at about 2650 Å. Exposure times on the 2-meter spectrograph for the more intense vibronic components



were about five minutes in the thick samples for both phosphorescence and fluorescence. Because of their sharpness, phosphorescence spectra on the larger photographic instrument required only slightly extended exposure times. A representative part of a microphotometer trace of the lower resolution phosphorescence spectrum of one of the isotopes is shown in Fig. 1. Phosphorescence line widths as observed on the large spectrograph are apparently less than  $1 \text{ cm}^{-1}$  and may be instrument limited. The best line width that could be obtained with the 2-meter spectrograph was around  $1 \text{ cm}^{-1}$ . Because of the lower  $\text{cm}^{-1}$  dispersion in the fluorescence region, the experimental linewidth was about a factor of two greater.



#### 4. VIBRONIC STRUCTURE OF FLUORESCENCE AND PHOSPHORESCENCE

Before discussing the details of the observed spectra we will briefly describe the general features of benzene phosphorescence and fluorescence as observed from isotopic guests in a  $C_6D_6$  host crystal. A more complete description of the spectra will be given in another paper. The lowest triplet state of undistorted benzene most likely has  $B_{1u}$  symmetry in point group  $D_{6h}$  and is thus both spin and electronically forbidden. Most of the transition probability is thought to arise from vibronic coupling of the  $^3B_{1u}$  state with the nearby  $^3E_{1u}$  state which in turn is mixed with the  $^1E_{1u}$  state by spin-orbit coupling.<sup>18</sup> The proposed reduction of the symmetry of the triplet state from  $D_{6h}$  does not appear to greatly alter this mixing scheme since the phosphorescence spectrum is basically that of a vibrationally-induced, electronically-forbidden transition. In fact the major vibronic features in both the fluorescence and phosphorescence spectra of all isotopic modifications are best described on the basis of an equilibrium nuclear configuration of hexagonal shape. That is to say, the vibrations most active in inducing the electronic transitions either have  $e_{2g}$  symmetry or correlate with these same  $D_{6h}$  normal coordinate motions for the partially deuterated species.

In a discussion of emission spectra at low temperatures it must be remembered that only ground state vibrations appear. The most active vibration in the phosphorescence spectrum of  $C_6H_6$  is the  $e_{2g}$  mode at  $1595\text{ cm}^{-1}$ . Within the line width of  $1\text{ cm}^{-1}$ , the twofold degeneracy of this vibration does not appear to be removed by the low symmetry of the crystal field, i. e., there is in general no observable site group splitting.<sup>19</sup>

This mode is somewhat complicated by Fermi resonance with the  $606 + 990 \text{ cm}^{-1}$  ( $e_{2g} + a_{1g}$ ) vibration. There is intensity stealing from the strong  $1595 + n \times 990 \text{ cm}^{-1}$  progression by the very weak  $606 + (n + 1) \times 990 \text{ cm}^{-1}$  progression. The  $606 \text{ cm}^{-1}$  mode alone is observed to be only ~10% as intense as it is when in resonance with the  $1595 \text{ cm}^{-1}$  modes. This fact is in qualitative agreement with the previously discussed conclusions of Moffitt that a primarily odd perturbation, such as would arise in a C-C stretching motion, is most effective in vibronic interactions between  $B_{1u}$  and  $E_{1u}$  states. The  $e_{2g}$  CH bending mode at  $1175 \text{ cm}^{-1}$  is also weakly active. Weaker yet are the  $b_{2g}$   $1004 \text{ cm}^{-1}$  <sup>20</sup> and  $703 \text{ cm}^{-1}$  vibrations and the totally symmetric  $a_{1g}$   $990 \text{ cm}^{-1}$  progression. It should be remembered at this point that in the crystal site, where the only symmetry element is inversion, <sup>23</sup> mixing among all of the  $g$ -vibrations can occur to various extents. The presence of  $b_{2g}$  and  $a_{1g}$  vibrations then need not be caused by any intrinsic property of the benzene molecule itself but may only be caused by the low symmetry of the crystal field in which the molecule resides. The fact that the other  $g$ -vibrations are not very intense implies, however, that the  $D_{6h}$  molecular classification for  $C_6H_6$  is still approximately valid even in the crystal.

Deuterium substitution changes the symmetry of the vibrational coordinates but leaves essentially unaltered the molecular electronic symmetry. For  $C_6H_5D$  the vibrational symmetry is reduced to  $C_{2v}$ , if undistorted, and the doubly-degenerate  $e_{2g}$  vibrations of  $C_6H_6$  correlate with  $a_1$  and  $b_1$  vibrations of  $C_{2v}$ . Thus in place of the  $1595 + n \times 990$  progression for  $C_6H_6$ , there are progressions of nearly equal intensity based upon the  $1591 \text{ cm}^{-1}$  ( $a_1$ ) and  $1574 \text{ cm}^{-1}$  ( $b_1$ ) vibrations. The components of



the split  $1178\text{ cm}^{-1}$  ( $e_{2g}$ ) vibration at  $1175\text{ cm}^{-1}$  ( $a_1$ ) and  $1158\text{ cm}^{-1}$  ( $b_1$ ) are seen, but they are relatively weaker than in  $C_6H_6$ . The  $1175\text{ cm}^{-1}$  component is somewhat more intense than the  $1158\text{ cm}^{-1}$  component. Very weak vibronic transitions are also seen to arise from the  $b_2$  vibrations (former  $b_{2g}$ ) at  $704\text{ cm}^{-1}$  and  $995\text{ cm}^{-1}$  as well as from other vibrations not seen in  $C_6H_6$ . A portion of the  $C_6H_5D$  phosphorescence is shown in Fig. 1.

For 1,4- $C_6H_4D_2$ , which has vibrational symmetry  $D_{2h}$  in the undistorted molecule, the degenerate  $e_{2g}$  vibrations of  $C_6H_6$  are again split. The main portion of the phosphorescence again involves the  $1569\text{ (}a_g\text{) cm}^{-1}$  and  $1587\text{ (}b_{1g}\text{) cm}^{-1}$  modes, which result from the splitting of the  $1595\text{ cm}^{-1}$  vibration of  $C_6H_6$ . All expected vibrations are seen.

There is a very strong resemblance between the phosphorescence spectra of 1,3- $C_6H_4D_2$ , 1,3- $C_6H_2D_4$ , and  $C_6H_5D$ , all of which have  $C_{2v}$  vibrational symmetry. For 1,3,5- $C_6H_3D_3$  having  $D_{3h}$  vibrational symmetry, the active degenerate modes, just as in  $C_6H_6$ , show little or no site group splitting. They occur as  $e'$  vibrations. The phosphorescence spectrum closely resembles that of  $C_6H_6$  except that Fermi resonance between the  $e'$  vibrations,  $1573\text{ cm}^{-1}$  and  $593 + 956\text{ cm}^{-1}$ , no longer occurs. The phosphorescence of 1,2,4- $C_6H_3D_3$  with vibrational symmetry  $C_{2v}$  mostly resembles that of the  $C_{2v}$  isotopes, but is more cluttered with false lines because of contamination by isotopic impurities.

In general the same ground-state vibrations are observed in fluorescence and phosphorescence, but with some intensity changes. While the  $e_{2g}\text{ }1595\text{ cm}^{-1}$  mode is the most strongly active in phosphorescence, the  $e_{2g}\text{ }606\text{ cm}^{-1}$  mode is the most active fluorescence vibration. The second strongest phosphorescence progression,  $1175 + n \times 990\text{ cm}^{-1}$  ( $e_{2g}$ ), is very weak in the fluorescence spectrum. The totally symmetric  $990\text{ cm}^{-1}$  progression is slightly more intense in fluorescence.

## 5. THE ANOMALOUS SPLITTINGS

Even though, as indicated in the preceding section, the similarities in the spectra of the isotopic benzenes can be understood in terms of group theory and the changes in the normal coordinates introduced by deuterium substitution, closer examination of the phosphorescence spectrum reveals several anomalies.

1. The phosphorescence spectra of  $C_6H_6$  and 1,3,5- $C_6H_3D_3$  in the  $C_6D_6$  host consist of single lines. However, the phosphorescence spectra of  $C_6H_5D$ , 1,3- $C_6H_4D_2$ , 1,4- $C_6H_4D_2$  and 1,3- $C_6H_2D_4$ , consist of closely spaced doublets, one component being about twice as intense as the other, while that of 1,2,4- $C_6H_3D_3$  is made up of triplets. This multiplet structure is in addition to the splitting of degenerate  $C_6H_6$  vibrations resulting from the reduced vibrational symmetry of partially deuterated benzene. It is present on all vibronic lines including the very weak 0,0.

2. Under higher resolution<sup>17</sup>, the most intense (high energy) multiplet component of the phosphorescence 0,0 band of 1,4- $C_6H_4D_2$  itself splits into a doublet. The measured splitting is  $1.9\text{ cm}^{-1}$ . For the 0,0 band of  $C_6H_5D$  no additional splittings were observed, but the high energy multiplet component is broader than the low energy component. Distinct splittings of  $1\text{--}3\text{ cm}^{-1}$  are observed on some of the other vibronic lines for  $C_6H_5D$ . One example is seen in the lower resolution spectrum shown in Fig. 1, where the high energy multiplet component of the  $1175\text{ cm}^{-1}$  band is further split by  $3\text{ cm}^{-1}$ .

3. The  ${}^1B_{2u} \rightarrow {}^1A_{1g}$  absorption spectra, insofar as they have been studied, show splittings of a nature qualitatively similar to those in the phosphorescence spectra but of a magnitude approximately eight times smaller. The observed line shapes suggest triplets for  $C_6H_5D$  and 1,4- $C_6H_4D_2$ , but the structure is not well resolved.

4. The magnitudes of the phosphorescence splittings are the same within  $\pm 1.0 \text{ cm}^{-1}$  for all vibronic transitions of a particular isotope. The magnitudes of these splittings for the various isotopic modifications of benzene are shown in Table I.

5. The relative intensities of the components of the phosphorescence multiplets depend on the concentration of solute molecules. In the limit of infinite dilution, the relative intensities of the components in descending order of frequency seem to approach 2:1 for  $C_6H_5D$ , 1,4- $C_6H_4D_2$ , and 1,3- $C_6H_4D_2$ ; approach 1:2 for 1,3- $C_6H_4D_2$ ; and 1:1:1 for 1,2,4- $C_6H_3D_3$ . This is discussed more completely in Sec. 9.

6. Within the lower resolution  $2 \text{ cm}^{-1}$  linewidth, the fluorescence spectrum of all isotopic benzenes shows no multiplet structure. In view of the small splittings observed in the electronic absorption spectrum and in the infrared<sup>24</sup> spectrum of isotopic mixed crystals of benzene, small splittings should show up in the fluorescence spectrum at higher resolution providing the intrinsic linewidths are sufficiently narrow.

## 6. INTERPRETATION OF THE SPECTRA

These observations can be explained if benzene in the crystalline state has an effective symmetry lower than  $D_{6h}$ . At low temperatures all phosphorescence emission originates from the zeroth vibrational level of the excited triplet state, and thus the symmetry reduction in the triplet state occurs in the vibrationally unexcited level of this state. The loss of symmetry is just what is expected when benzene is placed in any environment of low symmetry. The effect seems to be accentuated, however, in the  $^3B_{1u}$  state of benzene.

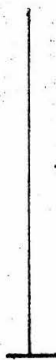
The symmetry reduction is such that the six carbon atom positions are no longer all equivalent. Considering the low resolution spectra first, where further splitting of the doublets into triplets was not accomplished, the intensity ratios of the multiplet components in the limit of low guest concentration indicate that the carbon positions are divided into two non-equivalent sets, of four and of two carbon atom positions each (vide infra). Using group theory<sup>25</sup>, it can readily be shown that only five subgroups of  $D_{6h}$  are consistent with this structural requirement. These are  $D_{2h}$ ,  $D_2$ ,  $C_{2v}$  (with the  $C_2$  perpendicular to the original molecular plane), and  $C_{2h}$  (with the  $C'_2$  or  $C''_2$  through the atoms or through the bonds). Other symmetries predict an incorrect number of components. In Fig. 2 the statistical weight and the positions of the deuteriums are shown for the distinct conformations of a given isotopic benzene assuming a particular  $D_{2h}$  symmetry. It is not possible from the data to eliminate any of the possible symmetries.

However, if the extrinsic distortion were sufficiently large, the molecular symmetry would be  $C_1$ . The finer features, which are currently

being studied in more detail, are undoubtedly the result of placing the guest molecule in the  $C_i$  site of the benzene crystal. For a  $C_i$  distortion of the  $^3B_{1u}$  state, three lines are predicted for  $C_6H_5D$ , 1,4- $C_6H_4D_2$ , 1,3- $C_6H_4D_2$ , and 1,3- $C_6H_2D_4$ ; one line for  $C_6H_6$  and 1,3,5- $C_6H_3D_3$ ; and six lines for 1,2,4- $C_6H_3D_3$ . The overall splitting is not symmetrically spaced since the interactions reflect the nearly  $C_{2h}$  site symmetry. Furthermore, orientation effects on ground state vibrations (see Sec. 8) contribute to the splittings. This is a small contribution, but observable even in the low resolution spectra. The measured multiplet splittings change reproducibly from band to band with an average deviation from the mean splitting of about  $\pm 1 \text{ cm}^{-1}$ . The additional splitting into three components is not only good spectroscopic support for the crystal structure of benzene, but also implies that the extrinsic distortion is comparable with or greater than any intrinsic distortion!

## 7. A MODEL FOR ZERO-POINT ENERGIES

To see better how the line multiplicity leads to the conclusion of a nonhexagonal benzene triplet we consider a very simple model for the explanation of the doublet structure. There is no advantage to be gained by extending this sort of model to the discussion of the triplet structure. We assume that the effect of isotopic substitution on electronic energies is





much smaller than the observed splittings in the multiplet line structure. This is reasonable since we are dealing here with a  $\pi-\pi^*$  transition mostly localized around the carbon frame. Even when the nuclear masses differ by a factor of two as for H and  $\text{He}^+$ , the Rydberg constants are the same to within about 0.05%.<sup>26</sup> We can conclude therefore that the mass effect on the electronic transition energies arises from zero-point vibrations. A quantitative calculation of the total zero-point energy in the benzene triplet state is not possible. Even the experimental data for the ground electronic state is not sufficiently reliable to calculate total zero-point energy to the degree of precision required here. In addition, no vibrational data presently exist for the triplet state.

The simple model that we use to treat zero-point energies in benzene considers the molecule to be composed of six CH or CD mass points that can oscillate independently<sup>27</sup> in three dimensions about their equilibrium positions. For simplicity, the effect of hydrogen or deuterium vibrations will be ignored for the moment. Let the force constants in the ground electronic state associated with coordinate  $i = x, y, z$  at the position of the  $j^{\text{th}}$  mass point be given by  $k_{ij}^0$ . The  $x$  coordinate at each mass point is defined as pointing outward from the center of the molecule, and the  $z$  coordinate is perpendicular to the molecular plane. The  $y$  coordinate is orthogonal to these. Because of hexagonal symmetry,  $k_{ij}^0$  for  $j = 1, 2 \dots 6$  are equal. Assigning reduced masses  $m_1$  and  $m_2$  to the CH and CD fragments, respectively, the zero point vibrational energy in  $\text{cm}^{-1}$  in the ground electronic state is,

$$(4\pi c)^{-1} \sum_{i=x,y,z} \sum_{j=1}^6 (k_{ij}^0 / m^j)^{\frac{1}{2}}$$

with  $m^j = m_1$  or  $m_2$  depending on whether the mass at  $j$  is that of CH or CD.

In the triplet state we assume a lower symmetry in accordance with the discussion. A cartesian coordinate system centered at each mass point is defined in such a way that there are two mass points bound to their equilibrium position by the force constants  $k'_{ij}$ , and four mass points by the force constants  $k''_{ik}$ . This analysis does not restrict the mechanism that leads to differing force constants. The zero point energy (in  $\text{cm}^{-1}$ ) in the triplet state becomes,

$$(4\pi c)^{-1} \sum_{i=x,y,z} \sum_{j=1,4} \sum_{k=2,3,5,6} (k'_{ij}/m^j)^{\frac{1}{2}} + (k''_{ik}/m^k)^{\frac{1}{2}}$$

where the index  $j = 1, 4$  refers to the mass points with force constants  $k'_i$  and the index  $k = 2, 3, 5, 6$  refers to mass points with force constants  $k''_i$ ; each  $m^j$  or  $m^k$  takes the value  $m_1$  or  $m_2$  whichever is appropriate.

Defining,

$$K^0 = (4\pi c)^{-1} \sum_{i=x,y,z} (k_i^0)^{\frac{1}{2}}$$

with similar definitions for  $K'$  and  $K''$ , the zero-point energy difference  $Z(D')$  between ground and excited state for monodeutero benzene with the deuterium atom in a primed position is

$$Z(D') = m_2^{-\frac{1}{2}} (K' - K^0) + m_1^{-\frac{1}{2}} (K' + 4K'' - 5K^0).$$

For a deuterium atom in a double-primed position, one has

$$Z(D'') = m_2^{-\frac{1}{2}} (K'' - K^0) + m_1^{-\frac{1}{2}} (2K' + 3K'' - 5K^0).$$

For the excited singlet state, where evidently  $K' \approx K''$ , these equations show, in agreement with observation, that each successive D atom substitution on  $C_6H_6$  contributes a constant contribution to  $Z$  equal to

$$(m_1^{-\frac{1}{2}} - m_2^{-\frac{1}{2}}) (K^0 - K)$$

where  $K = K' \approx K''$  for the singlet. The empirical value of this expression is  $+33 \text{ cm}^{-1}$ . Since  $m_1^{-\frac{1}{2}} > m_2^{-\frac{1}{2}}$ , the force constant  $K$  in the excited state is smaller than that in the ground state, a fact that is theoretically expected, and one that has already been pointed out by Ingold and co-workers.<sup>29</sup> For the triplet, where  $K'$  is not equal to  $K''$ , but where the difference  $2|K' - K''|$  is small compared with  $|K' + K'' - 2K^0|$ , a similar result obtains.

Using  $C_6H_5D$  as an example, the difference between the  $Z$ 's,

$$\Delta Z(C_6H_5D) = Z(D'') - Z(D') = (m_1^{-\frac{1}{2}} - m_2^{-\frac{1}{2}}) (K' - K'')$$

for the two nonequivalent substitutional positions in triplet benzene is the quantity equal to the observed doublet splitting in the spectrum. This splitting is measured to be  $+7 \text{ cm}^{-1}$ . The sign of this quantity is determined from the multiplet intensity ratio in the low concentration limit (see Sec. 9). For  $C_6H_5D$ , the higher frequency component corresponds to the one with the greater statistical weight, namely the component associated with a deuterium in the double primed position (Fig. 2). Since  $m_1^{-\frac{1}{2}} > m_2^{-\frac{1}{2}}$ , one sees that  $K' > K''$ . This line of reasoning gives a force constant difference between primed and double primed positions which is inconsistent with what at first sight would be expected for a quinoidal structure, where four of the six mass points are connected to positions having the greatest force constant. The above analysis shows that only two atoms are connected to such positions. However, a purely extrinsic perturbation is not necessarily governed by the rules of chemical binding. Therefore, a non quinoidal structure should not be too surprising.



The analysis, however, does not necessarily rule out the quinoidal structure. It could happen that the force constants for certain hydrogen vibrations are such that  $K'_H > K''_H$ , but for carbon vibrations  $K'_C > K''_C$ . This relationship could result in the observed sign of the splittings for the quinoidal structure, providing it is primarily hydrogen vibrations that determine the splitting, but primarily low frequency vibrations that determine the gross zero-point energy shifts. One cannot rule out the possibility that the frequencies of certain hydrogen stretching modes increase upon excitation into the lowest excited states of benzene, so such a relationship between the force constants is possible.

The multiplet splittings in the other isotopic modifications of benzene can readily be determined using the simplified model calculation just used for  $C_6H_5D$ . Defining  $\Delta Z$  as being determined by subtracting  $Z$  of the doublet component having the lower statistical weight from  $Z$  of the one with the higher statistical weight, one finds that:  $\Delta Z(1, 4-C_6H_4D_2) = 2\Delta Z(C_6H_5D)$ ;  $\Delta Z(1, 3-C_6H_4D_2) = -\Delta Z(C_6H_5D)$ ; and  $\Delta Z(1, 3-C_6H_2D_4) = \Delta Z(C_6H_5D)$ . For the  $1, 2, 4-C_6H_3D_3$  modification, a triplet is predicted with total splitting equal to that in  $1, 4-C_6H_4D_2$ . As can be seen from Table 1, these results are in exact agreement with the experimental findings at low resolution for both the multiplet splittings and the relative energies of the conformers.

#### 8. INTRINSIC OR ENVIRONMENTAL DISTORTION?

An intrinsic distortion of the lowest benzene triplet has experimental and theoretical support. However, as stressed earlier, the anisotropy of the benzene crystal alone can also give rise extrinsically to an effective symmetry lower than  $D_{6h}$ . The site symmetry of the benzene crystal is  $C_i$ .<sup>23</sup> However, to a fair approximation it is  $C_{2h}$ .<sup>30</sup> Therefore, within this latter approximation, the benzene molecule at a crystalline site has at

most  $C_{2h}$  symmetry in all electronic states. The magnitude of this symmetry reduction may or may not be appreciable depending on the strength of the coupling between the molecule and the crystal field. In other words, the difference between  $K'$  and  $K''$  in the model of Sec. 7 could arise entirely from intermolecular interactions. The distortion in general is expected to be different for different electronic states of the molecule.

The strongest argument in support of the distortion being caused by the extrinsic perturbation is in the vibronic structure of the phosphorescence and fluorescence transitions. No anomalies whatsoever were observed by Leach and Lopez-Delgado<sup>31</sup> in their lower resolution phosphorescence spectrum of  $C_6H_6$  and  $C_6D_6$  in a cyclohexane matrix. On this basis they concluded that the triplet state of benzene is hexagonal. Certainly the apparent absence of any strong progression, other than totally symmetric, built on one quantum of a perturbing  $e_{2g}$  vibration implies at most a small distortion, be it intrinsic or extrinsic; and it is intuitively more attractive to relate a small effect to an extrinsic, rather than an intrinsic, perturbation. The multiplet splittings in the phosphorescence do show that some kind of distortion occurs in the  $^3B_{1u}$  state above and beyond that which occurs in the  $^1B_{1u}$  state, but the experimental data can in no way distinguish an intrinsic distortion from one caused by external perturbations. One must remember that Moffitt's theoretical arguments reviewed in Sec. 2 may be applied to extrinsic as well as intrinsic perturbations.

In crystalline benzene some experimental evidence for a direct intermolecular perturbation on the molecular force field of the ground electronic state has been obtained by Bernstein and Robinson<sup>32</sup>. Using isotopic mixed crystals, they have observed splittings of nondegenerate

vibrations in the infrared spectrum of isotopic modifications of benzene having lower than  $D_{3h}$  symmetry. There are just two components observed at the resolution available, rather than three, because of the approximate  $C_{2h}$  site symmetry, and the magnitude of these orientational splittings, when observed, is around  $3-4 \text{ cm}^{-1}$ . The splittings, which are of similar magnitude as the site group splittings of degenerate vibrations and arise probably from the same kind of interaction, are observed primarily on  $u$ -vibrations or those vibrations that correlate with  $u$ -vibrations. Site group splittings and orientational splittings on  $g$ -vibrations appear to be extremely small in most cases.<sup>17, 32</sup> The main points of interest here are that only a part of the vibrations show orientational splittings and the magnitude of the splittings, when observed, is remarkably insensitive to the type of vibration concerned, its effective mass, its amplitude, or its infrequency.

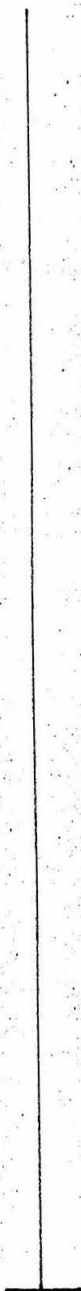
If these splittings were different in the ground and excited electronic states of benzene, their presence would contribute to a zero-point energy difference for molecules in the different orientations. "Electronic splittings" of the type observed in this work would result. The main reason we do not believe that extrinsic effects of this particular type contribute a measurable amount to the phosphorescence splittings is that no such splittings have yet been observed in the fluorescence spectrum, and even though they are expected their magnitude must be smaller than the  $2 \text{ cm}^{-1}$  low resolution linewidth. Since we know that orientational splittings exist, the lack of observable splittings in fluorescence is, at first sight, more remarkable than the presence of them in the phosphorescence spectrum. The smallness of the splittings in fluorescence implies that vibra-

tional orientational splittings in the ground and excited electronic states must be the same to within the experimental linewidth. Of course, one could say that there is some kind of cancellation effect in the singlet but not in the triplet. However, in view of the apparent insensitivity to vibrational state found for the vibrational orientational splittings in the ground electronic state, we prefer to believe (with some reservations) that this type of vibrational orientational effect is not important in the  $\geq 7 \text{ cm}^{-1}$  splittings discussed in this paper. Rather, we feel that the splittings observed in the phosphorescence, but less prominently in the fluorescence, reveal a real difference in the static geometry of the  $^3\text{B}_{1u}$  and  $^1\text{B}_{2u}$  states. The perturbation that causes the distortion of the  $^3\text{B}_{1u}$  state may still be either intrinsic or extrinsic, or it could be an intrinsic effect modified--magnified or even demagnified--by the environment.

The presence of additional (triplet) splitting in high resolution phosphorescence spectra and the orientation effects on ground state vibrations do show that the crystal-field-guest interaction is not negligible. In fact, the optical experiments are best interpreted in terms of a completely extrinsic distortion of the  $^3\text{B}_{1u}$  state or an inherent intrinsic distortion modified by the  $\bar{C}_i$  site symmetry of the crystal.

In an attempt to distinguish between intrinsic or extrinsic mechanisms for distorting the triplet state, the phosphorescence spectra of several isotopic benzenes were obtained in solid rare gas matrices. It was already known<sup>5</sup> that the spectrum of benzene in solid argon at  $4.2^\circ \text{K}$  is sufficiently sharp ( $4 \text{ cm}^{-1}$ ) that possible splittings might have been observed. No distinct splittings were observed for  $\text{C}_6\text{H}_5\text{D}$  and  $1,4\text{-C}_6\text{H}_4\text{D}_2$ . Line widths, however, increased to about 7 and  $10 \text{ cm}^{-1}$  respectively. This broadening could be associated with a distortion effect where the expected doublet for some reason is not resolved. If the broadened line

is really caused by such a distortion, and not by some extraneous effect, the distortion is then similar to what it is in crystalline benzene. This observation would then be more in keeping with an intrinsic distortion; but the rare-gas results are not very conclusive and should be given small weight. Mixed crystals of benzene and other substances, such as borazole, should be studied to clarify this point.





## 9. INTENSITY RATIOS

There are two limits that need be considered in the discussion of intensity ratios of the multiplet components. In the case where the rate of interconversion among the multiplet components of a nontrigonally symmetric isotopic modification of benzene is fast compared with the phosphorescence lifetime ( $\tau \approx 10$  sec.), the ratio of the emission intensities from the components should be equal to the ratio of their statistically weighted Boltzmann factors. If interconversion were slow compared with the phosphorescence lifetime, then the intensity ratio should be governed only by the probability of excitation of the various conformers. It is assumed that this probability is equal to the relative statistical weight of the conformer.

The mechanism for reaching Boltzmann equilibrium among the multiplet components may be different depending upon whether the interaction between the distorted molecule and the crystal field is strong or weak. For a strong interaction between molecule and environment, the potential surface describing interconversion between the conformers is highly unsymmetrical, trigonal symmetry being lost because of the low symmetry of the crystal field. As de Groot, Hesselmann, and van der Waals have pointed out,<sup>33</sup> for example, an intrinsically distorted molecule may have some highly preferred orientation in the cavity of the crystal. One minimum of the potential surface lies to much lower energy than the other two. The lowest-lying triplet state of each guest molecule is therefore spatially nondegenerate, the components associated with the other potential minima lying much higher. Tunneling among the levels is therefore not possible except at fairly high temperatures. Here "multiplet" components would be associated with this single low-lying energy in different

molecules, the zero-point energy difference between the components being a result of different orientations of the deuterium positions in the crystal field. The excited state orientation of a given molecule is fixed by its ground state orientation. There is no way for the conformers to interconvert at low temperatures except by molecular rotation in the solid, an event that cannot occur in normal crystalline benzene at 4.2°K during the triplet lifetime.<sup>34</sup> Boltzmann equilibrium can therefore be established only through intermolecular exchange of excitation, a process that is known<sup>16</sup> to take place in isotopic mixed crystals of benzene at low temperatures. Moreover, the rate of intermolecular excitation exchange is known<sup>16</sup> to be concentration dependent, the transfer becoming more efficient with increasing concentration of guests.

If the interaction between the molecule and its environment is weak, then, in all probability, any distortion of the benzene molecule in its triplet state would have to be intrinsic. Each benzene molecule possesses more than one conformation. Unsymmetrical isotopic substitution causes these conformers to have slightly different zero-point energies. Boltzmann equilibrium among the components is established by some sort of intramolecular process, thermally activated at very low temperatures. Intermolecular excitation exchange is not necessary for thermal equilibrium unless the intramolecular process is too slow.

The experimental intensities are subject to rather large errors, both in measurement and from errors due to effects caused by the presence, as impurities, of other isotopic traps. Furthermore, the Franck-Condon envelopes are slightly different for the multiplet components. Intensity ratios

integrated over the Franck-Condon envelope<sup>35</sup> should therefore be somewhat more reliable than line-to-line comparisons. The integration was performed by summing peak heights rather than areas under the lines. Fig. 3 shows the concentration dependence of the ratio of the integrated intensities of the upper to lower energy component for  $C_6H_5D$ . For isotopes other than  $C_6H_5D$  integrated intensities were obtained at concentrations less than 1% only. Integrated intensity ratios for all the isotopes at  $\leq 0.1\%$  guest are shown in Table I. Both photoelectric and photographic intensity measurements were used. The measured intensity ratios for both methods agree for identical concentrations within 10%.

As can be seen, the intensity ratios of the components are definitely concentration dependent. This fact shows that the dominant mechanism for thermal equilibration among the components is intermolecular excitation exchange, not intramolecular tunneling. This fact therefore forces us into one of two conclusions. The interaction between the molecule and its environment could be weak, but in that case the rate of the intramolecular tunneling process among the conformers would have to be much slower than the rate of disappearance of the triplet state,  $\sim 0.1 \text{ sec.}^{-1}$ . The other possibility is that the interaction between the molecule and the crystal field is strong, so that no intramolecular tunneling can occur at low temperatures. More will be said about these possibilities in the next section.

The zero concentration limits shown in Table I give the probability ratio for excitation of the multiplet components. These ratios are therefore associated with the relative statistical weights of the



conformers. In this way the statistical weight of a conformer can be related to its relative energy. In  $C_6H_5D$ , for example, the statistically favored conformation is the one at higher energy. In all cases it is found that the conformation with the most deuterium atoms on the double primed positions (see the third paragraph of Section 7) lies at highest energy. The lowest energy conformation is the one with the most deuteriums at the single primed positions. The observed statistical weights and energy ordering of the conformers are in exact agreement with those expected for a distorted benzene, as shown in Fig. 2. In the high concentration limit the intensity ratio should approach the Boltzmann ratio, which can be determined from the statistical weights and the measured energy differences between the multiplet components. The calculated Boltzmann ratio for the multiplet components of  $C_6H_5D$  is 0.2 at  $4.2^\circ K$  and 0.005 at  $1.7^\circ K$ . As shown in Fig. 3, the agreement with the experimental data is very good.

#### 10. COMPARISON WITH ESR RESULTS

de Groot and van der Waals<sup>15</sup> have observed the electron resonance spectrum of triplet benzene in rigid glass solution at  $20^\circ K$ . Their analysis indicates the absence of trigonal or greater symmetry in the benzene triplet state. In agreement with their theoretical predictions discussed in Section 2, the electron resonance spectrum at  $20^\circ K$  in glassy solvents is interpreted in terms of a dynamical equilibrium between three isomeric conformations with an inter-conformer conversion rate of  $>10^{10} \text{ sec}^{-1}$ .

This interpretation was extended<sup>33</sup> by observing the electron resonance spectra of mesitylene in a B-trimethylborazole crystal in the temperature range  $20^\circ K$  to about  $130^\circ K$ . Over this range of temperature

the  $\Delta M = \pm 1$  absorption lines for each crystal orientation remained sharp, but they shifted such that the zero-field splitting parameter  $Z$  remained nearly constant while  $|X - Y|$ , with increasing temperature, decreased from about  $0.050 \text{ cm}^{-1}$  to  $0.038 \text{ cm}^{-1}$ . This result shows the approach at high temperature to trigonal symmetry where  $|X - Y| = 0$ . The observation of only two sharp absorptions for each crystalline direction establishes a  $> 10^{10} \text{ sec}^{-1}$  conformer conversion rate.

The fast tunneling rate implied by the ESR experiments is at first sight inconsistent with the results of the optical experiments, which give an interconversion rate slow compared with the rate of triplet decay. The two results seem to differ by a factor of  $10^{11}$  or more! Differences in the experimental conditions of the two experiments of course exist. The optical experiments have been carried out at  $4.2^\circ \text{K}$ , or below, whereas the ESR experiments were at  $20^\circ \text{K}$ , or above; the optical experiments used crystalline benzene while the ESR experiments used mesitylene in B-trimethylborazole.

First, let's see if the assumption of weak interactions between the molecule and its environment is reasonable in the light of the ESR and optical experiments. The most probable mechanism for interconversion in this case would be intramolecular tunneling among the triad of nearly degenerate states of a nontrigonally symmetric isotopic modification of benzene. Theoretically, one would expect a fast tunneling rate.<sup>15, 36</sup> For example, taking a ring distortion corresponding to a carbon atom displacement of  $0.04 - 0.1 \text{ \AA}$ , tunneling of carbons between conformers would occur at a rate  $\sim 10^{12} \text{ sec}^{-1}$  for a barrier height of  $500 \text{ cm}^{-1}$ . In order to bring the theoretical tunneling rate into line with the optical experiments, a

distortion of at least 1 Å or an unreasonably high barrier would be required. While such a large distortion may be possible, there is no independent experimental evidence for it. We therefore conclude, in agreement with the discussion in Sec. 8, that the interaction between the molecule and the crystal field is not negligible.

If the distortion were purely intrinsic the effect of the crystal field is to present an energetically favored environment for one orientation of the distorted molecule. This is the picture given by van der Waals and de Groot. On the other hand, if the distortion were purely extrinsic, the potential surface with a triad of minima does not really exist. Any attempt to rotate the molecule results in distortion and the two things cannot be separately treated. In either case, only a single emitting state exists in each molecule. The observed splitting is therefore associated with zero-point energy differences among different molecules in the crystal with different orientations of the deuterium atoms in the  $C_i$  site symmetry of the crystal field.

If the distortion were intrinsic, emission or absorption studies at higher temperatures should reveal states resulting from the higher energy conformers. Failure, thus far, to photograph any emission from the higher energy conformers allows an estimate to be made of the minimum energy depression from Boltzmann considerations. For  $C_6H_6$  in  $C_6D_6$  a weak single line has been seen  $8\text{ cm}^{-1}$  to higher energy of the 0, 0 line of the  $C_6H_6$  phosphorescence when the latter was heavily exposed on the photographic plate. This has been tentatively assigned to  $^{13}C^{12}C_5H_6$  whose 0, 0 line is calculated<sup>37</sup> to be blue shifted some  $15\text{ cm}^{-1}$  from  $C_6H_6$ . A complete spectral analysis of the system built in this origin is prevented at this time by the heavy background of  $C_6H_6$  lines. Since its position is roughly where predicted and emission from it is expected, we will assume the assignment to

$^{13}\text{C}^{12}\text{C}_6\text{H}_6$  is correct. No other emission was detected to the high energy side of the  $\text{C}_6\text{H}_6$  0,0 line. Thus, it is probable that emission from the higher potential minima of the distorted molecule in the  $\text{C}_i$  cage was not observed at 4.2° K. Higher temperature experiments are planned in an attempt to observe these features. Estimating that emission  $10^{-2}$  as intense as the  $\text{C}_6\text{H}_6$  0,0 line would have been detected, a minimum energy difference of roughly  $15\text{ cm}^{-1}$  between the potential minima in the crystal is necessary. This is the correct order of magnitude for rapid conversion above 20° K where  $kT \cong 14\text{ cm}^{-1}$ .

Thus, at the present time, the optical experiments can be made consistent with the interpretation of the ESR experiments where an intrinsically distorted  $^3\text{B}_{1u}$  benzene molecule is preferentially oriented in the crystal site such that other orientations are energetically less stable by at least  $15\text{ cm}^{-1}$ . However, the detection of the relatively large splittings caused by the  $\text{C}_i$  site, the lack of vibronic evidence for distortions, the failure to find any optical evidence for the higher conformers, the likelihood of a nonquinoidal distortion (even in the  $\text{C}_{2h}$  site approximation), and the smallness of the zero-point energy effects would seem to be more consistent with a purely extrinsic distortion. On the other hand, the fact that the distortion appears larger for the  $^3\text{B}_{1u}$  state than for the  $^1\text{B}_{2u}$  state, and the agreement between the ESR experimental results and their quantitative interpretation on the basis of a quinoidal  $^3\text{B}_{1u}$  state give weight to the argument in favor of an intrinsic distortion.

ACKNOWLEDGEMENTS

We would like to thank Professor G. W. Robinson for his valuable discussions concerning the interpretation presented in this paper and for his help in the writing style. One of us (DST) would also like to acknowledge Drs. R. Kopelman and C. H. Ting and Messrs. E. R. Bernstein and S. D. Colson for many valuable discussions throughout the preparation of this paper. We are also grateful for the predoctoral fellowships from the National Science Foundation (GCN) and the National Aeronautics and Space Administration (DST). In addition, GCN thanks the Petroleum Research Fund for support of a portion of this work carried out at the University of Rochester. The 1.8 m Jarrell-Ash Spectrometer used in part of this work was made available by a grant to the California Institute of Technology from the Alfred P. Sloan Foundation.



## REFERENCES

1. G. N. Lewis and M. Kasha, J. Am. Chem. Soc. 66, 2100 (1944).
2. O. Redlich and E. K. Holt, J. Am. Chem. Soc. 67, 1228 (1945).
3. H. Sponer and E. Teller, Revs. Modern Phys. 13, 75 (1941).
4. H. Shull, J. Chem. Phys. 17, 295 (1949).
5. G. W. Robinson, J. Mol. Spectry. 6, 58 (1961).
6. R. S. Mulliken, Revs. Modern Phys. 14, 204 (1942); A. D. Walsh, J. Chem. Soc. pp 2260-2331 (1953); D. A. Ramsay in "Determination of Organic Structure by Physical Methods, "edited by F. C. Nachod and W. D. Phillips (Academic Press, Inc., New York, 1962), vol. 2, chap. 4. See also the elegant paper on the rotational analysis of the 2600 Å absorption system of benzene by J. H. Callomon, T. M. Dunn, and I. M. Mills [Phil. Trans. Roy. Soc. 259, 499 (1966)], where the geometry and symmetry of the lowest excited singlet state of gaseous benzene is discussed and proven to be exactly point group  $D_{6h}$ .
7. W. Moffitt, J. Chem. Phys. 22, 320 (1954).
8. A. D. Liehr, Z. Naturf. A16, 641 (1961).
9. M. Goeppert-Mayer and A. L. Sklar, J. Chem. Phys. 6, 645 (1938).
10. W. C. Price and A. D. Walsh, Proc. Roy. Soc. (London) A191, 22 (1947).
11. S. D. Colson and E. R. Bernstein, J. Chem. Phys. 43, 2661 (1965).
12. J. E. Lennard-Jones, Proc. Roy. Soc. (London) A158, 280 (1937).
13. W. D. Hobey and A. D. McLachlan, J. Chem. Phys. 33, 1695 (1960).
14. H. C. Longuet-Higgins and L. Salem, Proc. Roy. Soc. (London) A251, 172 (1959).
15. M. S. de Groot and J. H. van der Waals, Mol. Phys. 6, 545 (1963).

16. H. Sternlicht, G. C. Nieman, and G. W. Robinson, J. Chem. Phys. 38, 1326 (1963).
17. E. R. Bernstein, S. D. Colson, D. S. Tinti, and G. W. Robinson, to be published. See following section of this thesis.
18. A. C. Albrecht, J. Chem. Phys. 38, 354 (1963).
19. The only ground-state vibration of  $C_6H_6$  which has shown a site group splitting in the phosphorescence spectrum is the  $606\text{ cm}^{-1}$  ( $e_{2g}$ ) mode. The measured splitting is  $3\text{ cm}^{-1}$ .
20. This vibration ( $\nu_5, b_{2g}$ ) is assigned from combination bands a frequency of  $995\text{ cm}^{-1}$  by Mair and Hornig.<sup>21</sup> However, on the basis of the required symmetry<sup>18</sup> for vibronic interactions in a  $B_{1u}$  state and by comparison of the various isotopic benzenes, we feel that  $\nu_5$  should be correctly assigned a value of  $1004\text{ cm}^{-1}$  for crystalline benzene. Very recent Raman spectral studies<sup>22</sup> of solid benzene agree with this new assignment.
21. R. D. Mair and D. F. Hornig, J. Chem. Phys. 17, 1236 (1949).
22. M. Ito and T. Shigeoka, Spectrochim. Acta 22, 1029 (1966); A. R. Gee and G. W. Robinson, private communication.
23. E. G. Cox, Revs. Modern Phys. 30, 159 (1958); E. G. Cox, D. W. J. Cruickshank, and J. A. S. Smith, Proc. Roy. Soc. (London) A247, 1 (1958).
24. See Sec. 8 where certain splittings observed in the infrared spectrum of isotopic mixed crystals are briefly discussed.
25. R. Kopelman, to be submitted to J. Chem. Phys.
26. G. Herzberg, Atomic Spectra and Atomic Structure (Dover Publications, New York, 1944).

27. This model assumes all off-diagonal matrix elements of both the  $\underline{F}$  and  $\underline{G}$  matrices<sup>28</sup> to be zero and ignores translational and rotational degrees of freedom. While this may not be a good approximation, especially with regard to the  $\underline{G}$  matrix, it is hoped that these errors cancel when the differences in zero-point energies are taken.
28. E. B. Wilson, Jr., J. C. Decius, and D. C. Cross, *Molecular Vibrations* (McGraw-Hill Book Co., Inc., New York, 1955).
29. F. M. Garforth, C. K. Ingold, and H. G. Poole, J. Chem. Soc. 1948, 508
30. V. L. Broude, Usp. Fiz. Nauk 74, 577 (1961) [English translation Soviet Phys. -Usp. 4, 584 (1962)].
31. S. Leach and R. Lopez-Delgado, J. chim. phys. 61, 1636 (1964).
32. E. R. Bernstein and G. W. Robinson, private communication.
33. M. S. de Groot, I.A.M. Hesselmann, and J. H. van der Waals, Mol. Phys. 10, 91 (1965).
34. This is easily shown from the data given by E. R. Andrew and R. G. Eades, Proc. Roy. Soc. (London) A218, 537 (1953).
35. Approximately 75% of the total phosphorescence intensity in these mixed crystals arises from progressions built on vibrations that correlate with the  $e_{2g}$   $1178\text{ cm}^{-1}$  and  $1595\text{ cm}^{-1}$  vibrations of  $\text{C}_6\text{H}_6$ .
36. C. H. Townes and A. L. Schawlow, *Microwave Spectroscopy*, (McGraw-Hill Book Co., Inc., New York, 1955) p. 304.
37. C. H. Ting, private communication.



TABLE I.  
Multiplet Splittings and Intensity Ratios

Guest	Phosphorescence 0, 0 in C <sub>6</sub> D <sub>6</sub> host $\nu_{\text{vac}}$ (cm <sup>-1</sup> ) <sup>a</sup>	Multiplet Splitting (cm <sup>-1</sup> ) <sup>b</sup>	Multiplet Intensity Ratio <sup>c</sup>
C <sub>6</sub> H <sub>6</sub>	29658.1		
C <sub>6</sub> H <sub>5</sub> D	29690.5	7.0 ± 0.5	2.2
	29683.8		
1,4-C <sub>6</sub> H <sub>4</sub> D <sub>2</sub>	29720.4	13.5 ± 1.0	1.4 <sup>e</sup>
	29707.9		
1,3-C <sub>6</sub> H <sub>4</sub> D <sub>2</sub>	29724.2	7.6 ± 0.7	0.64
	29717.1		
1,3,5-C <sub>6</sub> H <sub>3</sub> D <sub>3</sub>	29753.2	7.2	1.0 <sup>f</sup>
	29755.8		
1,2,4-C <sub>6</sub> H <sub>3</sub> D <sub>3</sub> <sup>d</sup>	29748.6	7.1	1.0
	29741.5		
1,3-C <sub>6</sub> H <sub>2</sub> D <sub>4</sub>	29786.4	7.2 ± 0.3	2.0 <sup>f</sup>
	29779.5		

- a. Measured values, uncorrected for quasisonance interaction with the C<sub>6</sub>D<sub>6</sub> host exciton band.
- b. The limits given are the average error from the mean.
- c. Ratio of high energy to low energy conformation for a guest concentration ≤ 0.1%.
- d. Only the 0, 0 transition was accurately measured.
- e. This ratio is a lower limit since the high energy component is an unresolved doublet and peak-heights, not integrated intensities, were measured. See Sec. 8 of text.
- f. Visual estimates.

Figure 1

Microphotometer tracing of the phosphorescence of 1.0%  $\text{C}_6\text{H}_5\text{D}$  in  $\text{C}_6\text{D}_6$  host crystal at 4.2°K showing the  $7\text{ cm}^{-1}$  doublet structure in the vibronic transitions. The  $1574\text{ cm}^{-1}$  and  $1591\text{ cm}^{-1}$  bands were traced from a plate exposed a factor of three less. Intensity is in arbitrary units.

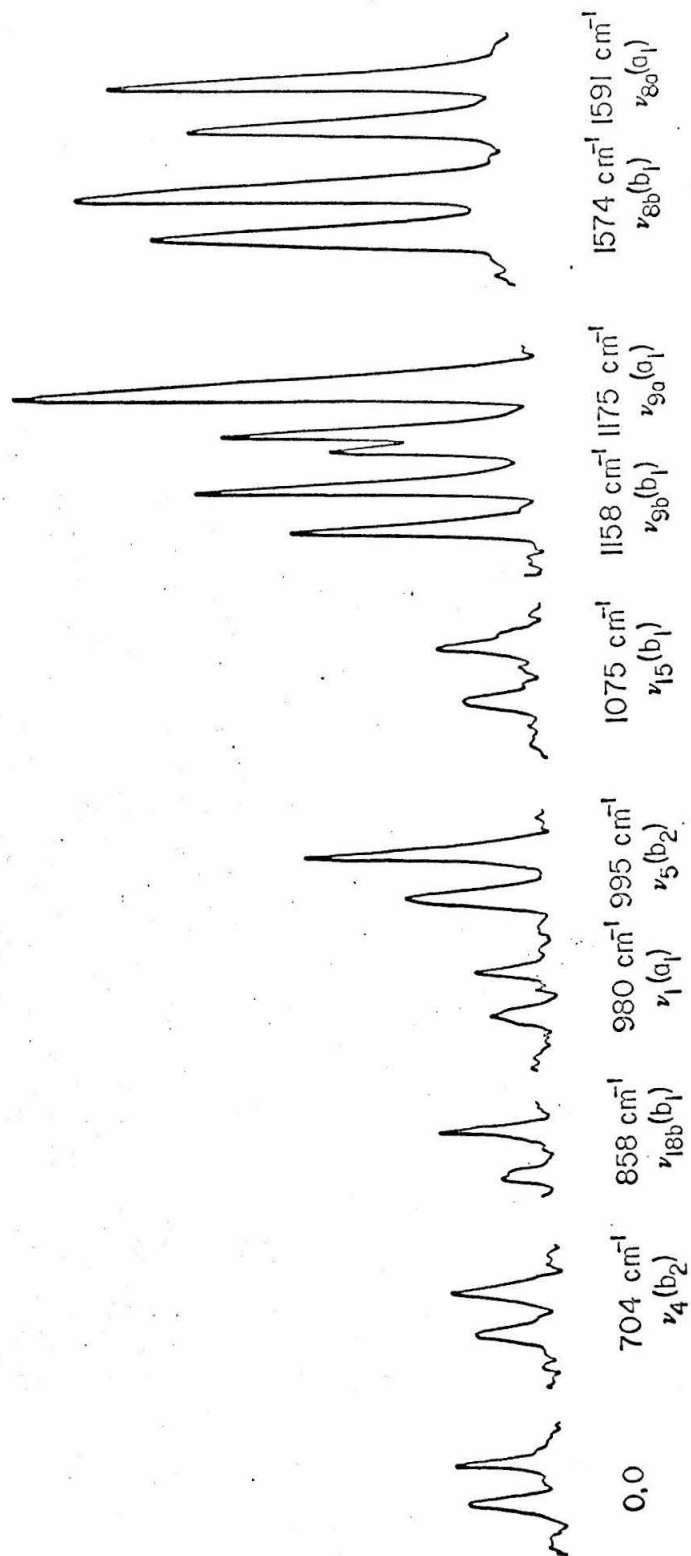
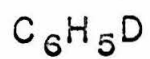
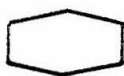
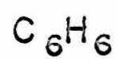
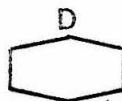


Figure 2

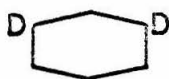
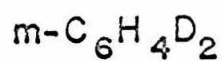
Conformations of an exaggerated  $D_{2h}$  benzene for various isotopic modifications. The number in parenthesis is the statistical weight of the conformation. The numbers at the bottom of the figure give the number of deuteriums in the apical or single primed position (see text) for the conformers in the column directly above. The prefixes m, p, s, and a denote meta, para, symmetric and asymmetric respectively.



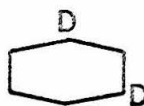
(2)



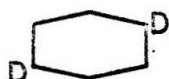
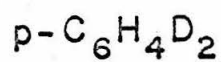
(1)



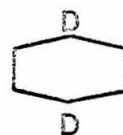
(1)



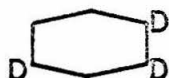
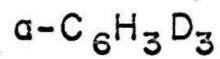
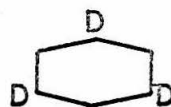
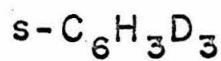
(2)



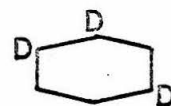
(2)



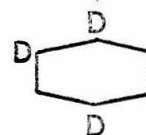
(1)



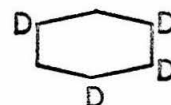
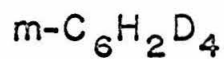
(1)



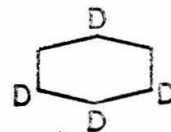
(1)



(1)



(2)



(1)

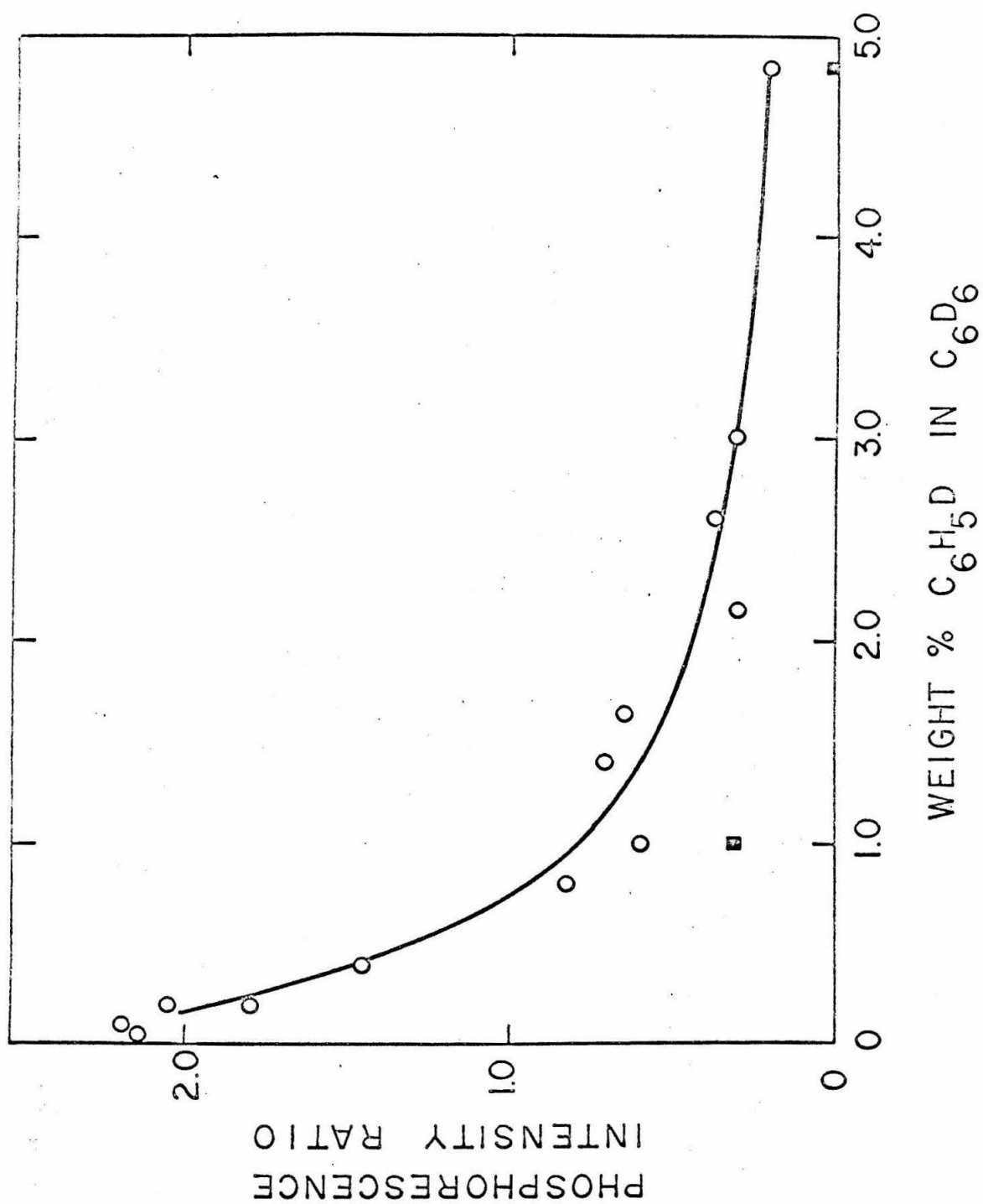
O

1

2

Figure 3

The integrated phosphorescence intensity ratio for the high energy to low energy conformer of  $C_6H_5D$  in  $C_6D_6$  host crystal as a function of guest concentration.  $\circ$  4.2°K;  $\blacksquare$  1.7°K.



Static Crystal Effects on the Vibronic Structure of the Phosphorescence,  
Fluorescence, and Absorption Spectra of  
Benzene Isotopic Mixed Crystals<sup>†</sup>

E. R. BERNSTEIN, S. D. COLSON, D. S. TINTI, and G. W. ROBINSON

Gates and Crellin Laboratories of Chemistry,<sup>‡</sup>

California Institute of Technology, Pasadena, California 91109

(Received

)

The phosphorescence, fluorescence and absorption spectra of the isotopic benzenes  $C_6H_6$ ,  $C_6H_5D$ ,  $p-C_6H_4D_2$ , and  $sym-C_6H_3D_3$ , present as dilute guests in a  $C_6D_6$  host crystal at 4.2°K, are obtained with sufficient spectral resolution to ascertain the magnitude of the crystalline site effects. Two such effects are emphasized: site splitting of degenerate fundamentals and orientational effects. The former can occur for the isotopes  $C_6H_6$  and  $sym-C_6H_3D_3$ , while the latter is possible only for isotopes with less than a molecular three-fold rotation axis. The observations show that both site-splitting and orientational effects do occur as a general rule on vibronic and vibrational states in benzene isotopic mixed crystals. We conclude, therefore, that the site interactions are not negligible.

---

<sup>†</sup>Supported in part by

<sup>‡</sup>Contribution No. 3546.



An empirical correlation of the magnitudes of the site splitting, orientation effect and site (gas-to-crystal) shifts for in-plane and out-of-plane modes is noted. Our results for the ground state vibrations are in good agreement with the findings of Bernstein from infrared spectra in those cases where levels can be observed by both techniques.

In order to characterize completely the above mentioned site effects it was necessary to analyze in some detail both the emission and absorption spectra of the isotopic guest molecules. The phosphorescence of  $C_6H_6$  and sym- $C_6H_3D_3$  has been completely analyzed out to  $0, 0-(\nu_8 + \nu_1)$  while for that of  $C_6H_5D$ , the analysis of only the more intense bands near the electronic origin has been carried out. Some ground state vibrations of p- $C_6H_4D_2$  are presented but the phosphorescence spectrum, complicated greatly by both ground and excited state orientational effects, is not analyzed in this present work. The fluorescence of these isotopes was used only to corroborate and supplement the conclusions and assignments extracted from the phosphorescence analysis and is not presented in detail. The relative vibronic intensities in the fluorescence spectrum are compared to those in the phosphorescence. From the general analysis it is possible to conclude that the effect of the crystal site on the molecule, while spectroscopically measurable, is quite small.

On heavily exposed photographic plates it has been possible to assign the  $^{13}CC_5H_6$  emission spectra in both the pure electronic and a few vibronic bands. Absorption spectra of these mixed crystals have yielded information concerning

the orientational effect on the first excited singlet state of  $C_6H_5D$  and  $p-C_6H_4D_2$  as well as site splitting of the  $\nu'_6$  vibrational levels of  $C_6H_6$ . The  $^{13}CC_5H_{6-n}D_n$  0,0 absorption spectra have also been identified. New absorptions, in the region of the 0,0 of  $C_6H_6$  and  $C_6H_5D$  have been tentatively assigned to resonance pair lines and  $^{13}C_2C_4H_{6-n}D_n$  on the basis of their intensity behavior as a function of guest concentration

## I. INTRODUCTION

Since the classic work of Halford,<sup>1</sup> Hornig,<sup>2</sup> and Winston and Halford<sup>3</sup> in the late 1940's, the effect of the crystal environment on molecular spectra has been of much interest. These early works deal in part with the effect of the crystal site on the degenerate molecular states. More recently, Bernstein<sup>4</sup> and Strizhevsky<sup>5</sup> have considered further site interactions not limited only to degenerate states, viz., orientational effects,<sup>4</sup> gas-to-crystal shifts,<sup>4</sup> and enhanced Fermi resonance<sup>4,5</sup> in the solid. For experimental as well as historical reasons, most of these investigations concern the ground state vibrations observable by means of infrared spectroscopy. Since it is of theoretical importance to know whether or not such effects are present for all the vibration classes and types, in the present work we look for the above effects in the vibronic transitions of  $C_6H_6$  and some of its deuterated isotopes: that is, the phosphorescence, fluorescence, and absorption spectra of various benzene isotopic mixed crystals. This allows us to study site interactions in vibrations which are not seen by infrared absorption.

For the case of a  $C_6H_6$  guest in the  $C_i$  site of a  $C_6D_6$  host crystal, the molecular  $\underline{u}, \underline{g}$  classification of guest states is retained, imposing the  $\underline{u} \leftrightarrow \underline{g}$  dipole selection rule for the  $C_6H_6$  transitions. Thus, in the infrared absorption spectra from the  $\underline{g}$ -ground state, only  $\underline{u}$ -vibrations are observed, while vibronic transitions involving  $\underline{u}$ -excited states can be utilized to study  $\underline{g}$ -vibrations. The emission spectra also supplement the vibrational data obtained employing the Raman effect. On the other hand, in an isotope that does not have inversion symmetry, the infrared absorption and the UV emission spectra can involve the same vibrations, and thus the data complement each other. For example, in the case of site splitting of degenerate fundamentals, the infrared and UV data for  $C_6H_6$  should supplement one another due to the  $\underline{u} \leftrightarrow \underline{g}$  selection rule, while for the case of sym- $C_6H_3D_3$  these data should overlap and check one another. Similarly, for the orientation effect, the  $C_6H_5D$  data should overlap with both techniques while for p- $C_6H_4D_2$ , there would be no direct overlap of data. It was from these considerations that  $C_6H_6$ ,  $C_6H_5D$ , p- $C_6H_4D_2$ , and sym- $C_6H_3D_3$  were chosen for this work. These were all studied as dilute guests in a  $C_6D_6$  host crystal at 4.2°K. By such a study we hope to provide a complete picture of crystal effects on vibrations of the benzene molecule for all classes and types and, therefore, furnish a good test for theoretical calculations of intramolecular and intermolecular force fields and potentials in solid benzene.

A vibrational analysis of the benzene phosphorescence spectrum in EPA at 77°K was first published by Shull.<sup>7</sup> Sveshnikov and co-workers<sup>8</sup> and Leach and Lopez-Delgado<sup>9</sup> have compared the vibronic structure of phosphorescence and fluorescence, again in glasses at 77°K. Nieman<sup>10</sup> and Nieman and Tinti (NT)<sup>11</sup> have analyzed the benzene phosphorescence under low resolution for many benzene isotopes in a  $C_6D_6$  host crystal at 4.2°K.

The benzene emission spectra in amorphous solids do not generally show resolvable crystal effects on the ground state vibrations. While a few of the larger of these effects were observed in the lower resolution crystal spectra of NT, it is only with the higher resolution employed here that the effects are discernible on nearly all vibronic bands as a general occurrence and can be quantitatively discussed with confidence.

## II. THEORETICAL CONSIDERATIONS OF CRYSTAL EFFECTS ON VIBRATIONS

Crystal effects on vibrations have been considered in great detail previously both in our laboratory and others. We will only discuss the general results as needed here, referring the reader to the more detailed work when necessary. Site splitting<sup>1,2</sup> for a molecular energy state occurs if this level has a degenerate representation in the group of the molecule which maps into one or more nondegenerate representations in the group of the crystal site. Thus, the doubly degenerate vibrations of  $C_6H_6$  and sym- $C_6H_3D_3$  are mapped into two nondegenerate components in the  $\bar{C}_i$  site of the benzene crystal. The energy difference between these two components in an "ideal mixed crystal" is defined as the site group splitting  $\delta_{ss}$ .<sup>4,12</sup> The concept of an "ideal mixed crystal" implies the absence of all resonance and quasi-resonance intermolecular interactions, while all other interactions remain as in the pure crystal. Dilute (<1%) isotopic mixed crystals of benzene have been shown to be an excellent approximation to the "ideal mixed crystal" for ground state vibrations.<sup>4</sup> This is found not to be true, however, for the lowest excited singlet state of benzene.<sup>13</sup>

For benzene isotopes without a molecular threefold axis, a different effect occurs.<sup>4</sup> It is clear that in the  $\bar{C}_i$  site there are three possible

orientations with respect to rotation about the original  $C_6H_6$  sixfold axis for the isotopic molecule that, at least in principle, could have different energies. Therefore, a nondegenerate molecular vibration could give rise in the spectrum to three lines, each of which is due to differently oriented molecules in three physically equivalent but distinct sites. For other site symmetries, in general a different number of physically distinct orientations are possible. Thus, the number of lines observed in the spectrum for a given vibration is an indication of the effective site symmetry. Table I summarizes the number of orientations group theoretically possible for benzene isotopes in various sites.

The observations of either effect measures the effect of the static field on the guest molecule. However, certain interaction terms present in one are absent in the other. In the orientational effect, which involves two or more guest molecules on different sites, the ground state terms do not necessarily cancel. These terms must cancel in transitions to the two site split components. Moreover, the two site split components have the same symmetry in the crystal site and can interact with each other, increasing the first-order splitting given by interaction with the static crystal field. This latter interaction can not, of course, occur for molecules on widely separated sites, i.e. for the orientational effect. Because of these differences, a direct comparison of the respective magnitudes of these effects is difficult at best and could be misleading.

### III. EXPERIMENTAL

The benzenes were obtained from Merck, Sharp and Dohme, Ltd., of Montreal, Canada. The mixed isotopic solutions were purified by the method described by Colson and Bernstein<sup>14</sup> and directly vacuum distilled into modified "Bridgman type" growing tubes, of the type depicted in Fig.1. Two

thicknesses of crystal were used: 3 mm and  $\sim 20 \mu$ . The thick crystals were grown by lowering the optical cells through a temperature gradient of about  $100^\circ\text{C}/\text{cm}$  directly into a liquid  $\text{N}_2$  cooled chamber at the rate of roughly 1 cm/day. These crystals, which are usually transparent and nearly free of cracks, are then cooled to  $4.2^\circ\text{K}$  with little decrease in quality. This same technique has been successful in growing crystals up to 3 cm in length. The thin crystals are grown in the same type tube by suspending the holder in a dewar approximately 20 cm above the liquid  $\text{N}_2$  surface and subsequently cooling to helium temperatures. Once the crystal holder is completely submerged under the liquid helium, the cell is broken open above the graded seal to insure good thermal contact with the coolant. If this is not done, the sample temperature has been found to remain well above  $4.2^\circ\text{K}$  for some length of time and increases when the sample is irradiated.

The emission spectra of the guest triplet and singlet states were excited by absorbing into the  $\text{C}_6\text{D}_6$  host singlet exciton band from which the excitation energy is rapidly transferred to the lowest excited singlet and triplet states of the guest. These lie approximately  $30 \text{ cm}^{-1}$  to lower energy for each hydrogen substituted into  $\text{C}_6\text{D}_6$ . The guests thus serve as effective energy traps from which emission is observed at low temperatures. Both low and high pressure Hg lamps were employed as excitation sources. Order sorting, where necessary, was accomplished by liquid Kasha or Corning glass filters in conjunction with 0.1 m-atm  $\text{Cl}_2$  and  $\text{Br}_2$  filters. When high orders were used, a small Bausch and Lomb monochromator was used as a predispersing element or as an order sorter.

The phosphorescence spectra of the mixed isotopic crystals were photographed at  $4.2^\circ\text{K}$  on a Jarrell-Ash 3.4 meter Ebert spectrograph. Two gratings were employed. The first had 15000 line/in yielding a plate



factor of roughly  $1.62 \text{ \AA/mm}$  in the third order. Exposure times for the more intense vibronic lines were about 5 min with  $20 \mu$  entrance slits. The weaker lines required approximately one hour exposures. A second grating was used in the eighteenth order where the plate factor was  $0.32 \text{ \AA/mm}$ . Only the more intense vibronic lines of  $\text{C}_6\text{H}_6$  were photographed, requiring exposure times with  $40 \mu$  entrance slits of four hours.

All fluorescence and some of the survey phosphorescence spectra were obtained on a 2.0 meter Czerny-Turner spectrograph, constructed in our laboratory, with a 15000 line/in grating blazed at  $1.0 \mu$ . Spectra were taken in third order where the dispersions are  $2.4 \text{ \AA/mm}$  and  $3.7 \text{ \AA/mm}$  in the phosphorescence and fluorescence regions, respectively. The exposure times for  $5 \mu$  slits were roughly 5 min. Some of the very weak phosphorescence lines were measured from these plates.

Absorption spectra were taken on the 3.4 meter instrument utilizing the fourth order of the lower resolution grating which gives a dispersion of roughly  $1.23 \text{ \AA/mm}$  at  $2650 \text{ \AA}$ . A few spectra were also photographed with the higher resolution grating.

#### IV. EMISSION SPECTRA

Both fluorescence and phosphorescence emissions have been photographed for the isotopic guest in a  $\text{C}_6\text{D}_6$  host crystal at  $4.2^\circ\text{K}$ . Exposure times for the more intense features are roughly equal for the two emissions at lower dispersions, implying nearly equal quantum yields for the singlet and triplet emissions of the guest molecule for the isotopes studies. Furthermore, the measured phosphorescence lifetime of the guest molecule for  $\text{C}_6\text{H}_6$ ,  $\text{C}_6\text{H}_5\text{D}$ ,  $p\text{-C}_6\text{H}_4\text{D}_2$ , and  $\text{sym-C}_6\text{H}_3\text{D}_3$  is independent of the isotopic composition of the guest and its concentration for less than about 1% guest by weight.

The phosphorescence intensity, followed over the first decade change for isolated vibronic lines, decayed exponentially within experimental error with an average lifetime of 8.7 sec. This constant triplet lifetime implies that the quantum yields remain approximately constant independent of the guest and thus appear to be crystal determined.

The phosphorescence does have somewhat sharper lines and is thus easier to photograph at higher dispersions. Due to this smaller linewidth and the greater  $\text{cm}^{-1}$  dispersion available in the phosphorescence spectral region, we have concentrated mainly on the phosphorescence spectrum as a means of studying ground state vibrations. The larger of the site splittings to be discussed is resolved in both emissions and we have used the fluorescence to complement the phosphorescence where possible.

The narrowest phosphorescence linewidth at the highest resolution employed was approximately  $0.1 \text{ cm}^{-1}$  and seemed to be limited by the quality of the crystal. This linewidth was observed only once in a very transparent, seemingly near perfect, crystal of 0.04%  $\text{C}_6\text{H}_6$  in  $\text{C}_6\text{D}_6$ . The linewidth of  $0.1 \text{ cm}^{-1}$  was superimposed on a weaker background whose width was approximately  $0.5 \text{ cm}^{-1}$ . This latter width probably corresponds to residual crystal imperfections. It should be noted that the narrowest linewidth we obtained roughly equals the expected zero-field splitting in the triplet state. Thus, the vibronic linewidth which would result from the uncertainty broadening of the ground state excited vibrational level may be much less than  $0.1 \text{ cm}^{-1}$ , implying that the vibrational relaxation time in the ground state is  $\geq 5 \times 10^{-11} \text{ sec}$ .

The lowest benzene triplet state most likely has  $B_{1u}$  symmetry in point group  $\underline{D}_{6h}$ .<sup>15</sup> It is thus both spin and electronically forbidden. This double forbiddenness can be formally removed in a second-order perturbation scheme



by some combination of spin-orbit and vibronic mixing such that the active vibrations must have symmetries contained in  $\Gamma_T \times \Gamma_S \times \Gamma_R$  where  $\Gamma_i$  is the irreducible representation in point group  $\underline{D}_{6h}$  of the phosphorescing triplet state, the dipole allowed singlet state, and the spin-orbit operator for  $i = T, S$ , and  $R$ , respectively. In this way  $e_{2g}$ ,  $b_{2g}$ , and  $e_{1g}$  vibrations are group theoretically predicted to be active in the phosphorescence spectrum for the free  $\underline{D}_{6h}$  molecule.

Albrecht<sup>16</sup> has analyzed various first- and second-order mechanisms for bringing dipole-allowed singlet character into the triplet state. From the polarized phosphorescence spectrum in solid glass at 77 °K, he concludes that the bulk of the transition probability arises from vibronic mixing, utilizing the  $e_{2g}$  vibrations  $\nu_8$  and  $\nu_9$ <sup>17</sup> of the lowest triplet with the  $^3E_{1u}$  state which is spin-orbit coupled to the dipole-allowed singlet states  $^1A_{2u}$  and  $^1E_{1u}$ . Assuming this mixing route and that the lowest excited singlet has  $B_{2u}$  symmetry, the vibronic structure of the phosphorescence implies the  $^3B_{1u}$  assignment for the lowest triplet state in point-group  $\underline{D}_{6h}$ .

For the lowest excited benzene singlet state,<sup>18</sup>  $B_{2u}$  symmetry in point-group  $\underline{D}_{6h}$  has been established with greater certainty than the triplet symmetry. The spatial forbiddenness of the transition between the ground  $^1A_{1g}$  state and the lowest excited  $^1B_{2u}$  state can be formally removed by vibronic mixing with the dipole allowed  $^1E_{1u}$  and  $^1A_{2u}$  states. The latter route requires a  $b_{1g}$  fundamental of which benzene has none. However,  $e_{2g}$  vibrations can mix a  $B_{2u}$  and an  $E_{1u}$  state. Thus, vibrations of species  $e_{2g}$  are group theoretically predicted to be active in the fluorescence and singlet absorption spectra. Vibronic calculations<sup>19</sup> predict that the  $e_{2g}$  vibration  $\nu_8$  should dominate.

In the  $C_i$  site of the  $C_6D_6$  host crystal, only the u, g-classification of molecular states is retained and, therefore, the above group-theoretical arguments are no longer rigorously correct. However, it is found experimentally (*vide infra*) that the above scheme predicts the dominant features of the spectrum, implying that the molecular classification of states is still approximately valid. The effect of the site is demonstrated by the appearance in both the fluorescence and phosphorescence of a totally symmetric progression built on a relatively weak 0,0 band.

One feature common to both emissions is the activity of a  $72\text{ cm}^{-1}$  lattice phonon. This frequency is apparently determined primarily by the  $C_6D_6$  host, independent of the guest, since the value does not measurably change for different isotopic guests. The phonon emission band is quite broad ( $\sim 5\text{ cm}^{-1}$ ) and is usually photographed only for the stronger molecular bands. Crystalline  $C_6D_6$  does have two observed<sup>20</sup> optical phonons in this range with frequencies of  $62$  and  $77\text{ cm}^{-1}$  at  $4.2^\circ\text{K}$ . Some unobserved optical phonons are also estimated<sup>20</sup> to have very similar frequencies so that the species of the phonon is not known with certainty. Symmetry arguments require that it be a gerade type.

#### 1. $C_6H_6$

The more active vibrations in the phosphorescence spectrum of  $C_6H_6$  in a  $C_6D_6$  host are the same as previously assigned in the solid glasses. However, the much sharper lines in the mixed crystal allow a more nearly complete analysis. For example, some of the fundamentals of  $^{13}C^{12}C_5H_6$  can be assigned (*vide infra*).  $C_6H_6$  has four degenerate fundamentals of  $e_{2g}$  symmetry in  $D_{6h}$ -- $\nu_6$ ,  $\nu_7$ ,  $\nu_8$ , and  $\nu_9$ --of which  $\nu_8$  dominates the phosphorescence in all solvents, being roughly a factor of five more intense than the

next strongest vibronic origin built on  $\nu_9$ . In a  $C_6D_6$  host many other weaker "false" origins are resolved and assigned. Progressions of the totally symmetric  $990\text{ cm}^{-1}$  ( $a_{1g}$ ,  $\nu_1$ ) quantum are also found built on  $\nu_6$ , on the two  $b_{2g}$  fundamentals  $\nu_4$  and  $\nu_5$ , the single degenerate  $e_{1g}$  fundamental  $\nu_{10}$ , the electronic 0,0 and combinations and overtones of overall symmetry  $e_{2g}$ ,  $b_{2g}$ , and  $e_{1g}$ .

Figure 2 shows a microphotometer tracing of the phosphorescence spectrum of  $C_6H_6$  from the 0,0 to 0,0 -  $2500\text{ cm}^{-1}$ . The analysis of the  $C_6H_6$  phosphorescence is given in Table II for energies greater than 0,0 - ( $\nu_8 + \nu_1$ ). Table III compares the relative intensity of the stronger vibronic origins in the  $C_6H_6$  phosphorescence and fluorescence spectra as determined from microphotometer tracings of photographic plates.

Fig. 2 and Tables II and III show the general dominance of  $e_{2g}$  vibrations, and in particular of  $\nu_8$  and  $\nu_9$  in activating the triplet emission spectrum in qualitative agreement with vibronic theory.<sup>16,19</sup> The almost exclusive activation of the benzene phosphorescence by the modes  $\nu_8$  and  $\nu_9$  is partially carried over to all the lower symmetry isotopes with an increase in the activity of certain other vibrations qualitatively predictable from mixing of the normal coordinates in the other isotopes. The only  $e_{2g}$  fundamental not assigned in the phosphorescence is  $\nu_7$ . The fundamental  $\nu_6$  is quite weak. However, when in combination with  $\nu_1$  it steals intensity from  $\nu_8$  by Fermi resonance. The totally symmetric progression built on the  $\nu_{10}(e_{1g})$  origin is the weakest progression analyzed, being weaker than some progressions based on combinations or overtones of  $\underline{u}$ -fundamentals of overall symmetry  $e_{2g}$ . The only  $\underline{g}$ -fundamentals which were not assigned in the phosphorescence of  $C_6H_6$  are  $\nu_2(a_{1g})$ ,  $\nu_3(a_{2g})$ , and  $\nu_7(e_{2g})$ . However,  $\nu_2$  and  $\nu_7$  are assigned from the fluorescence spectrum. No  $\underline{u}$ -vibrations are seen in either emission.

In general the same ground state vibrations are observed in the fluorescence spectrum as in the phosphorescence. However, the relative vibronic activity is substantially different, as can be seen from Table III. The relative intensities in the fluorescence also agree generally with the prediction of vibronic theory outlined earlier. In comparing the two emissions the following features seem noteworthy. The  $b_{2g}$  modes, both fundamentals and combinations, are relatively much more intense in the phosphorescence. The only  $b_{2g}$  mode we have assigned in the fluorescence is the fundamental  $\nu_4$ , which appears very weakly. No vibrations of species  $b_{2g}$  are seen in the gas phase  ${}^1B_{2u} - {}^1A_{1g}$  spectrum.<sup>18</sup> However, its intensity is so much less than  $\nu_1$  and, therefore, the electronic 0,0, that it is not possible to draw definitive conclusions from its appearance. The presence of a  $b_{2g}$  vibronic origin in the free molecule would support a  $B_{1u}$  assignment for the lowest singlet state, but in the crystal the  $b_{2g}$  origin could easily be due to crystal site interactions.

The intensity of the totally symmetric fundamental  $\nu_1$  relative to the most intense vibronic origin is much greater in the fluorescence than in the phosphorescence. It seems reasonable to attribute this to a greater enhancement of the 0,0 in the fluorescence since the transition is only symmetry and not spin forbidden. However, the possibility that vibronic mixing by  $\nu_8$  in the phosphorescence is enhanced simultaneously with the 0,0 in the crystal can not be eliminated.

Site splitting  $\delta_{ss}$  defined in Sec. II is observed for the degenerate  $e_{2g}$  fundamentals  $\nu_6$ ,  $\nu_7$ , and  $\nu_9$  amounting to  $3.1 \text{ cm}^{-1}$ ,  $5.5 \text{ cm}^{-1}$ , and  $0.54 \text{ cm}^{-1}$ , respectively. The splitting of  $\nu_9$  is seen only with the highest resolution employed and is not shown in Table II. Fig. 3 is a densitometer tracing of  $\nu_9$  and  $\nu_8$  with this highest resolution. No distinct splitting is seen in  $\nu_8$ , but, as seen in the Fig. 3, the  $\nu_8$  linewidth is roughly equal to the total bandwidth of the split  $\nu_9$  fundamental.  $\nu_8$  could be much more sensitive to

crystal quality than  $\nu_9$  so that its greater linewidth ( $0.5 \text{ cm}^{-1}$ ) need not completely represent unresolved site splitting. On the other hand, the absence of a splitting in  $\nu_8$  supports the assignment of the splitting in  $\nu_9$  as a genuine site splitting rather than a splitting due to different sites in a non-perfect crystal. A very weak line, which has not been assigned, is observed ca.  $8.5 \text{ cm}^{-1}$  to low energy of the very strong  $0, 0 - \nu_9 - n\nu_1$  progression. The intensity ratio of  $\nu_9$  to the unassigned line is  $> 100$  and much larger than the intensity ratio ( $\lesssim 10$ ) for the two components of any other observed site-split fundamental. We thus feel that this weak feature does not represent the other component of  $\nu_9$ .

The  $e_{1g}$  fundamental  $\nu_{10}$  is also split ( $\delta_{ss} = 6.8 \text{ cm}^{-1}$ ). The vibronic intensity of the two components is different in the fundamental (see Fig. 2), but in the observed combinations of  $\nu_{10}$  with  $\nu_5$  ( $e_{1g} \times b_{2g} = e_{2g}$ ) and with  $\nu_9$ ,  $\nu_8$  and  $\nu_6 + \nu_1$  ( $e_{1g} \times e_{2g} = b_{1g} + b_{2g} + e_{1g}$ ) the splitting repeats itself. The intensity of the components also tends to equalize in these combinations. For the totally symmetric progression built on  $\nu_{10}$  the intensity difference remains. The mode  $\nu_{10}$  is not observed in the fluorescence, apparently since it has  $e_{1g}$  symmetry in  $\underline{D}_{6h}$ , but the overtone  $2\nu_{10}$  ( $e_{2g}$ ) is seen very weakly and a site splitting of  $7 \text{ cm}^{-1}$  can be inferred. Thus, even though the vibronic intensities of the site split components of  $\nu_{10}$  in the phosphorescence is different, the reported site splitting and the frequencies of the components are certainly correct.

In the combination and overtone vibronic bands, site splitting in many u-fundamentals can be inferred. Consider for example the three lines at 808.3, 818.1, and  $826.8 \text{ cm}^{-1}$  removed from the 0, 0 which are assigned as  $2\nu_{16}$ ,  $(e_{2u})^2 = e_{2g} + a_{1g}$  in  $\underline{D}_{6h}$ . The observed splitting could arise by two different routes, both yielding three lines. The first mechanism assumes

the degenerate fundamental  $\nu_{16}$  is not split, but that the site and intramolecular anharmonic terms removes the threefold degeneracy of the overtone  $2\nu_{16}$ . If this were the case, the expected splitting would be small and the pattern not necessarily symmetric. If, however, the fundamental  $\nu_{16}$  is split in the site, then the overtone would be three symmetrically spaced lines for small anharmonicities with intensities determined by the binomial coefficients, i. e., 1:2:1, for equal vibronic activity among the three components. As seen from Fig. 2 and Table II the intensities are roughly in this ratio in the phosphorescence and the splitting nearly symmetrical. The fundamental  $\nu_{16}$  is thus predicted to occur at  $404.2\text{ cm}^{-1}$  and  $413.0\text{ cm}^{-1}$  with a site splitting  $\delta_{ss}$  of  $8.8\text{ cm}^{-1}$ . In the infrared spectrum of  $\text{C}_6\text{H}_6$  in a  $\text{C}_6\text{D}_6$  host crystal,<sup>4a</sup>  $\nu_{16}$  consists of a doublet at  $404.8\text{ cm}^{-1}$  and  $413.0\text{ cm}^{-1}$  ( $\delta_{ss} = 8.2\text{ cm}^{-1}$ ) in excellent agreement with the values inferred from the emission spectra. A small deviation is expected both from anharmonicities and from Fermi resonance among the trio of lines corresponding to  $2\nu_{16}$  each of which rigorously has only symmetry  $a_g$  in the  $\bar{C}_i$  site. The same band observed in the fluorescence, however, does not show this intensity pattern, the high-energy component at  $827\text{ cm}^{-1}$  being more intense relative to the other two.

Similarly, the doublet at  $1101.6$  and  $1110.9\text{ cm}^{-1}$ , which is assigned to  $\nu_{11} + \nu_{16}$ , is the combination of  $\nu_{11}$  with each of the site-split components of  $\nu_{16}$ . Assuming no anharmonic corrections or resonances, the inferred value of  $\nu_{11}$  is  $697.4\text{ cm}^{-1}$  which compares with  $696.9$  observed in the infrared. The quartet assigned to  $\nu_{16} + \nu_{17}$  at about  $1390\text{ cm}^{-1}$  yields for the degenerate fundamental  $\nu_{17}$  the frequencies  $978.3\text{ cm}^{-1}$  and  $982.8\text{ cm}^{-1}$  for an inferred site splitting of  $4.5\text{ cm}^{-1}$ . This should be compared with  $5.6\text{ cm}^{-1}$  observed in the infrared.



Table IV summarizes the fundamental ground state frequencies of  $C_6H_6$  in a  $C_6D_6$  host crystal and the site splittings for the degenerate fundamentals. The g-fundamentals were obtained directly from the emission spectra as false origins for totally symmetric progressions. For the u-fundamentals both the values inferred in this work from combinations and overtones and the values observed directly in the infrared are given. The latter should, of course, be taken for the frequencies of the u-fundamentals. Sixteen of the twenty benzene fundamentals are therefore accurately known and the site splitting of eight of the ten degenerate fundamentals is established for a crystalline benzene environment. For comparison, Table IV also includes the vapor and liquid phase fundamentals.

## 2. $^{13}C^{12}C_5H_6$

The isotope  $^{13}C$  is present in natural abundance in the amount of 1.1%. Thus, roughly 6.6% of any benzene will contain at least one  $^{13}C$  atom. For all the partially deuterated benzenes, more than one isomer with the chemical formula  $^{13}C^{12}C_5H_nD_{6-n}$  exists. The corresponding vibrational frequencies of each of these isotopes will be very similar and difficult to resolve. However, only one isomer  $^{13}C^{12}C_5H_6$  exists. Electronic spectra provide a means of obtaining some of the vibrational frequencies of  $^{13}C^{12}C_5H_6$  as an "impurity" in the  $C_6H_6$  guest in the  $C_6D_6$  crystal. This may have a definite advantage over a conventional infrared spectrum since in an electronic transition the corresponding vibronic lines are separated not by the vibrational energy difference, but by the vibrational energy difference plus the zero-point energy contribution. Thus, even if a particular vibrational frequency is unchanged by introducing  $^{13}C$ , the corresponding vibronic lines will be separated in energy by zero-point effects which may be much larger than any individual shift in a vibration. In actuality, however, the electronic

emission spectra have been only of limited usefulness in these mixed crystals for several reasons. Although  $\sim 6\%$  of the isotopic guest is  $^{13}\text{C}$ -benzene, the  $^{13}\text{C}$  to  $^{12}\text{C}$  phosphorescence intensity ratio is less than  $6\%$  since the transition energy for  $^{13}\text{C}$ -benzene lies above that of  $^{12}\text{C}$ -benzene. Thus, at low temperatures excitation energy transfer to the lowest lying trap, i. e., the  $^{12}\text{C}$ -benzene, can reduce the relative intensity of emission from the  $^{13}\text{C}$ -isotope. Definitive assignments of all but the more intense  $^{13}\text{C}$ -lines are further hampered by the intense background of  $^{12}\text{C}$ -lines along with phonon structure on very heavily exposed plates.

Since  $^{13}\text{C}^{12}\text{C}_5\text{H}_6$  has vibrational symmetry  $\underline{\text{C}}_{2v}$ , the degenerate vibrations of  $^{12}\text{C}_6\text{H}_6$  are split into a and b components. In the  $\underline{\text{C}}_i$  site the vibrations of  $^{13}\text{C}^{12}\text{C}_5\text{H}_6$  can be further perturbed by orientational effects and thus give rise to further apparent splittings or line broadening. However, the orientation effects due to one  $^{13}\text{C}$ -atom should be much smaller than that for one D-atom since the guest-host interaction is more sensitive to changes on the periphery of the interacting molecules. The orientation effects for  $^{12}\text{C}_6\text{H}_5\text{D}$ , discussed in a following section, are in general  $\lesssim 1\text{ cm}^{-1}$  and, thus, are expected to be vanishingly small for  $^{13}\text{C}^{12}\text{C}_5\text{H}_6$ . Therefore, the only new vibrational structure anticipated is the removal of the  $^{12}\text{C}_6\text{H}_6$  vibrational degeneracies.

A somewhat surprising result for  $^{13}\text{C}^{12}\text{C}_5\text{H}_6$  is that the isotope shifts from  $^{12}\text{C}_6\text{H}_6$  in the electronic origins of the phosphorescence and fluorescence are quite different, contrary to the observations for the deuterium substituted isotopes.<sup>21, 11</sup> These shifts to high energy from the corresponding  $^{13}\text{C}_6\text{H}_6$  transitions are  $3.7$  and  $7.8\text{ cm}^{-1}$  in the  $^1\text{B}_{2u} - ^1\text{A}_{1g}$  and  $^3\text{B}_{1u} - ^1\text{A}_{1g}$   $0, 0$  lines, respectively. The electronic origin in the singlet transition, as will be discussed in Section V, is determined from the  $0, 0$  line observed in



absorption. The assignment is confirmed by the presence in the fluorescence spectrum of a progression built on this origin involving a known fundamental<sup>22,23</sup> of  $^{13}\text{C}^{12}\text{C}_5\text{H}_6$ , viz.  $\nu_1$  of species  $a_1$ . The mixed crystal value observed for this fundamental is  $982.0\text{ cm}^{-1}$  compared to a liquid value<sup>22</sup> of  $984\text{ cm}^{-1}$ .

The other  $^{13}\text{C}^{12}\text{C}_5\text{H}_6$  fundamentals assigned with some certainty are  $\nu_4$ ,  $\nu_5$ ,  $\nu_{9a}$ , and  $\nu_{9b}$ . These were obtained from the phosphorescence wherein they serve as origins for progressions in  $\nu_1$ . The 0,0 and 0,0- $\nu_4$  lines are very weak and, thus, were only photographed with the faster, lower resolution spectrograph. The bands involving  $\nu_{9a,b}$  are seen in Fig. 2 as a weak doublet to high energy of the very strong 0,0- $\nu_9$ - $n\nu_1$  progression of  $^{12}\text{C}_6\text{H}_6$ . The progressions built on  $\nu_4$  and  $\nu_5$  are too weak to see on the exposure corresponding to Fig. 2 as is the  $^{13}\text{C}^{12}\text{C}_5\text{H}_6$  0,0. The fundamental frequencies are presented in Table V. The observed  $^{13}\text{C}$ -shifts are also tabulated and compared with the shift calculated from Whiffen's<sup>24</sup> force field employing the modifications of Albrecht.<sup>25</sup> The agreement between the predicted and observed shifts for the fundamentals  $\nu_1$ ,  $\nu_4$ ,  $\nu_5$ , and  $\nu_{9a,b}$  is excellent and generally within the experimental error limits of  $\pm 0.3\text{ cm}^{-1}$ . This range is imposed mainly by the uncertainty in the phosphorescence electronic origin. The vibronic bands terminating in the ground state fundamentals are nearly as sharp as the  $^{12}\text{C}_6\text{H}_6$  lines at the same resolution, confirming our expectations of a very small orientation effect for  $^{13}\text{C}^{12}\text{C}_5\text{H}_6$ .

Other lines are observed in both emissions which seem due to  $^{13}\text{C}$ -benzene, but the analysis leaves some doubt. For example,  $\nu_6$  is expected to be stronger than the assigned  $\nu_1$  in the fluorescence (cf. Table III). A single line of about the correct intensity relative to  $\nu_6$  of  $^{12}\text{C}$ -benzene is seen  $599.5\text{ cm}^{-1}$  from the  $^{13}\text{C}$ -0,0. If the  $\nu_{6a,b}$ -splitting is greater than about  $5\text{ cm}^{-1}$  and if the low energy component is the one observed, the other

component of  $\nu_6$  would be unresolved from the overexposed  $\nu_6$  band of  $^{12}\text{C}$ -benzene. Two very weak lines are seen in the phosphorescence at 600 and 606  $\text{cm}^{-1}$  from the  $^{13}\text{C}$ -0,0 and, thus, seemingly support the assignment to  $\nu_{6a,b}$ . However, this analysis can not be confirmed by a progression of  $\nu_1$  built on  $\nu_{6a,b}$ . Moderately intense lines are seen in the correct spectral region in both the fluorescence and phosphorescence emissions, but they are not easily assignable to  $\nu_{6a,b} + \nu_1$ . Because of the different  $^{13}\text{C}$ -shifts in the phosphorescence and fluorescence electronic origins, the  $^{13}\text{C}$ -lines are shifted relative to the  $^{12}\text{C}$ -lines in the two emissions. Some lines show the correct shift, but a sufficient number do<sup>not</sup> or are absent, to make an analysis difficult. Moreover,  $\nu_{6a,b} + \nu_1$  is most likely in Fermi resonance with  $\nu_{8a,b}$  and possibly also  $\nu_{6a,b} + \nu_{12}$ . Therefore, we do not conjecture a possible assignment for  $\nu_{8a,b}$ , even though in the phosphorescence it is expected to be stronger than the assigned  $\nu_{6a,b}$ , and present the results for  $\nu_{6a,b}$  only as tentative.

For the other  $^{13}\text{C}^{12}\text{C}_5\text{H}_n\text{D}_{6-n}$  isotopes, which are of course present in the other isotopic benzenes, no assignments to  $^{13}\text{C}$ -benzene are made. However, some of the unassigned weak lines, especially in the spectrum of sym- $\text{C}_6\text{H}_3\text{D}_3$ , could easily be due to  $^{13}\text{C}^{12}\text{C}_5\text{H}_3\text{D}_3$ .

### 3. sym- $\text{C}_6\text{H}_3\text{D}_3$

From the correlation diagram shown in Fig. 4, the active vibrations in the phosphorescence of sym- $\text{C}_6\text{H}_3\text{D}_3$  (point group  $\underline{\text{D}}_{3h}$ ) are predicted to have symmetry  $a_2''$ ,  $e'$ , and  $e''$ . However, only vibrations which correlate directly to the active  $\text{C}_6\text{H}_6$  vibrations given in Table III, viz.  $\nu_4$ ,  $\nu_5$ ,  $\nu_6$ ,  $\nu_8$ , and  $\nu_9$ , or are strongly mixed with them in the lower symmetry isotope are intense vibronic origins in the phosphorescence. For the mixing to be strong the vibrations must have similar frequencies and the same symmetry in the

free molecule. Thus, as shown by the normal coordinate analysis of Brodersen and Langseth,<sup>26</sup> relatively strong mixing occurs between  $\nu_9$  and  $\nu_{18}$ ,  $\nu_4$  and  $\nu_{11}$ , and  $\nu_8$  and  $\nu_{19}$ . Weaker mixing does occur to some extent among all vibrations of the same symmetry, and in particular in the  $C_{2v}$  site symmetry among all the vibrations of sym- $C_6H_3D_3$ . This latter mixing, however, does not appear to be very strong since the predicted vibrations are the more intense. Figure 5 shows a microphotometer tracing of the phosphorescence spectrum of sym- $C_6H_3D_3$  in crystalline  $C_6D_6$  near the electronic origin. All of the observed fundamentals serve as false origins for totally symmetric  $\nu_1$  ( $a_1'$ ,  $955\text{ cm}^{-1}$ ) and  $\nu_{12}$  ( $a_1'$ ,  $1003\text{ cm}^{-1}$ ) progressions. The analysis of the sym- $C_6H_3D_3$  phosphorescence out to  $0,0 - (\nu_8 + \nu_1)$  is given in Table VI. Some of the lines shown in Fig. 5 are due to m- $C_6H_4D_2$  and m- $C_6H_2D_4$  impurities. These were identified from the phosphorescence of the corresponding isotopes in a  $C_6D_6$  host. The frequencies are not included in Table VI. The possibility that some of the unassigned lines might be due to isotopic impurities other than the two above has not been investigated.

The vibrational degeneracies in sym- $C_6H_3D_3$ , as in  $C_6H_6$ , can also be removed by the low symmetry crystalline field, giving rise to site splittings. Nine of the ten degenerate vibrations have been assigned from the phosphorescence and fluorescence spectra. Site splitting is directly observed on four  $e'$  and two  $e''$  (vide infra) fundamentals and inferred for the third  $e''$  fundamental.  $\nu_{20}$  was obtained from the fluorescence. Because of the greater linewidth in the fluorescence, the site splitting in  $\nu_{20}$  could be as large as  $3\text{ cm}^{-1}$  and not be resolvable. For  $\nu_{19}$  the site splitting must be  $< 1\text{ cm}^{-1}$  assuming roughly equal intensities for the two components since only one line was observed. The results are summarized in Table VII.

None of the three possible  $a_2'$  vibrations --  $\nu_3$ ,  $\nu_{14}$ , and  $\nu_{15}$  -- were assigned from the emission spectra. These were observed in the infrared for sym- $C_6H_3D_3$  in both  $C_6H_6$  and  $C_6D_6$  hosts and are reported in Ref. 4. For the ground state fundamentals that are seen both in the infrared spectrum and in the electronic emission spectra the agreement is within experimental error except for  $\nu_{17}$ . The site split components of the fundamental  $\nu_{17}$  in the phosphorescence have quite different intensities and the high energy component of the vibration is too weak to observe in most combinations. The two components are seen only in  $\nu_{17}$  and in the doublets tentatively assigned to  $\nu_{17} + \nu_8$  and to  $\nu_{17} + \nu_5$ , where the splitting repeats but the intensities become more nearly equal. This behavior is similar to  $\nu_{10}$  in both  $C_6H_6$  and sym- $C_6H_3D_3$ , but for  $\nu_{17}$  the intensity difference is greater. The more intense component of  $\nu_{17}$  agrees with one of the infrared values in a  $C_6D_6$  host, but the weaker component differs from the other infrared value by ca.  $2\text{ cm}^{-1}$  which is outside the combined experimental errors. The infrared values for this sym- $C_6H_3D_3$  vibration in the two hosts  $C_6H_6$  and  $C_6D_6$  show larger than usual shifts (ca.  $1\text{ cm}^{-1}$ ), but this borders on the reported experimental error. Considering the weakness of the high energy component in the phosphorescence, the assignment to  $\nu_{17}$  may be questioned, but, if this is not the correct assignment and the other component of  $\nu_{17}$  is unobserved, then the vibronic intensities of the two components must be greatly different as  $\nu_{17}$  is seen as a doublet in the mixed crystal infrared spectrum. An alternate assignment of the very weak  $940.7\text{ cm}^{-1}$  component would be to  $\nu_1$  of either one (or both) of the two  $^{13}C^{12}C_5H_3D_3$  species present. Brodersen and Langseth have assigned a Raman line at  $947\text{ cm}^{-1}$ , observed in liquid sym- $C_6H_3D_3$ , to  $^{13}C^{12}C_5H_3D_3$ . If the  $^{13}C$ -isotope shift in the phosphorescence 0, 0 of  $^{13}C^{12}C_5H_3D_3$  is roughly equal to the  $7.8\text{ cm}^{-1}$   $^{13}C$ -shift seen for

$^{13}\text{C}^{12}\text{C}_5\text{H}_6$ , then the line at  $\Delta\nu = 940.7 \text{ cm}^{-1}$  becomes  $\Delta\nu = 948.5 \text{ cm}^{-1}$  based on the unobserved  $^{13}\text{C}-0, 0$ . This near agreement with the Brodersen and Langseth value and the weakness of the vibronic line suggests that perhaps the assignment to  $^{13}\text{C}$  is correct. We choose to report in Table VII a site splitting of  $4.1 \text{ cm}^{-1}$  based on (1) the few tentative combinations involving both components of  $\nu_{17}$  in the phosphorescence and (2) the observation of a comparable site splitting in the infrared.

At  $\Delta\nu \approx 1100 \text{ cm}^{-1}$  the fundamental  $\nu_9(e')$  is in resonance with the combination  $\nu_{10} + \nu_{16}(e' + a' + a_2')$ . The strongest two lines in this region, which might be assigned to  $\nu_9$  since this fundamental is expected to be strong in the phosphorescence, are degenerate with two of the harmonic values for  $\nu_{10} + \nu_{16}$ . Since six lines are observed, the  $\nu_9$  component of the Fermi multiplet is apparently responsible for two of these lines; however, unambiguous assignments can not be made. Similar problems occur  $2270 \text{ cm}^{-1}$  to the red of the  $0, 0$ . The fundamental  $\nu_7$  is expected to occur in this region, but again overlapping combinations make a unique assignment difficult especially from the phosphorescence (see Table VI). However, in the sym- $\text{C}_6\text{H}_3\text{D}_3$  fluorescence, as in that of  $\text{C}_6\text{H}_6$ , the relative vibronic intensity of  $\nu_7$  is increased and, therefore, the lines assigned to  $\nu_7$  stand out more clearly. Of course the higher the energy of the ground state vibration, i. e., the further it is removed from the  $0, 0$ , the more severe these problems become. Furthermore, for all the isotopes the emission lines at the same time become broader and an underlying continuum appears. Thus, the assignments to  $\nu_2$  and  $\nu_{20}$  in the  $3050 \text{ cm}^{-1}$  region are the least certain. As seen by comparing Figs. 3 and 5, the density of lines is less in the  $\text{C}_6\text{H}_6$  emissions and these complications are not so prevalent.

#### 4. $C_6H_5D$

$C_6H_5D$  has vibrational symmetry  $C_{2v}$  for a hexagonal carbon framework. As seen from the correlation diagram in Fig. 4, degenerate vibrations are split into a and b components in this lower symmetry and all vibrations group theoretically can be active in the phosphorescence spectrum. However, those vibrations which correlate directly to the more intense vibrations in the phosphorescence of  $C_6H_6$  or are strongly mixed with one of these active vibrations<sup>23</sup> again dominate. For example, the  $b_2$  vibrations  $\nu_{11}$  and  $\nu_{17b}$  are mixed with  $\nu_4$  and  $\nu_5$ , respectively. For the  $b_1$  vibrations strong mixing occurs among  $\nu_{9b}$ ,  $\nu_{15}$ , and  $\nu_{18b}$  and between  $\nu_3$  and  $\nu_{14}$ . Thus, besides the strong vibrations corresponding to those shown in Table III, the vibrations  $\nu_{11}$ ,  $\nu_{17b}$ ,  $\nu_{15}$ , and  $\nu_{18b}$  also serve as relatively strong vibronic origins of totally symmetric progressions. The weakness of the remaining vibrations again suggests that the molecular symmetry classifications are still approximately valid in the  $C_i$  site.

As a result of this mixing, the actual numbering of the fundamentals is somewhat arbitrary in a number of cases. We have generally followed Brodersen and Langseth, deviating from their labeling scheme only in one of the more arbitrary cases where the vibronic activity seemed to suggest a different assignment, i. e.,  $\nu_{9b}$  and  $\nu_{15}$  are interchanged.

Since there are no degenerate species in point group  $C_{2v}$ , site splitting cannot occur. As pointed out in Section II an apparently similar and related effect can and does occur. The latter has been termed the orientational effect.<sup>4</sup> The expected line pattern is given in Table I for the different isotopes for different choices of the effective site symmetry.



The phosphorescence spectrum near the electronic origin for 0.5%  $C_6H_5D$  in a  $C_6D_6$  host crystal is shown in Fig. 6. Table VIII gives the complete analysis for the measured bands out to  $0,0 - (\nu_{8a,b} + \nu_1)$ . The electronic origin consists of a pair of lines separated by  $6.5\text{ cm}^{-1}$  and all other vibronic bands are doublets or triplets with a total band width of approximately  $7\text{ cm}^{-1}$ . These general features have been previously described by NT. They assigned the  $0,0$  doublet to different orientations of the guest in the crystal, the  $6.5\text{ cm}^{-1}$  "splitting" representing the difference in zero-point energies among distinct guest molecules with different orientations of the deuterium atoms in the nearly  $C_{2h}$  site. Thus, based on each member of the  $0,0$  band vibronic lines appear with energy separations corresponding to vibrational frequencies. Due to the complications of the reduced molecular symmetry and of the orientational effect, the overall density of lines is greatly increased in the  $C_6H_5D$  phosphorescence. Therefore, we have primarily concentrated on the lower energy fundamentals and the more intense combinations.

For example, consider the doublet assigned to  $0,0 - \nu_1(a_1)$  in Fig. 6. Each of these represents the subtraction of a quantum of the totally symmetric mode  $\nu_1$  from its respective  $0,0$  line. NT have been able to show from concentration studies that for some of the more intense lines, the high (low) energy member of a vibronic doublet corresponds to the high (low) energy member of the  $0,0$  band. Therefore, in the analysis for  $\nu_1$  presented in Table VIII the subtractions are made assuming this correlation holds for all vibronic bands. Two values are in this manner obtained for  $\nu_1$ ,  $979.0\text{ cm}^{-1}$  and  $979.4\text{ cm}^{-1}$ . The difference in these two values results from the inequivalence of the guest-host interactions when two guest molecules undergo the same vibration in two physically different crystal directions corresponding

to the two different guest orientations. This apparent splitting, namely  $0.4 \text{ cm}^{-1}$  for  $\nu_1$ , is the orientational effect on this vibration for  $\text{C}_6\text{H}_5\text{D}$  in a  $\text{C}_6\text{D}_6$  host crystal. If this vibration were observed in the infrared or by the Raman effect with sufficient resolution, it would appear as a close doublet with a splitting of  $0.4 \text{ cm}^{-1}$ , instead of the apparent  $6.9 \text{ cm}^{-1}$  splitting observed in the phosphorescence.

Since the crystallographic site symmetry is  $\text{C}_i$  and not  $\text{C}_{2h}$ , triplets are predicted in Table I instead of the generally observed doublets. In fact, triplets are observed for some bands, e. g.,  $\nu_{13b}$  and  $\nu_5$  in Fig. 6, and inferred for many doublets since the high-energy line is broader. From this and the concentration studies of NT, two of the three electronic origins are assigned to the higher energy component of the  $0,0$ . In Table VIII this nearly degenerate pair are designated as  $0,0^1$  and  $0,0^2$ ; the third origin  $6.5 \text{ cm}^{-1}$  to lower energy is called  $0,0^3$ .

For the vibronic bands which appear as doublets, the vibrational energy quantum corresponding to origins  $0,0^1$  and  $0,0^2$  are again nearly degenerate. If the vibronic band is a triplet, the two lines at higher energy are subtracted from the assumed degenerate electronic origins  $0,0^1$  and  $0,0^2$  to obtain the respective vibrational quantum for these two guest orientations. The vibrational energy in the third orientation is obtained by



subtracting the low-energy line of the triplet vibronic band from  $0, 0^3$ . In this fashion, three different frequencies are generally obtained for a given vibrational mode as shown in Table VIII.

The results are summarized in Table IX which gives all the directly observed fundamental frequencies and the orientational effects determined. The near equivalence of the  $0, 0^1$  and  $0, 0^2$  orientations is demonstrated by the fact that only two of the fifteen observed fundamentals show a triplet structure and thus have non-zero entries in column 6 of Table IX. This indicates that the effective site symmetry is very nearly  $C_{2h}$ . However, the effect on the vibrational energy in these two cases is quite large, amounting to  $1-3 \text{ cm}^{-1}$ , compared to an average orientation splitting of  $0.7 \text{ cm}^{-1}$  between  $0, 0^3$  and  $0, 0^2$ . It should be noted that both positive and negative energy shifts are observed for the orientational effect. Where the fundamentals reported here overlap with bands observed directly in the infrared the agreement is excellent. No orientation effect has been reported for  $\nu_{9a}$  or  $\nu_{8b}$  as it is difficult to conclusively assign all the lines in these regions ( $1170$  and  $1575 \text{ cm}^{-1}$  removed from the  $0, 0$  band, respectively). It appears that these fundamentals are in Fermi resonance with combinations (see Table VIII).

Since these orientational effects are all small, it is necessary to carefully analyze the sources and the magnitudes of the errors and their propagation in obtaining the final result. The first consideration is, of course, the validity of the subtractions. These have been made subject to the following restrictions: the concentration studies referred to earlier and the fact that where the assignments are unambiguous the orientational effects are usually small (vide infra and Ref. 4). These considerations lead to the method of subtraction given above. Besides this fundamental problem, experimental errors in line frequencies can distort the final result. Such an analysis leads to an uncertainty in the orientational effect of  $\leq 0.5 \text{ cm}^{-1}$ .

This is a consequence mainly to the three differences involved and round-off error in the absolute energy of any given vibronic line which is reported only to  $\pm 0.1 \text{ cm}^{-1}$ .

### 5. p-C<sub>6</sub>H<sub>4</sub>D<sub>2</sub>

For p-C<sub>6</sub>H<sub>4</sub>D<sub>2</sub>, which has vibrational symmetry  $\tilde{D}_{2h}$  for a hexagonal carbon framework, the correlation diagram in Fig. 4 shows that all the g-vibrations  $a_{1g}$ ,  $b_{1g}$ , and  $b_{3g}$  can group theoretically be active in the phosphorescence spectrum. Besides those vibrations which correlate directly to the more active vibrations of C<sub>6</sub>H<sub>6</sub>, a significant activity is also seen of the vibrations  $\nu_{10b}(b_{3g})$  and  $\nu_3(b_{2g})$  which mix with  $\nu_4(b_{3g})$  and  $\nu_9b(b_{2g})$ , respectively. As in C<sub>6</sub>H<sub>5</sub>D, no degeneracies remain in the vibrational manifold of p-C<sub>6</sub>H<sub>4</sub>D<sub>2</sub>. However, inversion symmetry is preserved in the latter isotope so that in general the same fundamentals are not observed in the infrared and emission spectra.

As can be seen from the phosphorescence spectrum of 0.5% p-C<sub>6</sub>H<sub>4</sub>D<sub>2</sub> shown in Fig. 7, the electronic 0,0 and apparently all other vibronic bands are triplets. Because of the complex nature of this spectrum, it was not completely analyzed. A partial analysis of the spectrum is given in the figure, where the average band width of the triplets is about  $13 \text{ cm}^{-1}$ . The origin of the electronic splittings and their relative magnitude for various isotopes has been discussed by NT. Proceeding as in C<sub>6</sub>H<sub>5</sub>D, in general three different frequencies corresponding to  $0,0^1$ ,  $0,0^2$ , and  $0,0^3$  are observed for each vibrational mode summarized in Table X. These bands are the only ones for which an unambiguous assignment of the orientation effect could be made.

# V. $\overset{1}{B}_{2u} - \overset{1}{A}_{1g}$ ABSORPTION SPECTRA

The vibronic absorption spectra of the guest in an isotopic mixed crystal also provides a useful tool for studying the effects of the crystal environment on the molecular energy levels. Not only can some excited state vibrations be studied but the orientational structure of the 0,0 band can be observed directly. Unlike the fluorescence, the guest singlet - singlet absorption spectra can be very sharp in properly prepared crystals. Care must be exercised to avoid straining the crystal to obtain maximum sharpness.<sup>27</sup> In the thicker crystals of  $C_6H_6$  in  $C_6D_6$ , absorption linewidths as narrow as  $0.6\text{ cm}^{-1}$  have been measured. The structure of the guest 0,0 absorption bands is given in Table XI for mixed crystals of  $C_6H_6$ ,  $C_6H_5D$ ,  $p\text{-}C_6H_4D_2$ , and  $\text{sym-}C_6H_3D_3$  at  $\lesssim 0.005\%$  in  $C_6D_6$  at  $4.2^\circ\text{K}$ . This structure represents the differences in the orientational effects of the ground and lowest excited singlet states, including both the vibrational contribution to their zero-point energies and any electronic effect. That is, if the net contribution to the energy of the zeroth vibronic level for a given orientation were the same for both states and if this were true for all orientations, the 0,0 band would consist of one line. From a comparison of Tables VIII, X, and XI one can see that this difference for the  $\overset{1}{B}_{2u} - \overset{1}{A}_{1g}$  transition is about  $1/5$  that of the  $\overset{3}{B}_{1u} - \overset{1}{A}_{1g}$  transition, but in both transitions the overall splitting for  $p\text{-}C_6H_4D_2$  is about twice that for  $C_6H_5D$ . For a detailed discussion of the significance of these differences, see NT.

The thin crystals ( $\sim 20\text{ }\mu$ ) are required to observe the higher vibronic guest transitions as such absorptions are completely masked by the host absorption in the thick samples. Such guest lines are usually sharper than the fluorescence lines even in these "poorer" crystals. The vibrational frequencies obtained from these absorption lines are less significant than

those of ground state vibrations as excited state levels are more apt to be shifted by interactions with the host. The excitation exchange interactions are typically larger for the singlet vibronic bands than for the ground state vibrational bands and thus quasisresonance interactions<sup>28</sup> with nearby host bands could cause a different shift in each vibronic level. A few  $C_6H_6$  in  $C_6D_6$  levels are given in Table XII from which it can be seen that the  $\nu'_6$  site splitting ( $2.1\text{ cm}^{-1}$ ) is less than that of the  $\nu''_6$  ( $3.1\text{ cm}^{-1}$ ). This splitting should not necessarily be the same as that of the  $\nu'_6$  in a pure  $C_6H_6$  crystal, which has been reported<sup>29</sup> to be  $9\text{ cm}^{-1}$ , since resonance interactions must contribute to the splitting in the pure crystal.

Absorptions due to  $^{13}C$ -containing benzene have also been observed (see Table XI). In thick crystals of about 0.04%  $C_6H_6$ , considerable fine structure is seen surrounding the 0,0 line. The spectrum is shown in Fig. 8 and analyzed in Table XIII. The additional absorptions are tentatively assigned to  $^{13}C$ -benzene,  $^{13}C_2$ -benzene, and to pairs of guest molecules in adjacent sites ("dimers" or "resonance pairs"). The line at  $37856.9\text{ cm}^{-1}$  is assigned to  $^{13}C^{12}C_5H_6$  based on the presence of a  $982\text{ cm}^{-1}$  ( $\nu_1, a_1$ ) progression built on this origin in the  $^1B_{2u} \rightarrow ^1A_{1g}$  emission spectrum, as described earlier, and on its intensity relative to the  $^{12}C_6H_6$  0,0 absorption at very low concentrations. The  $^{13}C_2$ -benzene assignment is made from an analogy with the deuterium isotope effect;<sup>11,21</sup> that is, the  $^{13}C_2$ -line is expected to be shifted twice as much as the  $^{13}C_1$ -line. Also in analogy with the deuterium effect, the o-, m-, or p- $^{13}C_2$ -shifts are expected to be nearly equal (within 10% of one another). The assignment of the line at  $37848.6\text{ cm}^{-1}$  to a resonance pair is made on the basis of its concentration dependence; that is, its intensity decreases more rapidly than that of the  $C_6H_6$  "monomer" absorption with decreasing  $C_6H_6$  concentration. The line at  $37851.2\text{ cm}^{-1}$ , which may also be due to a dimer on a different pair of crystallographic sites, has not been shown to have the expected concentration dependence since it is

too near the intense monomer absorption. At the highest resolution employed, additional absorption lines very near the monomer line are resolved. These are given in Table XIII, but are unresolved in the lower resolution spectrum shown in Fig. 8. Their concentration dependence and, therefore, their definite assignment is unknown. Similar lines were seen for the other deuterated isotopes. The  $C_6H_5D$  data is also given in Table XIII; note the consistency of the orientational effects.

It should be pointed out that polarized absorption spectra of pairs of molecules in isotopic mixed crystals allow the magnitudes and relative signs of pairwise intermolecular excitation exchange interactions to be determined directly, and therefore may be quite important in the interpretation of the pure crystal spectrum. Within the Frenkel limit, assuming short range terms dominate, these interactions are responsible for exciton mobilities and Davydor splittings, as well as for the full exciton band structures of molecular crystals.<sup>30</sup>

## VI. DISCUSSION AND CONCLUSIONS

From the results presented in the summary Tables, both site splittings and orientational effects are seen to be a general occurrence in the benzene crystal. The magnitude of the effects are generally insensitive to isotopic substitution, u- or g-symmetry classification, or to the vibration type as long as the vibration is either in- or out-of-plane. Even the gas-to-crystal frequency shifts (vide infra) follow this general pattern. However, differences are seen comparing in-plane and out-of-plane vibrations. Apparent exceptions for the site shifts are the particular in-plane vibrations  $\nu_2$ ,  $\nu_7$ ,  $\nu_8$ , and  $\nu_{13}$ . However, the anomalously large gas-to-crystal shift for these vibrations parallels an anomalously large gas-to-liquid shift, while for the



other fundamentals the gas-to-liquid shifts are very small. This implies that the gas-to-solid shifts for these vibrations are due to environmentally induced interactions among the molecular vibrations, rather than, for example, repulsive interactions in the solid phase. The average site shift for the in-plane vibrations is very nearly zero and certainly within gas phase experimental error ( $2\text{--}3\text{ cm}^{-1}$ ) for unresolved bands. For the out-of-plane vibrations the average site shift (solid-gas) is greater than  $10\text{ cm}^{-1}$ .

This trend is followed in the site splittings (see Tables IV and VII). The average site splitting for the out-of-plane vibrations is  $\sim 7\text{ cm}^{-1}$  while the in-plane vibrations have an average site splitting of roughly  $3\text{ cm}^{-1}$ . For the orientational effect the distinction between in-plane and out-of-plane bands is less clear and it appears that the effect is more dependent on the particular vibrational mode. We note, however, that for  $\nu_{16}(\text{CC}^{\perp})$  the orientational effect as seen in the infrared<sup>4</sup> in  $\text{C}_6\text{H}_5\text{D}$  and  $p\text{-C}_6\text{H}_4\text{D}_2$  is the largest observed. Furthermore, the average maximum splitting among the orientational components is generally less than site splitting.

We suggest that the distinction between in-plane and out-of-plane modes is probably due to the greater vibrational amplitudes<sup>24</sup> for the out-of-plane displacements. This could imply that interaction with the crystal environment is greater and, therefore, larger site shifts, site splittings, and orientational effects result for larger vibrational displacements. For the lower symmetry isotopes which exhibit orientational effects, the mixing among vibrations, especially in the  $\text{C}_i$  site, tends to equalize the vibrational amplitudes. Hence, one might not expect a clear distinction into certain vibrational classes or types, but rather a general effect larger only for certain motions with large vibrational amplitudes.

The site splitting observed in the fundamental  $\nu_6$  for  $\text{C}_6\text{H}_6$  is  $3.1\text{ cm}^{-1}$ .

When totally symmetric additions are made to  $\nu_6$ ,  $(\nu_6 + \nu_1) + n\nu_1$  comes into Fermi resonance with  $\nu_6 + n\nu_1$  and the measured splitting decreases to roughly  $1.2 \text{ cm}^{-1}$  as shown in Table XIV. The assignment of the " $\nu_6$  component" in the Fermi doublet is made by comparison of the intensities of the members of the Fermi couple with the  $\nu_6$  fundamental in the fluorescence and phosphorescence emissions (cf. Table III and Fig. 3). The decrease in the measured splitting of  $\nu_6$  for  $\text{C}_6\text{H}_6$  in the Fermi couple is apparently due to the resonance. Note, however, that the "lost splitting" does not appear in the other half of the couple  $\nu_8$ . In  $\text{sym-C}_6\text{H}_3\text{D}_3$  this same resonance does not appear to be as strong since the observed value for  $\nu_6 + \nu_1$  is closer to the harmonic value. The site splitting in this progression is more nearly constant and equals  $1.7$ ,  $1.9$  and  $1.5 \text{ cm}^{-1}$  for  $n = 0$ ,  $1$ , and  $2$  respectively. Furthermore,  $\nu_8$  in  $\text{sym-C}_6\text{H}_3\text{D}_3$  is split by  $1.0 \text{ cm}^{-1}$ .

Even though the site-split components of a degenerate fundamental usually have very nearly equal vibronic intensities, the fundamentals  $\nu_{10}$  in both  $\text{C}_6\text{H}_6$  and  $\text{sym-C}_6\text{H}_3\text{D}_3$  and  $\nu_{17}$  in  $\text{sym-C}_6\text{H}_3\text{D}_3$  are exceptions. Exactly how to evaluate this difference in vibronic intensities is not clear at present. An unknown amount of mixing and Fermi resonance between the components contributes to the site splitting and, if substantial, these interactions would tend to equalize the vibronic intensities. Therefore, one might conclude that for the bands where significant intensity differences are seen such intra-site interactions are small. The inverse, however, need not be true; that is, nearly equal intensities does not necessarily imply strong intra-site interactions. It may just be that in these cases the site-split components are equally good "intensity stealers." In combination and overtone bands the relative intensity of the components is variable. For example, the components of  $(\nu_{16} + \nu_{11})$  and  $2\nu_{16}$  in  $\text{C}_6\text{H}_6$  appear as expected in the phosphorescence,



but in the fluorescence  $2\nu_{16}$  differs from this intensity pattern, whereas  $(\nu_{11} + \nu_{16})$  does not. Other examples are evident both from the approximate intensities given in Tables IV and VII and Figs. 2 and 5. Some of these have been previously discussed.

One would also expect an increased mixing and interaction among different molecular vibrations. These effects are expected to show up most clearly where they are symmetry forbidden or weak in the molecule but allowed in the crystal site. For example, for the well known case of  $(\nu_6 + \nu_1) + n\nu_1$  interacting with  $\nu_8 + n\nu_1$ , as given in Table XIV, crystal effects are not obvious. However, for sym- $\text{C}_6\text{H}_3\text{D}_3$   $\nu_{16} + \nu_{10}$  and  $\nu_9$  (see Fig. 5 and Table VI) and  $\nu_{20}$  and  $\nu_2$  seem to be examples of crystal site induced interactions. A further possible indication of the magnitude of the crystal site induced effects can be obtained from anharmonicities. Observing  $n\nu_1$  out to  $n = 5$  in the  $\text{C}_6\text{H}_6$  fluorescence, the anharmonic effects are small in accordance with the above observations. The only other vibrations whose overtones are observed are  $\nu_{16}$  and  $\nu_{10}$ , but in these cases Fermi resonance in the crystal site among the three components of the overtone complicates the analysis of the anharmonicities. Similar difficulties are encountered in the combination bands.

The general conclusion from the gross vibrational structure is that neither the energies nor the symmetry classifications of the vibrations are strongly perturbed by the crystal. This is specifically shown by the magnitude of the site shifts, splittings, and orientational effects and by the dominance of the  $e_{2g}$  vibrations in the singlet and triplet spectra. The most pronounced effect of the crystal is the appearance of the 0, 0 progressions in the two emissions. This, along with the observation of site splittings, indicates that the molecular symmetry is not strictly  $\bar{D}_{6h}$ , but these effects could correspond to very small molecular distortions.

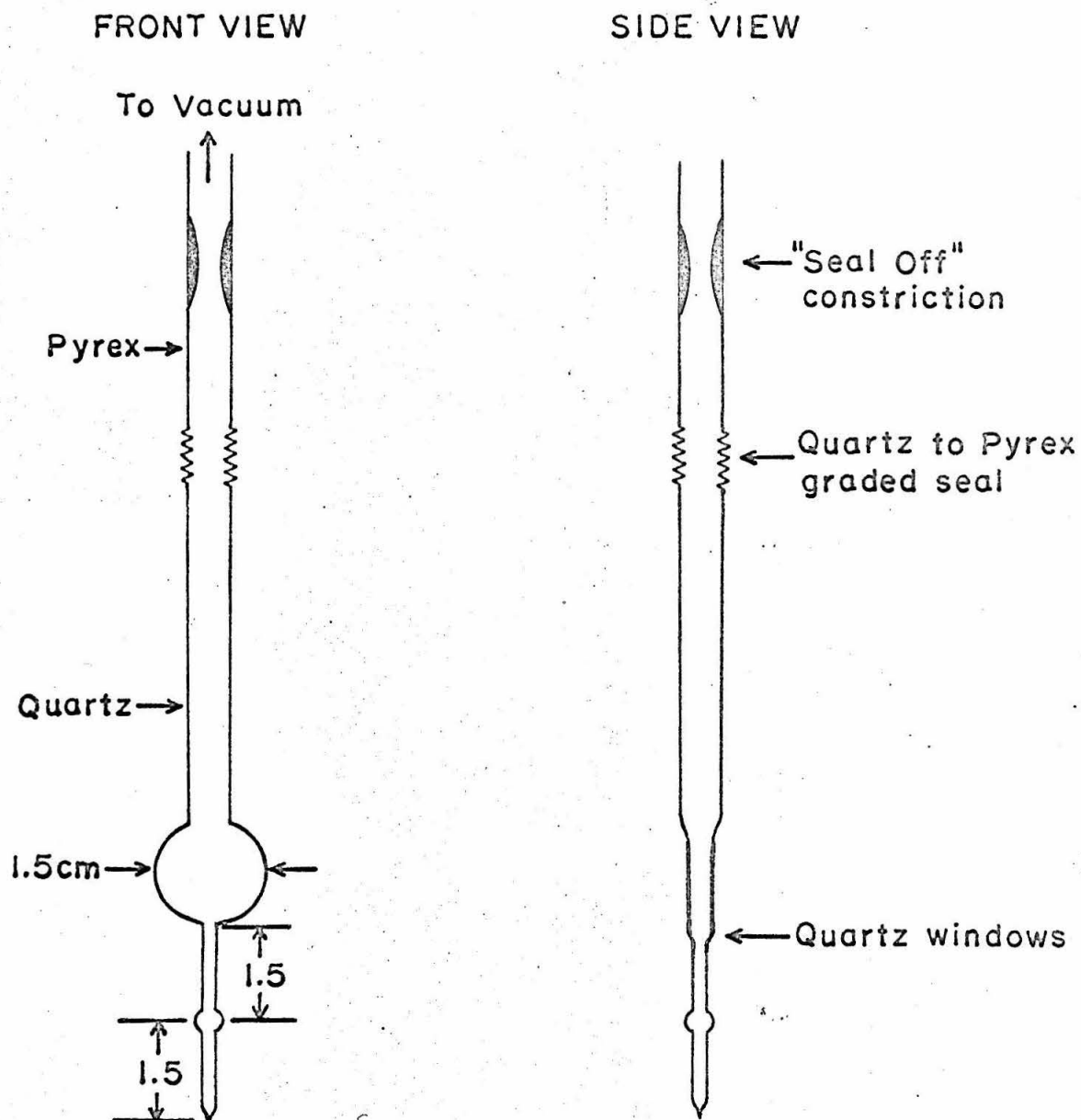
References

- <sup>1</sup>R. S. Halford, J. Chem. Phys. 14, 8 (1946).
- <sup>2</sup>D. F. Hornig, J. Chem. Phys. 16, 1063 (1948).
- <sup>3</sup>H. Winston and R. S. Halford, J. Chem. Phys. 17, 607 (1949).
- <sup>4(a)</sup>E. R. Bernstein, "Site Effects in Molecular Crystals--Site Shift, Site Splitting, Orientational Effect and Intermolecular Fermi Resonance for Benzene Crystals," J. Chem. Phys. (to be published). <sup>(b)</sup>E. R. Bernstein and G. W. Robinson, "Vibrational Exciton Structure in Crystals of Isotopic Benzenes," J. Chem. Phys. (to be published). <sup>(c)</sup>E. R. Bernstein, "Calculation of the Ground State Vibrational Structure and Phonons of the Isotopic Benzene Crystals," J. Chem. Phys. (to be published).
- <sup>5</sup>V. L. Strizhevsky, Opt. i Spektroskopiya 8, 86 (1960).
- <sup>6</sup>E. G. Cox, Rev. Mod. Phys. 30, 159 (1958); E. G. Cox, D. W. J. Cruickshank, and J. A. S. Smith, Proc. Roy. Soc. (London) A247, 1 (1958).
- <sup>7</sup>H. Shull, J. Chem. Phys. 17, 295 (1949).
- <sup>8</sup>B. Ya. Sveshnikov and P. P. Dikun, Dokl. Akad. Nauk SSSR 65, 637 (1949); Zhur. Eksperim. i Teor. Fiz. 19, 1000 (1949); T. V. Ivanova and B. Ya. Sveshnikov, Opt. i Spektroskopiya 11, 322 (1961).
- <sup>9</sup>S. Leach and R. Lopez-Delgado, J. chim. phys. 61, 1636 (1964).
- <sup>10</sup>G. C. Nieman, Thesis, California Institute of Technology, 1965.
- <sup>11</sup>G. C. Nieman and D. S. Tinti, J. Chem. Phys. 46, 1432 (1967).
- <sup>12</sup>E. R. Bernstein, S. D. Colson, R. Kopelman, and G. W. Robinson (manuscript in preparation).
- <sup>13</sup>S. D. Colson, "Electronic Absorption Spectra of Isotopic Mixed Benzene Crystals," J. Chem. Phys. (to be published).
- <sup>14</sup>S. D. Colson and E. R. Bernstein, J. Chem. Phys. 43, 2661 (1965).
- <sup>15</sup>See, however, G. Castro and R. M. Hochstrasser, J. Chem. Phys. 46, 3671 (1967), who suggest that the lowest triplet is  ${}^3B_{2u}$ .

- <sup>16</sup>A. C. Albrecht, J. Chem. Phys. 38, 1326 (1963).
- <sup>17</sup>Here and elsewhere in this work, the normal coordinates are numbered after E. B. Wilson, J. C. Decius, and P. C. Cross, Molecular Vibrations, McGraw-Hill Book Co., Inc., New York, New York, 1955.
- <sup>18</sup>J. H. Callomon, T. M. Dunn, and I. M. Mills, Phil. Trans. Roy. Soc. (London) A259, 499 (1966).
- <sup>19</sup>A. C. Albrecht, J. Chem. Phys. 33, 156, 169 (1960); D. P. Craig, J. Chem. Soc. 1950, 59 2146; J. N. Murrell and J. A. Pople, Proc. Phys. Soc. (London) A69, 245 (1956); A. Liehr, Z. Naturforsch. A16, 641 (1961).
- <sup>20</sup>M. Ito and T. Shigeoka, Spectrochim. Acta 22, 1029 (1966).
- <sup>21</sup>F. M. Garforth, C. K. Ingold, and H. G. Poole, J. Chem. Soc. 1948, 508.
- <sup>22</sup>A. Langseth and R. C. Lord, Jr., J. Chem. Phys. 38, 203 (1938); W. Gerlach, Ber. d. Bayr. Akad. d. Wiss. 1, 39(1932).
- <sup>23</sup>A. R. Gee and G. W. Robinson, J. Chem. Phys.       , (1967).
- <sup>24</sup>D. H. Whiffen, Phil. Trans. Roy. Soc. (London) A248, 131 (1955).
- <sup>25</sup>A. C. Albrecht, J. Mol. Spectry. 5, 236 (1960).
- <sup>26</sup>S. Brodersen and A. Langseth, Danske Videnkab. Selskab, Mat. Fys. Skrifter Kgl. 1, No. 1 (1956).
- <sup>27</sup>S. D. Colson, J. Chem. Phys. 45, 4746 (1966).
- <sup>28</sup>G. C. Nieman and G. W. Robinson, J. Chem. Phys. 38, 1928 (1963).
- <sup>29</sup>V. L. Bronde, Usp. Fiz. Nauk 74, 577 (1961) [English transl. Soviet Phys.-Usp. 4, 584 (1962)].
- <sup>30</sup>A. S. Davydov, Usp. Fiz. Nauk. 82, 393 (1964) [English transl. Soviet Phys.-Usp. 6, 145 (1964)].

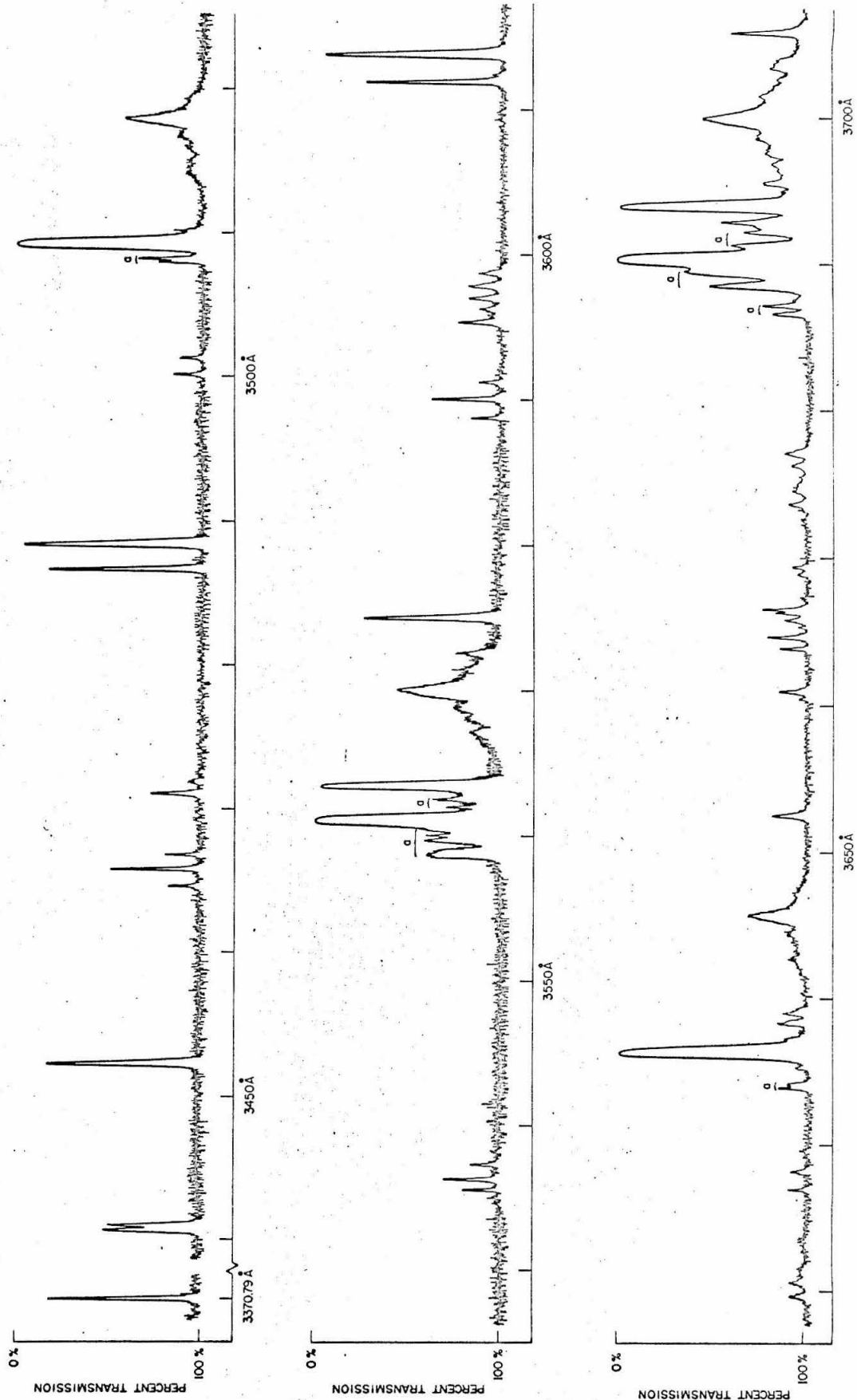
Caption for Fig. 1.

Modified "Bridgman-type" sample cell.

SAMPLE CELL

Caption for Fig. 2.

Microphotometer tracing of a lower resolution plate of the  $C_6H_6$  phosphorescence. The bands labeled "a" are due to  $^{13}C^{12}C_5H_6$  and discussed in the text.





Caption for Fig. 3.

Microphotometer tracing of the  $0, 0-\nu_9$  and  $0, 0-\nu_8$   $C_6H_6$  phosphorescence lines at the highest resolution employed.

PLATE TRANSMISSION  
↓

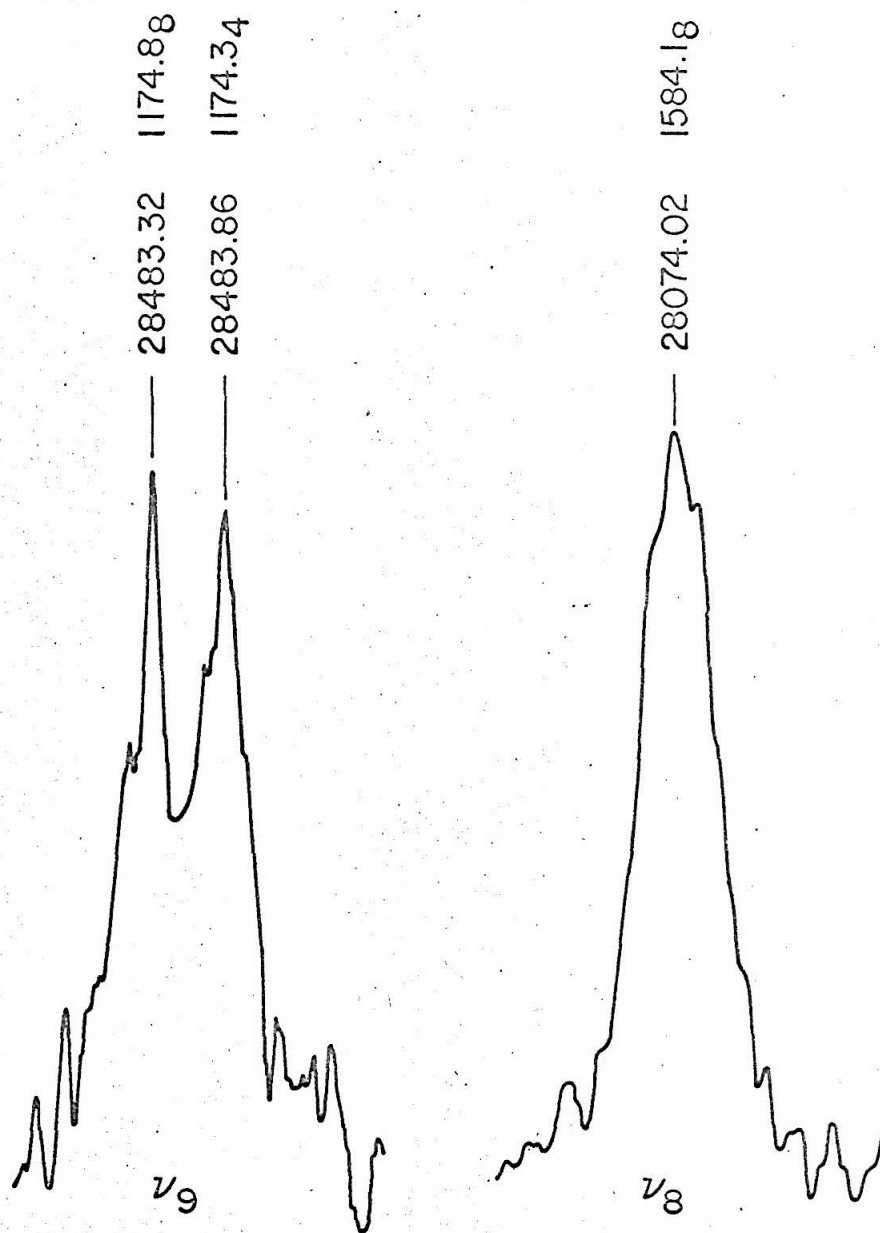
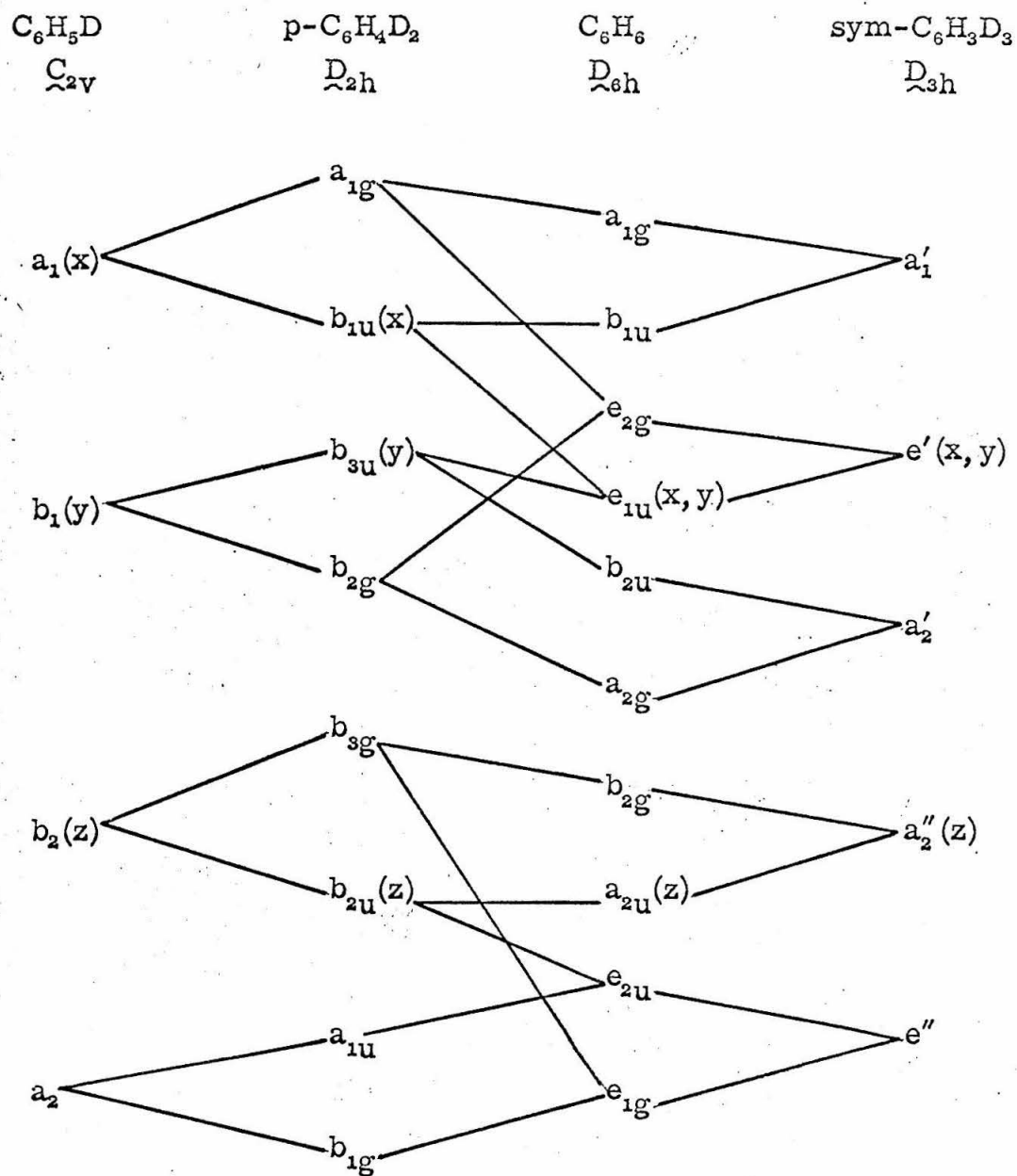


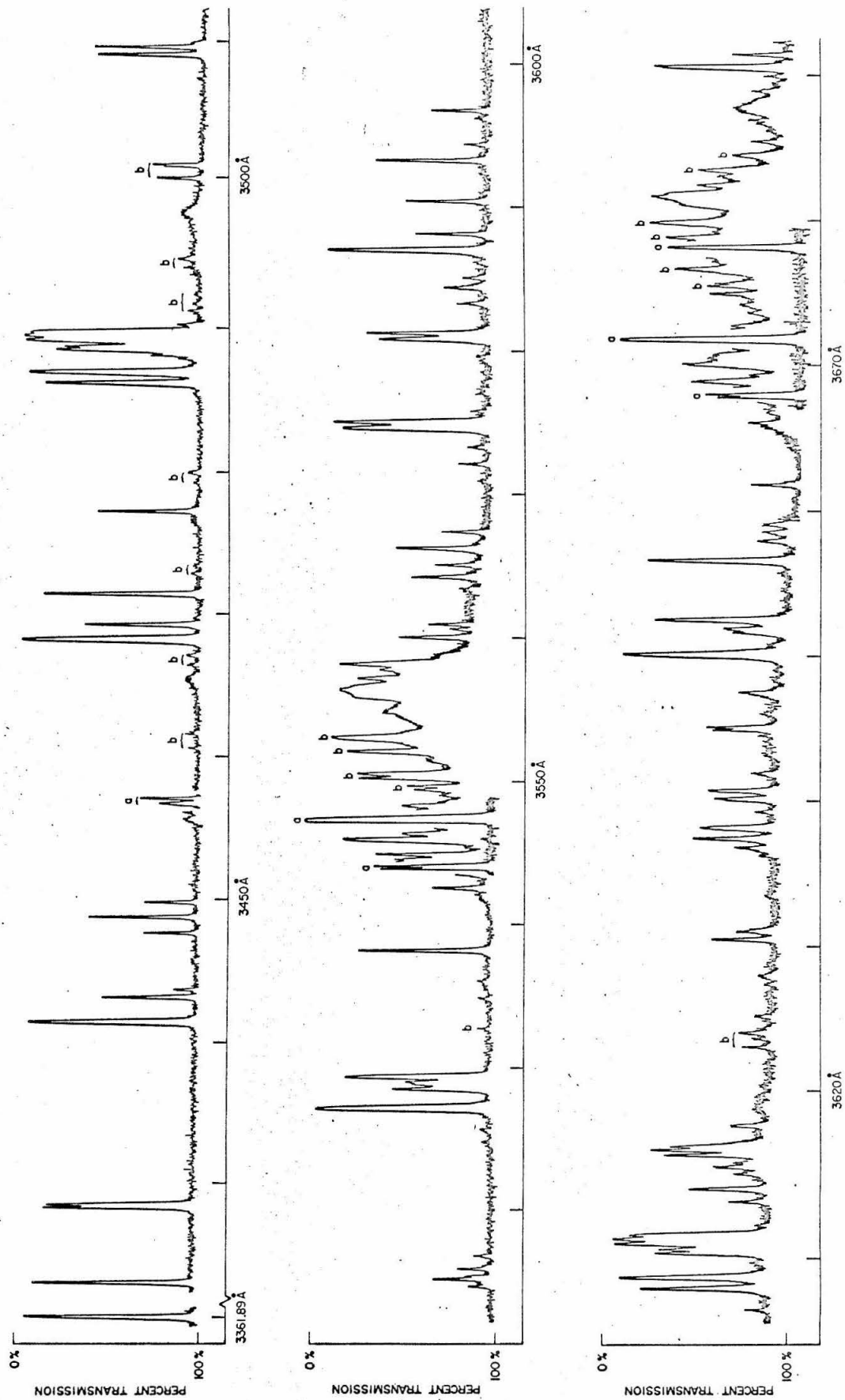
FIG. 4. Correlation diagram for the groups of benzene isotopes<sup>a</sup>.



<sup>a</sup> $z$ -axis always perpendicular to the plane of molecule;  $y$ -axis through  $C_1$ ; and  $x$ -axis between  $C_2$  and  $C_3$ .

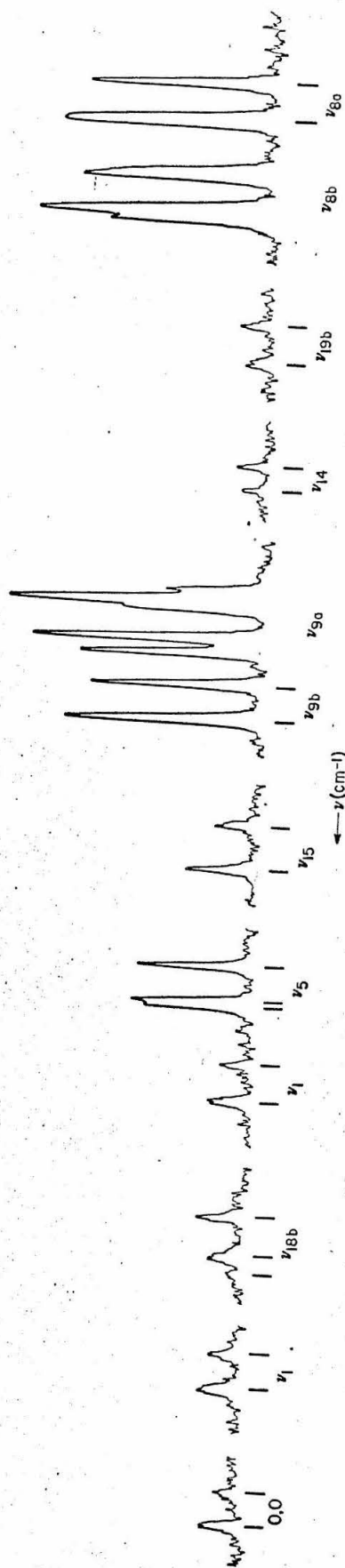
Caption for Fig. 5.

Microphotometer tracing of a lower resolution plate of the sym- $\text{C}_6\text{H}_3\text{D}_3$  phosphorescence. The bands labeled "a" are from a plate exposed 1/20 as long as the rest of the spectrum; "b" denotes bands assigned to m- $\text{C}_6\text{H}_4\text{D}_2$  and m- $\text{C}_6\text{H}_2\text{D}_4$  impurities.



## Caption for Fig. 6.

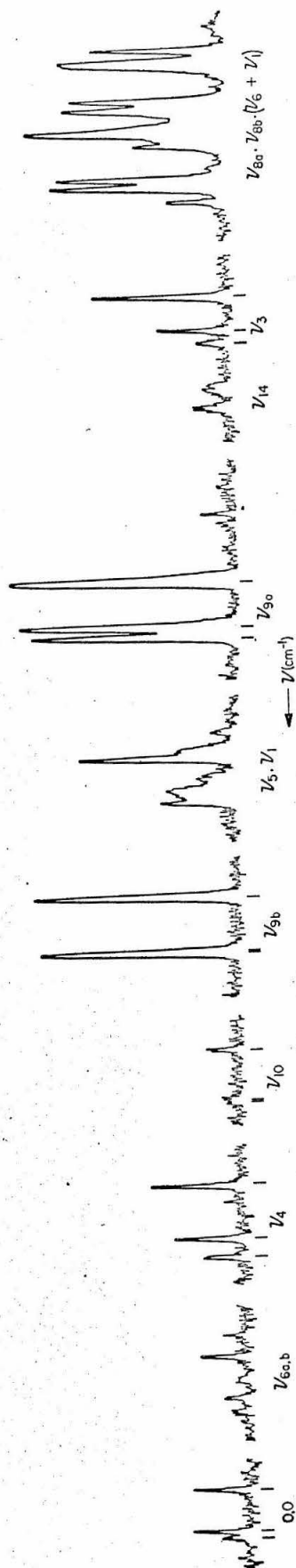
Microphotometer tracing of the stronger bands of the  $C_6H_5D$  phosphorescence. The  $\nu_{8a,b}$  bands are taken from a plate exposed  $1/5$  as long as the rest of the spectrum. Lines under the trace indicate assignments.





## Caption for Fig. 7.

Microphotometer tracing of the stronger bands of the  $p\text{-C}_6\text{H}_4\text{D}_2$  phosphorescence. The  $\nu_8$  region is taken from a plate exposed 1/5 as long as the rest of the spectrum. Lines under the trace indicate assignments.



Caption for Fig. 8.

Microphotometer tracing of the  $C_6H_6$  electronic origin at two concentrations in a 2 mm. thick  $C_6D_6$  host crystal. See Table XIII for the frequencies.

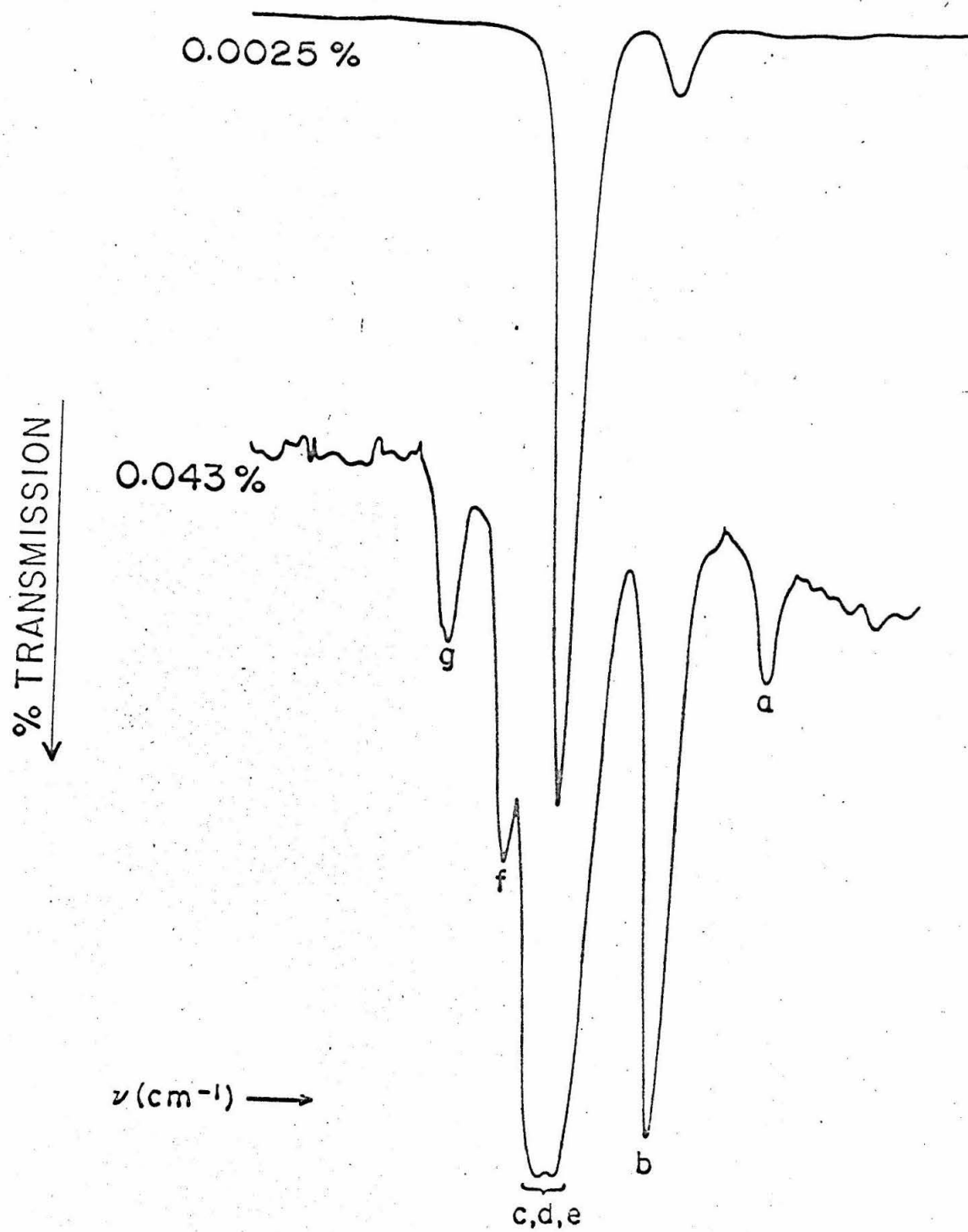


TABLE I. Number of possible orientations for benzene isotopes in sites of different symmetries.

Molecule	Molecular Symmetry	Site Symmetry			
		$\bar{C}_1$	$\bar{C}_i$	$\bar{C}_{2h}$	$\bar{D}_{2h}$
$C_6H_6$	$D_{6h}$	1	1	1	1
$C_6D_6$					
sym- $C_6H_3D_3$	$D_{3h}$	2	1	1	1
p- $C_6H_4D_2$	$D_{2h}$	3	3	3, <sup>a</sup> 2	2
$C_6H_5D$	$C_{2v}$	6	3	3, <sup>a</sup> 2	2
o- $C_6H_4D_2$					
m- $C_6H_4D_2$					
vic- $C_6H_3D_3$					
asym- $C_6H_3D_3$	$C_s$	12	6	6, <sup>a</sup> 3	3

<sup>a</sup>Plane of the site same as the molecular plane.

TABLE II. Analysis of the  $C_6H_6$  phosphorescence.

$\lambda_{\text{air}}(\text{\AA})$	$\nu_{\text{vac}}(\text{cm}^{-1})$	Relative intensity	$\Delta\nu(\text{cm}^{-1})$	Assignment <sup>a</sup>	Vibrational symmetry in $D_{6h}$	Predicted harmonic value ( $\text{cm}^{-1}$ )
3369.90	29666.0	vw		$^{13}\text{C } 0,0$		
70.79	658.2	m	0	0,0		
3441.13	051.9	mw	606.3	$\nu_6$	$e_{2g}$	
41.49	048.8	mw	609.4			
52.85	28953.3	m	704.9	$\nu_4$	$b_{2g}$	
65.22	849.9	w	808.3	$2\nu_{16}$	$e_{2g} + a_{1g}$	809.6
66.40	840.1	mw	818.1			817.8
67.45	831.4	w	826.8			826.0
71.75	795.7	w	862.5	$\nu_{10}$	$e_{1g}$	
72.57	788.9	vw	869.3			
87.25	667.7	m	990.5	$\nu_1$	$a_{1g}$	
87.90	662.4	vw	995.8	$^{13}\text{C } \nu_5$		
89.00	653.3	s	1004.9	$\nu_5$	$b_{2g}$	
3500.82	556.6	w	1101.6	$\nu_{11} + \nu_{16}$	$e_{2g}$	1101.7
01.96	547.3	w	1110.9			1109.9
08.58	493.4	w	1164.8	$^{13}\text{C } \nu_{9a,b}$		
08.83	491.4	w	1166.8			
09.79	483.6	vs	1174.6	$\nu_9$	$e_{2g}$	
10.84	475.1	vw	1183.1	?		
18.63	412.0	w, b	1246.2	$\nu_9 + 71.6$		

TABLE II. (Cont'd)

$\lambda_{\text{air}} (\text{\AA})$	$\nu_{\text{vac}} (\text{cm}^{-1})$	Relative intensity	$\Delta\nu (\text{cm}^{-1})$	Assignment <sup>a</sup>	Vibrational symmetry in $D_{\infty h}$	Predicted harmonic value ( $\text{cm}^{-1}$ )
3535.51	28276.4	w	1381.8	$\nu_{16} + \nu_{17}$	$e_{2g} + a_{2g} + a_{1g}$	1383.1
36.21	270.8	mw	1387.4			1387.5
36.8	266.	vw	1392.			1391.3
37.25	262.5	w	1395.7			1395.7
58.53	093.4	mw	1564.8	$^{13}\text{C} ?$		
59.01	089.6	mw	1568.6			
59.65	084.6	mw, b	1573.6			
60.43	078.4	mw, b	1579.8			
61.00	073.9	vs	1584.3	$\nu_8$ $^{13}\text{C} ?$	$e_{2g}$	
62.56	061.7	mw, b	1596.5			
63.35	055.4	s	1602.8			
63.51	054.2	s	1604.0			
64.32	047.8	vw	1610.4	$\nu_6 + \nu_5$	$e_{1g}$	1596.8
64.52	046.2	vw	1612.0			
70.10	002.4	w, b	1655.8	$\nu_8 + 71.5$		
72.59	27982.9	w, b	1675.3			
74.99	964.1	m	1694.1	$\nu_6 + \nu_1 + 71.3$ $\nu_4 + \nu_1$	$b_{2g}$	1695.4
88.75	856.9	w	1801.3			
90.08	846.5	mw	1811.7	$2\nu_{16} + \nu_1$	$e_{2g} + a_{1g}$	1800.1
91.20	837.9	w	1820.3			
95.31	806.0	w	1852.2	$\nu_{10} + \nu_1$	$e_{1g}$	1808.3
96.24	798.8	vw, b	1859.4			
						1816.5
						1853.0
						1859.8

TABLE II. (Cont'd)

$\lambda_{\text{air}} (\text{\AA})$	$\nu_{\text{vac}} (\text{cm}^{-1})$	Relative intensity	$\Delta\nu (\text{cm}^{-1})$	Assignment <sup>a</sup>	Vibrational symmetry in $D_{6h}$	Predicted harmonic value ( $\text{cm}^{-1}$ )
3597.02	27792.8	w	1865.4	$\nu_{10} + \nu_5$	$e_{2g}$	1867.4
97.86	786.3	w	1871.9			1874.2
98.77	779.3	w	1878.9	$\nu_9 + \nu_4$	$e_{1g}$	1879.5
3611.63	680.4	vw, sh	1977.8	$^{13}\text{C } \nu_5 + \nu_1$		
11.89	678.4	m	1979.8	$2\nu_1$	$a_{1g}$	1981.0
12.42	674.4	vw	1983.8	?		
13.78	664.0	s	1994.2	$\nu_5 + \nu_1$	$b_{2g}$	1995.4
19.30	621.8	w	2036.4		$e_{1g} + b_{2g} + b_{1g}$	2037.1
20.35	613.8	w	2044.4	$\nu_{10} + \nu_9$		2043.9
26.75	565.1	w	2093.1	$\nu_{11} + \nu_{16} + \nu_1$		2092.2
28.00	555.6	w	2102.6			2100.4
29.39	545.0	vw	2113.2	?		
33.76	511.8	w	2146.4			
34.05	509.6	w	2148.6	$^{13}\text{C } \nu_{9a}, b + \nu_1$		
35.32	500.0	vw	2158.2	$\nu_{12} + \nu_{15}$ ?	$a_{2g}$	2158.2
36.13	493.9	vs	2164.3	$\nu_9 + \nu_1$	$e_{2g}$	2165.1
37.23	485.6	vw	2172.6	?		
38.20	478.3	w	2179.9	$\nu_9 + \nu_5$	$e_{1g}$	2179.5
38.35	477.1	w, sh	2181.0			2181.7
38.90	473.0	w	2185.2	$\nu_{15} + \nu_{18}$	$e_{2g}$	2185.5
45.57	422.7	w, b	2235.5	$\nu_9 + \nu_1 + 71.2$		
52.47	370.9	w	2287.3	$\nu_8 + \nu_4$	$e_{1g}$	2289.2



TABLE II. (Cont'd)

$\lambda_{\text{air}} (\text{\AA})$	$\nu_{\text{vac}} (\text{cm}^{-1})$	Relative intensity	$\Delta\nu (\text{cm}^{-1})$	Assignment <sup>a</sup>	Vibrational symmetry in $D_{\infty h}$	Predicted harmonic value ( $\text{cm}^{-1}$ )
3660.46	27311.2	vw	2347.0	$\nu_{14} + \nu_{18}$	$e_{2g}$	2347.4
60.98	307.3	w	2350.9			2351.2
63.87	285.8	w	2372.4	$\nu_{16} + \nu_{17} + \nu_{11}$	$e_{2g} + a_{2g} + a_{1g}$	2373.6
64.65	280.0	w	2378.2			2378.0
65.31	275.1	vw	2383.1			2381.8
65.83	271.2	w, b	2387.0			2386.2, 2387.2
66.31	267.6	w	2390.6	$2\nu_6 + \nu_9$	$2e_{2g} + a_{2g} + a_{1g}$	2390.3
66.53	266.0	w	2392.2			2393.4
68.94	248.1	w	2410.1	?		
69.46	244.2	w	2414.0	?		
73.73	212.5	w	2445.7	$\nu_8 + \nu_{10}$	$e_{1g}$	2446.8
74.58	206.2	w, b	2452.0			2453.6
76.39	192.8	w	2465.4	$\nu_6 + \nu_{11} + \nu_{10}$	$e_{1g}$	2465.9
77.15	187.2	w, b	2471.0			2472.7
86.68	116.9	mw	2541.3	$^{13}\text{C}$ ?		
87.24	112.8	mw	2545.4			
88.60	102.8	m	2555.4			
89.58	095.6	m	2562.6			
90.34	090.1	vs	2568.1	$\nu_8 + \nu_{11}$	$e_{2g}$	2574.8
91.38	082.4	mw	2575.8			
92.27	075.9	mw	2582.3	$^{13}\text{C}$ ?		
93.00	070.6	mw	2587.6			2589.2

TABLE II. (Cont'd)

$\lambda_{\text{air}}(\text{\AA})$	$\nu_{\text{vac}}(\text{cm}^{-1})$	Relative intensity	$\Delta\nu(\text{cm}^{-1})$	Assignment <sup>a</sup>	Vibrational symmetry in $D_{6h}$	Predicted harmonic value ( $\text{cm}^{-1}$ )
3693.91	27063.9	s	2594.3	$\nu_6 + 2\nu_1$	$e_{2g}$	2587.3
94.07	062.7	s	2595.5			2590.4
95.54	052.0	vw	2606.2	$\nu_6 + \nu_1 + \nu_5$	$e_{1g}$	2601.7
95.70	050.8	vw	2607.4			2604.8
3700.06	018.9	w, b	2639.3	$\nu_8 + \nu_1 + 71.2$		
05.92	26976.2	mw	2682.0	$\nu_4 + 2\nu_1$	$b_{2g}$	2685.9

<sup>a</sup>Bands in Fermi resonance are connected by square brackets.

TABLE III. Relative intensity estimates for the stronger vibronic origins in the  $C_6H_6$  phosphorescence and fluorescence spectra.

Symmetry	Vibration	$^3B_{1u} \rightarrow ^1A_{1g}$	$^1B_{2u} \rightarrow ^1A_{1g}$
$e_{2g}$	$\nu_6$	1	100
	$\nu_7$	—	3
	$\nu_8^a$	100	20
	$\nu_9$	25	3
	$2\nu_{16}$	1	3
	$\nu_{11} + \nu_{16}$	<1	5
$b_{2g}$	$\nu_4$	1+	<1
	$\nu_5$	6	—
$a_{1g}$	$\nu_1$	1	22
	$\nu_2$	—	1
$e_{1g}$	$\nu_{10}$	<1	—
0, 0		1	b

<sup>a</sup>Uncorrected for Fermi resonance with  $\nu_8 + \nu_1$ .

<sup>b</sup>Due to appreciable reabsorption, no relative intensity estimate is given.

TABLE IV. Summary of  $C_6H_6$  data ( $cm^{-1}$ ).

$D_{6h}$ symmetry class	Vibration number and type <sup>a</sup>	Fundamental frequency			Site splitting
		gas <sup>b</sup>	liquid <sup>c</sup>	solid <sup>d</sup>	
$a_{1g}$	$\nu_1(CC)$	995.4	(993)	990.5	
		(3073)	(3062)	3063.3	
$a_{2g}$	$\nu_3(H^{\parallel})$	(1350)	1346		
$b_{2g}$	$\nu_4(C^{\perp})$	(707)	(707)	704.9	
	$\nu_5(H^{\perp})$	(990)	(991)	1004.9	
$e_{2g}$	$\nu_6(C^{\parallel})$	608.0	(606)	606.3, 609.4	3.1
	$\nu_7(CH)$	(3056)	(3048)	3042.0, 3047.5	5.5
	$\nu_8(CC)^e$	(1590)	1586	1584.2	$\leq 0.3$
	$\nu_9(H^{\parallel})$	(1178)	1177	1174.3 <sub>4</sub> , 1174.8 <sub>8</sub>	0.5 <sub>4</sub>
$e_{1g}$	$\nu_{10}(H^{\perp})$	(846)	850	862.5, 869.3	6.8
$a_{2u}$	$\nu_{11}(H^{\perp})$	674.0	675	696.9	
				[697]	
$b_{1u}$	$\nu_{12}(C^{\parallel})$	(1010)	1010	1011.3	
	$\nu_{13}(CH)$	(3057)	(3048)	[1011]	
$b_{2u}$	$\nu_{14}(CC)$	(1309)	1309	1312.6	
	$\nu_{15}(H^{\parallel})$	(1146)	1146	[1313]	
				1146.9	
$e_{2u}$	$\nu_{16}(C^{\perp})$	398.6	404	404.8, 413.0	8.2
	$\nu_{17}(H^{\perp})$	(967)	969	[404, 413]	
				978.3, 983.9	
				[978, 983]	

TABLE IV. (Cont'd)

$D_{sh}$ symmetry class	Vibration number and type <sup>a</sup>	Fundamental frequency			Site splitting
		gas <sup>b</sup>	liquid <sup>c</sup>	solid	
$e_{1u}$	$\nu_{18}(H^{\parallel})$	1037	1035	1034.8, 1038.6 [1034, 1038]	3.8
	$\nu_{19}(CC)$	1482	1479		
	$\nu_{20}(CH)^e$	3047	3036		

<sup>a</sup>The vibrational numbering for this and the other isotopes follows Refs. 17 and 26.

<sup>b</sup>Taken from summary given in Ref. 26. ( ) indicates calculated values.

<sup>c</sup>Ref. 18.

<sup>d</sup>The frequencies of the u-fundamentals are from Ref. 4. The values inferred from the u. v. spectra, rounded-off to the nearest  $cm^{-1}$ , are given in parentheses.

<sup>e</sup>Uncorrected for Fermi resonance.

TABLE V. Some observed and calculated fundamental frequencies of  $^{13}\text{C}^{12}\text{C}_5\text{H}_6$ .

$^{13}\text{C}^{12}\text{C}_5\text{H}_6$ fundamental frequency (cm $^{-1}$ ) <sup>a</sup>		$\Delta\nu(^{12}\text{C} - ^{13}\text{C})$	
		observed <sup>b</sup>	predicted <sup>c</sup>
$\nu_1$	982.0	8.5	8.4
$\nu_4$	702.0	2.9	3.5
$\nu_5$	1003.8	1.1	1.0
$\nu_{9a, b}$	1174.6	0.0	0.3
	1172.6	2.0	2.4

<sup>a</sup>The experimental error is  $\pm 0.3$  cm $^{-1}$ .

<sup>b</sup>The mean of the site-split fundamental  $\nu_9$  of  $^{12}\text{C}_6\text{H}_6$  was used to calculate the  $\Delta\nu$  observed.

<sup>c</sup>See text.

TABLE VI. Analyses of the sym-C<sub>6</sub>H<sub>3</sub>D<sub>3</sub> phosphorescence.

$\lambda_{\text{air}} (\text{\AA})$	$\nu_{\text{vac}} (\text{cm}^{-1})$	Relative intensity	$\Delta\nu (\text{cm}^{-1})$	Assignment <sup>†</sup>	Vibrational symmetry in $D_{3h}$	Predicted harmonic value ( $\text{cm}^{-1}$ )
3361.89	29,753.8	m	0			
3422.78	29,207.6	m	546.2	$\nu_{11}$	$a_2''$	
28.14	162.0	m	591.8	$\nu_6$	$e'$	
28.33	160.3	m	593.5			
41.33	050.2	m	703.9	$\nu_4$	$a_2''$	
43.06	035.6	mw	718.2	$\nu_{10}$	$e''$	
43.59	031.1	vw	722.7			
47.55	28,997.8	w	756.0			
48.65	988.6	mw	765.2	$2\nu_{16}$	$a_1' + e'$	
49.70	979.7	w	774.1			
56.55	922.3	ms	831.5	$\nu_{18}$	$e'$	
56.97	918.8	ms	835.0			
68.10	825.9	m	927.9	$\nu_5$	$a_2''$	
69.17	817.1	mw	936.7	$\nu_{17}$	$e''$	
69.66	813.1	vww	940.7			
71.33	799.2	m	954.6	$\nu_1$	$a_1'$	
77.15	750.9	mw	1002.9	$\nu_{12}$	$a_1'$	
86.06	677.5	m	1076.3	$\nu_4 + \nu_{16} ?$	$e'$	1081.9
86.80	671.3	ms	1082.5			1090.9
87.89	662.4	vw	1091.4	$2\nu_{11} ?$	$a_1'$	1092.4

TABLE VI. (Cont'd)

$\lambda_{\text{air}}(\text{\AA})$	$\nu_{\text{vac}}(\text{cm}^{-1})$	Relative intensity	$\Delta\nu(\text{cm}^{-1})$	Assignment	Vibrational symmetry in $D_{3h}$	Predicted harmonic value ( $\text{cm}^{-1}$ )
3488.02	28,661.4	vW	1092.4	?		
88.35	658.6	m	1095.2	$\nu_9$ and $\nu_{10} + \nu_{16}$	$e'$	
88.60	656.5	m	1097.3			
88.99	653.4	ms	1100.4			
89.35	650.4	ms	1103.4			
89.65	848.0	m	1105.8			
90.19	643.5	vW	1110.3			
3508.92	490.6	mW	1263.2	$\nu_{11} + \nu_{10}$	$e'$	1263.0
09.46	486.3	mW	1267.5			1267.5
14.70	443.8	vW	1310.0	$\nu_{16} + \nu_{5'}$ $\nu_{10} + \nu_{6'}$ $\nu_{16} + \nu_{17}$	$e'$	
15.22	439.6	w	1314.2			
15.44	437.8	vW	1316.0			
15.97	433.5	vW	1320.3			
16.88	426.2	vW	1327.6			
27.23	342.8	ms	1411.0	$\nu_{19}$	$e'$	
28.63	331.5	mW	1422.3	$\nu_6 + \nu_{18}$ $\nu_4 + \nu_{10}$	$e' + a'_1 + a'_2$	
29.02	328.3	w	1425.5			
29.52	324.4	m	1429.4			
35.07	279.9	vW	1473.9	$\nu_{11} + \nu_5$	$a'$	1474.1
36.18	271.0	vW	1482.8	$\nu_{11} + \nu_{17}$	$e'$	1482.9
38.32	253.9	mW	1499.9	$\nu_{11} + \nu_1$	$a''_2$	1500.8



TABLE VI. (Cont'd)

$\lambda_{\text{air}}(\text{\AA})$	$\nu_{\text{vac}}(\text{cm}^{-1})$	Relative intensity	$\Delta\nu(\text{cm}^{-1})$	Assignment	Vibrational symmetry in $D_{3h}$	Predicted harmonic value ( $\text{cm}^{-1}$ )
3542.63	28,219.5	w	1534.3	?		
43.90	209.5	s	1544.3	$\nu_6 + \nu_1$	$e'$	1546.5
44.13	207.6	s	1546.2			1548.2
44.67	203.3	w	1550.5			1549.1
45.00	200.7	mw	1553.1	$\nu_{11} + \nu_{12}$	$a_2''$	
45.98	192.9	m	1560.9	$\nu_{18} + \nu_{10}$ ?	$e'' + a_1'' + a_2''$	
46.43	189.3	w	1564.5	?		
47.28	182.6	vs	1571.2	$\nu_8$	$e'$	
47.41	181.6	vs	1572.2			
48.39	173.7	w	1580.1	?		
49.12	168.0	vw	1585.8	?		
56.44	110	m, vb	1644	$\nu_8 + 72$		
57.24	103.6	w	1650.2	$\nu_5 + \nu_{10}$ ?	$e'$	1646.0
57.82	99.1	vw	1654.7			1650.5
58.22	95.9	mw	1657.9	$\nu_4 + \nu_1$	$a_2''$	1658.5
60.09	81.2	w	1672.6	$\nu_{10} + \nu_1$	$e''$	1672.8
60.68	76.5	vw	1677.3			1677.3
61.01	73.9	w	1679.9	?		
64.26	48.3	w	1705.5	$\nu_4 + \nu_{12}$	$a_2''$	1706.8
65.09	41.8	w	1712.0			1710.6
66.29	32.3	mw	1721.5	$2\nu_{16} + \nu_1$	$a_1' + e'$	1719.8
67.42	23.5	w	1730.3			1728.7

TABLE VI. (Cont'd)

$\lambda_{\text{air}} (\text{\AA})$	$\nu_{\text{vac}} (\text{cm}^{-1})$	Relative intensity	$\Delta\nu (\text{cm}^{-1})$	Assignment	Vibrational symmetry in $D_{3h}$	Predicted harmonic value ( $\text{cm}^{-1}$ )
3570.96	27,995.7	vvw	1758.1	$2\nu_{16} + \nu_{12}$	$a'_1 + e'$	1758.9
72.14	986.4	vw	1767.4			1768.1
73.28	977.5	vvw	1776.3			1777.0
74.54	967.6	m	1786.2	$\nu_{18} + \nu_1$	$e'$	1786.1
75.00	964.0	m	1789.8			1789.2
80.71	919.6	mw	1834.2	$\nu_{18} + \nu_{12}$	$e'$	1834.4
81.14	916.1	mw	1837.7			1837.5
83.19	899.9	vw	1853.9	$2\nu_5$ ?	$a'_1$	1855.8
84.27	891.7	vw	1862.1	$\nu_5 + \nu_{17}$	$e'$	1864.5
84.93	886.6	vw	1867.2			1868.6
86.83	871.8	m	1882.0	$\nu_5 + \nu_1$	$a''_2$	1882.4
87.97	863.0	w	1890.8	$\nu_{17} + \nu_1$	$e''$	1891.3
90.45	845.3	w	1908.5	$2\nu_1$	$a'_1$	1909.2
93.05	823.5	mw	1930.3	$\nu_5 + \nu_{12}$	$a''_2$	1930.8
94.18	814.8	vw	1939.0	$\nu_{17} + \nu_{12}$	$e''$	1939.5
96.52	796.7	w	1957.1	$\nu_{12} + \nu_1$	$a'_1$	1957.5
3604.60	734.4	vvw	2019.4	?		
06.13	722.6	mw	2031.2	$\nu_4 + \nu_{16} + \nu_1$ ?	$e'$	2036.0
06.91	716.6	m	2037.2			2043.5
08.03	708.0	vvw	2045.8			

TABLE VI. (Cont'd)

$\lambda_{\text{air}}(\text{\AA})$	$\nu_{\text{vac}}(\text{cm}^{-1})$	Relative intensity	$\Delta\nu(\text{cm}^{-1})$	Assignment	Vibrational symmetry in $D_{3h}$	Predicted harmonic value ( $\text{cm}^{-1}$ )
3608.59	27,703.7	mw	2050.1	$\left. \begin{array}{l} \nu_9 + \nu_1 \\ \nu_{10} + \nu_{16} + \nu_1 \end{array} \right\}$	$\left. \begin{array}{l} e' \\ e' + a'_1 + a'_2 \end{array} \right\}$	
08.88	701.5	mw	2052.3			
09.27	698.8	m	2055.0			
09.67	695.8	m	2058.0			
09.92	693.5	m	2060.3			
12.23	675.8	vw	2078.0	$\left. \begin{array}{l} \nu_4 + \nu_{16} + \nu_{12} \end{array} \right\}$	$\left. \begin{array}{l} e' \end{array} \right\}$	$\left. \begin{array}{l} 2084.8 \\ 2093.8 \end{array} \right\}$
13.08	669.3	w	2084.5			
13.74	664.3	vvw	2089.5	?		
14.12	661.4	vw	2092.4	?		
14.62	657.5	vvw	2096.3	$\left. \begin{array}{l} \nu_9 + \nu_{12} \\ \nu_{10} + \nu_{16} + \nu_{12} \end{array} \right\}$	$\left. \begin{array}{l} e' \\ e' + a'_1 + a'_2 \end{array} \right\}$	
14.95	655.0	vvw	2098.8			
15.45	651.2	w	2102.6			
15.80	648.5	mw	2105.3			
16.05	646.6	w	2107.2			
17.42	636.1	vvw	2117.7	?		
23.59	589.1	vvw	2164.7	?		
24.33	583.4	vvw	2170.4	?		
26.60	566.2	vvw	2187.6	?		
27.37	560.3	vvw	2193.5	?		
28.83	549.2	vvw	2205.6	?		

TABLE VI. (Cont'd)

$\lambda_{\text{air}}(\text{\AA})$	$\nu_{\text{vac}}(\text{cm}^{-1})$	Relative intensity	$\Delta\nu(\text{cm}^{-1})$	Assignment	Vibrational symmetry in $D_{3h}$	Predicted harmonic value ( $\text{cm}^{-1}$ )
3630.37	27,537.6	w	2216.2	$\nu_{11} + \nu_{10} + \nu_1$	$e'$	2219.0
30.93	533.3	vw	2220.5			2223.5
36.21	493.3	vvw	2260.5	$\nu_{11} + \nu_{10} + \nu_{12}; \nu_{10} + \nu_6 + \nu_1$	] — [	
36.69	489.7	vw	2264.1	$\nu_7; \nu_{16} + \nu_5 + \nu_1$		
37.32	484.9	w	2268.9	$\nu_8 + \nu_4; \nu_{16} + \nu_{17} + \nu_1$		
38.09	479.1	w, b	2274.4			
39.14	471.2	vw	2282.6	$\nu_{13}$		
40.08	464.1	w, b	2289.7	$\nu_8 + \nu_{10}$	$e'' + a_1'' + a_2''$	
40.64	459.9	w, b	2293.9			
41.80	451.1	vw	2302.7			
43.14	441.1	vw, b	2312.7	$\nu_6 + \nu_{12} + \nu_{14}$	] — [	
44.41	431.5	vvw	2322.3	$2\nu_{16} + \nu_{12} + \nu_{11}$		
44.97	427.2	vvw	2326.6	$2\nu_{16} + \nu_8$		
45.93	420.0	vvw	2333.8	$\nu_{19} + \nu_{17}$		
47.40	409.0	w	2344.6			
47.55	407.1	w	2346.6			
48.44	401.2	vw, b	2352.6			
50.02	389.3	m	2364.5	$\nu_{19} + \nu_1$	$e'$	2365.4
50.82	383.3	w	2370.5	$\nu_6 + \nu_{18} + \nu_1$	$e' + a_1' + a_2'$	
51.81	375.9	w	2377.9	$\nu_4 + \nu_{10} + \nu_1$	$e'$	
52.40	371.5	mw	2382.3			

TABLE VI. (Cont'd)

$\lambda_{\text{air}}(\text{\AA})$	$\nu_{\text{vac}}(\text{cm}^{-1})$	Relative intensity	$\Delta\nu(\text{cm}^{-1})$	Assignment	Vibrational symmetry in $D_{3h}$	Predicted harmonic value ( $\text{cm}^{-1}$ )
3656.52	27, 340.6	mw	2413.2	$\nu_{19} + \nu_{12}$	$e'$	2413.7
57.86	330.6	vw	2423.2	$\nu_6 + \nu_{18} + \nu_{12}$	$e' + a'_1 + a'_2$	
58.50	325.8	vw	2428.0	$\nu_4 + \nu_{10} + \nu_{12}$	$e'$	
59.04	321.8	vw	2432.0	$\nu_{11} + \nu_5 + \nu_1$	$a'_1$	
60.84	308.4	vvw, b	2445.4	?		
61.79	301.3	vw	2452.5	$\nu_{11} + 2\nu_1$	$a''_2$	2455.4
64.49	281.2	vw, vb	2472.6	?		
65.85	273.0	vvw	2480.8	?		
65.96	270.2	vvw	2483.6	$\nu_{11} + \nu_{12} + \nu_{17}$	$e'$	2484.4
67.63	257.8	ms	2496.0	$\nu_6 + 2\nu_1$	$e'$	
67.83	256.3	ms	2497.5	$(\nu_8 + \nu_5)$	$e''$	
68.71	249.7	vw	2504.1	?		
69.15	246.4	mw	2507.4	$\nu_8 + \nu_{17}(?)$	$e'' + a''_1 + a''_2$	2508.3
69.89	241.0	vw	2512.8			2512.4
70.49	236.6	mw, vb	2517.2	?		
71.54	228.8	vs, b	2525.0	$\nu_8 + \nu_1$	$e'$	2525.8
72.56	221.2	vw	2532.6	?		
73.46	214.5	vw	2539.1	?		
74.04	210.2	vw	2543.6	?		

TABLE VI. (Cont'd)

$\lambda_{\text{air}}(\text{\AA})$	$\nu_{\text{vac}}(\text{cm}^{-1})$	Relative intensity	$\Delta\nu(\text{cm}^{-1})$	Assignment	Vibrational symmetry in $D_{3h}$	Predicted harmonic value ( $\text{cm}^{-1}$ )
3677.84	27, 182.2	s	2571.6	$\nu_8 + \nu_{12}$	$e'$	2574.1
81.34	156.3	mw, vb	2597.5	$\nu_8 + \nu_1 + 72.0$		
82.77	145.7	vw	2608.1	$\nu_4 + 2\nu_1$	$a_2''$	2613.1
85.19	127.9	vw	2625.9	$\nu_{10} + 2\nu_1$ ?		2632.0
86.44	118.7	vw	2635.1	$\nu_6 + 2\nu_{11} + \nu_1$	$e'$	2638.9
86.66	117.1	vw	2636.7			2639.6
87.5	111.3	w, vb	2643.5	$\nu_8 + \nu_{12} + 71.9$		
88.67	102.4	vww	2651.4	?		
89.22	098.3	vww	2655.5	?		
89.71	094.7	vww	2659.1	?		
90.32	090.3	m-b	2663.5	$\nu_8 + 2\nu_{11}$	$e'$	2664.1

† Square brackets connect possible Fermi resonances.

‡ Splitting only resolved at higher resolution.

TABLE VII. Summary of the sym-C<sub>6</sub>H<sub>3</sub>D<sub>3</sub> data (cm<sup>-1</sup>)

$D_{3h}$ symmetry class	Vibration number	Fundamental frequency			Site splitting
		gas <sup>a</sup>	liquid <sup>a</sup>	solid <sup>b</sup>	
a <sub>1</sub> '	$\nu_1$	(956)	955	954.6	
	$\nu_2$	(3074)	(3062)	3046.3	
	$\nu_{12}$	(1004)	1003	1002.9	
	$\nu_{13}$	(2294)	2282	2281.4	
a <sub>2</sub> ''	$\nu_4$	697	697	703.9	
	$\nu_5$	917	918	927.8	
	$\nu_{11}$	531	533	546.2	
e'	$\nu_6$	594	594	591.8 593.5	1.7
	$\nu_7$	2282	2274	2269.0 2274	5
	$\nu_8$	1580	1575	1571.2 1572.2	1.0
	$\nu_9$	1101	1101	FR	
	$\nu_{18}$	833	833	831.5 834.6	3.1
	$\nu_{19}$	1414	1412	1410.8	<1
	$\nu_{20}$	3063	3553	3060.6	<3
e''	$\nu_{10}$	(707)	711	718.2 722.7	4.5
	$\nu_{16}$	(370)	375	[378] [387]	[8.5]
	$\nu_{17}$	(924)	(926)	936.6 940.7	4.1 <sup>c</sup>

<sup>a</sup>Ref. 26. Values in parentheses are calculated.<sup>b</sup>Not corrected for possible Fermi resonance (FR). Values in brackets are inferred from combinations.<sup>c</sup>See text.

TABLE VIII. Analysis of the  $C_6H_5D$  phosphorescence

$\lambda_{\text{air}}$ ( $\text{\AA}$ )	$\nu_{\text{vac}}$ ( $\text{cm}^{-1}$ )	Relative intensity	$\Delta\nu$ ( $\text{cm}^{-1}$ )	Assignment <sup>a</sup>	Vibrational symmetry in $C_{2v}$	Predicted harmonic value ( $\text{cm}^{-1}$ )
3367.85	29690.3	w	0	0, 0 <sup>1</sup>		
67.11	683.8	w	6.5	0, 0 <sup>2</sup>		
3436.53	090.8	vw, b	599.5	0, 0 <sup>3</sup>		
37.37	083.7	vw, b	606.6	$\nu_{6a}$	$a_1$	
39.14	068.8	vw, b	621.5	600.1	$b_1$	
40.11	060.6	vw, b	629.7	$\nu_{11}$	$b_2$	
48.81	28987.2	w	703.1	623.2		
49.60	980.6	w	709.7	$\nu_4$	$b_2$	
66.88	836.1	vw	854.2	703.2		
67.23	833.2	w	857.1	( $\nu_{10a}$ )	$a_2$	
68.15	825.6	w	864.7	$\nu_{18b}$	$b_1$	
76.86	755.3	vw	937.0	857.1		
77.56	747.5	vw	942.8	936.3	$b_2$	
81.95	711.3	w	979.0	$\nu_{17b}$		
82.78	704.4	w	985.9	$\nu_1$	$a_1$	
84.09	693.7	w	996.6	979.4		
84.21	692.7	w	997.6	$\nu_5$	$b_2$	
84.99	686.2	mw	1004.1	997.6		



TABLE VIII. (Cont'd)

$\lambda_{\text{air}}$ (Å)	$\nu_{\text{vac}}$ (cm <sup>-1</sup> )	Relative intensity	$\Delta\nu$ (cm <sup>-1</sup> )	Assignment <sup>a</sup>	Vibrational symmetry in $\zeta_{2v}$	Predicted harmonic value (cm <sup>-1</sup> )
3493.76	28614.3	w	1076.0	1076.0	b <sub>1</sub>	$\nu_{15}$ 1077.7
94.76	606.1	w	1084.2			
3503.58	534.1	m	1156.2	1156.2	b <sub>1</sub>	$\nu_{9b}$ 1156.3
04.39	527.5	mw	1162.8			
05.09	521.8	mw	1168.5	1168.5	b <sub>2</sub>	$3\nu_{16}$
05.43	519.0	mw	1171.3	1171.3	a <sub>1</sub>	$\nu_{9a}$
06.07	513.8	w	1176.5	1176.5	b <sub>1</sub>	$(\nu_{16b} + \nu_{10a})$
06.21	512.2	m	1178.1		a <sub>1</sub>	$\nu_{9a}$
07.51	510.3	w	1180.0	1180	b <sub>2</sub>	$3\nu_{16}$
07.90	499.0	vw	1191.3		b <sub>1</sub>	$(\nu_{16b} + \nu_{10a})$
21.08	392.3	vvw	1297.5	1297.5	b <sub>1</sub>	$\nu_3$ 1298.5
21.95	385.3	vvw	1305.0			
23.88	369.7	vw	1320.6	1320.6	b <sub>1</sub>	$\nu_{14}$ 1318.4
24.43	365.2	vw	1325.1			
39.72	242.8	vw	1447.5		b <sub>1</sub>	$\nu_{19b}$ 1417.7
40.56	236.1	vw	1454.2			
53.27	135.0	vw, b	1555.3	1555.3	a <sub>1</sub>	$\nu_{11} + \nu_{17b}$ 1555.7
54.15	128.1	vw, b	1562.7			
						1558.6
						1566.0

TABLE VIII. (Cont'd)

$\lambda_{\text{air}}$ (Å)	$\nu_{\text{vac}}$ (cm <sup>-1</sup> )	Relative intensity	$\Delta\nu$ (cm <sup>-1</sup> )	Assignment <sup>a</sup>	Vibrational symmetry in $\zeta_{2v}$	Predicted harmonic value (cm <sup>-1</sup> )
3555.41	28118.1	s	1572.2	1572.2	$(\nu_6 + \nu_1)$ b <sub>1</sub> , a <sub>1</sub>	
55.68	115.9	s	1574.4	1574.4	$\nu_{8b}$ b <sub>1</sub>	
56.39	110.3	s	1580.0	1573.5	$(\nu_6 + \nu_1)$ b <sub>1</sub> , a <sub>1</sub>	
56.55	109.1	s	1581.2	1574.7	$\nu_{8b}$ b <sub>1</sub>	
57.67	100.2	s	1590.1	1590.1	$\nu_{8a}$ a <sub>1</sub>	
58.52	093.5	s	1596.8	1590.3		
64.38	047.3	vw, b	1643.0	$\nu_{8b} + 69.7$		
66.52	030.5	vw, b	1659.8	$\nu_{8a} + 69.7$		
69.31	008.6	w	1681.7	1683.1	$\nu_4 + \nu_1$ b <sub>2</sub>	1682.1
70.19	001.7	w	1689.6			1689.1
81.91	27910.1	vw	1780.2	1778.8	$(\nu_{10b} + \nu_1)$ b <sub>2</sub>	
82.57	905.0	vw	1785.3			
89.19	853.5	vw, b	1836.8	1837.6	$\nu_{18b} + \nu_1$ b <sub>1</sub>	1833.2
90.13	846.2	vw	1844.1			1836.1
99.29	775.4	vw	1914.9	1915.5	$\nu_{17b} + \nu_1$ b <sub>2</sub>	1844.1
3600.21	768.3	vw	1922.0			1916.0
04.73	733.4	vw	1956.9	1957.3	$2\nu_1$ a <sub>1</sub>	1922.0
05.68	726.1	vw	1964.2			1958.0
						1965.3

TABLE VIII. (Cont'd)

$\lambda_{\text{air}}$ (Å)	$\nu_{\text{vac}}$ ( $\text{cm}^{-1}$ )	Relative intensity	$\Delta\nu$ ( $\text{cm}^{-1}$ )	Assignment <sup>a</sup>	Vibrational symmetry in $\zeta_{2v}$	Predicted harmonic value ( $\text{cm}^{-1}$ )
3607.12	27715.0	w	1975.3	1975.3		1975.6
07.25	714.0	w	1976.3	1976.3	$\nu_5 + \nu_1$	1976.6
08.09	707.6	w	1982.7	1982.7		1983.5
17.50	635.5	vw	2054.8	2054.8	$\nu_{15} + \nu_1$	2055.0
18.62	627.0	vw	2063.3	2063.3		2063.6
28.03	555.3	m	2135.0	2135.0	$\nu_9 + \nu_1$	2135.2
28.92	548.6	mw	2141.7	2141.7		2142.2
29.67	542.9	mw	2147.4	2147.4	$3\nu_{16} + \nu_1$	
30.04	540.1	m	2150.2	2150.2	$\nu_{9a} + \nu_1$	
30.86	533.9	vw	2156.4	2156.4	$(\nu_{16a} + \nu_{10a}) + \nu_1$	
30.95	533.2	m	2157.1	2157.1	$\nu_{9a} + \nu_1$	
31.30	530.5	vw	2159.8	2159.8	$3\nu_{16} + \nu_1$	
49.54	392.9	vvw	2297.4	2297.4	$(\nu_3 + \nu_1), \nu_{7a}$	
49.87	390.4	vw	2299.9	2299.9		2299.6
50.38	386.6	vw	2303.7	2303.7	$\nu_{14} + \nu_1$	2304.3
66.64	265.0	vw	2425.3	2425.3	$\nu_{19b} + \nu_1$	2426.5
67.60	258.1	vw	2432.2	2432.2		
83.06	143.6	s	2546.7	2546.7	$\nu_{8b} + \nu_1$	
83.34	141.5	s	2548.8	2548.8	$\nu_6 + 2\nu_1$	
84.18	135.3	s	2555.0	2555.0		

TABLE VIII. (Cont'd)

$\lambda_{\text{air}}$ (Å)	$\nu_{\text{vac}}$ (cm <sup>-1</sup> )	Relative intensity	$\Delta\nu$ (cm <sup>-1</sup> )	Assignment <sup>a</sup>	Vibrational symmetry in $\bar{C}_{2v}$	Predicted harmonic value (cm <sup>-1</sup> )
3686.20	27120.5	s	2569.8	2569.8		2569.1
87.18	113.3	s	2577.0	2570.5	$\nu_{8a} + \nu_1$ $a_1$	2582.7

<sup>a</sup> Bands in Fermi resonance are connected by square brackets.

TABLE IX. Summary of  $C_6H_5D$  data ( $cm^{-1}$ )

$C_{2v}$ symmetry class	Vibration number	Gas <sup>a</sup>	Liquid <sup>a</sup>	Solid sites			Orientational effect (arbitrary)		Comments <sup>b</sup>
				1	2	3	2-1	3-2	
a <sub>1</sub>	$\nu_1$	(983)	(983)	979.0		979.4	+0.4		FR: $\nu_5$
	$\nu_{8a}$	(1600)	1593	1590.1		1590.3	+0.2		FR: $\nu_{8a}$ , $\nu_{8b}$ and ( $\nu_6 + \nu_1$ )
	$\nu_{9a}$	(1177)	1177	1171		—			FR: ( $\nu_{10} + \nu_{16b}$ ) and 3 $\nu_{16b}$ ; F
b <sub>1</sub>	$\nu_3$	(1295)	1291	1297.5		1298.5	0	+1.0	
	$\nu_{6b}$	(607)	602	599.5		600.1	0	+0.6	$\nu_{6a}$ and $\nu_{6b}$ in resonance
	$\nu_{8b}$	(1590)	1576	1575.2		—	0		FR: $\nu_{8a}$ , $\nu_{8b}$ and ( $\nu_6 + \nu_1$ ); F
	$\nu_9$	(1157)	1158	1156.2		1156.3	0	+0.1	
	$\nu_{14}$	(1327)	(1325)	1320.6		1318.4	0	-2.2	
	$\nu_{15}$	1077	1077	1076.0		1077.7	0	+1.7	
	$\nu_{16b}$	858	857	854.2	857.1	858.2	+2.9	+1.1	FR: $\nu_{10a}$
	$\nu_{19b}$	1440- 1490	1448	1447.5		1447.7	0	+0.2	FR: $\nu_{19a}$

TABLE IX. (Cont'd)

$\zeta_{2v}$ symmetry class	Vibration number	Gas <sup>a</sup>		Liquid <sup>a</sup>			Solid sites			Orientational effect (arbitrary)			Comments
		Gas <sup>a</sup>		Liquid <sup>a</sup>	1	2	3	2-1	3-2				
$b_2$	$\nu_4$	698		699	703.1		703.2	0	+0.1				
	$\nu_5$	(984)		978	996.6	997.6	997.6	+1.0	0				FR: $\nu_1$
	$\nu_{11}$	607		602	621.4		623.6	0	+2.2				FR: $\nu_6$ in liquid
	$\nu_{17}$	924		925	937.0		936.3	0	-0.7				

<sup>a</sup>Ref. 26 ( ) indicates calculated values.<sup>b</sup>FR = Fermi resonance; F = frequency observed in the fluorescence.

Table X. Summary of p-C<sub>6</sub>H<sub>4</sub>D<sub>2</sub> Data (cm<sup>-1</sup>)

D <sub>2h</sub> symmetry class	Vibration number	Gas <sup>a</sup>	Liquid <sup>a</sup>	Solid sites			Orientational effect (arbitrary)	
				1	2	3	2-1	3-2
b <sub>3g</sub>	ν <sub>4</sub>	(633)	633	637.9	641.2	643.6	+3.3	+ 2.4
	ν <sub>10b</sub>	(739)	736	744.3	742.4	742.9	-1.9	+ 0.5
	ν <sub>3</sub>	(1307)	1311	1310.2	1311.5	1308.1	+1.3	- 3.4
a <sub>1g</sub>	ν <sub>9a</sub>	(1177)	1173	1171.4	1172.9	1171.8	+1.5	- 1.1
b <sub>2g</sub>	ν <sub>9b</sub>	(913)	908	908.4	906.5	909.1	-1.9	+ 2.6
<sup>1</sup> B <sub>3u</sub>	0,0			29721.4	29719.5	29708.0	-1.9	-11.5

<sup>a</sup>Ref. 26 ( ) indicates calculated values.

Table XI.  ${}^1B_{2u} \leftarrow {}^1A_{1g}$  Electronic Transition Energy for Isotopic Guests in a  $C_6D_6$  Host Crystal at 4.2°K.

	mixed crystal <sup>a</sup> (cm <sup>-1</sup> )		gas <sup>b</sup> (cm <sup>-1</sup> )
	${}^{12}C_6H_nD_{6-n}$	${}^{13}C {}^{12}C_5H_nD_{6-n}$	${}^{12}C_6H_nD_{6-n}$
$C_6H_6$	37853.3	37856.9	38086.1
$C_6H_5D$	37885.2 37884.0	37888.8 37887.7	38124
p- $C_6H_4D_2$	37915.7 37912.9		38154
sym- $C_6H_3D_3$	37947.9	37951.4	38184

<sup>a</sup>Uncorrected for interaction with the  $C_6D_6$  host.

<sup>b</sup>The  $C_6H_6$  value is from Ref. 18. For the other isotopes the 0,0 is taken from Ref. 21.



Table XII. Analysis of the  ${}^1\text{B}_{2\text{u}} \leftarrow {}^1\text{A}_{1\text{g}}$  Absorption Spectrum of  
1%  $\text{C}_6\text{H}_6$  in  $\text{C}_6\text{D}_6$  at 4.2°K.

$\lambda_{\text{air}}$	$\nu_{\text{vac}}$	$\Delta\nu$	Assignment	Gas $\Delta\nu$
2641.00	37,853.3	0	0-0	
2605.34	38,371.3	518.0	$\nu_6'$	522.4 <sup>a</sup>
2605.20	38,373.4	520.1		
2577.89	38,779.8	926.5	$\nu_1'$	923 <sup>b</sup>
2543.9	39,297(b)	1444	$\nu_1' + \nu_6'$	

<sup>a</sup>Ref. 18.

<sup>b</sup>F. M. Garforth and C. K. Ingold, J. Chem. Soc., 1948, 417.

Table XIII. Structure Observed Near the Electronic Origin for  $C_6H_6$  and  $C_6H_5D$  at Higher Concentrations in a  $C_6D_6$  Host.

$C_6H_6$ <sup>†</sup>				$C_6H_5D$ <sup>†</sup>			
$\nu$ cm <sup>-1</sup>	I	Assignment		$\nu$ cm <sup>-1</sup>	I	Assignment	
a <sup>‡</sup> 37,860.9	w	$^{13}C_2^{12}C_4H_6$		37,892.5	w	$^{13}C_2^{12}C_4H_5D$	
				37,891.6	w		
b 37,856.9	s	$^{13}C C_5H_6$		37,888.8	s	$^{13}C^{12}C_5H_5D$	
				37,887.7	s		
c ~37,854.1	w,sh			—			
d 37,853.3	vs	Monomer		37,885.2	vs	Monomer	
				37,884.0	vs		
e 37,852.3	w			—			
f 37,851.2	w			37,882.7	w		
				37,881.8	w		
g 37,848.6	w	Resonance Pair		37,880.0	w,b	Resonance Pair	

<sup>†</sup>0.04% guest in a ~ 2 mm  $C_6D_6$  host crystal.

<sup>‡</sup>See Fig. 8.

Table XIV: Change in the  $1600\text{ cm}^{-1}$   $\nu_8$  and  $\nu_6 + \nu_1$  Fermi Couple Splitting with Totally Symmetric  $n\nu_1$  Additions

n	$\nu_8 + \nu_1$ ( $\text{cm}^{-1}$ )	$(\nu_6 + \nu_1) + n\nu_1$ ( $\text{cm}^{-1}$ )	Site splitting ( $\text{cm}^{-1}$ )	Fermi splitting ( $\text{cm}^{-1}$ )	
				solid <sup>a</sup>	gas <sup>b</sup>
0	1584.3	1602.8 1604.0	1.2	19.1	20
1	2568.1	2594.3 2595.5	1.2	26.8	26
2	3551.6	3583.5 3584.8	1.3	32.5	31
3	4534.1	4571.5 <sup>c</sup>		37.4	37
$\nu_6$		606.3 609.4	3.1		

<sup>a</sup>The mean of the split  $(\nu_6 + \nu_1) + n\nu_1$  component is used to calculate the Fermi splitting.

<sup>b</sup>F. M. Garforth, C. K. Ingold and H. G. Poole, J. Chem. Soc., 1948, 427.

<sup>c</sup>This band is too weak to observe any splitting.

THE GUEST PHOSPHORESCENCE LIFETIME IN ISOTOPICALLY  
MIXED BENZENE CRYSTALS

The benzene phosphorescence lifetime has been previously measured in glassy media<sup>1</sup> and in low molecular weight condensed gases.<sup>2</sup> We\* have measured the lifetime of several isotopic benzenes, each as a guest in a  $C_6D_6$  host crystal at 4.2°K.

All experiments were performed by isolating individual vibronic lines with either a 1.0 or 1.8 meter Jarrell-Ash spectrometer. In general, a minimum of two separate determinations on each of two different vibronic lines was performed for each lifetime reported. The vacuum-line distilled and degassed samples were prepared as described earlier in Part III of this thesis. Purification<sup>3</sup> with metallic cesium did not change the phosphorescence lifetime. The exciting light was either a low energy xenon flash lamp of 20  $\mu$ sec duration or a mechanically shuttered c.w. mercury or high pressure xenon lamp. All light sources yielded identical triplet decay times. The phosphorescence intensity was monitored from  $t \approx 0.1$  sec to  $t \approx 40$  sec with an oscilloscope and decayed exponentially in all cases.

As shown in Table I, the triplet lifetimes of the isotopic benzene guest in a  $C_6D_6$  host crystal are independent of the guest and its concentration for less than about 1% guest by weight with a total average lifetime  $\bar{\tau} = 8.7$  sec. For higher guest concentrations, the triplet lifetime decreases and presumably becomes nonexponential due to rapid triplet-triplet annihilation as has been previously reported.<sup>4</sup>

---

\*The author acknowledges the collaboration of S. D. Colson in this work.

Table I. Phosphorescence Lifetimes of Isotopically Mixed Benzene Crystals

host	guest	weight % guest	$\tau^a$ (sec)
$C_6D_6$	$C_6H_6$	0.82	8.7
		0.093	8.5
		0.014	8.7
$C_6D_6$	$C_6H_5D$	0.94	8.5
		0.15	8.5
		0.013	8.6
$C_6D_6$	p- $C_6H_4D_2$	0.86	8.6
		0.16	8.9
		0.016	8.9
$C_6D_6$	sym- $C_6H_3D_3$	1.05	8.7
		0.22	8.3
		0.0088	9.0
sym- $C_6H_3D_3$	$C_6H_6$	0.009	8.4

 $a \pm 0.2$  sec

The only other determination at 4.2°K yielded lifetimes of 16 sec and 26 sec for  $C_6H_6$  and  $C_6D_6$ , respectively, when the respective isotope was trapped in low molecular weight solidified gases.<sup>2</sup> Robinson and Frosch<sup>5</sup> have suggested that the phosphorescence lifetime of a perdeutero compound is very nearly equal to the actual radiative lifetime  $\tau_R$ , the shorter  $\tau$  for the protonated species being attributed to a decreased nonradiative lifetime  $\tau_{NR}$  from Franck-Condon arguments. This has been confirmed for benzene by the quantum yield measurements of Lim.<sup>6</sup> The arguments of Robinson and Frosch would predict a monotonic dependence of the radiationless rate on the number of deuteriums present, which is in agreement with the experimental observations of the benzene phosphorescence lifetime in glassy solutions at 77°K<sup>7</sup> and of the naphthalene phosphorescence lifetime in perdeuterated durene.<sup>8</sup> Thus, both the magnitude of the benzene triplet lifetime, 8.7 sec, and its constancy with partial deuteration suggest anomalous behavior in the crystal.

The results imply that the triplet lifetime is entirely crystal determined, either by a shortening of the radiative lifetime or by an unknown radiationless mechanism. The usual nonradiative process for depopulating triplet states can be eliminated. From the absence of a concentration effect and the constancy of the lifetime for different excitation conditions and degree of purification, impurity or photo-product quenching and triplet-triplet annihilation are ruled out as possible mechanisms for shortening the lifetime. Appreciable inter-system crossing to the ground state is apparently also eliminated by the absence of a deuterium effect. Moreover, Hirota and Hutchison<sup>8</sup>

have found that the naphthalene triplet lifetime generally lengthens with complete deuteration of the durene host, which they attribute to a decrease of the intersystem crossing rate. It seems reasonable to assume that the  $C_6D_6$  host behaves similarly. As seen from Table I, the phosphorescence lifetime of 0.01%  $C_6H_6$  in 1,3,5- $C_6H_3D_3$  host is  $(8.4 \pm 0.2)$  sec, which is equal to the mean lifetime of 8.7 sec observed in the  $C_6D_6$  host within our experimental error. If a host effect is present, it appears to be in the correct direction. However, from our data we can only conclude that degree of deuteration in the host is also not rate determining at 4.2°K. If the radiative lifetime is shortened from 26 sec to 8.7 sec in the crystal, it is easy to account for the absence of a deuterium effect. Namely, the nonradiative rate is sufficiently small relative to the radiative rate even for  $C_6H_6$  that a further decrease in the nonradiative rate from deuteration does not measurably affect the overall triplet lifetime.

We can not at this time definitively identify the process by which the lifetime becomes "crystal determined". However, it is interesting to note that the triplet state in the crystal has been shown<sup>9</sup> to have an effective symmetry lower than  $\bar{D}_{6h}$  such that the benzene phosphorescence is no longer orbitally forbidden. The remaining spin forbiddance can be formally removed in the lower symmetry by a direct spin-orbit interaction with a dipole allowed singlet state. In addition, other vibronic mechanisms group theoretically forbidden for the free molecule can occur. Thus, there are reasons one might expect the radiative lifetime to be shortened.

## REFERENCES

1. D. S. McClure, J. Chem. Phys 17, 905 (1949).
2. M. R. Wright, R. P. Frosch and G. W. Robinson, J. Chem. Phys 33, 934 (1960).
3. S. D. Colson and E. R. Bernstein, J. Chem. Phys. 43, 2661 (1965).
4. H. Sternlicht, G. C. Nieman, and G. W. Robinson, J. Chem. Phys. 38, 1326 (1963).
5. G. W. Robinson and R. P. Frosch, J. Chem. Phys. 37, 1962 (1962); 38, 1187 (1963).
6. E. C. Lim, J. Chem. Phys. 36, 3497 (1962).
7. A. Kalantar, private communication.
8. N. Hirota and C. A. Hutchison, Jr., J. Chem. Phys. 46, 1561 (1967).
9. G. C. Nieman and D. S. Tinti, J. Chem. Phys. 46, 1432 (1967); see, also, the earlier sections of Part III of this thesis.



## PROPOSITION I

Although relatively slow vibrational relaxation in simple van der Waals solids has now been established, no quantitative measurement of the kinetics have been obtained.

We suggest the systems OH and CN in solid matrices for further study of vibrational relaxation in excited electronic states.

The work described in Part II of this thesis shows that vibrational relaxation in excited electronic states of diatomic guest molecules in solid hosts can be quite slow. However, this work suffers from the inadequate manner in which the data can be treated and many questions surrounding vibrational relaxation in solids remain unanswered. The most obvious are (1) the manner in which the relaxation rate changes with vibrational level, (2) the importance of  $\Delta v = 2$  transitions, and (3) the dependence of the relaxation rate on the vibrational quantum. We here suggest two systems wherein these questions may be answerable.

One of the major difficulties in the earlier work arises from the use of X-irradiation to excite the diatomic emission spectrum, since the excitation mechanism can be quite complicated. The kinetics for the relaxation greatly simplify if only one vibrational level of the excited electronic state is initially populated. This condition can be experi-

mentally chosen in an allowed band system by absorbing directly into only one level of the excited state.

The  $A^2\Sigma^+ - X^2\Pi_1$  system of OH is an allowed transition for which emission from  $v' > 0$  is seen in solid Ne at 4.2°K. Some preliminary work on this system using X-irradiation to excite the emission spectrum is described in this thesis. It is proposed that the intensity of emission from various  $v'$  in the  $A^2\Sigma^+$  state be studied as a function of the vibrational level initially excited by direct absorption. The Franck-Condon factors<sup>1</sup> for this system are such that  $v' = 0, 1, 2$ , and perhaps 3 can be reasonably populated by absorption from the  $v'' = 0$  level. Moreover, all strong emission bands, except for the 0,0 band, occur considerably to lower energy. Therefore, filtering problems are minimized.

A second diatomic, from which emission has not been reported in solid matrices, is the cyanogen radical. CN has two well-known allowed band systems which connect with the ground state:  $A^2\Pi - X^2\Sigma^+$  and  $B^2\Sigma^+ - X^2\Sigma^+$ .<sup>2</sup> Both of these have been seen in absorption in an Ar matrix.<sup>3</sup> The red system  $A \rightarrow X$  lies in a difficult spectral region for this study ( $\nu_{00} = 9114 \text{ cm}^{-1}$ ), but the violet system  $B \rightarrow X$  ( $\nu_{00} = 25798 \text{ cm}^{-1}$ ) can probably be excited in emission. The latter system involves a very small change in intermolecular distance and, therefore, the strong bands of the system involve the  $\Delta v = 0$  sequence. However, published Franck-Condon factors<sup>4</sup> suggest that  $v = 0, 1$  and perhaps 2 can be reasonably populated. A more serious problem is the small change in  $\omega_e$  between the ground and excited states, which means that members of the strong  $\Delta v = 0$  sequence lie close together ( $\sim 10 \text{ Å}$ ) and, thus, cause a filtering problem. This is much less serious for the red system of CN and for OH.

The experimental procedure to be employed for either diatomic suggested can be generally outlined as follows.  $\text{H}_2\text{O}$  - Ne or  $\text{HCN}$ -rare-gas mixtures are deposited onto a liquid helium cooled optical window. OH or CN is formed in situ by photolysis with ultraviolet light, whose wavelength is chosen to give the products desired:  $\lambda < 1860 \text{ \AA}$  for OH<sup>5</sup> and  $\lambda < 1810 \text{ \AA}$  for CN.<sup>5</sup> Alternately the system can be prepared by photolysis in the gas phase during deposition of  $\text{H}_2\text{O}_2$  or  $\text{C}_2\text{N}_2$  plus matrix gas. This may have the advantage of producing only OH and CN,



whereas photolysis of  $\text{H}_2\text{O}$  and  $\text{HCN}$  in the rare gas solid leads to H-atoms which may diffuse through the solid. Photolysis of  $\text{H}_2\text{O}_2$  or  $\text{C}_2\text{N}_2$  in situ is expected to be less effective since the OH and CN formed in the decomposition may not be able to escape the matrix cage. A third method of producing the radicals would be a microwave discharge.

A given vibrational level of the upper electronic state is then continuously populated by absorption of monochromatic light while the steady state intensities of emission bands originating from various  $v'$  is simultaneously recorded photoelectrically.

The data obtained can be related to the relative populations of the various excited state vibrational levels and, thus, values of the vibrational relaxation rate as a function of vibrational level in the excited electronic state determined. The kinetic

equations for such a system are discussed earlier in this thesis. In brief, by populating the level  $v' = 1$  and measuring the relative intensities of emission from  $v' = 1$  and  $v' = 0$ , the vibrational relaxation rate for  $v' = 1 \rightarrow v' = 0$  can be determined if the radiative lifetime as a function of vibrational level is known. The radiative lifetime of the  $A \rightarrow X$  system of  $\text{OH}$  <sup>6</sup> and the violet <sup>7</sup> and red <sup>8</sup> systems of  $\text{CN}$  are known for the free molecules. It is a reasonable assumption that these are not appreciably perturbed in solids and that they do not vary with vibrational level since the transitions are allowed and the internuclear distances for the two states are nearly the same. By next exciting  $v' = 2$  and monitoring the emission from  $v' = 2, 1$  and  $0$ , the relaxation rates for  $2 \rightarrow 1$  and  $1 \rightarrow 0$  are obtained. Clearly the rate for  $1 \rightarrow 0$  must agree in the two determinations. If they do not, multi-quantum jumps are strongly suggested. These can be incorporated into the relaxation kinetics and their rates determined.

The big "if" in the proposed investigation is whether emission will be seen from lower vibrational levels when excitation is carried out into higher vibrational levels. If the vibrational relaxation rate is very slow relative to the electronic radiative lifetime only resonance emission will be seen and, therefore, only a rough limit to the relaxation rate obtained. In this case it may be possible to increase the vibrational relaxation rate significantly by changing the solid host. For example, by using  $\text{CO}_2$  or other polyatomics for a matrix, near resonances between the guest and host vibrational levels occur and the relaxation rate may be greatly increased.

## References

1. R. W. Nicholls, Proc. Phys. Soc. A69 , 741 (1956).
2. G. Herzberg, Molecular Spectra and Molecular Structure I. (D. Van Nostrand Co., Inc. New York, 1950), p. 520.
3. M. McCarty and G.W. Robinson, J. chim. phys. 56, 723 (1959);  
D.E. Milligan and M.E. Jacox, J. Chem. Phys. 47, 278 (1967).
4. R.J. Spindler, J. Quant. Spectrosc. Radiat. Transfer 5, 165 (1965).
5. G. Herzberg, Electronic Spectra of Polyatomic Molecules (D. Van Nostrand Co., Inc., New York, 1966), p. 484.
6. R.G. Bennett and F.W. Dalby, J. Chem. Phys. 40, 1414 (1964).
7. V.H. Reis, J. Quant. Spectrosc. Radiat. Transfer 5, 585 (1965).
8. T. Wentink, Jr., L. Isaacson, and J. Morreal, J. Chem. Phys. 41, 278 (1964).

## PROPOSITION II

It is proposed to investigate the crystal electronic spectrum of p-benzoquinone and search for either absorption or emission involving vibronic states arising from interaction between the two carbonyl groups.

Two chromophoric groups or molecules at finite distances can interact and, thereby, remove the twofold degeneracy of the excited states of the pair. This kind of interaction gives rise to the well-known Davydov splitting in molecular crystals.<sup>1</sup> As a limiting case of a "crystal with only two molecules", McClure<sup>2</sup> has studied the spectra of molecules containing two benzene moieties connected by  $-(CH_2)_n-$  groups ( $n = 0, 1$ , and  $2$ ). The spectra were explained by considering excitation exchange interactions between the benzene rings.

Similar interactions are expected in smaller molecules which contain two identical chromophoric groups. The experimental confirmation of this expectation is, however, limited to only one observation. El-Sayed and Robinson<sup>3</sup> have observed additional absorption features to low energy of the  $3200 \text{ \AA}$  system of pyrazine at low temperatures which they assigned to the symmetry forbidden component of the lowest  $\pi^* \leftarrow n$  transition. Herzberg<sup>4</sup> has questioned this interpretation, while Cohen and Goodman<sup>5</sup> have recently employed the ordering of states suggested by El-Sayed and Robinson to explain radiationless transitions in the diazines. In light of its singular

importance, a re-examination of the solid spectrum of the diazines is indicated. An alternate approach, although not designed to settle the above controversy, is to search for absorption to the two components in other similar systems expected to show this type of splitting. We, thus, propose to investigate the absorption spectra of p-benzoquinone at low temperatures.

The pure crystal spectrum of p-benzoquinone has been investigated previously under low resolution at room temperature<sup>6</sup> and at 20°K.<sup>7</sup> The strong bands observed by Sidman<sup>7</sup> at 20°K correlate well with the recent high resolution analysis of the visible spectrum of the free molecule by Hollas.<sup>8</sup> Two transitions are seen in the visible:  ${}^3A_u \leftarrow {}^1A_{1g}$  at  $\sim 5500 \text{ \AA}$  and  ${}^1B_{1g} \leftarrow {}^1A_{1g}$  at  $\sim 5000 \text{ \AA}$ . Both are assigned as  $\pi^* \leftarrow n$ .

In the simplest approximation,<sup>6</sup> these states arise from the following electron configurations:

$$\begin{array}{ll} A_u & \dots n_+^2 n_- \pi_5 \quad (b_{2u} \leftarrow b_{2g}) \\ B_{1g} & \dots n_+ n_-^2 \pi_5 \quad (b_{3g} \leftarrow b_{2g}) \end{array}$$

where  $\pi_5$  is the lowest unfilled  $\pi$ -orbital and

$$n_{\pm} = \frac{1}{\sqrt{2}} (n_1 \pm n_2)$$

are the pair of n-orbitals resulting from the degenerate nonbonding orbitals on the oxygen atoms. Thus, besides the transitions assigned by Hollas,  ${}^3B \leftarrow {}^1A_{1g}$  and  ${}^1A_u \leftarrow {}^1A_{1g}$  are expected. The purpose of this proposal is to search for these states, which are anticipated to be nearly degenerate with the observed states. The degeneracy is presum-

ably removed by a small interaction between the two equivalent carbonyl groups.

Hollas reports no evidence for the  ${}^1A_u \leftarrow {}^1A_{1g}$  transitions in the gas. Sidman's crystal spectrum is less clear. Although he does not consider this transition, many weak lines in his spectrum are unassigned, even in light of the more recent gas phase analysis. Moreover, many lines are assigned to phonon additions, some of which appear with an intensity greater than the no-phonon line. In particular, all phonon addition lines are weaker than the corresponding vibronic line except for the two bands near the first false origin. This apparent additional absorption may possibly represent unresolved structure due to the other component of the lowest  $\pi^* \leftarrow n$  singlet transition, i. e.,  ${}^1A_u \leftarrow {}^1A_{1g}$ . This observation of Sidman's spectrum was apparently first made by Hollas, who suggested that this region of strong absorption may be the region of the  ${}^1A_{1u} \leftarrow {}^1A_{1g}$  system. Assuming this to be the origin, a splitting of the  ${}^1B_{1g}$  and  ${}^1A_u$  states of 200-300  $\text{cm}^{-1}$  in the crystal is implied with the  ${}^1B_{1g}$  state lower in energy.

This conjecture may, however, be in error for the following reasons. The  ${}^1A_u \leftarrow {}^1A_{1g}$  system is forbidden in the free molecule and requires  $b_{1g}$ ,  $b_{2g}$  or  $b_{3g}$  vibrations to gain vibronic intensity. Although it does become group theoretically allowed in the  $C_i$  site<sup>9</sup> of the *p*-benzoquinone crystal, it most likely will still give the appearance of a forbidden system made vibronically allowed. Therefore, the tentative splitting given above may be too large by the energy of



the perturbing vibration and may in fact even invert the energy ordering of the two states.

Another observation by Sidman seems to suggest that the  $^1A_u$  state is at lower energy, viz., no emission was seen from "crystalline p-benzoquinone at 20°K, or in a glassy solution at 77°K, when illuminated with either blue or ultraviolet light." The recent mechanism for radiationless transitions in diazines suggested by Cohen and Goodman would qualitatively predict this observation if the  $^1A_{1u}$  state does lie beneath the  $^1B_{1g}$  state. However, the emission spectrum should certainly be reinvestigated since this could aid in establishing the existence or nonexistence of lower lying states.

Extension of the above suggested studies to the spectrum of other molecules containing two carbonyl groups would also be of interest.

## References

1. See, for example, D. S. McClure, Solid State Physics (Academic Press, Inc., New York, 1959), Vol. 8, pp. 1-48.
2. D. S. McClure, *Can. J. Chem.* 36, 59 (1958).
3. M. A. El-Sayed and G. W. Robinson, *Molec. Phys.* 4, 273 (1961); *J. Chem. Phys.* 34, 1840 (1961); 35, 1896 (1961).
4. G. Herzberg, Electronic Spectra of Polyatomic Molecules (D. Van Nostrand Co., Inc., New York, 1966), p. 551.
5. B. J. Cohen and L. Goodman, *J. Chem. Phys.* 46, 713 (1967).
6. J. C. D. Brand and T. H. Goodwin, *Trans. Far. Soc.* 53, 295 (1957).
7. J. W. Sidman, *J. Amer. Chem. Soc.* 78, 2363 (1956); *J. Chem. Phys.* 27, 820 (1957).
8. J. M. Hollas, *Spectrochimica Acta* 20, 1563 (1964).
9. J. Trotter, *Acta Cryst.* 13, 86 (1960).

## PROPOSITION III

As a means of studying the bonding in alkali halide dimers, it is proposed to investigate the infrared spectrum of mixed alkali halides.

In the vapor most of the alkali halides form dimers, and in some cases even trimers.<sup>1</sup> The actual structure of the dimers have been investigated only for some of the lithium halides where electron diffraction measurements indicate a planar rhombic structure with  $D_{2h}$  symmetry.<sup>2</sup> The structures of the dimers of the other halides is not known with certainty, but they are thought to have similar geometries.<sup>1</sup>

Klemperer and Norris<sup>3</sup> have assigned two gas phase infrared absorptions to the dimers of the lithium halides, but the vibrational frequencies could not be accurately determined because of the large bandwidths that result from the high temperatures used to obtain a sufficient concentration of dimers in the gas phase. In addition a series of workers<sup>4</sup> have investigated the infrared spectra of lithium fluoride dimers in matrices at low temperatures. Much sharper lines are obtained and a more nearly complete analysis of the spectrum in terms of the species present and their geometry is possible.

However, even in the most recent matrix study the vibrational analysis is incomplete since only three vibrational modes are assigned, whereas a tetratomic non linear molecule has six normal modes. The reason for this is of course clear if the lithium halide dimers belong

to point group  $\underline{D}_{2h}$ , namely only the three  $\underline{u}$  vibrations are infrared active.

The frequencies for the alkali halide dimers have been theoretically calculated by Berkowitz<sup>5</sup> on the basis of an ionic model. The agreement with the three known frequencies is fair ( $\sim 25\%$ ), but this is certainly an inadequate test of the potential used. To obtain a better understanding of the binding in these dimers, one would like to have more of the vibrational frequencies.

A systematic study of the infrared spectra of mixed alkali halide dimers which contain either a common anion or cation is proposed. These have not been observed by infrared spectroscopy although it is known, for example, that in the LiF-NaF system the vapor consists mostly of  $\text{LiNaF}_2$  when the LiF-NaF composition of the melt is about 1:1.<sup>6</sup> The mixed dimers have lower symmetry than the pure dimer and, therefore, an accordingly greater number of infrared active modes.

Assuming that the planar rhombic-type structure is carried over to the mixed dimer, the symmetry is reduced to  $\underline{C}_{2v}$  and all vibrational modes become infrared active. Therefore, a complete vibrational analysis is in principle possible. The ionic model of Berkowitz can be extended to the mixed dimer and the comparison between observed and calculated frequencies for a series of mixed dimers would serve as a sensitive test for the model potential.

As indicated above, two techniques are available for studying the infrared frequencies of these molecules, involving two temperature extremes. The low temperature trapping technique is probably required, at least as a check, in the proposed work since the bandwidths at high

temperatures will be broad and, therefore, it will be difficult to separate the features due to different species. A combination of the two techniques is undoubtedly best. Thus, the frequencies and assignments obtained from the low temperature study can be compared with the unperturbed gas phase spectra. The samples are prepared for low temperature infrared investigation as follows.<sup>4</sup> A Knudsen cell containing the salt (or salts) is electrically heated to obtain a vapor pressure of a few microns. The gases effuse from the cell and are mixed with a matrix gas subsequent to deposition on a low temperature infrared window. The gas phase spectra are recorded employing phase sensitive detection to reduce the strong infrared emission at high temperatures.<sup>3</sup>

The monomer and some dimer frequencies for the alkali halides are known so that the dimer frequencies for some of the mixed halides will probably be easily identified. Varying the relative salt concentration in the Knudsen cell will aid the identification and, of course, the spectrum of the individual halides can be obtained separately for comparison in those cases where the pure alkali halide frequencies are unknown. In the gas phase monomer and dimer bands can be distinguished using a double-oven technique.<sup>3</sup>

## References

1. For a recent review see S.H.Bauer and R.F.Porter in Molten Salt Chemistry, ed. by M.Blander (Interscience Publisher, New York, 1964), pp. 607-680.
2. S.H.Bauer, T.Ino, and R.F.Porter, J.Chem.Phys. 33, 685 (1960).
3. W.Klemperer and W.G.Norris, J.Chem.Phys. 34, 1071 (1961).
4. A.Snelson, J.Chem.Phys. 46, 3652 (1967) and references cited therein.
5. J.Berkowitz, J.Chem.Phys. 29, 1386 (1958); 32, 1519 (1960).
6. R.G.Schoonmaker and R.F.Porter, J.Chem.Phys. 30, 283 (1959).

## PROPOSITION IV

It is suggested that the nuclear quadrupole resonance spectra of the halogen nuclei in crystalline addition compounds of the type 1,4-dioxane · 2ICl be investigated.

Certain chemically "saturated" molecular species combine to form solids whose composition is a simple molecular ratio of the component molecules. A well known and often studied example is the 1:1 solid complex between Br<sub>2</sub> and benzene. The binding in these complexes is usually described in terms of "charge-transfer" from the donor to the acceptor component.<sup>1, 2</sup>

A series of complexes which have received relatively little attention, but which seem well suited for a comparative study, are the crystalline addition compounds formed between halogens and ethers. The available crystal structure determinations<sup>3</sup> for these complexes have shown that the "charge-transfer" bond length is considerably shorter than the sum of the van der Waals radii and that the halogen-halogen bond length is typically longer than the bond length in the free halogen. The crystallographic data thus imply that bonding occurs between the ether oxygen and the halogen, and has been interpreted<sup>3</sup> in terms of charge-transfer from the non bonded ether electrons to the halogen. The bond lengths and crystal structures further imply that the strength of the interaction increases in the order Cl<sub>2</sub> < Br<sub>2</sub> < I<sub>2</sub> < ICl for the halogen, but the data are not yet complete.

As particular examples, we consider the addition compounds formed between halogens and 1,4-dioxane, 1,4-dithiane, and 1,4-diselenane. The 1,4-dioxane-Br<sub>2</sub> or Cl<sub>2</sub> crystal contains "zigzag" chains of alternating donor and acceptor molecules and the participation of one halogen atom in a bond to the ether oxygen does not appear to influence the ability of the other halogen atom to form a similar bond. However, in the stronger complexes between the corresponding thio- and seleno-ethers and I<sub>2</sub>, only one iodine atom is bonded to the ether and the complexes contain the molecular species in the proportion 1:2, e.g., 1,4-dithiane·2I<sub>2</sub>. A similar 1:2 complex results for dioxane and ICl with the ether oxygens linked to the iodine.

To further characterize the nature and the relative strength of the bonding in these complexes, the nuclear quadrupole resonance spectra of the halogen nuclei would be useful. Examples of the application of quadrupole coupling data to investigate intermolecular bonding in the solid state are given by Das and Hahn,<sup>4</sup> but these examples all relate to neat crystals. A study of complexes involving aromatic donors has been reported<sup>5</sup> and interpreted in terms of very weak, if any, charge-transfer, as might have been anticipated from the crystallographic results for these particular complexes.<sup>6</sup>

On the other hand, the addition compounds of n-donors with halogens show strong evidence for intermolecular interactions in the solid. It is, therefore, of interest to obtain the halogen coupling constants in these complexes and attempt to relate the values for a series of complexes to the bonding.



The pertinent theory will be briefly outlined for the example addition compound 1,4-dioxane·2ICl. The structural data discussed above imply that this is one of the more strongly bound complexes, so that the effects should be near maximum. The nuclear quadrupole coupling constants for  $^{127}\text{I}$  and for  $^{35}\text{Cl}$  are known for ICl both in the gas phase<sup>7</sup> and in the pure solid<sup>8</sup> and, therefore, the observed frequencies for the complex can be compared to uncomplexed ICl. Moreover, the iodine and chlorine resonances are expected to be well separated in frequency. The above considerations at least in part apply to all interhalogens and point out the advantages of using an interhalogen instead of a halogen for a nuclear quadrupole resonance study of the 1:2 addition complexes.

In the complex the atomic grouping O—I—Cl is linear and directed in the equatorial direction with respect to the 1,4-dioxane molecule. Considering only the fragment O—I—Cl and assuming the field is symmetric about the linear axis, the quadrupole energy levels are<sup>4</sup>

$$W_M = \frac{e^2 Qq}{4I(2I-1)} [3M^2 - I(I+1)] .$$

$\text{Cl}^{35}$  has a nuclear spin  $I = \frac{3}{2}$  and only one line results in the quadrupole spectrum at a frequency

$$\omega = \frac{e^2 Qq}{2\hbar}$$

corresponding to  $M = \pm \frac{1}{2} \leftrightarrow \pm \frac{3}{2}$ . Two frequencies are obtained for

$I^{127}$ , which has  $I = \frac{5}{2}$ , and these are given by

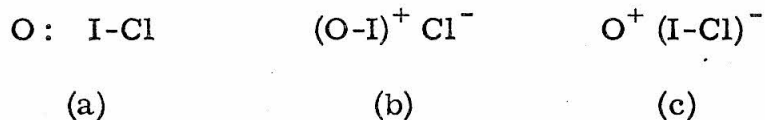
$$\begin{aligned}\omega_1 &= \frac{3e^2 Qq}{20\hbar} & M &= \pm \frac{1}{2} \leftrightarrow \pm \frac{3}{2} \\ \omega_2 &= \frac{3e^2 Qq}{10\hbar} & M &= \pm \frac{3}{2} \leftrightarrow \pm \frac{5}{2}\end{aligned}$$

Thus, for a given nucleus with quadrupole moment  $eQ$ , the transition frequencies are determined by

$$eq = \frac{\partial^2 V}{\partial z^2}$$

where  $z$  refers to the unique axis and  $V$  is the electrostatic potential at the nucleus due to the surrounding charges. We, therefore, must inquire into how  $q$  changes in the complex relative to the uncomplexed ICl molecule. Das and Hahn review and discuss the factors influencing  $q$ .

The complex may be roughly approximated as a resonance hybrid of the structures (a), (b), and (c), where all groups attached to the oxygen and all oxygen electrons except for the equatorial lone-pair are neglected.



In (a) no intermolecular bond exists, and the ICl molecule approaches the case of an oriented gas. Therefore, the quadrupole coupling constants for both  $I^{127}$  and  $Cl^{35}$  are expected to have roughly the free

molecule values. In the full charge separation implied by structure (b), the chlorine ion has a completely closed, spherically symmetric valence shell and the quadrupole coupling vanishes. Thus, the larger the contribution made by structure (b) to the total wavefunction of the complex, the greater the lowering of the Cl resonance frequency. The  $I^{127}$  coupling in structure (b) would seem to increase from the value in ICl due to the larger electronegativity of oxygen compared to chlorine and the formal positive charge, if the hybridization about the iodine does not change. Structure (c) represents the "dative-bond" structure in charge-transfer theory and is intermediate between (a) where no bond exists and (b) where the interaction is sufficiently strong to form an oxygen-iodine bond.

Clearly the above discussion is highly qualitative, but it does indicate the type of changes expected in the quadrupole coupling with intermolecular interactions. By comparing the observed changes in a family of related complexes, trends may be ascertained which might allow a more quantitative discussion of the bonding. It is, therefore, proposed to investigate the nuclear quadrupole resonance spectra of the halogen nuclei in the crystalline addition compounds of 1,4-dioxane, 1,4-dithiane, and 1,4-diselenane with the interhalogens and halogens.

## References

1. G. Briegleb, Elektronem-Donator-Acceptor-Komplexe (Springer-Verlag, Berlin-Göttingen-Heidelberg, 1961).
2. R. S. Mulliken and W. P. Person, *Ann. Rev. Phys. Chem.* 13, 107 (1962).
3. O. Hassel and Chr. Rømming, *Quart. Rev.* 16, 1 (1962).
4. T. P. Das and E. L. Hahn, Nuclear Quadrupole Resonance Spectroscopy, Solid State Physics, Supplement 1 (Academic Press Inc., New York, 1958).
5. H. O. Hooper, *J. Chem. Phys.* 41, 599 (1964).
6. F. J. Streiter and D. H. Templeton, *J. Chem. Phys.* 37, 161 (1962).
7. C. H. Townes and E. L. Schawlow, Microwave Spectroscopy (McGraw-Hill Book Co., Inc., New York, 1955), p. 634.
8. S. Kojima, K. Tsukada, S. Ogawa, and A. Schimauchi, *J. Chem. Phys.* 23, 1963 (1955); P. J. Bray, *ibid.* 23, 703 (1955).

## PROPOSITION V

Recent work has shown that molecules are preferentially oriented in deposited solids. It is suggested that this be further investigated and applied to obtain the electron spin resonance spectra of CCO and NCN.

Recent observations by Kasai, et al.<sup>1,2</sup> demonstrate that radicals in solid matrices at low temperatures can have preferential orientations with respect to the substrate. For example, NO<sub>2</sub> was found from electron spin resonance (ESR) studies to be not rotating and to be oriented mainly parallel to a planar sapphire substrate in a Ne matrix. The mechanism where by this occurs is not known. Kasai, et al. propose that the thermal gradients at the substrate surface might be important, but only minor variations in the experimental conditions are reported.

If such partially oriented solutes were a general occurrence in matrices, this would aid the ESR study of many molecules which can not be incorporated into a single crystal. The technique would be especially useful for chemically unstable molecules such as small, highly reactive, ground state triplets. It is suggested that the ESR spectrum of CCO and NCN be obtained in solid matrices following the general experimental technique of Kasai, et al. By extending the study to a number of hosts and varying the conditions of sample preparation,

optimum conditions for any preferential orientation and the perturbation by the environment on the parameters of the triplet state may be determined. These systems are considerably different than those studied by Kasai in that the radicals are chemically unstable. Preferential orientation of the precursor may or may not occur more readily than the radical. Thus, both in situ photolysis and photolysis during deposition should be investigated.

CCO and NCN are isoelectronic and, therefore, the electronic energy levels are expected to be similar. The lowest electronic configuration of NCN is

$$\dots 1\sigma_g^2 1\sigma_u^2 2\sigma_g^2 2\sigma_u^2 1\pi_u^4 1\pi_g^2$$

which yields  $^3\Sigma_g^-$ ,  $^1\Sigma_g^+$ , and  $^1\Delta_g$  states.<sup>3</sup> The lowest energy state of this configuration is expected to be  $^3\Sigma_g^-$  with the  $^1\Delta_g$  and  $^1\Sigma_g^+$  states low lying excited states. For the unsymmetrical radical CCO, the u, g-classification is of course no longer correct. However, the expectation that both of these fourteen electron radicals are linear in accordance with theoretical predictions<sup>3, 4</sup> and ground state triplets is still valid.

Herzberg and Travis<sup>5</sup> have examined a portion of the NCN spectrum under high resolution and have assigned the observed bands to a  $^3\Pi_u \leftarrow ^3\Sigma_g^-$  transition. Moreover, they were able to ascertain the spin-spin splitting in the ground  $^3\Sigma_g^-$  state. Wasserman, et al.<sup>6</sup> have in addition observed the ESR spectrum of NCN in a fluorocarbon glass at 77°K. No ESR studies have been reported for CCO, although there

has been considerable interest in photochemical systems involving this radical.<sup>7</sup>

A reason for choosing the NCN molecule for further investigation is that the zero-field splitting for the free radical is known from the analysis of Herzberg and Travis. The zero-field splitting of no other polyatomic molecule in a triplet state has been determined both for the free molecule and in a condensed solvent. The results show that for NCN in a fluorocarbon glass the zero-field splitting is decreased from the gas phase value by about 2%. The extension to other solvents with different molecular properties is, therefore, of interest to establish whether this magnitude change is characteristic. The direct confirmation of a triplet ground state for CCO relates of course directly to its behavior in photochemical systems. The energies of the excited states of CCO are similarly of interest and not currently known.

The ESR spectrum of triplet states of randomly oriented molecules in solids has been discussed by Wasserman, Snyder, and Yager (WSY).<sup>8</sup> We will present a brief outline of the theory, following mainly these authors. The spin Hamiltonian of two electrons in a triplet state in the presence of an external magnetic field  $\underline{H}$  may be written

$$\mathcal{H} = g_e \beta \underline{H} \cdot \underline{S} + D(S_z^2 - 2/3) + E(S_x^2 - S_y^2)$$

where the symbols have their usual meaning. D and E are the experimentally determined zero-field splitting constants. When two of the principal axes are equivalent, as in a linear molecule, the third

direction corresponds to the  $z$  axis and  $E = 0$ . The zero-field splittings in triplet states of molecules containing mainly light atoms arise primarily from the dipolar interaction of the electron spins, but in the more general case spin-orbit interactions can also contribute to the splitting.<sup>9</sup>

WSY have shown that there is a sharp change in the number of molecules which are in resonance at those fields where  $\underline{H}$  is parallel or nearly parallel to one of the principal axis. This feature gives rise to peaks in the ESR spectrum that are centered at these fields. From these axial resonance fields and the solutions of the spin Hamiltonian, the zero-field splitting constants are obtained. In our case, the axial resonance fields are related to the zero-field splitting as follows.

$$H_{xy1}^2 = H_0 (H_0 - D')$$

$$H_{xy2}^2 = H_0 (H_0 + D')$$

$$H_{z1} = |H_0 - D'|$$

$$H_{z2} = H_0 + D'$$

where  $H_0 = h\nu/g\beta$ ,  $\nu$  is the microwave frequency,  $D' = D/g\beta$ , and, for example,  $H_{z1}$  and  $H_{z2}$  are the low and high axial fields when  $\underline{H}$  is parallel to  $z$ .

As seen from the above equations for the axial resonance fields,  $H_{xy1}$  and  $H_{z1}$  move to lower fields as  $D'$  increases relative to  $H_0$ . For  $D' > H_0$ ,  $H_{xy1}$  no longer occurs and the two  $z$ -absorptions are then transitions between the same energy levels.<sup>10</sup> The case  $D' > H_0$



applies for the radicals CCO and NCN. Whereas typical spectrometers employ a microwave quantum of  $\sim 0.3 \text{ cm}^{-1}$ ,  $D$  for NCN equals  $1.568 \text{ cm}^{-1}$ .<sup>5</sup> We reasonably expect CCO to also have  $D \approx 1\text{-}2 \text{ cm}^{-1}$ . This means that the ESR spectrum of NCN or CCO, randomly oriented in a solid host, should show absorptions for those radicals that have their  $z$ -axis perpendicular to the external field at the resonance field  $H_{xy2}$ . The absorptions for  $\underline{H} \parallel z$  are much weaker than  $\underline{H} \perp z$  and the former have not been observed for cases where  $D' > H_0$ .

If the radicals preferentially orient with their  $z$ -axis parallel to a planar substrate, the ESR spectrum can be easily obtained by placing the substrate plane perpendicular to the magnetic field. Thus, a majority of the molecules have  $\underline{H} \perp z$ . Moreover, now the resonance for  $\underline{H} \parallel z$  might also be seen by rotating the substrate perpendicular to the magnetic field. This then allows two independent measurements of the zero-field splitting. If these do not agree, then the assumption made in the above discussion that  $g$  equals the free electron value  $g_e$  is not valid. The degree of orientation can be obtained by monitoring the intensity of the  $H_{xy2}$  absorption as the substrate is rotated relative to  $\underline{H}$ .

Precursors that have been used to obtain CCO and NCN are carbon suboxide<sup>7</sup> and cyanogen azide.<sup>6</sup>

## References

1. P. A. Kasai, W. Weltner, Jr., and E. P. Whipple, J. Chem. Phys. 42, 1120 (1965).
2. P. A. Kasai, E. P. Whipple, and W. Weltner, Jr., J. Chem. Phys. 44, 2581 (1966).
3. G. Herzberg, Molecular Spectra and Molecular Structure III. Electronic Spectra and Electronic Structure of Polyatomic Molecules (D. Van Nostrand Co., Inc., New York, 1966).
4. A. D. Walsh, J. Chem. Soc. 1953, 2266.
5. G. Herzberg and D. N. Travis, Can. J. Phys. 42, 1658 (1964).
6. E. Wasserman, L. Barash, and W. A. Yager, J. Am. Chem. Soc. 87, 2075 (1965).
7. See, for example, D. G. Williamson and K. D. Bayes, J. Am. Chem. Soc. 89, 3390 (1967) and references cited therein.
8. E. Wasserman, L. C. Snyder and W. A. Yager, J. Chem. Phys. 41, 1763 (1964).
9. M. Tinkman and M. W. P. Strandberg, Phys. Rev. 97, 937 (1955); K. Kayama and J. C. Baird, J. Chem. Phys. 46, 2604 (1967).
10. A calculated absorption spectrum for molecules that have  $E' \ll H_0 < D'$  is given by J. A. R. Coope, J. B. Farmer, C. L. Gardner, and C. A. McDowell, J. Chem. Phys. 42, 54 (1965).